**UNIVERSITY OF SOUTHAMPTON**

FACULTY ENGINEERING, SCIENCE AND MATHEMATICS

INSTITUTE OF SOUND AND VIBRATION RESEARCH

# SHOCK ISOLATION USING SWITCHABLE STIFFNESS

**by**

**Diego Francisco Ledezma Ramirez.**

**Thesis submitted for the degree of**

**Doctor of Philosophy**

**September 2008**

UNIVERSITY OF SOUTHAMPTON

## ABSTRACT

FACULTY OF ENGINEERING, SCIENCE AND MATHEMATICS

INSTITUTE OF SOUND AND VIBRATION RESEARCH

DOCTOR OF PHILOSOPHY

# Shock Isolation using Switchable Stiffness.

By Diego Francisco Ledezma Ramirez.

This study investigates a novel stiffness control strategy applied to the problem of shock isolation. This is based on the principle that the stiffness and mass are the principal physical properties that control the passive system shock response.

The problem of shock response control is divided in two stages. Firstly, the maximum response whilst a shock is applied is considered, and the effectiveness of a switchable isolation stiffness strategy is evaluated. This strategy aims to reduce the shock response by switching the stiffness to a low value during the shock input. Two different models are considered for the theoretical analysis, namely, a single mass supported by two elastic elements one of which can be disconnected, and a second model where the switchable element comprises a secondary mass-stiffness system. The performance of the two strategies is analyzed in terms of response parameters such as the absolute and relative displacement and absolute acceleration. The single degree-of-freedom system is considered as a benchmark for comparison.

The issue of residual vibration suppression is then presented. For the latter a different switchable stiffness strategy is identified, and the analysis is mainly concerned with the energy dissipation mechanism used to suppress residual vibration. As in the first stage of shock isolation, two models are considered. Optimum configurations and stiffness changes are identified for both the shock response reduction and the decay of the residual vibration. The effect of viscous damping is subsequently incorporated.

The practical implementation and experimental validation is then presented and a experimental system is developed. It is based on a conceptual model comprising a magnetic suspension element that is able to change its effective stiffness by altering the magnetic force. This novel configuration has the advantages of achieving a high stiffness change in a very short amount of time and with very low damping, which is required to validate the theoretical studies. The design and properties of the model are discussed and then both stiffness strategies are implemented. This model is used to show the feasibility and evaluate the isolation performance of the different switchable stiffness strategies and the issues and limitations of the implementation.

# ACKNOWLEDGEMENTS.

I would like to express my gratitude to my supervisors, Dr, Neil Ferguson, and Prof. Mike Brennan, not only because of their excellent academic guidance during the last four years, but also for their advice and suggestions which will help me to develop my professional career.

I also wish to thank the valuable advices during my research project given by Prof. Brian Mace, Dr. Tim Waters, and Prof. Paolo Gardonio. Their suggestions helped to greatly improve this work.

Many thanks also to the administrative personal of the ISVR, especially to Mrs. Maureen Mew, Miss Anne-Marie McDonell and Miss Joanne Hazell, for their help and support during the last years. I would also like to mention the technicians from the electronic and mechanical workshops, and especially thanks to Rob Stansbridge, Keith Sims and Dave Edwards for their help and suggestions to develop the experimental rig. Many thanks to my colleagues and friends from the ISVR for their company and all the memorable moments. Also, many thanks to all the good friends whom I have meet during my time in the UK, because they have contributed to making my stay more enjoyable.

Additionally, I want to acknowledge the Mexican Council of Science and Technology (CONACyT) for providing the funding and scholarship for the development of this project.

Last but not least, thanks to my mother, my sisters and all my family for their constant support and understanding during this stage of my life.

# CONTENTS

**ABSTRACT……i**
**AKNOWLEDGEMENTS……ii**
**CONTENTS……iii**
**LIST OF FIGURES……vi**
**LIST OF TABLES……xviii**
**NOMENCLATURE……xix**

**1. INTRODUCTION ……1**
**1.1. Background……1**
**1.2. Vibration Isolation for shock……2**
1.2.1. Vibration control and isolation……2
1.2.2. Passive shock isolation……3
1.2.3. Active and semi-active shock isolation……5
1.2.4. Variable stiffness for vibration isolation and control……7
**1.3. Objectives and contributions……10**
**1.4. Thesis overview……11**

**2. INTRODUCTION TO SHOCK ISOLATION……12**
**2.1. Introduction……12**
**2.2. Fundamentals of shock analysis……13**
**2.3. Shock Response Spectrum……18**
**2.4. Shock response for damped systems……20**
**2.5. Summary……21**

**3. SHOCK RESPONSE CONTROL USING SWITCHABLE STIFFNESS……29**
**3.1. Introduction……29**
**3.2. Motivation……30**
**3.3. Simple model (massless secondary spring)……31**
3.3.1. Analytical solution……32
3.3.2. Parametric analysis and numerical results……35
3.3.3. Effect of delay……40
3.3.4. Effect of damping……42
**3.4. Compound model (mass-spring secondary system)……43**

3.4.1 Fundamentals and description of the model…..……..44
3.4.2 Re-connection issues…….……..46
3.4.3 Compound model results…….……..……49
3.4.4 Effect of damping……..……..……51
**3.5. Conclusions……52**

**4. RESIDUAL VIBRATION SUPPRESSION USING VARIABLE STIFFNESS……...…….76**
**4.1. Introduction……...76**
**4.2. Simple model (massless secondary spring)…….……77**
4.2.1 Effect of damping……84
**4.3. Compound model (mass-spring secondary system)……..86**
4.3.1 Undamped model…….……86
4.3.2 Effect of damping……...……96
**4.4. Conclusions……99**

**5. DESIGN OF A SWITCHABLE STIFFNESS EXPERIMENTAL MODEL…….……...116**
**5.1. Introduction…….116**
**5.2. Description of the rig and tests……...117**
**5.3. Procedure…….119**
**5.4. Results……..120**
**5.5. Discussion…….120**
**5.6. Conclusions……..……124**

**6. EXPERIMENTAL VALIDATION OF THE SWITCHING STIFFNESS SRATEGIES…….……...…..…137**
**6.1. Introduction…….137**
**6.2. Generation of a shock pulse……...138**
6.2.1 Experimental measurement of SRS……...139
6.2.2 Modified shock pulse…….……140
**6.3 Maximax response control strategy tests……..…142**
6.3.1 Set-up information……..……..……142
6.3.2 Results……..……..143

6.3.3 Discussion…….……143

**6.4. Decay and switching logic tests…….....147**

6.4.1 Set-up information……..……..…….147

6.4.2 Results……..……..148

6.4.3 Discussion…….……149

**6.5. Energy dissipation in the experimental design……..…151**

**6.6. Full implementation of the switching strategies……...153**

**6.7. Conclusions……...…154**

**7. GENERAL CONCLUSIONS AND RECOMMENDATIONS FOR FURTHER WORK……..…….…170**

**7.1. General conclusions……..…170**

**7.2. Recommendations for further work……..……173**

**REFERENCES……...175**

**APPENDIX A: SOLUTION OF THE EQUATIONS OF MOTION USING LAPLACE TRANSFORMATIONS…….……..……..184**

**APPENDIX B: PROOF OF ZERO RESIDUAL RESPONSE FOR SYMMETRICAL PULSES APPLIED TO UNDAMPED SYSTEMS…….…….…….189**

**APPENDIX C: SHOCK RESPONSE SPECTRA FOR RECTANGULAR AND VERSED SINE PULSES…….……..…192**

**APPENDIX D: EFFECT OF DELAY IN THE SWITCHING STIFFNESS STRATEGY FOR RESIDUAL VIBRATION……..…194**

**APPENDIX E. MAXIMUM ENERGY DISSIPATION FOR THE IMPACTING MODEL: AN ANALYTICAL DERIVATION FOR THE OPTIMUM PARAMETERS ……...……..…200**

**APPENDIX F. DETAILS OF THE SWITCHING CIRCUIT……...202**

# LIST OF FIGURES.


| Section | | Page |
|---|---|---|
| 2.1. | Single degree-of-freedom undamped model subjected to different types of shock excitations. (a) Transient force excitation on the mass, (b) transient base displacement, (c) transient base acceleration | 24 |
| 2.2. | Graphical representations of the Dirac delta function. $\delta(t-a)$ as $\varepsilon \to 0$ | 24 |
| 2.3. | Typical displacement response of an undamped single degree-of-freedom model to the impulse function applied at $t = a$ | 24 |
| 2.4. | Displacement response curves for an undamped single degree-of-freedom corresponding to several symmetrical pulses representing base displacement excitation; rectangular, half sine, and versed sine, for different values of $\tau/T$ . The vertical axis is for the normalised displacement response $v/\xi$ and the horizontal axis represents the normalised time $t/\tau$ . (— System response; – – Pulse ) | 25 |
| 2.5. | Shock response spectra for a single degree-of-freedom undamped model subjected to a rectangular pulse (— Maximax; – – Residual –·–Relative) | 26 |
| 2.6. | Shock response spectra for a single degree-of-freedom undamped model subjected to a half sine pulse (— Maximax; – – Residual –·– Relative) | 26 |
| 2.7. | Shock response spectra for a single degree-of-freedom undamped model subjected to a versed sine pulse (— Maximax; – – Residual –·–Relative) | 27 |
| 2.8. | Shock response spectra for a single degree-of-freedom viscously damped model subjected to half sine excitation. (— $\zeta = 0$ ···$\zeta = 0.2$ ; – – $\zeta = 0.4$; –··– $\zeta = 0.6$; — — $\zeta = 0.8$; –·– $\zeta = 1$) | 27 |
| 2.9. | Effect of damping in the reduction of maximax response for a half sine pulse. Vertical axis represents the ratio between the maximax for a damped system and the maximax for an undamped system. The horizontal axis is the value of damping ratio.(— $\tau/T = 0.8$ ; ··· $\tau/T = 0.25$ ; – – $\tau/T = 0.5$ ; –··– $\tau/T = 1.5$ ) | 28 |
| 3.1. | Single degree-of-freedom model with switchable stiffness under a shock excitation $\xi(t)$ applied to the base. | 55 |

3.2. Schematic representation of the stiffness variation $k_{\text{efffective}}$ during a shock pulse excitation $\xi(t)$. The time $\Delta t_1$ represents the delay between the beginning of the shock, and the reduction of the stiffness. The stiffness is recovered at time $\Delta t_2$ after the pulse has finished at $t = \tau$. 55

3.3. Normalised period ratio $\frac{\hat{\tau}_{\text{low}}}{\hat{\tau}_{\text{high}}} = \sqrt{1-\sigma}$ as function of the stiffness reduction ratio $\sigma = \frac{\Delta k}{k}$. (continuous). Linear approximation $1-\sigma/2$. for small values of the period ratio (dashed) 56

3.4. Time response for absolute displacement (dashed) and relative displacement (dash-dot) for stiffness reduction factor $\sigma$ =0.5 and different values of the period ratio $\hat{\tau}_{\text{high}}$. The solid line represents the versed sine excitation. (a) $\hat{\tau}_{\text{high}} = 0.25$. (b) $\hat{\tau}_{\text{high}} = 0.5$. (c) $\hat{\tau}_{\text{high}} = 1$. (d) $\hat{\tau}_{\text{high}} = 2$. 57

3.5. Time responses for absolute acceleration considering stiffness reduction factor $\sigma$ =0.5 and different values of the period ratio. (a) $\hat{\tau}_{\text{high}} = 0.25$. (b) $\hat{\tau}_{\text{high}} = 0.5$. (c) $\hat{\tau}_{\text{high}} = 1$. (d) $\hat{\tau}_{\text{high}} = 2$. 58

3.6. Ratio between the absolute displacement responses of the switchable stiffness model $\nu_{\text{adaptive}}$, and the passive model $\nu_{\text{passive}}$, as a function of the stiffness reduction factor (— $\hat{\tau}_{\text{high}} = 0.25$. — — $\hat{\tau}_{\text{high}} = 0.5$. ··· $\hat{\tau}_{\text{high}} = 1$. -·- $\hat{\tau}_{\text{high}} = 2$). 59

3.7. Ratio between the relative displacement responses of the switchable stiffness model $(\nu_{rel})_{\text{adaptive}}$ and the passive model $(\nu_{rel})_{\text{passive}}$ as a function of the stiffness reduction factor $\sigma$ (— $\hat{\tau}_{\text{high}} = 0.25$. — — $\hat{\tau}_{\text{high}} = 0.5$. ··· $\hat{\tau}_{\text{high}} = 1$. -·- $\hat{\tau}_{\text{high}} = 2$). 59

3.8. Ratio between the absolute acceleration responses of the switchable stiffness model $(\ddot{\nu}_{rel})_{\text{adaptive}}$ .and the passive model $(\ddot{\nu}_{rel})_{\text{adaptive}}$ as a function of the stiffness reduction factor (— $\hat{\tau}_{\text{high}} = 0.25$. — — $\hat{\tau}_{\text{high}} = 0.5$. ··· $\hat{\tau}_{\text{high}} = 1$. -·- $\hat{\tau}_{\text{high}} = 2$). 60

3.9. Effect of a time delay in the stiffness reduction $\Delta_1 = \frac{\Delta t_1}{\tau}$ and in the stiffness recovery $\Delta_2 = \frac{\Delta t_2}{\tau}$ on the maximax response of the normalised absolute displacement, for a switchable stiffness system, under a versed sine pulse excitation. (a) $\hat{\tau}_{\text{high}} = 0.25$. (b) $\hat{\tau}_{\text{high}} = 0.5$. 61

3.10. Effect of a time delay in the stiffness reduction $\Delta_1 = \frac{\Delta t_1}{\tau}$ and in the stiffness recovery $\Delta_2 = \frac{\Delta t_2}{\tau}$ on the maximax response of the normalised absolute acceleration, for a switchable stiffness system, under a versed sine pulse excitation. (a) $\hat{\tau}_{\text{high}} = 0.25$. (b) $\hat{\tau}_{\text{high}} = 0.5$. 62

3.11. Example of time responses for a system with switchable stiffness for versed sine excitation. $\sigma = 0.7$, $\hat{\tau}_{\text{high}} = 0.25$. and delays $\Delta_1 = \Delta_2 = 0.1$. (— Pulse, --- $\frac{\nu}{\xi_c}$ . ··· $\frac{\dot{\nu}}{\dot{\xi}_c}$ . -·- $\frac{\ddot{\nu}}{\ddot{\xi}_c}$). 63

3.12. Shock Response Spectra of the switching stiffness model for versed sine pulse and delays $\Delta_1 = \Delta_2 = 0.01$. The bold line represents the passive system. (— $\sigma = 0$; — $\sigma = 0.1$; – – $\sigma = 0.3$; – $\sigma = 0.5$; —— $\sigma = 0.7$; ·· $\sigma$=0.9) 63

3.13. Viscously damped single degree-of-freedom model with switchable stiffness under a shock excitation $u(t)$ applied at the base. 64

3.14. Shock Response Spectra for a versed sine pulse considering the effect of viscous damping, for a stiffness reduction factor $\sigma = 0.5$. The bold line is for a passive undamped model. (— $\zeta = 0.05$; – – $\zeta = 0.1$; - - $\zeta = 0.3$; – - – $\zeta = 0.5$) 64

3.15 Displacement Shock Response Spectra for a versed sine pulse considering the effect of viscous damping, for a stiffness reduction factor $\sigma = 0.5$. The bold line is for a passive undamped model. (— $\zeta = 0.05$; – – $\zeta = 0.1$; - - $\zeta = 0.3$; – - – $\zeta = 0.5$). 65

3.16 Acceleration Shock Response Spectra for a versed sine pulse 65

considering the effect of viscous damping, for a stiffness factor of $\sigma =$ 0.5. The bold line is for a passive undamped model. ( — $\zeta$ = 0ñ – – $\zeta = 0.1$; - - $\zeta = 0.3$; – - – $\zeta = 0.5$).

3.17. Conceptual sketch for a variable stiffness/mass system. The secondary mass can oscillate independently inside the main mass while it is disconnected. 66

3.18. Compound model comprising two single degree-of-freedom models that can oscillate together (a) or independently (b). 66

3.19. Values of the mass ratio $\mu = \frac{\Delta m}{m}$ and the stiffness reduction ratio $\sigma = \frac{\Delta k}{k}$ .corresponding to several integer values of the frequency ratio $\Omega = \frac{\omega_s}{\omega_p}$. (— $\Omega$ = 1; — $\Omega$ = 2; --- $\Omega$ = 3; ··· $\Omega = 4$; -·- $\Omega = 5$) 67

3.20. Displacement time response for the primary (---) and secondary (····) masses, showing the moment when the systems recombine with an inelastic impact. The continous bold line represents the versed sine input. The thin line represents the response after the systems reconnect The period ratio is $\hat{\tau}_{\text{initial}} = 0.25$ and the values of frequency ratio $\Omega$ are: (a) $\Omega$ = 2 and (b) $\Omega$ = 3. 68

3.21. Variation in the period ratio $\hat{\tau}$ . as a result of the stiffness and mass change. (a) Primary system, (b) Secondary system. 69

3.22. Ratio between the displacement response of the compound model and the passive model under a versed sine pulse as a function of the stiffness reduction factor $\sigma$ given for two values of the frequency ratio between the primary and secondary systems . (a) $\Omega$ = 2 and (b) $\Omega$ = 3 .(— $\hat{\tau}_{\text{initial}} = 0.25$ . --- $\hat{\tau}_{\text{initial}} = 0.5$ . ··· $\hat{\tau}_{\text{initial}} = 1$ . -·- $\hat{\tau}_{\text{initial}} = 2$ . 70

3.23. Ratio between the relative displacement response of the compound model and the passive model under a versed sine pulse, as a function of the stiffness reduction factor $\sigma$ given for two values of the frequency ratio between the primary and secondary systems . (a) $\Omega$ = 2 and (b) $\Omega$ = 3. (— $\hat{\tau}_{\text{initial}} = 0.25$ . --- $\hat{\tau}_{\text{initial}} = 0.5$ . ··· $\hat{\tau}_{\text{initial}} = 1$ . -·- $\hat{\tau}_{\text{initial}} = 2$ . 71

3.24. Ratio between the absolute acceleration response of the compound model and the passive model under a versed sine pulse, as a function of the stiffness reduction factor $\sigma$ given for two values of the frequency ratio between the primary and secondary systems (a) $\Omega = 2$ and (b) $\Omega = 3$. (— $\hat{\tau}_{\text{initial}} = 0.25$ . --- $\hat{\tau}_{\text{initial}} = 0.5$ . ··· $\hat{\tau}_{\text{initial}} = 1$ . -·- $\hat{\tau}_{\text{initial}} = 2$ . 72

3.25. Shock response spectra for the compound model. (a) $\Omega = 2$ and (b) $\Omega = 3$. The bold line represents the SRS corresponding to the undamped single degree-of-freedom model, while the other curves are given for different values of the stiffness ratio $\sigma$.
(— $\sigma = 0$; – $\sigma = 0.1$; – – $\sigma = 0.3$; - - $\sigma = 0.5$; – - – $\sigma = 0.7$; ··· $\sigma = 0.9$) 73

3.26. Conceptual compound model with viscous damping. 74

3.27. Effect of viscous damping in the different switchable stiffness models considered. The input is a versed sine considering a period ratio of $\hat{\tau}_{\text{initial}} = 1$. The compound model comprises two single degree-of-freedom systems considering $\sigma = 0.7$, $\mu = 0.085$ and and undamped frequency ratio of $\Omega = 5$. The damping ratio is given by the initial state as $\zeta = \frac{c}{2\sqrt{km}}$ . (— Simple model; --- Compound model) 74

3.28. Shock Response Spectra for the switchable compound models showing the effect of viscous damping for a stiffness ratio of $\sigma = 0.5$, The bold line included represents the passive undamped model. The mass ratio $\mu$ is chosen so that the frequency ratio is $\Omega = 5$. (– $\zeta$ = 0.05; – – $\zeta = 0.1$; - - $\zeta = 0.3$; – - – $\zeta = 0.5$ 75

4.1. Single-degree-of-freedom system with variable stiffness. 100

4.2. Phase plane representation of the motion of a single degree-of-freedom undamped system. (a) low stiffness and (b) high stiffness for a fixed mass *m*. 100

4.3. Phase plane representation of the motion of a single degree-of-freedom viscously damped system. 100

4.4. Single-degree-of-freedom system with on-off switchable stiffness. 101

4.5. Free vibration of the on-off switchable variable system illustrating the effects of the stiffness change (—— High stiffness; --- low stiffness). (a) Phase plane plot (b) Time history of the displacement response. 101

4.6. Typical response for the on-off variable stiffness system of figure 4.4 showing curves for displacement, velocity and acceleration. $T_m = \frac{T_{on}}{2} + \frac{T_{off}}{2}$. where $T_{on}$ and $T_{off}$ are the natural period during the high and the low stiffness states respectively. (a) $\sigma = 0.5$ (b) $\sigma = 0.8$. (——Displacement; ----- Velocity; ····· Acceleration) 102

4.7. Example of energy levels for the on off switchable stiffness system with a stiffness reduction ratio of $\sigma = 0.5$. Horizontal axis represents time normalised with respect to the mean period and vertical axis is the energy normalised with respect to the initial energy (—— Total energy; --- Kinetic energy; ···· Potential energy) 103

4.8. Switchable on-off model with viscous damping. (a) High stiffness state with both elastic elements connected and the dashpot disconnected. (b) Low stiffness state, the secondary spring has been disconnected and the dashpot is connected. 103

4.9. Maximum damping permissible in the secondary spring-damper system as a function of the stiffness reduction ratio $\sigma$ to allow the secondary spring to return to the equilibrium position whilst it is disconnected. 104

4.10. Response of the combined main system (▬) and the secondary spring-damper system for different damping values considering a stiffness ratio of $\sigma = 0.5$. (···· $c/2\sqrt{km} = 0.1$ . --- $c/2\sqrt{km} = 0.01$ . 104

4.11. Equivalent damping ratio as a function of the stiffness reduction ratio $\sigma$, where the straight line represents the asymptote given by $\zeta_{eq} = \sigma/2\pi$ for small values of $\sigma = \Delta k/k$. 105

4.12. Single-degree-of-freedom viscously damped system with on-off switchable stiffness. 105

4.13. Equivalent damping ratio as a function of the stiffness reduction factor for different values of the actual damping ratio in the system. (——$\zeta = 0$; --$\zeta = 0.1$; — $\zeta = 0.3$; – – $\zeta = 0.5$; - - $\zeta = 0.7$; – - –$\zeta = 0.9$) 106

4.14. Effect of the switching stiffness in the actual damping ratio for various values of the stiffness reduction ratio $\sigma$ (—$\sigma$ = 0.1; -- $\sigma$ = 0.3; ···· $\sigma$ = 0.5; –·– $\sigma$ = 0.7; – $\sigma$ = 0.8) 106

4.15. Acceleration response for the on-off variable stiffness system with damping. (——$\zeta = 0$; — $\zeta = 0.01$; – – –$\zeta = 0.1$; - - - - $\zeta = 0.1$) 107

4.16. On-off stiffness model considering a secondary spring with mass: (a) The systems are rigidly attached. (b) The secondary mass is disconnected and oscillates independently from the main mass. 107

4.17. Response of the main mass $m - \Delta m$ before the stiffness reduction (—) and after the reduction (— —) 108

4.18. Percentage of energy dissipated as a function of the frequency ratio Ω, for several values of the stiffness ratio $\sigma$. (●$\sigma$= 0.1; × $\sigma$= 0.3; +$\sigma$= 0.5; ✳$\sigma$= 0.7) 108

4.19. Percentage of energy dissipated as a function of the stiffness reduction ratio $\sigma$ for different values of the secondary to primary system frequency ratio Ω. (—— Ω = 3; --- Ω = 7; ···· Ω = 11; — Ω = 5; – – Ω = 9; - - - Ω = 13) 109

4.20. Equivalent damping ratio as a function of the stiffness reduction ratio $\sigma$ for different values of the secondary to primary system frequency ratio Ω.(—Ω = 3; -- Ω = 7; ··· Ω = 11; — Ω = 5; – – Ω = 9; - - Ω = 13) 109

4.21. Values of the stiffness reduction ratio $\sigma$, and mass ratio $\mu$ corresponding to different values of secondary to primary systems frequency ratio Ω which give maximum energy dissipation in the impacting model. (—— $\sigma$; --- $\mu$) 110

4.22. Combinations of the stiffness reduction ratio $\sigma$, and mass ratio $\mu$ causing the secondary mass to be exactly at the static equilibrium position at the moment of impact, for optimum vales of the secondary to primary system frequency ratio Ω. (—— Ω = 3; --- Ω = 7; ····· Ω = 11) 110

4.23. Time response for the impacting model. The time is normalised with respect to the mean period $T_m$. (a) $\sigma = 0.5$ and $\mu = 0.1$, (b) $\sigma = 0.75$ and $\mu = 0.25$. The frequency ratio between secondary and primary system is $\Omega = 3$. (——Displacement; ----- Velocity; ····· Acceleration) 111

4.24. (a) Displacement response for both the main (——) and the secondary system (---). (b) Energy levels in the system. (—— Total energy; --- Kinetic energy; ···· Potential energy). Time is normalised with respect to the mean period $T_m$. For this example the stiffness reduction ratio is $\sigma = 0.5$ and the mass ratio $\mu = 0.1$, giving a secondary to primary system frequency ratio $\Omega = 3$ 112

4.25. (a) Displacement response for both the main (——) and the secondary system (---). (b) Energy levels in the system. (—— Total energy; --- Kinetic energy; ···· Potential energy). Time is normalised with respect to the mean period $T_m$. For this example the stiffness reduction ratio is $\sigma = 0.75$ and the mass ratio $\mu = 0.25$, giving a secondary to primary system frequency ratio $\Omega = 3$ and maximum energy dissipation. 113

4.26. On-off stiffness viscously damped model considering a secondary spring with mass: (a) The systems are rigidly attached. (b) The secondary mass is disconnected and oscillates independently from the main mass 114

4.27. Equivalent damping ratio for the impacting system considering viscous damping in both primary and secondary systems. Damping ratio in both systems is equal. The frequency ratio is $\Omega_d = 3$ (—$\zeta = 0$; —$\zeta = 0.01$; – –$\zeta = 0.1$;- -$\zeta = .3$) 114

4.28. Equivalent damping ratio comparison between impacting model, considering a frequency ratio is $\Omega = 3$ (——), and the same model when the secondary mass approaches to zero (·····).The viscous damping ratio considered for both models is the same and is equal to 1%. 115

5.1. Concept of magnetic levitation. Two magnets with the same poles facing will produce a repulsive force $F_m$. 125

5.2. (a) Diagram of the switchable stiffness experimental rig. The permanent magnets (1, 2) are suspended between two electromagnets (3, 4) using four wires (6, 7) that also join the magnet to the main frame (5). (b) Photograph of the actual rig. 126

5.3. Schematic diagram of the setup used for the laboratory tests. 127

5.4. Example of frequency response function magnitude measured for two different amplitudes of the excitation signal. The bold line represents the minumum amplitude and the thin line represents the maximum amplitude. This particular example corresponds to nylon wires in the off setting. 127

5.5. Transmissibility of the magnetic spring with no electromagnets attached and supported by nylon wires. (a) Magnitude, (b) phase angle. (c) Coherence function. 128

5.6. Transmissibility of the magnetic spring with the electromagnets attached but turned off. The permanent magnet is supported by nylon wires. (a) Magnitude, (b) phase angle. (c) Coherence function. 129

5.7 Transmissibility of the magnetic spring with the electromagnets powered with 12 V. The permanent magnet is supported by nylon wires. (a) Magnitude, (b) phase angle. (c) Coherence function. 130

5.8 Transmissibility of the magnetic spring with the electromagnets powered with 18 V. The permanent magnet is supported by nylon wires. (a) Magnitude, (b) phase angle. (c) Coherence function. 131

5.9. Transmissibility of the magnetic spring with no electromagnets attached and supported by titanium wires. (a) Magnitude, (b) phase angle. (c) Coherence function. 132

5.10. Transmissibility of the magnetic spring with the electromagnets attached but turned off. The permanent magnet is supported by titanium wires. (a) Magnitude, (b) phase angle. (c) Coherence function. 133

5.11. Transmissibility of the magnetic spring with the electromagnets powered with 12 V. The permanent magnet is supported by titanium wires. (a) Magnitude, (b) phase angle. (c) Coherence function. 134

5.12. Transmissibility of the magnetic spring with the electromagnets powered with 18 V. The permanent magnet is supported by titanium wires. (a) Magnitude, (b) phase angle. (c) Coherence function. 135

5.13. Transmissibility magnitude of the system supported by nylon wires. The solid line gives the off state (low stiffness) and the dotted line represents the on state for 12 V (high stiffness). 136

6.1. Ideal versed sine pulse generated as a WAV file using MATLAB. This particular pulse was generated to give $\tau/T = 0.25$. 157

6.2. Acceleration response (g's) measured on top of the shaker showing the decaying sinusoidal nature of the shock response of the shaker (dotted). The solid curve represents the expected theoretical acceleration pulse. The vertical acceleration axis is given in *g* and the time in seconds. 157

6.3. Shock response spectra obtained experimentally and theoretically for a decaying sinusoidal for both low and high stiffness states. Nylon wires used. (— High stiffness simulated, – Low stiffness simulated, – High stiffness experimental, -- Low stiffness experimental). 158

6.4. Suppression of residual vibration using two impulses. The second impulse is applied at $t = 0.5T$ in order to cancel the response of the first impulse. 158

6.5. Effective shaker acceleration resulting from two impulses sent to the shaker (bold line). The second impulse is applied at $t = 0.5T$ . o gain residual vibration suppression. The thin line represents the response when only the first impulse is applied. The vertical axis is given in g´s and the time in seconds. 159

6.6. Passive shock response of the experimental rig. (a) Shock pulse, (b) low stiffness response, (c) high stiffness response. The vertical axis is given in *g* and the time in seconds. 160

6.7. Stiffness switching strategy for shock response. (a) Passive response, (b) switching response, (c) shock pulse, (d) voltage. Acceleration is given in *g*, voltage in volts and time in seconds. 161

6.8. Stiffness switching strategy for shock response considering a longer pulse obtained adding a mass of 1 kg to the rig, resulting in a pulse of duration 0.03s. (a) Passive response, (b) switching response, (c) shock pulse, (d) voltage. Acceleration is given in g´s, voltage in volts and time in seconds. 162

6.9. Stiffness switching strategy for shock response considering a longer pulse obtained adding a mass of 2 kg to the rig, resulting in a pulse of duration 0.035s. (a) Passive response, (b) switching response, (c) shock pulse, (d) voltage. Acceleration is given in *g*, voltage in volts and time in seconds. 163

6.10. Displacement response for the model with stiffness control during shock (a) absolute displacement for switching system, (b) absolute displacement for passive system. (c) relative displacement for switching system, (d) relative displacement for passive system. The vertical axis is given in metres and the horizontal axis in seconds. 164

6.11. Switching stiffness response for residual vibration suppression applied to nylon wires suspension. (a) Passive response, (b) switching response, (c) voltage. Acceleration is given in *g*, voltage in volts and time in seconds. 165

6.12. Absolute displacement free response for the experimental rig. (a) switching strategy applied. (b) passive response. The vertical axis is given in metres and the horizontal axis in seconds. 166

6.13. Comparison between the experimental response of the switching strategy for residual vibrations (bold line) and a simulation considering the parameters of the actual model (thin line). Acceleration is given in g´s, and time in seconds. 167

6.14. RL circuit representing the switchable stiffness system based in electromagnets. The switch moves from A to B to disconnect the electromagnets thus generating a transient as the current decays exponentially. 168

6.15. Schematical representation of the voltage variation of the electromagnetic system. The points shown are A for the stiffness recovery and B for the stiffness reduction. The instantaneous current for points A and B is calculated as $I = \frac{V}{R}$. 168

6.16. Response of the switchable stiffness model to both stiffness control during the shock, and control for residual vibration. (a) Passive response, (b) switching response, (c) shock pulse, (d) voltage. Acceleration is given in g´s, voltage in volts and time in seconds. 169

# LIST OF TABLES


| Section | | Page |
|---|---|---|
| 2.1. | Response-excitation pairs for a system subjected to shock excitation. | 23 |
| 3.1. | Values of mass ratio $\mu$ and stiffness ratio $\sigma$ corresponding to two values of the frequency ratio $\Omega$. The values are for the compound model with a secondary mass-stiffness system. | 54 |
| 5.1. | Properties of the switchable stiffness model for the different configurations considered. | 125 |
| 6.1. | Comparison between the theoretically predicted acceleration response reduction using the shock stiffness control, and the experimental results, for the particular shock pulses used in the tests. | 156 |
| 6.2. | Reduction of the absolute and relative displacement response for the system with stiffness switching during the shock in terms of percentage. The results are for the shortest pulse. i.e. $\tau/T = 0.44$. | 156 |
| 6.3. | Comparative results of the theoretical damping ratio, and the experimental results for the different configurations considered. | 156 |

# NOMENCLATURE

## Abbreviations

| | |
|---|---|
| FRF | Frequency response function. |
| SDOF | Single Degree-of-Freedom model. |
| SRS | Shock Response Spectra. |
| MK | Mass-Spring System. |
| MKC | Mass-Spring-Damper System. |
| RL | Resistor-Inductor circuit |

## Symbols

English capitals

| | |
|---|---|
| $E$ | Energy |
| $E_d$ | Energy dissipated. |
| $F$ | Force. |
| $I$ | Impulse, current. |
| $L$ | Inductance. |
| $R$ | Resistance. |
| $T_n$ | Natural period. |
| $T_m$ | Mean or effective period. |
| $T_{off}$ | Natural period for the off state. |
| $T_{on}$ | Natural period for the on state. |
| $V$ | Voltage |
| $X$ | Initial displacement. |

English lower case

| | |
|---|---|
| $a$ | Arbitrary constant. |
| $c$ | Viscous damping constant. |
| $c_c$ | Critical damping constant. |
| $k$ | Stiffness. |
| $k_{effective}$ | Effective stiffness. |
| $k_v$ | Variable stiffness. |

| | |
|---|---|
| $m$ | Mass. |
| $t$ | Time. |
| $t_0$ | Disconnection time. |
| $u$ | Base displacement. |
| $x$ | Displacement. |
| $x_{max}$ | Maximum displacement. |
| $\dot{x}$ | Velocity. |
| $\ddot{x}$ | Acceleration. |
| $z$ | Relative displacement. |
| $\ddot{z}$ | Relative acceleration. |

Greek capitals

| | |
|---|---|
| $\Delta_1$ | First delay normalized. |
| $\Delta_2$ | Second delay normalized. |
| $\Delta m$ | Secondary mass. |
| $\Delta k$ | Secondary stiffness. |
| $\Delta t_1$ | First delay. |
| $\Delta t_2$ | Second delay. |
| $\Omega$ | Frequency ratio. |
| $\Omega_d$ | Damped frequency ratio. |

Greek lower case

| | |
|---|---|
| $\delta$ | Dirac Delta function. |
| $\hat{\delta}$ | Logarithmic decrement. |
| $\varepsilon$ | Duration of function. |
| $\mu$ | Mass ratio. |
| $v$ | Absolute displacement. |
| $v_{final}$ | Final velocity of primary mass. |
| $v_m$ | Maximax absolute response, |
| $v_r$ | Residual absolute response. |

| | |
|---|---|
| $v_{rel}$ | Relative displacement response. |
| $\dot{v}$ | Absolute velocity response. |
| $\dot{v}_0$ | Common velocity after impact. |
| $\dot{v}_1$ | Velocity of primary mass. |
| $\dot{v}_2$ | Velocity of secondary mass. |
| $\dot{v}_{\max}$ | Maximum velocity response. |
| $\ddot{v}$ | Absolute acceleration response. |
| $\sigma$ | Stiffness ratio. |
| $\tau$ | Pulse duration. |
| $\hat{\tau}$ | Period ratio. |
| $\hat{\tau}_{\text{low}}$ | Low stiffness period ratio. |
| $\hat{\tau}_{\text{high}}$ | High stiffness period ratio. |
| $\omega$ | Angular frequency. |
| $\omega_1$ | Natural frequency for high stiffness state. |
| $\omega_2$ | Natural frequency for low stiffness state. |
| $\omega_{\text{effective}}$ | Effective natural frequency. |
| $\omega_p$ | Natural frequency of primary mass. |
| $\omega_s$ | Natural frequency of secondary mass. |
| $\omega_n$ | Natural frequency. |
| $\xi$ | Generic impulsive excitation. |
| $\xi_c$ | Displacement amplitude of shock pulse |
| $\ddot{\xi}$ | Second derivative of a generic impulsive excitation. |
| $\zeta$ | Viscous damping ratio. |
| $\zeta_1$ | Viscous damping ratio of primary system. |
| $\zeta_2$ | Viscous damping ratio of secondary system. |
| $\zeta_{eq}$ | Equivalent viscous damping ratio. |

# Chapter 1

# Introduction

## 1.1. Background.

Mechanical vibration is a natural phenomenon, present in many situations. Its effects are often undesirable, because excessive vibration can lead to damage, wear, noise and human discomfort. For instance, excessive vibration in rotating machinery may cause failures, buildings, which are subjected to earthquakes, can collapse if not properly designed, and persons travelling in a ship can feel sickness due to the vibration. Although sometimes it can be beneficial such as the case of vibration based conveyors, most of the time its effects are negative. These reasons have motivated engineers to look for ways to control or isolate undesirable vibrations. It is important to know the nature of the source of vibration, since this is a key point in the method used to control vibrations. Mechanical vibrations can be harmonic, such as the vibration coming from a rotating machine, random, for example the profile of a rough road, or impulsive, like the shocks produced by a punch press. The latter kind of vibration is the object of study in this thesis. Shock, or transient vibration is a sudden excitation, normally of short duration, which can be highly detrimental because it typically involves high forces, displacements or stresses.

Shock inputs are typically discrete disturbances, very often non-predictable in occurrence, for example a car passing over a bump in the road, a wave that hits a ship, etc. The description of the input requires knowledge of the variation of the input displacement versus time, from which the velocity and acceleration profiles can be derived. In general terms, a specific input can be qualitatively described as being of "short" or "long" duration, and in engineering terminology such descriptions will be more explicitly defined later. The research scope in this thesis has been restricted to shock isolation, rather than harmonic or random excitation where other approaches could be considered.

For sensitive or supported equipment the response might cause damage through exceeding the allowable levels of stress or strain resulting from the transmitted displacement, velocity or acceleration. Alternatively, the equipment might be positioned in a finite space and a large relative displacement could cause the equipment to impact another structure.

This study is concerned with an investigation of alternative means to reduce the vibration suffered when items, typically electronic equipment, are subjected to transient vibration inputs. This chapter comprises a brief overview of the aims and objectives of the study, description of the thesis contents and the questions that have been considered in detail. The background and context of vibration isolation will be presented herein so as to identify the main existing status of the topic.

## 1.2. Vibration isolation for shock.

### 1.2.1. Vibration control and isolation.

A vibratory system can be represented by three components, namely the vibration source, the path and the receiver [1]. There are several techniques used to limit or alter in some way the vibration response of the receiver, which is the component that might be affected by external vibrations. One way is to control the vibration source in order to reduce the subsequent response. However, this measure could be difficult to implement most of the times due to the design of the systems involved. Another possibility is the structural modification of the receiver in order to reduce its response, i.e. by adding or changing the damping, mass and stiffness properties. Finally, one of the most common methods is to place a vibration isolator

in between the vibration source and the receiver, i.e. to modify the path of vibration transmission. This isolator has the objective of reducing or modifying the vibratory forces transmitted to the receiver, and it normally takes the form of a resilient element. These anti-vibratory mounts are readily available in many different forms, such as helical spring and shock absorber combinations, rubber pads, leaf springs, etc. In order to design a suitable isolator, it is necessary to have a good knowledge of the vibrations levels and nature, i.e. if the vibration source is harmonic or impulsive, and of the system to be isolated. If the isolators are properly selected or designed, the vibration levels can be attenuated to a high degree. When the physical properties of the isolator, i.e. stiffness and damping are fixed for a particular application, it is said that the isolators are *passive* [2]. This form of vibration isolation is generally a low cost and reliable solution, but is normally designed for a particular problem and there might not be good performance for different situations for example under very unpredictable excitation. In general, passive isolation is the most commonly used solution for shock excitation problems and is reviewed briefly below.

### 1.2.2. Passive shock isolation.

One of the first applications of shock isolation was to the package and transport of fragile items. The monograph by Mindlin [3] is one of the first and probably the most comprehensive study related to shock dynamics and isolation. This publication incorporates practical package cushioning techniques and supporting theoretical analysis. Much of the study is concerned with the dynamics of objects subjected to free fall, whilst the isolator element is modelled considering a combination of different types of linear and nonlinear elastic and damping elements. Later, a subsequent study by Ayre [4] extended the shock response analysis by investigating the response of single degree-of-freedom undamped and damped models. To date, this is one of the best studies into shock response. The results obtained by Ayre were subsequently compiled into the Shock and Vibration Handbook, edited by Harris and Crede [2]. The latter is generally regarded as the core textbook on the topic.

One of the principal characteristics of the work by Ayre [2, 3] is the fact that the observations were intended to be useful in many types of situations. Contrary to the work of Mindlin [1], which is mainly concerned with systems subjected to acceleration pulses due to free fall, the compilation by Ayre [2, 3] aimed to standardise the nomenclature used. As a result the fundamental equations can be applied in different scenarios. Later Snowdon [5] analyzed the

shock behaviour of linear resilient mountings, used to isolate items from foundation displacements, explaining how the absolute and relative displacements, as well as the maximum acceleration due to a shock, are indicators of the potential damage in the mounted item. Moreover, it was reported in the aforementioned paper [5] that even though the effect of viscous damping is generally beneficial, it also has adverse effects on the transmitted acceleration. By implementing a two degree-of-freedom model the adverse effects of damping were reduced. Snowdon [5] also extended the analysis to nonlinear elastic elements, showing that a softening elastic element with light damping is able to reduce both displacement and acceleration transmitted due to a shock. These investigations were made considering an impulsive step excitation. The analysis was later extended for pulse excitations [6] and for a viscous relaxation model [7, 8]. Furthermore, a number of shock isolator configurations were studied both analytically and experimentally by Eshleman [9], including helical springs, ring springs, friction snubbers, pneumatic springs, liquid springs and solid rubber elastomers. By the time these papers were published the shock response spectra (SRS which is to be further explained in chapter 2) had been established and defined as a means to evaluate the shock severity and to assist in the selection of isolators. However, Snowdon [10] also pointed out some disadvantages in using the SRS. He introduced new tools for shock analysis, namely shock acceleration ratio and shock displacement ratio. Although these parameters have been used recently in shock research [11], the shock response spectra seems to have been the more popular terminology quoted within the scientific community [12, 13].

Regarding nonlinear shock mounts, several investigations have been published [14-26]. Apart from the ones previously mentioned, there are some other notable works. One of the first of these works is also related to vehicle suspension dynamics, studying the ground shock response of a four-degree-of-freedom suspension model [14]. A ground surface bump was modelled as a versed sine displacement input. The authors studied the effects of nonlinearity and optimum parameters were determined. Another study regarding nonlinear stiffness was published by He [15], where the response under exponential pulses was evaluated. The effect of non-linear damping was studied by Hundal [16], Guntur [17] and more recently by Chandra and Shekhar [11, 18]. Many works involving non-linear shock mounts have been considered in the area of air springs, e.g. by Hundal [19-22]. The use of shock isolators based on dry friction has been also explored by Mercer [23] who developed an optimum shock isolator with great advantages over a common resilient mount. The use of non-linear energy sinks is a relatively new idea that has also been considered, through the concept of energy

pumping [24]. In this concept the authors considered an energy flow through a system of damped coupled oscillators. The authors claimed that this system is capable of absorbing large portions of energy from transient excitations. Naval engineering is another area of study where shock isolation and effects have been investigated [25]. The use of non-linear shock mounts for naval applications has also been considered with good results [26].

Closely related to shock phenomena is earthquake engineering. The family of cycloidal pulses, along with oscillatory pulses, have been used theoretically and experimentally to replicate and study real earthquakes [27, 28]. A comprehensive review on seismic shock response has been published [29]. Additionally, shock vibration is also a common problem in machinery like punch presses. As a result, the dynamics of these systems have been studied, particularly modelled as block foundations under the action of cycloidal pulses [30]. Several designs of passive isolators for such systems have been proposed [31, 32].

More recently, attention has been paid to the development of shock isolators for electronic equipment. Fragile electronic items such as printed circuit boards and hard disk drives e.g. for laptops, are commonly subjected to shock vibration. Consequently, methods for efficient shock isolation have been developed [33-36]. Many of these situations find application in naval and aeronautical engineering [37, 38], where sometimes commercially "off the shelf" isolation solutions might provide acceptable results [39-41].

### 1.2.3. Active and semi-active shock isolation.

Although the use of passive vibration isolators is extensive and typical due to their reliability, simplicity and relatively low cost, there are some major disadvantages. For example, in the case of harmonic vibration isolation there is a trade off between the isolation performance at the resonance frequency where high damping is necessary, and at higher frequencies, where the damping effectively increases the transmissibility and response [2]. Moreover, isolation systems are normally designed for a certain application and they might not provide an adequate isolation under other circumstances [42]. In order to overcome the drawbacks of passive vibration isolators, active vibration controllers have been developed [43]. The active isolation systems are classified into three categories, i.e. fully active systems, semi-active systems and adaptive-passive systems [44]. The first category involves sensors and actuators that measure the response and subsequently provide an active force used to suppress or reduce

the vibration of the system. Although the isolation performance is normally better and the system is adjustable to different situations compared to passive systems, the resultant active system is complex and the energy consumption could be high. Also, if the system fails, it should be designed such that the isolation performance is not worse than the passive scenario case. However, semi-active and adaptive systems have the advantages of a fully active configuration, combined with the simplicity of a passive model [44]. In these models the properties of the system, namely the stiffness and the damping, are changed depending upon a specified control law. The difference between the semi-active and the adaptive configurations, is that in the semi-active models the properties are changed within each cycle of vibration, while in the adaptive systems the properties vary relatively slowly [45]. Much has been published [46-48] regarding the use of fully active and semi-active/adaptive approaches, especially in applications such as structural control, automotive suspensions, aeronautics, etc. Most of the studies are dedicated to harmonic and random vibration sources, whilst fewer studies have been published concerning shock applications. The objective of this section is to present a review of the most relevant work related to the application of semi-active/adaptive and fully active isolation approaches to shock isolation.

One of the first approaches for active shock isolation was the concept of optimum vibration isolation. The concept means that the isolators are chosen for a particular performance index and a certain design constraint of the system that is optimized. Usually an additional constraint is also involved. For example, the maximum acceleration of the system might be the performance index, whilst the relative displacement represents the design constraint. This analysis gives the time-optimal functions for the isolator. However, for most of the cases the passive isolators might not be able to behave in that way, being more appropriate for active isolators [49-52]. One interesting conclusion from these early studies was the idea of an "early warning" or preview isolator, in which some information is available before the excitation begins. It has been shown that a substantial performance increase was obtained by using such an isolator [49] and this has been recently validated [53].

Many of the investigations regarding the active or semi-active/adaptive isolation approaches for shock excitations are related to automotive suspensions. Normally semi-active and adaptive approaches have been considered. Air springs have been used for some time in order to obtain variable spring/damper rates [54]. Variable damping has been extensively used in automotive suspension research [55-60]. In general, the use of this kind of variable damping

suspension has been oriented to eliminate the compromise between ride comfort and handling. Preview systems have also been used in automotive applications [61]. Moran [61] claims to have achieved improvement over common adaptive suspensions. However, research into this area is not only related to shock but to different input types. Moreover, most of the research focuses on the control methods for the active suspension and the robustness of the control systems, particularly $H_{inf}$ control theory, linear quadratic control (LQ) and recently sliding mode control. [62-65]. Variable damping strategies have also been used in other automotive applications, such as suspension for seats in order to reduce the severity of end stop impacts [66, 67]. In addition, there are a number of studies regarding general shock isolation systems using variable damping devices [68-71].

Fully active control strategies have been less commonly applied in shock isolation. Some notable exceptions are the studies of Tanaka [72-74], who has published several papers regarding the theoretical and practical implementation of fully active control systems in forging hammers, using feedforward control. Tanaka [75, 76] has also studied the use of semi-active dampers and preview control systems for the same application. He claimed that the impact vibration was almost eliminated.

There are some other different approaches to semi-active/adaptive shock isolation. Variable damping devices based on dry friction have been also investigated [77, 78]. Variable stiffness elements have also been considered in [79, 80], where a variable stiffness device is considered which comprises a working fluid that can move between chambers hence dissipating energy when it is released.

### 1.2.4. Variable stiffness for vibration isolation and control.

Several variable stiffness methods and strategies have been previously developed. The work by Winthrop *et al* [81] reviewed the most notable variable stiffness related studies, and he also presented a method for selection and understanding the performance of several variable stiffness devices. In contrast to variable damping strategies for vibration control, variable stiffness strategies have been more widely used in adaptive schemes rather than semi-active methods. To the author's knowledge, there are only two published studies where the stiffness is varied within each cycle of vibration in systems under harmonic excitation. The first [82] uses a friction lock to vary the stiffness in an on-off fashion, where the stiffness is turned off

when the relative velocity across the support is greater than a specified design value. The authors claim that the strategy is capable of reducing the vibration levels for base harmonic input. Another investigation [83] considered a two degree-of-freedom model with variable damping, where the resulting equivalent single degree-of-freedom model had variable stiffness. The performance under variable damping, variable stiffness and combined variable damping and stiffness strategies were analyzed and presented. The control law used in all the cases is the on-off skyhook control. The concept of sky-hook control is a strategy used mainly for damping control based in a theoretical model that comprises a damper attached between the mass and a fixed reference, originally proposed by Crosby and Karnopp [84]. The reason behind this concept is that one of the principal drawbacks of a passive mount is the poor performance at high frequencies in highly damped systems. This model is intended to overcome the issue of damping compromise at resonance and higher frequencies. The sky-hook model is useful as a theoretical concept, but is not always realisable or possible in practice. However, using a controllable damping device it is possible to obtain the benefits of the sky-hook concept.

Variable stiffness and damping devices have also been widely used in tunable vibration absorbers and neutralizers. Since a vibration absorber/neutralizer is normally designed to work well over a narrow frequency band, tunable absorbers, which can vary both stiffness and damping, have recently been investigated. There are a few notable studies, both theoretical and experimental. Walsh and Lamancusa [85] investigated a vibration absorber using a variable geometry element comprising a compound leaf spring, where the gap between two parallel beams is adjusted. A similar configuration, where fuzzy control was applied, was investigated by Kidner and Brennan [86]. Variable curvature members to induce stiffness changes have also been considered. The development of a variable spring using variable curvature piezoelectric actuators can be found in references [87, 88]. Additionally, the use of a switchable on-off stiffness strategy has been applied to vibration absorbers, with application to beams and plates [89].

Another area in which active vibration control has been used is in residual vibration suppression. There are many engineering applications, especially those involving lightweight structures, where there are low damping levels. In this situation, vibration suppression can be difficult to achieve using conventional methods and alternative solutions have to be developed. Several strategies have been proposed using different actuators (fully active

systems) or variable members (adaptive or semi active systems). Most of the work in this field has been concerned with fully active isolation and variable damping members, whilst some work has been related to variable stiffness members. A particular control strategy for transient vibration suppression is based on an on-off logic to connect/disconnect a stiffness element. Although the strategy was originally proposed by Onoda and Watanabe [90-92], it is based in the variable structure system theory, which considers a main system comprised of several continuous subsystems with a suitable control logic [93]. The strategy of Onoda and Watanabe attempted to provide a high amount of energy dissipation for lightly damped systems. The authors [92] proposed a model with two springs in parallel. One of the springs can be disconnected depending upon the system response and a specified control law. Some experimental validation was presented using a truss structure with variable stiffness members. Several variations of the latter variable stiffness concept have been used in other applications. Yamaguchi *et al* [94] investigated the vibration isolation behaviour of a single degree of freedom system with two springs in parallel, one of which can be disconnected using a friction lock. Warkentin and Semercigil [95] applied this concept to suppress vibration on robotic arms using a system with two parallel beams, one cantilevered and the other controlled by a mechanical brake. The latter produced a change of the boundary conditions between being a pinned beam and a fixed beam as required. Pun and Semercigil [96] took the latter concept further using only one beam and using a variable torque at the pinned end to emulate a cantilever beam. Lately the concept has been studied by Jalili and Ramaratnam [97]. The work by Jalili and Ramaratnam [97] considered a theoretical model and experimental validation using a helical spring with variable coils. A number of studies alternatively consider piezoelectric actuators to achieve the on-off stiffness [98-101]. However, the concept of switchable on-off stiffness offers a wider scope for research, since some of the basic concepts such as the energy dissipation mechanism are not fully explained, and more validation is needed. This will improve the understanding and possible applications for the concept.

## 1.3. Objectives and contributions.

Given the background of shock isolation literature, this project was conceived. The objectives of the study were as follows:

- To conduct a state of the art review regarding passive and active/semi-active shock isolation.

- To perform a rigorous analysis of a switchable stiffness strategy for use in shock isolation problems, to identify the governing parameters and optimum configurations for obtaining reductions in the response.

- To determine the advantages and disadvantages of such a strategy, considering the problem in two stages, namely the reduction of response during a shock impulse and the suppression of the residual vibration after the shock.

- To investigate a practical realisation of the stiffness control strategy and compare the experimental results with the theoretical predictions.

The contributions in this thesis are:

- Presentation and analysis of a novel method for shock isolation using switchable stiffness control.

- An explanation for the energy dissipation mechanism of a switchable variable on-off stiffness control strategy used to suppress free vibrations.

- Identification of the optimum configuration for the suppression of residual shock vibration.

- The development of an experimental switchable stiffness element based upon a magnetic suspension element.

## 1.4. Thesis overview.

The presentation of the research incorporating the modelling, simulation and experimental validation is given in detail in the remaining chapters. Chapter 2 is a brief introduction to the performance of a passive isolation system modelled as a single degree-of-freedom (SDOF) system. With this established it will then be possible to investigate the possibilities of an adaptive system. Chapter 2 also acts to assist in identifying the key features and parameters involved in passive isolation and its assessment. The study does not consider a fully active system, but instead considers the potential advantages and disadvantages of adapting the isolation system properties in real time in order to reduce and minimise the severity of the response. The problem of vibration isolation using adaptive stiffness is divided into two stages, namely the control of the response during a shock event, and the later suppression of the residual vibration. The theoretical basis for the shock isolation strategy using switchable stiffness is presented in chapter 3. In this chapter the performance of the switchable stiffness strategy is comprehensively analyzed, with the reduction of the maximum response of the system subjected to shock being the main objective. Several single degree-of-freedom models are considered for the analysis, and their respective response parameters are studied depending upon the configuration of the switchable stiffness strategy. The second stage, concerned with the residual vibration suppression, is presented in chapter 4. A switchable stiffness strategy is presented and analyzed, focusing on the energy dissipation mechanism of a simple single degree-of-freedom undamped model. Later in the chapter, the effects of damping are considered, with an improved simple model studied. The experimental validation of the theoretical studies is presented in chapter 5. This chapter introduces a conceptual design used for the laboratory tests. This rig comprises a switchable stiffness element based on electromagnetic forces. The physical properties of the system are measured and presented, and its characteristic behaviour discussed. Chapter 6 presents the implementation of the switching strategies for shock maximum response reduction and residual vibration suppression using custom made analogue control circuits. The results are then compared with the theoretical predictions. Chapter 7 presents overall concluding remarks and suggestions for future investigations. Finally, the appendices included show further analysis and extended results for some of the aspects presented in the thesis, which assists in gaining a better understanding of the concepts and methodology used in this work.

# Chapter 2

# Introduction to shock isolation

## 2.1. Introduction.

Transient vibration is defined as a temporarily sustained vibration of a mechanical system. It may consist of forced or free vibrations, or both [2]. Transient loading, also known as impact or mechanical shock, is a nonperiodic excitation, which is often characterized by a sudden and severe application. In real life, mechanical shock is very common. Examples of shock could be a forging hammer, an automobile passing across a road bump, the free drop of an item from a height, etc.

In most cases, to analyse systems involving mechanical shock it is convenient to represent the forcing function (displacement, velocity, acceleration or force) as a step or pulse excitation. This impulsive forcing function can be approximated to a certain shape depending on the situation and the structural characteristics of the system, in particular the natural frequency and damping ratio of the system.

The objective of this chapter is to provide an overview into the behaviour of the common linear passive single degree of freedom system under shock excitation for different impulsive forcing inputs. The aim of passive shock isolation in its simplest form is to reduce or minimise the response compared to the input, and the way that this is achieved is outlined in this chapter. The terminology introduced here will be used when examining and comparing the performance of the switchable stiffness system discussed in this thesis as a means to quantify any potential benefits or limitations of the switchable stiffness system for shock excitation.

## 2.2. Fundamentals of shock analysis

Because of the negative effects produced by impacts, shock-produced vibration has been a topic of research interest over many years. As a result, the dynamics of shock have been extensively studied, and methods of isolation and control developed. Consider the single degree of freedom model shown in figure 2.1. It comprises a mass *m* supported on an elastic stiffness, which could be an undamped resilient isolator represented by the stiffness *k*. The input is a function of time, that can be a force acting on the mass or a displacement of the base or foundation. Sometimes it is more convenient to express it as a ground or base acceleration. The corresponding differential equations of motion for these three systems can be expressed respectively as follows:

$$m\ddot{x} = -kx + F(t) \tag{2.1}$$

$$m\ddot{x} = -k\left[x - u(t)\right] \tag{2.2}$$

$$m\left[\ddot{z} + \ddot{u}(t)\right] = -kz \tag{2.3}$$

where $x$ is the displacement of the mass relative to a fixed reference, and $z$ is the displacement relative to a moving ground. The relationship between these displacements and the ground displacement is $x = u + z$. Equations (2.1-2.3) can be conveniently normalised considering the definition of natural frequency $\omega_n = \sqrt{k/m}$ [2]. Moreover, if the response of the system and the excitation are expressed in a general form, i.e. $v$ is the response of the system and $\xi$

the excitation being both functions of time, the equations of motion (2.1-2.3) can be expressed in a general way as:

$$\frac{\ddot{v}}{\omega_n^2} + v = \xi(t) \tag{2.4}$$

Equation (2.4) can be used to calculate the shock response of an undamped single degree-of-freedom system to a shock excitation. When a specific response to a particular type of excitation is required, a suitable pair of excitation-response can be used, as presented in table 2.1 and in [2].

Impulsive excitation produces vibration responses in elastically supported systems, and the maximum values of these responses may be less than, equal to or greater than the corresponding static response [103]. In general, the response depends upon the system properties and the nature of the load. For single degree of freedom systems (SDOF), one characteristic that determines the response is the natural period $T$ (or the natural frequency $\omega_n = \frac{2\pi}{T}$). In addition, the shape and duration of the impulse plays an important role in the response. Shock phenomena can be modelled using ideal step and pulse functions, which represent very well the features of real transient inputs and which produce similar system behaviour. However, when the duration of the shock is very short in comparison with the natural period, it can be simply represented by a scaled version of the unit impulse. In this case situations involving shock excitation of linear systems can be considered as the result of applying a unitary impulse to the system. This sort of transient excitation can be considered mathematically using the Dirac delta function $\delta(t)$ [102] which is defined as:

$$\delta(t) = 0 \qquad t \neq 0 \tag{2.5}$$

$$\int_{-\infty}^{\infty} \delta(t)dt = 1 \tag{2.6}$$

Figure 2.2 shows two alternative graphical representations of the Dirac delta function, applied at $t = a$. Its representation is a single impulse of area equal to unity.

When a sudden impulse of magnitude $I$ is applied at a time $t = a$ to an undamped single degree of freedom system at rest the subsequent response is given by [102]:

$$x(t) = \frac{I}{m\omega_n} \sin \omega_n (t - a) \qquad \text{for} \quad t \geq 0 \tag{2.7}$$

where $x(a) = 0$ and $\dot{x}(a) = I/m$.

This is represented graphically in figure 2.3. It is noticeable that the maximum response occurs after the impulse has been applied. If $I$ is of unit magnitude, then the response is the impulse response function given by equation (2.7) with $I = 1$ typically written for an impulse applied at $t = 0$.

However, for many shock tests [104] and when it is necessary to select or design isolators for a particular application, the excitation function is normally a pulse function. A pulse like excitation is a more complex function. It can often be considered as being equivalent to the superposition of two or more successive input functions. For example, a half sine pulse can be obtained by the addition of two sine inputs with one delayed by half the sinusoid period. Alternatively, a general input $\xi(t)$ can be considered to be composed of an infinite set of scaled impulses, and the system response given by the sum of the responses to each individual pulse is described by the convolution integral [102].

There are many different types of pulse excitations, which can be symmetric or non symmetric. Examples include rectangular, triangular, trapezoidal and versed sine pulses. They can, in many cases, be used to replicate real shock situations. The dynamics and characteristics for a comprehensive collection of pulse functions can be found in the work by Lalane [13]. However, the category of pulses more widely used is the family of versed sine pulses and the rectangular pulse. These pulses are represented by piecewise functions. However, there are pulses represented by continuous functions, for example the round pulse. These types of excitation pulses have been used by a number of authors, particularly Snowdon [105]. Generally, the overall results are similar and the use of the family of versed

sine pulses is more extensive. In order to explain the fundamentals of shock analysis three pulses are considered , namely a rectangular pulse, a half sine pulse and a versed sine pulse.

The excitation functions $\xi(t)$ and the equations governing the time response $v(t)$ are given by the following equations. Residual response factors are also given and correspond to the solutions after the pulse has ceased, i.e. $t \geq \tau$. There are several methods for obtaining the response of a particular pulse, most of them can be found in reference [2]. An example of determining the solution using Laplace transforms is included in appendix A. Given below are the most common inputs and the corresponding undamped single degree-of-freedom responses.

a) Rectangular pulse input

$$\left\{\begin{array}{l}\xi(t)=\xi_c \\ v(t)=\xi_c\left(1-\cos\left(\omega_n t\right)\right)\end{array}\right\} \qquad \left[0 \leq t \leq \tau\right] \qquad (2.8)$$

$$\left\{\begin{array}{l}\xi(t)=0 \\ v(t)=\xi_c\left[2\sin\left(\frac{\pi\tau}{T}\right)\right]\sin\omega_n\left(t-\frac{\tau}{2}\right)\end{array}\right\} \qquad \left[\tau < t\right] \qquad (2.9)$$

b) Half cycle sine input

$$\left\{\begin{array}{l}\xi(t)=\xi_c \sin\left(\frac{\pi t}{\tau}\right) \\ v(t)=\frac{\xi_c}{1-T^2/4\tau^2}\left(\sin\left(\frac{\pi t}{\tau}\right)-\frac{T}{2\tau}\sin\omega_n t\right)\end{array}\right\} \qquad \left[0 \leq t \leq \tau\right] \qquad (2.10)$$

$$\left\{\begin{array}{l}\xi(t)=0 \\ v(t)=\xi_c\left[\frac{\left(T/\tau\right)\cos\left(\pi\tau/T\right)}{\left(T^2/4\tau^2\right)-1}\right]\sin\omega_n\left(t-\frac{\tau}{2}\right)\end{array}\right\} \qquad \left[\tau < t\right] \qquad (2.11)$$

c) Versed sine input

$$\left\{\begin{array}{l}\xi(t)=\dfrac{\xi_c}{2}\left(1-\cos\left(\dfrac{2\pi t}{\tau}\right)\right)\\ v(t)=\dfrac{\xi_c/2}{1-\tau^2/T^2}\left(1-\dfrac{\tau^2}{T^2}+\dfrac{\tau^2}{T^2}\cos\left(\dfrac{2\pi t}{\tau}\right)-\cos(\omega_n t)\right)\end{array}\right\} \qquad \left[0\le t\le\tau\right] \qquad (2.12)$$

$$\left\{\begin{array}{l}\xi(t)=0\\ v(t)=\xi_c\left[\dfrac{\sin(\pi\tau/T)}{1-\tau^2/T^2}\right]\sin\omega_n\left(t-\dfrac{\tau}{2}\right)\end{array}\right\} \qquad \left[\tau<t\right] \qquad (2.13)$$

where $\xi_c$ is the maximum amplitude of the shock input, $T$ is the natural period of the system, $\tau$ is the duration of the pulse and $\omega_n$ is the natural frequency of the system.

It is important to note at this point the classification used to categorize the shock response. As mentioned previously, the response $v(t)$ can represent an absolute displacement, velocity or acceleration depending upon the excitation. The maximum response $v$ occurring at <u>any</u> time as a result of the forcing function, is called the *maximax response* , denoted by $v_m$ [2].

In contrast, the maximum response of the system during the residual vibration phase, after the loading has been removed, is called the residual response denoted by $v_r$ [2]. This is measured with respect to the final position of equilibrium. The maximax response can occur either during the pulse or after. When the maximum response occurs after the pulse has finished $v_m = v_r$.

The normalised response curves (the response is divided by the maximum amplitude of the input disturbance) for the excitation pulses given by equations (2.8), (2.10) and (2.12) are presented as functions of time in figure 2.4, for different values of the ratio $\tau/T$ for the undamped single degree-of-freedom system. This parameter is the duration of the input pulse compared to the period of the single degree-of-freedom system. The solutions of the equations of motion were obtained using Laplace transformations for the various cases. When the impulse is very short (approximately $\tau/T$ < 0.25) the pulse tends to approach a scaled version

of the Dirac delta function, and the response can be approximated using a scaling of the simple unit impulse expression. As a result, the shape of the pulse is of negligible importance. On the other hand, when the period of the impulse is very long compared to the natural period (approximately $\tau/T > 2$), the response follows the shape of the impulse more closely during the time when the input is applied. In all of the input types considered here for certain values of $\tau/T$ there is no residual response. The physical interpretation of this phenomenon being that the net work done on the undamped system by the applied input is zero at the end of the time $\tau$, so that there is no residual energy and hence no residual response. There is a further discussion for this phenomenon included in appendix B.

## 2.3. Shock Response Spectrum

The fundamental effect of a shock is to perturb mounted equipment and excite its modes of vibration, depending upon the frequency content of the shock. Consequently, a risk of damage is present if the shock mount is not able to reduce the energy transmitted by the shock. After a shock input the subsequent vibration decay is dependent upon the amount of damping present in the system. The peak acceleration and peak relative displacement of the system are particularly important, as these often indicate whether damage or failure may occur. These parameters are likewise an indicator of the forces transmitted to the mounted equipment, and the stresses experienced by the isolator. Furthermore the relative and absolute displacement are related to the available space for the mounted item, or rattle space [13, 105].

One of the most important tools to evaluate the severity or the potential damage which might occur due to a particular shock, and to select a proper isolator for a certain application, is the Shock Response Spectrum (SRS) [104]. A shock response spectrum is simply the normalised peak response (either absolute, relative or residual normalised considering the maximum amplitude of the shock input) produced by the shock on the isolated mass as a function of the natural frequency of the mass on its elastic support, or more commonly as a function of the ratio between the duration of the pulse and the natural period of the system. Shock spectra can either be measured experimentally, computed from waveforms, or determined theoretically [104].

The shock spectrum gives a full and realistic measure of the damaging potential of a shock disturbance. To select a damage criterion (acceleration or displacement), the duration of the pulse and the natural period of the system $\tau/T$ are of great importance (considering a SDOF undamped system). If $T << \tau$ the motion of the mass closely follows the motion of the support during the shock input (see figure 2.4 for values of $\tau/T$ greater than 2). The acceleration then becomes the primary quantity of concern. Otherwise, when $T >> \tau$, the mass remains substantially at rest until motion of the support has ceased (as shown in figure 2.4 for values of $\tau/T$ less than 0.5), and it is the value of the maximum displacement that determines potential damage. Moreover, if the transient disturbance is neither short nor long duration to fit into one of the previous cases, no simple damage criterion can be found [104]. As a result, both acceleration and displacement responses must be considered.

Shock response spectra for symmetrical pulses, i.e. rectangular, half sine and versed sine pulses are shown in figures 2.5, 2.6 and 2.7 respectively for the general case of equation (2.4).

The response parameters include maximax, residual and relative responses. A further analysis of these plots and the time response curves (figure 2.4) reveals that for values of $\tau/T$ less than 0.25 (corresponding to short duration pulses), the shape of the pulse is of less importance in determining the maximum value of the response. This behaviour can be explained by considering that the response is essentially due to an impulse, because the pulse has a very short duration. It is in this regime where best shock isolation can occur i.e. the amplitude of the response is smaller than the amplitude of the shock. In contrast, when $\tau/T$ is approximately higher than 0.5 but smaller than 2 (depending upon the excitation) the maximum response of the system is effectively greater in comparison with the maximum input amplitude. This region of the response spectrum is called the amplification region. Finally, if $\tau/T$ is larger than 2, the shape may be of greater significance. The response tends to become quasi static and it follows closely the shape of the input. As a result, this zone is called quasi-static region. As mentioned previously, there are some cases when the residual and maximax responses are equal, and this applies also for the relative response.

## 2.4. Shock response for damped systems.

Generally, if one compares the effect of viscous damping on the shock response and the effect of damping on harmonic response, it is found that in the case of shock the effect is of less importance. Nevertheless, there is still a reduction in the response, especially in the residual response, as the damping helps to reduce the maximum residual responses and ultimately it will suppress the residual vibrations in a shorter time.

Consider the analysis of a viscously damped single degree-of-freedom system subjected to an impulsive base displacement $\xi(t)$ The equation of motion under normal notation is:

$$\frac{m}{k}\ddot{v} + \frac{c}{k}\dot{v} + v = \frac{c}{k}\dot{\xi}(t) + \xi(t) \tag{2.14}$$

which can be written as:

$$\frac{1}{\omega_n^2}\ddot{v} + \frac{2\zeta}{\omega_n}\dot{v} + v = \frac{2\zeta}{\omega_n}\dot{\xi}(t) + \xi(t) \tag{2.15}$$

where $c$ is the viscous damping constant and $\zeta$ is the viscous damping ratio of the system, defined as $\zeta = c/c_c$ and $c_c = 2m\omega_n$.

Figure 2.8 shows the maximax response spectrum for the displacement response of a single degree of freedom system with viscous damping, subjected to a half sine pulse excitation as a function of the viscous damping ratio. These results were evaluated numerically. Comparing figure 2.8 with figure 2.6 one can observe that in all cases there is benefit of having damping present. Progressively increasing the amount of damping results in a decrease in the maximax response for $\tau/T < 2$. The effect for the different type of pulses, i.e. versed sine, or rectangular amongst others, is typically similar. Examples for rectangular and versed sine pulses are included in appendix C.

Further insight into the behaviour of damped systems under shock excitation can be obtained from figure 2.9, which is a plot of the ratio of the maximum value of the shock response

spectra for a damped system to the undamped system, for various values of damping. This plot has been produced considering the maximum value of the undamped maximax response as a reference for different values of the period ratio $\tau/T$ . Although the SRS plots for other pulses are not included, the effect of damping is similar for other transient excitation inputs and is also similar for the different values of $\tau/T$ considered. Large reductions in the response can be achieved for larger values of damping, but care has to be taken because of the derivatives of the response, i.e. the velocity and acceleration can take higher values as damping increases. Some studies have shown that high levels in damping in systems subjected to shock might result in increased acceleration levels [1]. Another result of damping values higher than the critical value is a longer time for the system to return to the initial equilibrium position.

## 2.5. Summary

The most important quantities in shock measurements are the maximax response and the residual response, both used to determine the severity of the shock. The most important parameters in damage assessment due to shock problems are the displacement, both absolute and relative and the absolute acceleration. A powerful tool in the analysis of shock motion is the *shock response spectrum* (SRS), which gives information about the relationship between the maximax response, the duration of the shock and the natural period of the system.

For pulse inputs the response depends upon the ratio of the duration of the pulse to the natural period of the system and the shape of the pulse. When the pulse is of short duration compared to the natural period of the system, the shape of the pulse is not important (for $\tau/T$ less than 0.5), and the maximax occurs after the excitation has ceased. In contrast, when the pulse is long compared to the natural period of the system, the shape plays an important role, and the maximax response can occur during the pulse or after it has ceased. This is reflected in the three characteristic regions of the SRS, namely the isolation (or impulsive) region, the amplification region and the quasistatic region.

Inclusion of viscous damping in the system generally results in a decrease in the maximax response. Most of the work has been carried out considering only viscous damping. However, the reduction in the response is not as significant if compared with the effect of damping in

harmonically excited systems. Moreover, damping can cause acceleration levels to rise.

Considering that the system shock response is mainly controlled by the stiffness of the system as the mass is normally fixed, the concepts presented in this chapter are used in chapter 3 to determine a switchable stiffness strategy to achieve better shock isolation.

| **Excitation $\xi(t)$** | | **Response $v(t)$** | |
|---|---|---|---|
| Force | $\frac{F(t)}{k}$ | Absolute displacement | $x$ |
| Base displacement | $u(t)$ | Absolute displacement | $x$ |
| Base acceleration | $-\frac{\ddot{u}(t)}{\omega_n^2}$ | Relative displacement | $z = x - u$ |
| Base acceleration | $\ddot{u}(t)$ | Absolute acceleration | $\ddot{x}$ |
| Base velocity | $\dot{u}(t)$ | Absolute velocity | $\dot{x}$ |
| $n$th derivative of the ground displacement | $\frac{d^n u}{dt^n}$ | $n$th derivative of absolute displacement | $\frac{d^n x}{dt^n}$ |

Table 2.1. Response-excitation pairs for a system subjected to shock excitation.

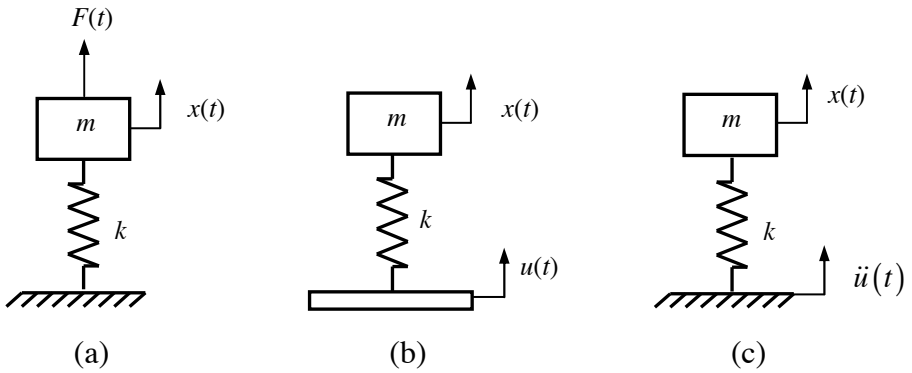


Figure 2.1. Single degree-of-freedom undamped model subjected to different types of shock excitations. (a) Transient force excitation on the mass, (b) transient base displacement and (c) transient base acceleration.

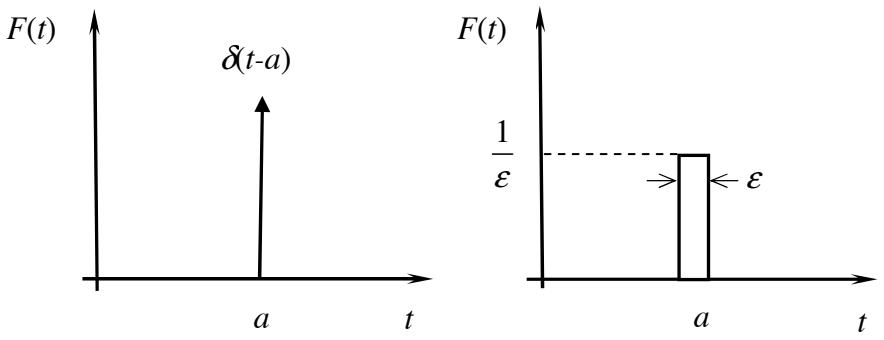


Figure 2.2 Graphical representations of the Dirac delta function. $\delta(t-a)$ as $\varepsilon \to 0$.

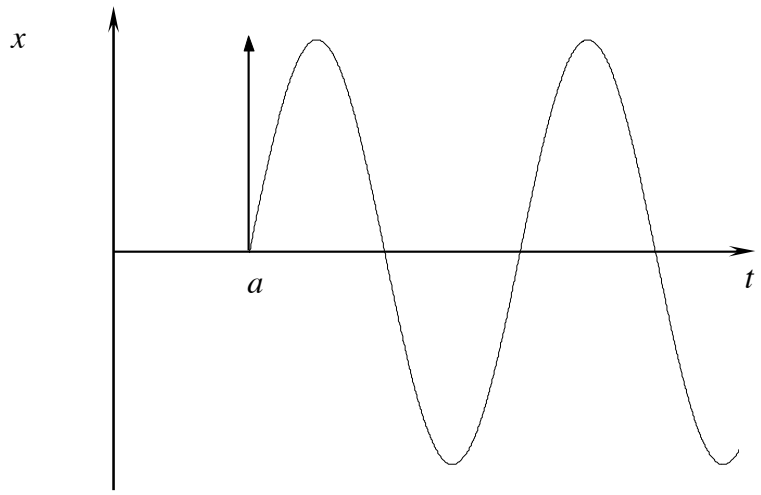


Figure 2.3. Typical displacement response of an undamped single degree-of-freedom model at rest to the impulse function applied at $t = a$.

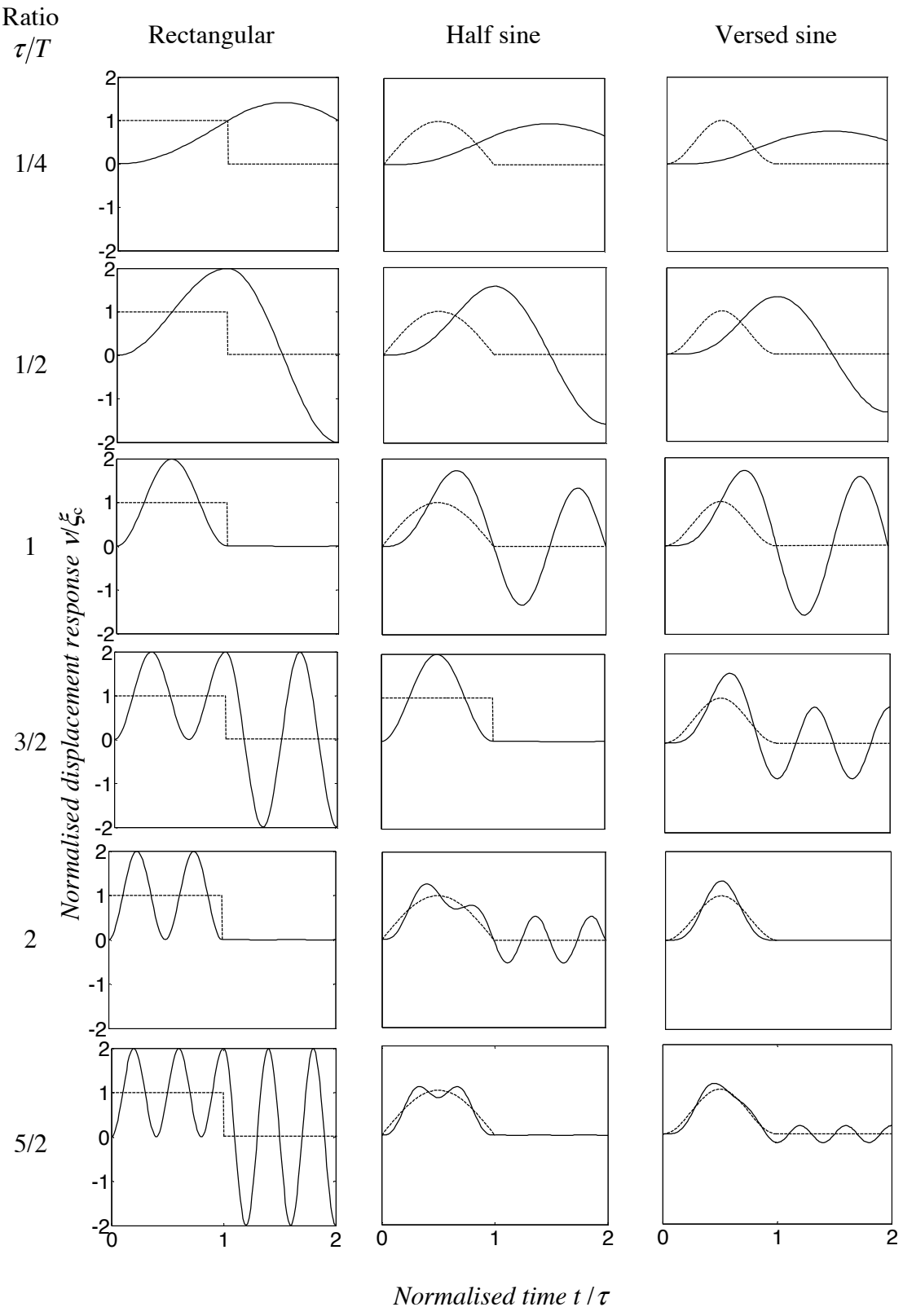


Figure 2.4. Displacement response curves for an undamped single degree-of-freedom system corresponding to several symmetrical pulses representing base displacement excitation; rectangular, half sine, and versed sine, for different values of the ratio $\tau/T$ . The vertical axis is normalised considering the maximum pulse amplitude $\xi_c$ and the time considering the duration of the pulse $\tau$. (— System response; – – Pulse )

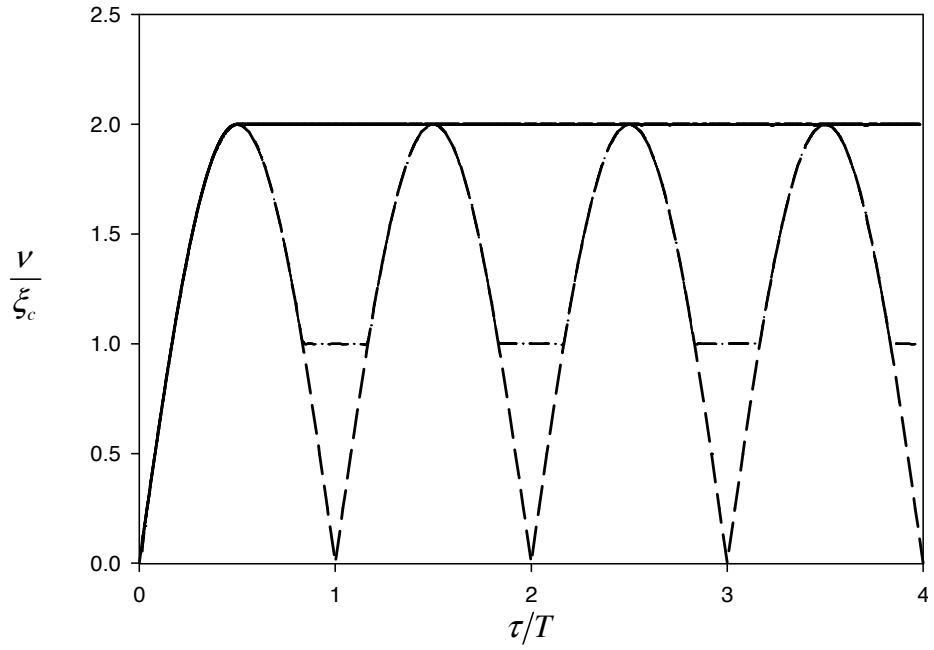


Figure 2.5. Shock response spectra for a single degree-of-freedom undamped model subjected to a rectangular pulse (— Maximax; – – Residual – · – Relative).

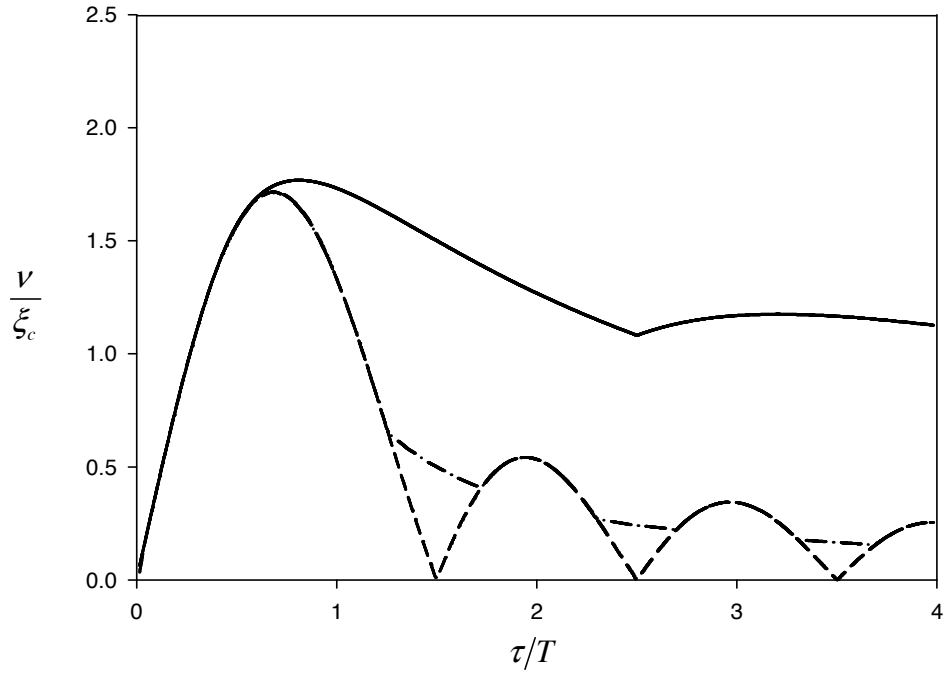


Figure 2.6. Shock response spectra for a single degree-of-freedom undamped model subjected to a half sine pulse (— Maximax; – – Residual – · – Relative).

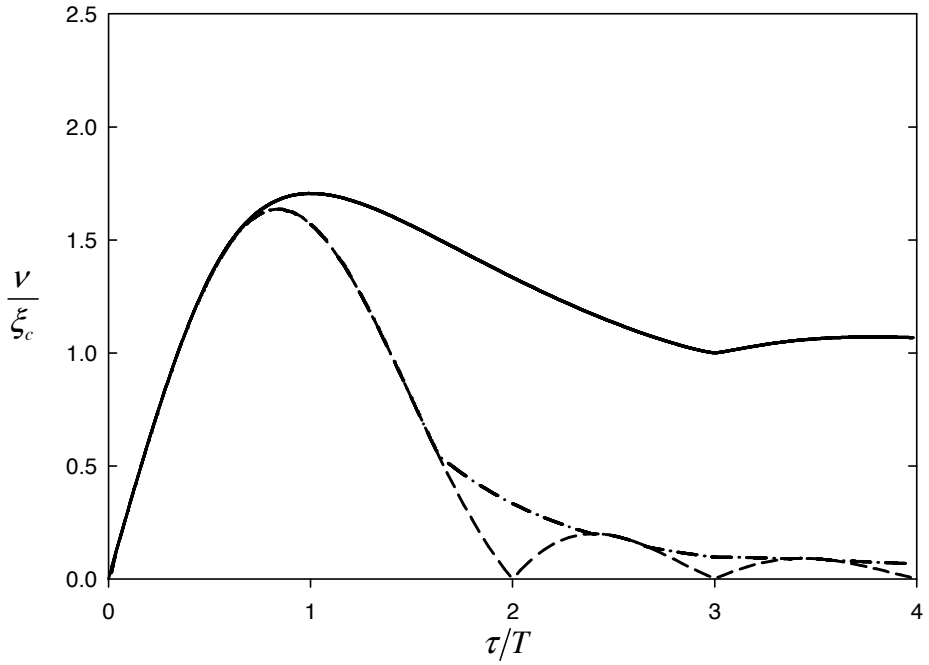


Figure 2.7. Shock response spectra for a single degree-of-freedom undamped model subjected to a versed sine pulse (— Maximax; – – Residual – · – Relative).

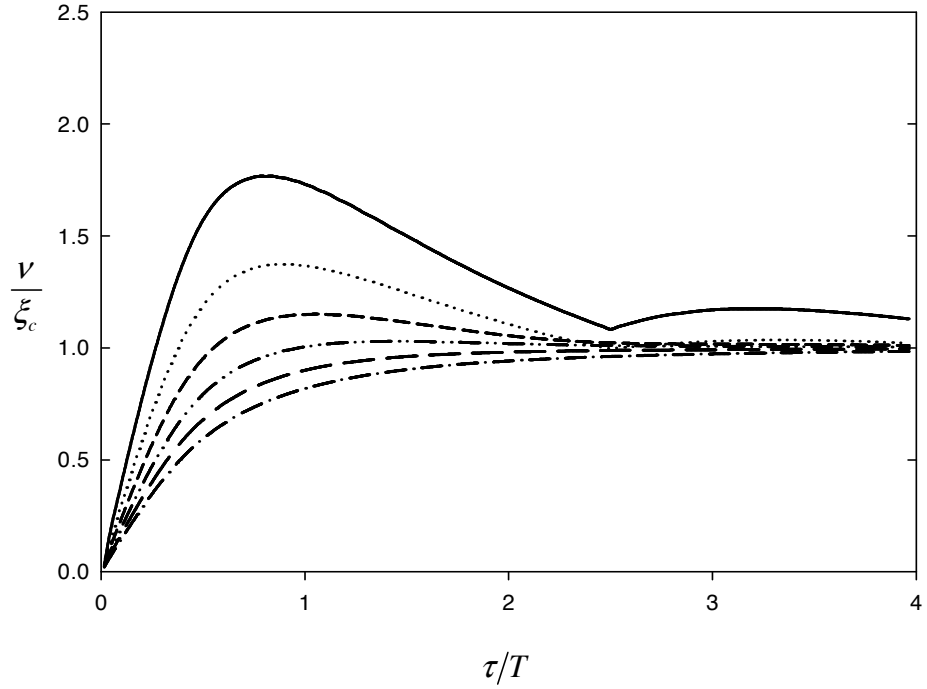


Figure 2.8. Shock response spectra for a single degree-of-freedom viscously damped model subjected to half sine excitation. (— $\zeta = 0$ ···$\zeta = 0.2$ ; – – $\zeta = 0.4$; —··— $\zeta = 0.6$; — — $\zeta = 0.8$; – · – $\zeta = 1$).

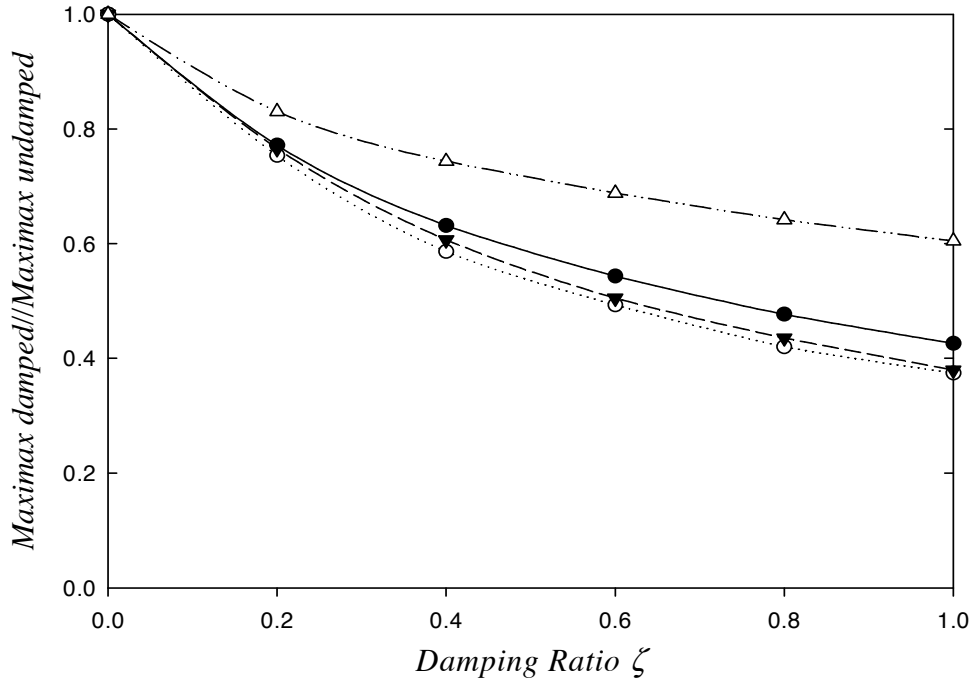


Figure 2.9. Effect of damping in the reduction of maximax response for a single degree-of-freedom system under a half sine pulse. Vertical axis represents the ratio between the maximax for a damped system and the maximax for an undamped system. The horizontal axis is the value of damping ratio.($-\tau/T = 0.8$; $\cdots\ \tau/T = 0.25$; $- -\ \ \tau/T = 0.5$; $-\cdot\cdot-\ \tau/T = 1.5$).

# Chapter 3.

# Shock response control using switchable stiffness.

## 3.1. Introduction.

This chapter describes an analytical study into the effects of a switchable stiffness control strategy applied to a single degree-of-freedom model subjected to shock excitation. Such a control strategy is intended to provide an alternative to the common passive isolation methods used for shock excitation [2]. The approach involves a semi-active control scheme, which is based on an on-off stiffness variation. The principal objective throughout is to investigate the reduction of the maximax response. Several response parameters such as the absolute displacement, the relative displacement and the absolute acceleration of an isolated mass are used to evaluate the performance of the strategy. The response is considered for a certain shock pulse typically used to evaluate the shock response of a passive model. The issues and advantages of using a switchable stiffness strategy are investigated to determine the possible benefits, the conditions required for practical implementation and any problems or difficulties that might exist. To begin, a simple undamped model with a secondary switchable massless stiffness element is considered, subsequently the effect of damping is investigated. This is followed by the analysis of a compound model, involving primary and secondary mass spring

systems, which are both initially considered to be undamped. Subsequently, the effect of damping is analyzed afterwards. Both the simple and the compound models are evaluated in terms of several response parameters according to the nature of the excitation. Moreover, the effect of a time lag in the implementation of the strategy is considered, as this might inevitably occur in any practical realization or demonstration.

## 3.2. Motivation.

Chapter 2 summarized the idealised response of a single degree-of-freedom system subjected to several shock excitations, e.g. step, rectangular and half sine pulses excitation types. One of the most important features observed is that the maximax response for an isolated mass is mainly controlled by the relationship between the duration of the pulse (pulse period $\tau$) and the natural period $T$ of the system involved, expressed as the ratio $\tau/T$ . This can be easily seen when examining the shock response spectra (SRS). The other important factor, which affects the response, is the shape of the pulse. However, provided that the duration of the pulse is short enough compared to the natural period, the shape of the pulse has a negligible effect on the response of the system. When the pulse is long compared to the natural period the excitation becomes quasi-static, and the shape of the pulse is important, since the response follows the shape of the pulse quite closely. It was also noted that the effect of viscous damping in reducing the maximax response is generally insignificant, if compared to the effect of damping when the excitation has a different nature, i.e. harmonic. As a result, an ideal shock mount should be as soft as possible to reduce the response to the shock by deformation of the elastic element. In the SRS this is known as the isolation region where the maximum response of the system is smaller than the amplitude of the shock, and in this region the ratio $\tau/T$ is normally small. In practice, there is a limitation on the allowable softness of the mount to achieve a low $\tau/T$ ratio mainly because of two reasons. The first reason is that certain stiffness is required to support the static weight of the mass. Secondly, due to the space limitations, because a soft mount will normally involve large elastic deformations that might be unacceptable.

The basic idea behind the implementation of a variable or switchable stiffness strategy is to provide a softer support for the isolated mass only during the time when the pulse is applied. This can be achieved if the stiffness of the system is capable of change from a high state to a

low state during the application of the pulse. The initial value of stiffness is then recovered when the shock is over. In this way the maximax response is expected to decrease. The system is therefore adaptive and piecewise linear in this situation. The advantages and limitations of this strategy are analyzed in the following section for an undamped system.

## 3.3. Simple model (massless secondary spring)

To investigate the switchable stiffness strategy, a simple single degree-of-freedom undamped model is considered. The conceptual model is depicted in figure 3.1. It comprises a mass $m$ supported by two springs in parallel. The stiffness $k - \Delta k$ is known as the primary stiffness and the stiffness $\Delta k$ is known as the secondary stiffness. The secondary stiffness $\Delta k$ can be disconnected at some point in time depending upon a particular control law. The system is subjected to a generic shock excitation represented by $\xi(t)$ in the form of a base displacement. The equation of motion is thus given by:

$$m\ddot{v} + k_{\text{effective}} v = k_{\text{effective}} \xi(t) \tag{3.1}$$

The stiffness $k_{\text{effective}}$ can take either the values of $k - \Delta k$ or $k$ depending upon whether the secondary stiffness $\Delta k$ is disconnected or connected respectively. The excitation $\xi(t)$ typically has the form of a symmetrical pulse. In this chapter a versed sine pulse is considered for the analysis. The use of a versed sine type pulse is justified because its derivatives are continuous, since it smoothly rises from zero to its maximum, and then back to zero [4, 13]. As a result, no acceleration discontinuities are produced. Additionally, this sort of excitation has been widely used for shock testing and simulation [13, 104]. The versed sine pulse is represented mathematically as:

$$\xi(t) = \begin{cases} \frac{\xi_c}{2}\left(1 - \cos\left(\frac{2\pi t}{\tau}\right)\right) & 0 \le \mathrm{t} \le \tau \\ 0 & \tau < \mathrm{t} \end{cases} \tag{3.2}$$

where $\xi_c$ is the maximum amplitude of the pulse and $\tau$ is its duration, or pulse period.

At this point it is important to clarify the nature of the analysis of the system response and excitation. Although the analysis performed in this chapter considers base excitation in the form of a single displacement pulse and then the response is obtained, the results presented in this chapter can be applied to a number of different scenarios. For instance, if the excitation is regarded as generic, as considered by Ayre [2,4], the results obtained can be extended to different excitation-response pairs, as explained in table 2.1. Although absolute and relative responses are obtained, the analysis is focused on the situation where a system suffers a sudden base motion, and the absolute parameters, namely displacement and acceleration are of concern. Additionally, this will form the basis for further simulations and the experimental validation.

### 3.3.1. Analytical solution

The fundamental idea is to reduce the stiffness for the duration of the pulse. In theory this change in stiffness is immediate. It is desirable to have preliminary information about the shock pulse, in order to change the system properties before or just at the time of the excitation. It has already been shown that using a pre-acting control strategy for shock excitation will result in better isolation performance [53]. This can be challenging due to the sudden nature of shock excitation, which can be highly unpredictable, and typically of very short duration. Although there might be some applications in which this may be possible, in many situations there would be a delay between sensing a shock pulse and changing the stiffness. In this study a specified delay can be incorporated between the beginning of the shock and the stiffness reduction to account for this. Additionally, if there is a delay at the moment of stiffness reduction, there could be another delay at the stiffness recovery, either due to the circuitry and devices involved in implementing the control logic, or to the type of the actuators used. This can be shown schematically using figure 3.2, which depicts the time history of a versed sine pulse excitation, and the system stiffness as it changes over time. The stiffness is reduced at a delayed time $\Delta t_1$ after the pulse has initiated and then increased again at $\tau + \Delta t_2$, which happens shortly after the pulse has finished at time $\tau$. The effect of this time lag is analyzed and presented in section 3.3.3.

Considering the stiffness changes and the nature of the excitation, the response of the conceptual system can be evaluated during four stages. The system is considered to be at rest

at the moment of excitation, hence the initial conditions are $v(0)=0$ and $\dot{v}(0)=0$. Then a certain pulse $\xi(t)$ is applied. Firstly, the system has the high stiffness state $k$ during a short interval of the pulse excitation. Secondly, after a time $\Delta t_1$ the stiffness is reduced to $k-\Delta k$ while it is still under the pulse excitation. Thirdly, the pulse has ended at time $\tau$ and the system is undergoing free vibration, but the stiffness value is still $k-\Delta k$ until the time $\tau+\Delta t_2$. Finally, after $\tau+\Delta t_2$ the original stiffness is again recovered. At the reconnection, the displacement of the mass is unaltered, so that the effective stiffness is assumed to have the same extension as the reduced stiffness at that time, and the system continues under free vibration. Mathematically the equation of motion (3.1) in this case represents a piecewise linear system and it can be expressed as:

$$\begin{aligned} &m\ddot{v}+kv=k\xi(t) && 0\le t\le \Delta t_1\\ &m\ddot{v}+(k-\Delta k)v=(k-\Delta k)\xi(t) && \Delta t_1< t\le \tau\\ &m\ddot{v}+(k-\Delta k)v=0 && \tau< t\le \tau+\Delta t_2\\ &m\ddot{v}+kv=0 && \tau+\Delta t_2< t \end{aligned} \tag{3.3}$$

The solution of the set of equations given by equation (3.3) will be obtained for each interval of time. At the corresponding times of which switching occurs the solution will be assumed continuous in both the displacement and velocity. It will be shown later that he acceleration is not continuous and also energy considerations will be presented. This latter point is further discussed in chapter 4.

The response for a particular pulse $\xi(t)$ can be calculated using the convolution integral [102].

$$v(t)=\int_0^t \xi(\varepsilon)h(t-\varepsilon)\,d\varepsilon \tag{3.4}$$

where $h(t)$ is the impulse response function, which for an undamped single degree-of-freedom system under base excitation is given by:

$$h(t)=\omega_n \sin(\omega_n t) \tag{3.5}$$

where $\omega_n$ is the instantaneous undamped natural frequency of the system. The term instantaneous refers to the fact that the natural frequency changes depending upon the stiffness state, as a result the instantaneous natural frequency is the value of the natural frequency for a particular instant of time. There are two different values of natural frequency corresponding to the high and low stiffness states respectively as given by:

$$\omega_1 = \sqrt{\frac{k}{m}} \tag{3.6}$$

$$\omega_2 = \sqrt{\frac{k - \Delta k}{m}} \tag{3.7}$$

The response is divided into four stages $v_1$, $v_2$, $v_3$ and $v_4$ corresponding to the different stiffness states as expressed by equation (3.3). Combining equations (3.4), and (3.5), the response for the first part, from 0 to $\Delta t_1$, with stiffness $k$ can be written as:

$$v_1(t) = \xi_c \omega_1 \int_0^t \xi(\varepsilon) \sin \omega_1 (t - \varepsilon) d\varepsilon, \text{ for } 0 \le t \le \Delta t_1 \tag{3.8}$$

The second part from $\Delta t_1$ to $\tau$ is also calculated using a convolution integral. However, for this part of the response the system has non-zero initial conditions. In general terms, the response can be expressed as:

$$v_2(t) = \omega_2 \int_{\Delta t_1}^t \xi(\varepsilon) \sin \omega_2 (t - \Delta t_1 - \varepsilon) d\varepsilon + v_1(\Delta t_1) \cos\left(\omega_2 (t - \Delta t_1)\right) + \left(\frac{\dot{v}_1(\Delta t_1)}{\omega_2}\right) \sin\left(\omega_2 (t - \Delta t_1)\right)$$
$$\text{for } \Delta t_1 \le t \le \tau \tag{3.9}$$

The solution given by equation (3.9) is valid during the pulse. From time $\tau$ until time $\tau + \Delta t_2$ the stiffness has the lower value $k - \Delta k$, and the system undergoes free vibration. The response can be simply written as:

$$v_3(t) = v_2(\tau)\cos\left(\omega_2\left(t-\tau\right)\right) + \left(\frac{\dot{v}_2(\tau)}{\omega_2}\right)\sin\left(\omega_2\left(t-\tau\right)\right), \text{ for } \tau \le t \le \tau + \Delta t_2 \tag{3.10}$$

The final stage is the free vibration response for the high stiffness state, from the time $\tau + \Delta t_2$ onwards, and it can be expressed as

$$v_4(t) = v_3(\tau+\Delta t_2)\cos\left(\omega_1\left(t-\left(\tau+\Delta t_2\right)\right)\right) + \left(\frac{\dot{v}_3(\tau+\Delta t_2)}{\omega_1}\right)\sin\left(\omega_1\left(t-\left(\tau+\Delta t_2\right)\right)\right) \quad \text{for } \tau+\Delta t_2 < t \tag{3.11}$$

It is important to note at this point that although the displacement and velocity are continuous, the acceleration response will display sudden step changes due to the corresponding stiffness switching points.

3.3.2. Parametric analysis and numerical results.

As mentioned previously, one of the most important parameters that affect the shock response of a passive single degree-of-freedom system is the ratio between the duration of the shock $\tau$ and the natural period of the system $T$. The additional analysis considered in this chapter involves a parameter that changes in time, namely the stiffness. Moreover, for practical reasons the effect of the time lag mentioned above has to be considered. This section presents and discusses the results of numerical simulations, focusing on the effects of the stiffness reduction ratio and its delay on the system response.

The stiffness reduction can be expressed in terms of a stiffness ratio, which is the ratio between the secondary stiffness and the total stiffness, i.e. when the secondary stiffness $\Delta k$ is connected to the main system:

$$\sigma = \frac{\Delta k}{k} \tag{3.12}$$

The SRS for the passive single degree-of-freedom system is taken as a performance benchmark for this switchable mass-stiffness model. As in chapter 2, the shock response of a

particular system can fall into three categories, or zones of the SRS, namely isolation region, amplification region and the quasi-static region. These zones are determined mainly by the aforementioned ratio $\tau/T$, which is called $\hat{\tau}$ henceforth. In a passive system, the physical properties, i.e. the stiffness, damping and mass, are fixed. Effectively the result of changing the system properties is a shift in the SRS region. If this change is known, then the response of the system can be estimated for any pulse, having the SRS of the passive model as an approximate basis for evaluation. Initially the system has a certain value for the ratio $\hat{\tau}_{\text{high}}$ for the initial or high value of stiffness, which will determine the maximum response. However, when the stiffness is changed, the system has a new ratio, which can be referred as an effective or low stiffness ratio $\hat{\tau}_{\text{low}}$. The objective is to shift the system to the isolation region of the SRS, i.e. where the response amplitude is smaller than the pulse amplitude.

Effectively, the reduced natural frequency as a result of the stiffness variation can be written as:

$$\omega_{\text{low}} = \omega_n \sqrt{1-\sigma} \tag{3.12}$$

Equation (3.12) can be rewritten in terms of the period ratio of the input duration to the period of the system as:

$$\frac{\hat{\tau}_{\text{low}}}{\hat{\tau}_{\text{high}}} = \sqrt{1-\sigma} \tag{3.13}$$

Equation (3.13) can easily be used to obtain the period ratio for the low stiffness state of the system $\hat{\tau}_{\text{low}}$. In this way the response of the system can be predicted for the ideal case when no delay occurs for the stiffness reduction. Figure 3.3 shows the effective period ratio normalised with respect to the initial period ratio. The fundamental result of the stiffness reduction is to reduce the ratio $\hat{\tau}$, i.e. move the system SRS response towards the origin. As expected, as the stiffness ratio increases the reduction of the period ratio is more accentuated. This can be advantageous for some values of the initial period ratio, but not for other values. For instance, the new effective period ratio could make the system response fall into the amplification zone. This is especially the case when the shock approaches the quasi-static region for the original passive system, as explained later. Furthermore, it can be observed

from figure 3.3 that the change in the period ratio of the system behaves approximately linearly when the stiffness ratio is small, ($\sigma < 0.2$). For this situation the variation of the period ratio can be simplified and calculated using the linear approximation $\frac{\hat{\tau}_{\text{low}}}{\hat{\tau}_{\text{high}}} = 1 - \frac{1}{2}\sigma$. This is also shown in figure 3.3.

Three response parameters are studied in this section, which are the absolute displacement $v(t)$, the relative displacement $v_{rel}(t) = v(t) - \xi(t)$ and the absolute acceleration $\ddot{v}(t)$. These are the most important parameters when studying shock problems, since they are related to the space available (rattlespace), the stress in the supporting mount and the potential damage that might occur in the supported equipment [104, 105]. The maximax response is considered (which can occur either during or after the pulse). The normalised values of maximax response are represented by the symbols $v_m = \max\left|\frac{v(t)}{\xi_c}\right|$ for the absolute displacement, $v_{rel} = \max\left|\frac{v(t) - \xi(t)}{\xi_c}\right|$ for the relative displacement and $\ddot{v}_m = \max\left|\frac{\ddot{v}(t)}{\ddot{\xi}_c}\right|$ the for absolute acceleration, where $\ddot{\xi}_c$ is the maximum input acceleration. The analysis of the residual response is presented later in the next chapter.

Ideally, using a shock mount should minimize all of these parameters. However, there is a compromise between the maximum absolute displacement, the absolute acceleration, and the relative displacement. A softer mount will reduce the maximum displacement and acceleration of the supported mass, but at the cost of increasing the relative motion, which means more space is required. This can be a problem where space is limited. Moreover, if the mount comprises helical springs, there is a risk of the coils making contact thus forming a rigid link and possibly damage might occur. As this switchable stiffness strategy is based upon a stiffness reduction, the relative displacement might increase, but the absolute responses are expected to decrease. As a result, the parameters to be controlled are the maximum absolute displacement and acceleration. However, one of the objectives here is to evaluate the performance of the system considering this strategy, taking into account all the response parameters involved. The possible advantages and disadvantages of this strategy are discussed.

For the analysis considered in this chapter the type of input pulse considered is the versed sine pulse, given in equation (3.2). Whilst equations (3.8-3.11) provide analytical expressions, the evaluations are required for a range of stiffness reductions and there is no explicit means to determine the maximum response. The simulations presented were calculated using variable step numerical integration routines (fourth order Runge-Kutta method) available in MATLAB. Essentially the results are the solutions for the piecewise linear system as presented by the differential equations of motion (3.3), and the maximax responses are then obtained.

The ideal case is when no time lag occurs and the stiffness is reduced immediately when the excitation begins, and then recovered exactly when the pulse ends. This can be regarded as the best case scenario, where one knows the excitation and when it is going to start, although for most practical applications this is not the case. In order to investigate the overall effect of the stiffness reduction the first step in the analysis is to study the behaviour of the response as a function of the stiffness reduction, for several values of the initial period ratio $\hat{\tau}_{\text{high}}$.

Several examples of time histories are presented in figures 3.4 and 3.5 for representative values of the initial period ratio $\hat{\tau}_{\text{high}}$ ( $\hat{\tau}_{\text{high}} = 0.25$, $\hat{\tau}_{\text{high}} = 0.5$, $\hat{\tau}_{\text{high}} = 1$ and $\hat{\tau}_{\text{high}} = 2$ ). These values represent typical situations of short pulses (isolation area) as well as pulses in the amplification and the beginning of the quasistatic regions. These examples consider a stiffness switching during the shock, for a stiffness reduction of 50% as an illustrative example. Figure 3.4 shows the responses corresponding to absolute (dashed line) and relative displacement (dash dot). The pulse is depicted by the solid line. Subplots are as follows: (a) $\hat{\tau}_{\text{high}} = 0.25$, (b) $\hat{\tau}_{\text{high}} = 0.5$, (c) $\hat{\tau}_{\text{high}} = 1$, and (d) $\hat{\tau}_{\text{high}} = 2$ Figure 3.5 presents the absolute acceleration responses corresponding to the same values of $\hat{\tau}_{\text{high}}$ as before. It is important to note the sudden acceleration change observed in figure 3.5 when the stiffness is recovered, which occurs at a point different from the equilibrium position.

To illustrate the benefits, and to quantify the performance of the switchable stiffness strategy, the maximax response of the passive model is taken as the reference for comparison. Consequently, the parameter results are presented as the ratio between the maximax responses of the adaptive and the passive models. As a result, if this ratio has a value higher than 1, it

means the response of the adaptive model exceeds the response of the passive model, otherwise there is a performance gain. The maximax response has been calculated for values of the period ratio between 0 and 1, where 0 means no stiffness change is made, and 1 means the stiffness is completely removed from the system. The results are presented in figure 3.6 for absolute displacement, figure 3.7 for relative displacement and figure 3.8 for absolute acceleration. Each curve represents a different value of the initial ratio which are $\hat{\tau}_{high} = 0.25$, $\hat{\tau}_{high} = 0.5$, $\hat{\tau}_{high} = 1$, and $\hat{\tau}_{high} = 2$ with no delay considered.

Regarding the absolute displacement, shown in figure 3.6, it can be seen that the maximax response is effectively reduced depending upon the percentage of stiffness reduction for short duration pulses ($\hat{\tau}_{high} < 1$). Higher stiffness reduction results in a smaller displacement response. For instance, in the case of absolute displacement a decrease of approximately 40% in the response is achieved for $\sigma = 0.5$ and $\hat{\tau}_{high} = 0.25$. However, as the period ratio increases the reduction in the response becomes smaller and higher stiffness reductions are needed in order to obtain any advantage. Furthermore, the maximax response can be amplified if the period ratio $\hat{\tau}_{high} > 1$, as can be seen for example in figure 3.6 when $\hat{\tau}_{high} = 2$. In this latter case the response increases except when the stiffness reduction is very high, i.e. more than 90%. This is related to the fact that the stiffness reduction modifies the effective period ratio of the system, as mentioned previously. Effectively a higher stiffness ratio is needed to shift the system to the SRS isolation zone, and if it is not enough the system might shift to the amplification region. This effect begins to manifest itself when the period ratio is higher than 1, where a small increase in the displacement response actually occurs.

For the relative displacement, depicted in figure 3.7, the behaviour is slightly different. Recalling the situation when the system is passive, a softer support will experience a larger relative displacement. This improves the shock isolation since the elastic support is capable of storing more strain energy, which potentially can be dissipated later via a damping mechanism. However, this requires more space for the isolated mass above the base. For $\hat{\tau}_{high} = 0.25$, the relative displacement is very similar to that of the passive system regardless of the stiffness reduction. There is some benefit obtained for values of $\hat{\tau}_{high}$ between 0.5 and 1. Moreover, the

relative displacement increases when the period ratio is higher than 2. This is basically as a result of the greater deformations in a softer system. Also, in the passive system the absolute and relative displacement responses are effectively equal in certain zones of the SRS, near the region when the period ratio is approximately equal to 1. This behaviour is likewise present in the switchable stiffness model. For these situations, both response quantities are identical for some values of the stiffness ratio. Again, this effect is a result of the effective period ratio change, which shifts from one SRS region to another.

The remaining response parameter is the normalised absolute acceleration presented in figure 3.8. Broadly the behaviour is similar to the absolute displacement. High stiffness reductions generally lead to a decrease in the acceleration levels. As the period ratio increases the advantages obtained are less evident. However, the sudden stiffness changes will cause acceleration discontinuities that might affect the isolation performance.

In general, it can be seen that the strategy does not give very good results if $\hat{\tau}_{\text{high}}$ is larger than 1 unless the reduction in stiffness is very high, i.e. larger than 90%. It is in this region that the shock input is no longer impulsive, being closer to a quasi-static input due to the high natural frequency of the passive system or a long pulse duration. The best benefits are observed for the absolute displacement and acceleration, with little or no change observed for relative motion. In contrast a disadvantage occurs when $\hat{\tau}_{\text{high}}$ is larger than 2, where the relative displacement increases under stiffness reduction changes.

### 3.3.3. Effect of delay.

Now that the effect of the stiffness reduction is clear, it is interesting to investigate and quantify the effect of any time delay in switching the stiffness. A similar numerical procedure is performed, but in this case the delays $\Delta t_1$ and $\Delta t_2$ are considered, corresponding to the beginning and the end of the shock respectively. These delays are presented as non-dimensional parameters for simplicity with respect to the pulse duration $\tau$ and are now expressed as $\Delta_1 = \frac{\Delta t_1}{\tau}$ and $\Delta_2 = \frac{\Delta t_2}{\tau}$. The results are presented in the form of 3D surface plots where the *x* and *y* axes are the delays $\Delta_1$ and $\Delta_2$ respectively, ranging from 0 to 1. The *z*-

axis represents the response parameter. For this analysis only the absolute displacement and acceleration are presented, since they are the most important. The effect of the delay in the relative motion is very similar to the other parameters. Moreover, the results are given for only two values of the initial period ratio, which are $\hat{\tau}_{\text{high}} = 0.25$ and $\hat{\tau}_{\text{high}} = 0.5$. This decision was made because when the period ratio increases the effect of stiffness reduction diminishes. Additionally, the effect of the delay can be explained with these representative values since its effect is generally the same for other values of the period ratio. The figures presented were calculated considering $\sigma = 0.7$ as a representative value for the stiffness reduction. The choice of this value was made because the effect of delay is very similar regardless of the stiffness reduction factor, and the effect of the stiffness reduction in the response has already been discussed. Moreover the effect of stiffness reduction can be more easily appreciated as this stiffness ratio is relatively large.

Examination of figures 3.9 and 3.10 shows that the initial switching delay $\Delta_1$ has an important effect on the response for the parameters considered. Whilst relatively small values of delay will cause no difference in the response, if this time delay increases a higher response might occur. This phenomenon is a consequence of the reduction in the restoring force as the mass is moving following the pulse, especially at the time when the mass is close to its maximum displacement, the reduction of the elastic force will cause the mass to move further in the same direction as the applied base input. The effect is the same for both absolute displacement and acceleration.

In contrast, the second switching delay $\Delta_2$, which corresponds to the stiffness recovery once the pulse has finished, has a small effect and the response is not greatly affected. This is basically because the response of a system subjected to a shock is smaller when the stiffness is reduced, a delay in recovering the stiffness to the original high state after the shock will not cause a greater response. However, it is necessary to ensure that the system returns to its original stiffness state soon after the shock, since the system is undergoing free vibration. If the stiffness is not recovered after the shock finishes, when the residual oscillations end the static stiffness will be lower than the original design value, which might not be acceptable for the system at rest.

An example of a characteristic time history comprising the normalised absolute responses for displacement, velocity and acceleration is included in figure 3.11, in order to show the effect of the stiffness variation on the responses. This example has been produced considering representative values of the stiffness reduction ratio of 0.7, and a period ratio $\hat{\tau}_{high} = 0.25$. The values of delay used are $\Delta_1 = \Delta_2 = 0.1$, in order to appreciate better the effect. The most significant effect is a discontinuity in the acceleration as a result of the stiffness recovery after the pulse has finished and also at the point of stiffness reduction at the beginning of the shock.

To consolidate the results discussed previously, figure 3.12 presents the Shock Response Spectra for several values of the stiffness reduction factor $\sigma$. The bold line represents the SRS for a passive undamped model. For this figure a small value for the delays $\Delta_1 = \Delta_2 = 0.01$ is considered, for both the stiffness reduction and recovery. The ratio $\hat{\tau}_{initial}$ considered for reference corresponds to the initial value of stiffness, i.e. the highest stiffness state. Fundamentally, for higher stiffness reduction, then greater response reduction will take place, especially when the pulse duration is short compared to the system natural period, i.e. when $\hat{\tau}_{high} \leq 1$ and otherwise very high stiffness reductions are needed. Generally, for long duration pulses, i.e. if $\hat{\tau}_{high} \geq 1$ it is preferable not to have any stiffness reduction.

### 3.3.4. Effect of damping

In practice, all real systems have damping or energy dissipation to a certain extent. Hence, the effect of damping is briefly considered in this section. For simplicity, viscous damping is incorporated as depicted in figure 3.13. For a concise representation of the behaviour of the damped model, the SRS is again used as a basis of comparison. Figures 3.14 and 3.15 show a displacement Shock Response Spectra for stiffness reduction factors of $\sigma = 0.5$ and $\sigma = 0.7$, each one considering different values of damping $\zeta = \frac{c}{2\sqrt{km}} = 0.05,\ 0.1, 0.3$ and $0.5$. These results are given for a versed sine input. The effect obtained when viscous damping is present is very similar compared with the results for the passive case, and also compared to the switchable undamped stiffness model in figure 3.12. The benefit of damping alone is not very significant, but the combination of the switchable stiffness strategy and viscous damping can yield better isolation performance, especially in the amplification region of the SRS,

i.e. $\hat{\tau}_{\text{high}} \approx 1$. On the other hand, when $\hat{\tau}_{\text{high}} \leq 0.5$ (impulsive zone) and $\hat{\tau}_{\text{high}} \geq 3$ (quasi-static zone) for $\sigma < 0.5$ the effect of damping is not very significant. In contrast, the effect of damping on acceleration response is a little different. Recalling that the scenario studied in this chapter is that of a system having base displacement excitation, high values of damping can cause the acceleration to increase, as it has been shown for the passive situation [3]. Figure 3.16 presents a characteristic acceleration SRS of a base excited system for a versed sine pulse. The acceleration response was computed by substituting the numerical solutions for displacement and velocity into the equation of motion of the system given by equation (2.14) for the corresponding values of high and low stiffness. A representative value of $\sigma < 0.5$ was considered. In general, it can be seen how damping causes the maximum acceleration response to increase for short duration pulses, i.e. typically for $\hat{\tau}_{\text{high}} \leq 0.5$ because of the force transmitted by the viscous damper due to base excitation. In the amplification region damping reduces the acceleration levels to some extent, but in the quasi-static region the effect of increasing damping because the spring and damper behave almost like a rigid link. This behaviour is very similar to the passive system with base excitation.

## 3.4. Compound model (mass-spring secondary system)

In the previous section it was assumed that the model involved massless elastic elements. The incorporation of mass with the secondary elastic element represents a further step in the modelling of the system. This is now studied in this section for an undamped system so that the effect of the mass can be established. The effect of damping in this system is investigated later.

The concept introduced here considers a secondary spring-mass system that is allowed to connect and disconnect from a main system following a switching logic. A particular consideration must be made in order for this system to work according to the control law. Considering that the secondary mass-spring system will oscillate independently during the off part of the control law (low stiffness stage), it is envisaged that it would be possible to design or configure the system to ensure that the secondary mass is exactly at the static equilibrium position at the moment of stiffness recovery, when the secondary stiffness $\Delta k$ reconnects to the primary mass. If this is achieved, both the main and the secondary system will coincide at

the correct time. This also requires that the primary and secondary systems oscillate in such a way that they do not collide during the time they are disconnected. One possible arrangement to ensure that the reconnection can effectively be performed is idealised in the system shown in figure 3.17. This represents two masses of mass ($m$-$\Delta m$)/2 each, supported by springs ($k$-$\Delta k$)/2, and between these masses there is the secondary mass $\Delta m$ supported by $\Delta k$, which can be disconnected or connected from the main masses following a suitable control law. This schematic model can be thought of as a small mass oscillating inside a larger, hollow mass which can be connected or separated depending upon the control law. As a result, if the oscillation amplitude of the secondary mass is between the height limits of the primary masses they can oscillate independently without problem. If the several parameters related to the model are correctly chosen, the system can be designed so the reconnection takes place as expected or preferred. The analysis of this system and the relationship between the parameters involved is performed later in this section.

Taking into account the previous considerations, the model can be simplified for the purpose of analysis, as shown in figure 3.18. It comprises a mass $m - \Delta m$ supported by a massless spring $k - \Delta k$ and is rigidly connected to the secondary mass-spring system consisting of mass $\Delta m$ and secondary spring $\Delta k$. At some point in time the systems can be disconnected and oscillate independently. It is assumed that the masses do not collide whilst they are disconnected but they experience an impact at the moment of reconnection, and that they move together immediately after impact, i.e. a perfectly inelastic impact.

### 3.4.1. Fundamentals and description of the model.

The model comprises two masses, which are attached in normal conditions. For this model, it is useful to express the mass change in terms of a mass ratio:

$$\mu = \frac{\Delta m}{m} \tag{3.13}$$

Considering a base displacement excitation, the equation of motion for the system with a high stiffness is given by:

$$m\ddot{v} + kv = k\xi(t) \qquad 0 \le t \le \Delta t \tag{3.14}$$

When the stiffness is reduced, the masses are disconnected. The primary mass $m-\Delta m$ and the secondary mass $\Delta m$ oscillate independently, while they are both being excited by the same base input shock. Thus the equations of motion are given by:

$$(m-\Delta m)\ddot{v}_1 + (k-\Delta k)v_1 = (k-\Delta k)\xi(t) \qquad \Delta t \le t \le \tau \tag{3.15}$$

$$\Delta m\ddot{v}_2 + \Delta k v_2 = \Delta k\xi(t) \qquad \Delta t \le t \le \tau \tag{3.16}$$

Once the pulse is over, after a certain time it is assumed that both systems are reconnected and vibrate freely as a combined single mass. However determining the time when and how the systems can physically reconnect is not trivial and the next section is concerned with this matter.

It is important to note that, as the properties of the system will change over time (mass and stiffness) the system will exhibit a switchable natural frequency. As a result, when the masses are connected, the original natural frequency is given by:

$$\omega_n = \sqrt{\frac{k}{m}} \tag{3.17}$$

Then when the systems are disconnected, the natural frequency for the main or primary system is given by:

$$\omega_p = \sqrt{\frac{k-\Delta k}{m-\Delta m}} \tag{3.18}$$

and for the secondary system:

$$\omega_s = \sqrt{\frac{\Delta k}{\Delta m}} \tag{3.19}$$

3.4.2. Re-connection issues

In order to ensure that the systems can recombine once the pulse is over it is necessary to predict the next point when they coincide. For simplicity in this part of the analysis, the effect of delay is ignored so that the stiffness is reduced exactly when the shock pulse begins. Considering the free response equations for the primary and the secondary systems once the pulse has finished, the later condition for coincidence of the masses can be expressed as:

$$v_1(\tau)\cos\omega_p(t-\tau)+\left(\frac{\dot{v}_1(\tau)}{\omega_p}\right)\sin\omega_p(t-\tau)-v_2(\tau)\cos\omega_s(t-\tau)-\left(\frac{\dot{v}_2(\tau)}{\omega_s}\right)\sin\omega_s(t-\tau)=0 \qquad (3.20)$$

Equation (3.20) can be solved to find the possible times when both systems coincide however, this condition might not be the most suitable for their reconnection. Effectively, both systems will coincide, but they can be at any point in their free vibration cycles. It is preferable to reconnect the systems when they are at the static equilibrium position corresponding to $v_1 = v_2 = 0$, since the elastic elements have no strain energy at that moment. The effect of gravity is ignored now for both simplicity and the configuration could be designed such that the static equilibrium position of the two systems coincides. Moreover there will possibly be an impact between the masses, which if considered completely inelastic (i.e. the masses oscillate together after the impact) will cause an immediate loss of energy and a reduction in the response. The residual free vibration stage after the base input has finished is analyzed in the next chapter to identify a method to reduce it.

A simplified form of the free response equations after a versed sine pulse as given in equation (2.13) is used in the following analysis. Equation (2.13) can be re-written for the primary and secondary systems as [2]:

$$v_p = \xi_c\left[\frac{\sin\left(\pi\tau/T_p\right)}{1-\tau^2/T_p{}^2}\right]\sin\omega_p\left(t-\frac{\tau}{2}\right) \qquad \text{for } t>\tau \qquad (3.21)$$

$$v_s = \xi_c \left[ \frac{\sin\left(\pi\tau/T_s\right)}{1-\tau^2/T_s^2} \right] \sin\omega_s\left(t-\frac{\tau}{2}\right) \qquad \text{for } t > \tau \tag{3.22}$$

where $T_p$ and $T_s$ are the natural periods of the primary and secondary systems respectively. The systems are required to coincide at the static equilibrium position, i.e. both systems have a value of displacement equal to zero. This is more convenient since at this point the velocity of the masses will be maximum and they will impact inelastically dissipating energy. However this phenomenon is analyzed in chapter 4. Hence, the following conditions need to be satisfied:

$$\omega_p\left(t-\frac{\tau}{2}\right) = n\pi \qquad n\text{=0, 1, 2, 3...} \tag{3.23}$$

$$\omega_s\left(t-\frac{\tau}{2}\right) = q\pi \qquad q\text{=0, 1, 2, 3...} \tag{3.24}$$

where the terms $q$ and $n$ are integer values. By arranging equations (3.23) and (3.24), the possible solutions can occur when the ratio between the natural frequencies $\omega_p$, and $\omega_s$ can be expressed as:

$$\Omega = \frac{\omega_s}{\omega_p} = \frac{q}{n} \tag{3.25}$$

As a result, the frequency ratio needs to be a value resulting from the terms $q$ and $n$ being integers, for both systems to coincide at the equilibrium position. However, it is important to note that this condition applies only for symmetric pulses such as the versed sine considered here. For non-symmetric pulses the phase angle in the free response will depend upon the amount of non-symmetry in the pulse. The equations for free response in the case of non symmetric pulses are different, hence the required frequency ratio for the masses to coincide at zero will be given by a different relationship. As a result the frequency ratio will not necessarily be an integer value [2].

Depending upon the value of the frequency ratio, there are many combinations of the stiffness and mass ratios that satisfy the required condition. Figure 3.19 presents the required mass ratio $\mu$ as a function of the stiffness reduction ratio $\sigma$ for several values of the frequency ratio $\Omega$. Additionally, the representative values of mass ratio and stiffness ratio for the values of frequency ratio used in the following discussion is presented in table 3.1 for guidance. A numerical example comprising a time response for different values of the frequency ratio is given in figure 3.20. From this figure it can be clearly seen how the masses can be configured to recombine within the first half of the residual free vibration cycle of the primary mass system. This example considers an initial value of the ratio $\tau/T = 0.25$ and a value of the stiffness reduction ratio $\sigma = 0.5$. Thus the mass ratio $\mu$ is selected to give the required value of frequency ratio. The corresponding values of mass ratio $\mu$ and frequency ratio $\Omega$ are in figure 3.20(a) $\mu = 0.2$, giving $\Omega = 2$, and for figure 3.19(b) $\mu = 0.1$ giving $\Omega = 3$. The situation when $\Omega = 1$ (mass and stiffness ratio are equal) is not considered since both systems will have the same behaviour vibrating in amplitude and phase together and will recombine with no energy dissipation. It is clear how the secondary mass oscillates at a higher frequency in figure 3.20(b) as a result of the frequency ratio. It can also be observed the reduction of the amplitude after the masses recombine represented by the solid thin line, due to an inelastic impact, which causes a certain amount of energy being lost. However, the calculation of the amount of energy lost due to this impact and the importance of the parameters involved is analyzed in chapter 4 as it is related to the residual response of the system. In all of the simulations shown in figure 3.20, the parameters chosen mean that the secondary system with mass $\Delta m$ has a natural frequency higher than the mass $m - \Delta m$.

As introduced in section 3.2, the result of a variation in the stiffness is essentially a shift from one SRS region to another. This compound model also has this behaviour, but now two different systems are involved and two variables, i.e. the mass and stiffness ratios. The effective natural frequencies for the primary and secondary systems are given respectively by:

$$\omega_p = \omega_n \sqrt{\frac{\sigma}{\mu}} \tag{3.26}$$

$$\omega_s = \omega_n \sqrt{\frac{1-\sigma}{1-\mu}} \tag{3.27}$$

As a result, the frequency ratio can be expressed in terms of the mass and stiffness ratios as

$$\Omega = \sqrt{\frac{(1-\mu)\sigma}{(1-\sigma)\mu}} \tag{3.28}$$

Figure 3.21 shows the variation in the period ratio, normalised with respect to the initial period ratio $\hat{\tau}_{\text{high}}$, for the primary and the secondary systems, as a result of the changes in the system properties. Since the objective is to minimize the response of the primary mass, the main function of the secondary system is to reduce the stiffness of the main system. Hence typically the response of the secondary system is increased, but the main system will benefit from a reduction in its response. From figure 3.21 it is clearly seen that high stiffness reductions and a small mass ratio (i.e. a small secondary mass) yield a reduction in the period ratio $\hat{\tau}_{\text{high}}$ which is the preferred situation in most cases and corresponds to a lower mounted natural frequency. In this situation, as the secondary mass is smaller, the system approaches to the simple model with no secondary mass. As a result, the secondary system will have a large period ratio $\hat{\tau}_{\text{high}}$ due to its higher natural frequency. Otherwise, a bigger secondary mass will cause the effective ratio of the main supported mass to increase, in this way the system could fall into the amplification or into the quasistatic regions.

### 3.4.3. Compound model results

The response parameters numerically evaluated in this section are the absolute and relative displacement, as well as the absolute acceleration. It has already been shown in the previous section that it is desirable to have as small a delay as possible, and the simulations for the compound model have shown the same behaviour. Nonetheless, in this model a fixed value for the delay $\Delta_1 = 0.01$ is considered. For this model the results are presented as a function of the mass and stiffness ratio for several values of the ratio $\hat{\tau}_{\text{high}}$, i.e. $\hat{\tau}_{\text{high}} = 0.25$, $\hat{\tau}_{\text{high}} = 0.5$, $\hat{\tau}_{\text{high}} = 1$ and $\hat{\tau}_{\text{high}} = 2$. It is important to recall that the response parameter presented here is for the primary mass, i.e. the one to be isolated from the shock.

As with the analysis of the simple model, the results presented here for the response parameters are given as the ratio between the maximax responses corresponding respectively to the adaptive compound and the passive undamped models for two values of the frequency ratio $\Omega$, as a function of the stiffness reduction ratio. The results are presented as follows: Figure 3.22 for the absolute displacement, figure 3.23 for the relative displacement and figure 3.24 for absolute acceleration, each one given for values of $\Omega$ equal to 2 and 3.

The general behaviour is very similar compared to the basic model. Considering the response of a passive system as a reference it is easily observed that the best results are in general achieved when the stiffness reduction is large, and the mass ratio is small. When the frequency ratio increases for a particular fixed value of stiffness reduction the secondary mass is smaller, thus the system approaches the simple model and the isolation performance is slightly better. Effectively, reducing the mass in the system has the contrary effect to reducing the stiffness. As a result, it is preferable to have a small secondary mass. For this case, the effect is always beneficial, although not very significant in the case of relative displacement. As in the previous model, the benefits are mainly seen in the absolute responses, but not in the case of relative displacement. The latter remains almost unaltered in the best case, and might even suffer an increase if the period ratio is greater than 1.

It is clear that the benefits in reducing the response are increased for higher values of the frequency ratio, mainly because the secondary mass becomes very small, while the stiffness reduction might be relatively high. In this case the system approaches the simple model considered in the first part of the chapter and the behaviour is very similar. It is also seen that the strategy works well for values of the period ratio $\hat{\tau}_{\text{high}}$ smaller than 1. In contrast, when $\hat{\tau}_{\text{high}} \geq 1$ the response remains almost unaltered or it may even be amplified unless the stiffness reduction is very high.

To summarize, the results discussed above are presented in the form of Shock Response Spectra plots, which are shown in figure 3.25 The results are shown for various values of the stiffness reduction ratio $\sigma$ and frequency ratio $\Omega$, which then produces a corresponding mass ratio of $\mu = \dfrac{1}{1+\Omega^2\left(\dfrac{1}{\sigma}-1\right)}$. There are two SRS corresponding to the system natural frequency

ratios of $\Omega$ = 2, and $\Omega$ = 3. Several values of the stiffness ratio $\sigma$ are considered. As observed before, an increase in the stiffness ratio $\sigma$ will cause a reduction of the response. However, there is also a mass reduction involved, which has the opposite effect and as a result the advantages may not be as significant if compared with the simple model considered initially. This effect becomes less important as the frequency ratio $\Omega$ increases, because if the stiffness ratio is kept constant, the mass ratio decreases.

### 3.4.4. Effect of damping.

In this section the addition of damping to the compound system in its initial state i.e. when the masses are attached is considered. An initial viscous damping ratio $\zeta = \frac{c}{2\sqrt{km}}$ is considered and the damping constant $c$ remains unaltered and connected to the main mass $m - \Delta m$. As a result, the effective damping ratio will change when the systems are disconnected as a result of the stiffness and mass changes. This model is shown in figure 3.26. As in the simple model considered initially, damping effectively helps in further reducing the response. Moreover, its effect is very similar if compared to the passive mass-spring-damper model. However, the combination of the switchable stiffness strategy plus some external form of damping (viscous damping in this case) will result in better isolation performance. The effect of damping can be more easily illustrated by figure 3.27, for both the simple and the compound models. The figure shows the ratio between the maximax response of the damped compound model and the passive undamped model. The passive model is taken as a reference in order to have a point of comparison of the performance of the damped compound model. For this plot a representative value of the stiffness reduction ratio of $\sigma = 0.7$ has been considered, and for the compound model (dashed line) with a frequency ratio of $\Omega$ = 5 which requires a corresponding mass ratio of 0.085. The period ratio is $\hat{\tau}_{\text{initial}} = 1$ for this case, because this is the zone where viscous damping has the greatest effect in the passive model. In general the reduction in the response is not very significant (very similar to the passive case), and the behaviour is almost the same for the simple (only switchable stiffness) and the compound model. However, the performance of the simple model is slightly better as the mass does not change. The effect of damping on both models is very similar, showing slightly lower levels of response for the simple model. As a result, the optimum situation for the compound model, which can be more realisable in the practice, is when the secondary mass is very small and it

approaches the simple model. In the situation of acceleration response, the behaviour is very similar to the simple model as well, where high levels of acceleration might cause the response to increase in the quasistatic region.

These conclusions can be further justified considering the SRS plots presented in figure 3.28. The bold line included represents the SRS for the passive model, which is included for comparison. Although the overall response reductions are more considerable, this is a result of the combination of both damping and switchable stiffness strategies, as the effect of damping alone remains fairly insignificant, and it is very similar to the effect observed in the simple mass-spring-damper model.

## 3.5. Conclusions

The dynamics of a switchable stiffness single degree-of-freedom model subjected to a shock pulse excitation have been analyzed. The switchable stiffness strategy considers a reduction in the system effective stiffness whilst a shock pulse is being applied, and then recovers the original stiffness after the pulse is over. In the first part of the chapter a conceptual simple model with two parallel springs was considered. One of the springs is disconnected at some point in time. It has been shown theoretically that a stiffness reduction will cause a reduction in the absolute displacement and acceleration responses, i.e. when the duration of the pulse is less than the natural period of the system. Otherwise, very high stiffness reductions are needed to obtain a reduction in the response, i.e. more than 90% stiffness reduction. The effect of a delay in the stiffness change has been studied, showing that if the delay is small enough (less than 1% of the shock pulse duration) the effect is negligible, but for larger delays the response in some situations can be amplified. The effect of viscous damping was also considered, and though its effect is small, it improves the shock isolation.

The second part of the chapter introduced the concept of a compound model, where a combined secondary mass-spring system is the element that connects and disconnects in order to change the primary system dynamic characteristics. The dynamics of both systems have been considered in order to determine the moment when the systems might reconnect after the input with an inelastic connection. Since this new model also involves a mass change, it is desirable to have a small secondary mass compared to the main mass, since the effect of the

mass reduction is opposite to the stiffness reduction. As a result, the system reduces to the simple model studied initially, which is the optimum situation. The effect of damping was also considered. As before, damping improves shock isolation, but still the effect is small and not as significant as the possible benefits of applying the stiffness reduction strategy.

In conclusion, for a practical realisable model, the first simple model could be more feasible in practice. The performance of both systems is very similar, with a slightly better isolation in the case of the simple model. Moreover a secondary mass element is not required which eliminates the issues of clamping or attaching two masses as the compound model requires. If a variable or switchable stiffness device capable of a quick and high stiffness reduction (at least 50%) with low damping is available or designed the switching strategy could be implemented practically. As a result, the main use of such a system will be reducing the peak shock responses of absolute acceleration and displacement. There will be no great advantages for relative motion but the performance will not be worst than the passive case.

The rapid suppression of the residual vibration resulting after the shock has ended is the subject of study in the next chapter. The approach is also based on stiffness switching but different strategies are analyzed to achieve the objective.

| | $\Omega = 2$ | $\Omega = 3$ |
|---|---|---|
| $\sigma$ | $\mu$ | $\mu$ |
| 0.1 | 0.027 | 0.012 |
| 0.2 | 0.0588 | 0.027 |
| 0.3 | 0.096 | 0.045 |
| 0.4 | 0.14 | 0.068 |
| 0.5 | 0.2 | 0.1 |
| 0.6 | 0.272 | 0.142 |
| 0.7 | 0.368 | 0.205 |
| 0.8 | 0.5 | 0.307 |
| 0.9 | 0.692 | 0.5 |

Table 3.1. Values of mass ratio $\mu$ and stiffness ratio $\sigma$ corresponding to two values of frequency ratio $\Omega$. The values are for the compound model with a secondary mass-stiffness system.

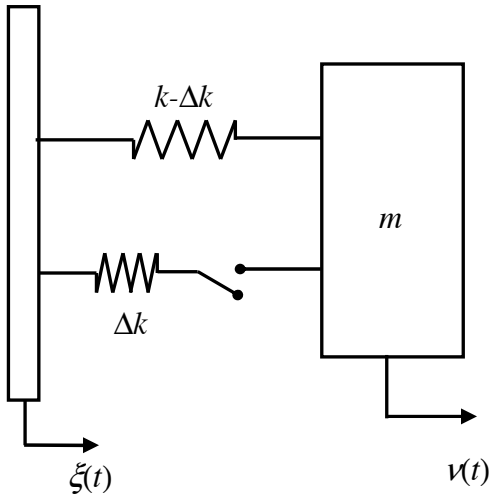


Figure 3.1. Single degree-of-freedom conceptual model with switchable stiffness under a shock excitation $\xi(t)$ applied to the base.

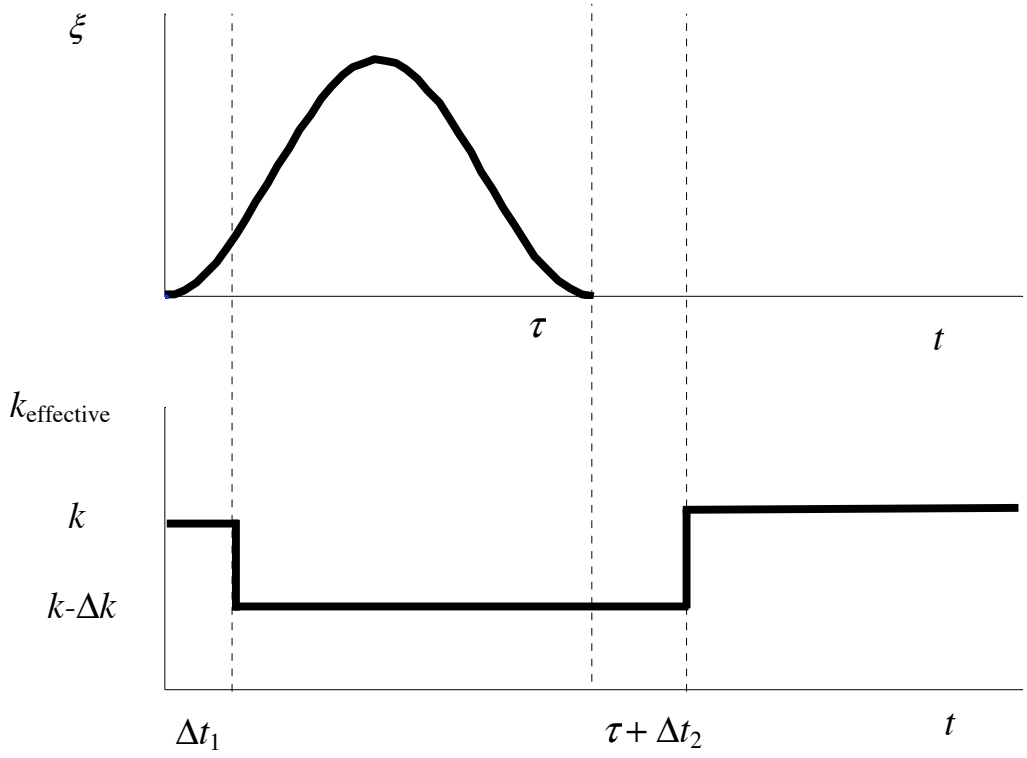


Figure 3.2. Schematic representation of the stiffness variation $k_{efffective}$ during a shock pulse excitation $\xi(t)$. The time $\Delta t_1$ represents the delay between the beginning of the shock, and the reduction of the stiffness. The stiffness is recovered at time $\Delta t_2$ after the pulse has finished at $t = \tau$.

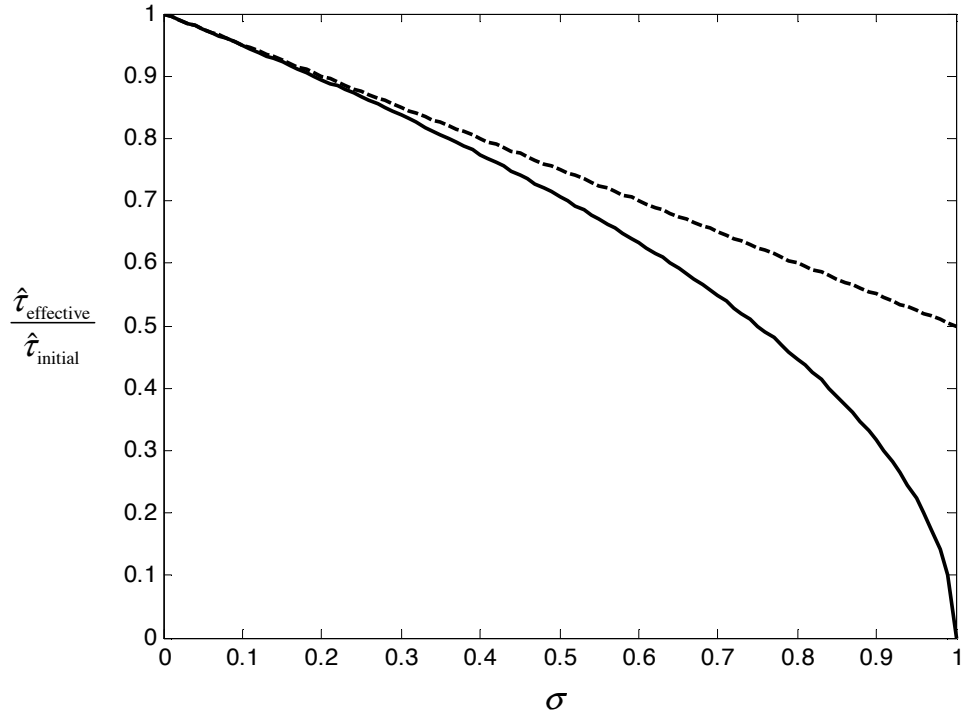


Figure 3.3 Normalised period ratio $\frac{\hat{\tau}_{\text{low}}}{\hat{\tau}_{\text{high}}} = \sqrt{1-\sigma}$ as a function of the stiffness reduction ratio $\sigma = \frac{\Delta k}{k}$ (continuous). Linear approximation $1-\sigma/2$ for small values of the period ratio (dashed).

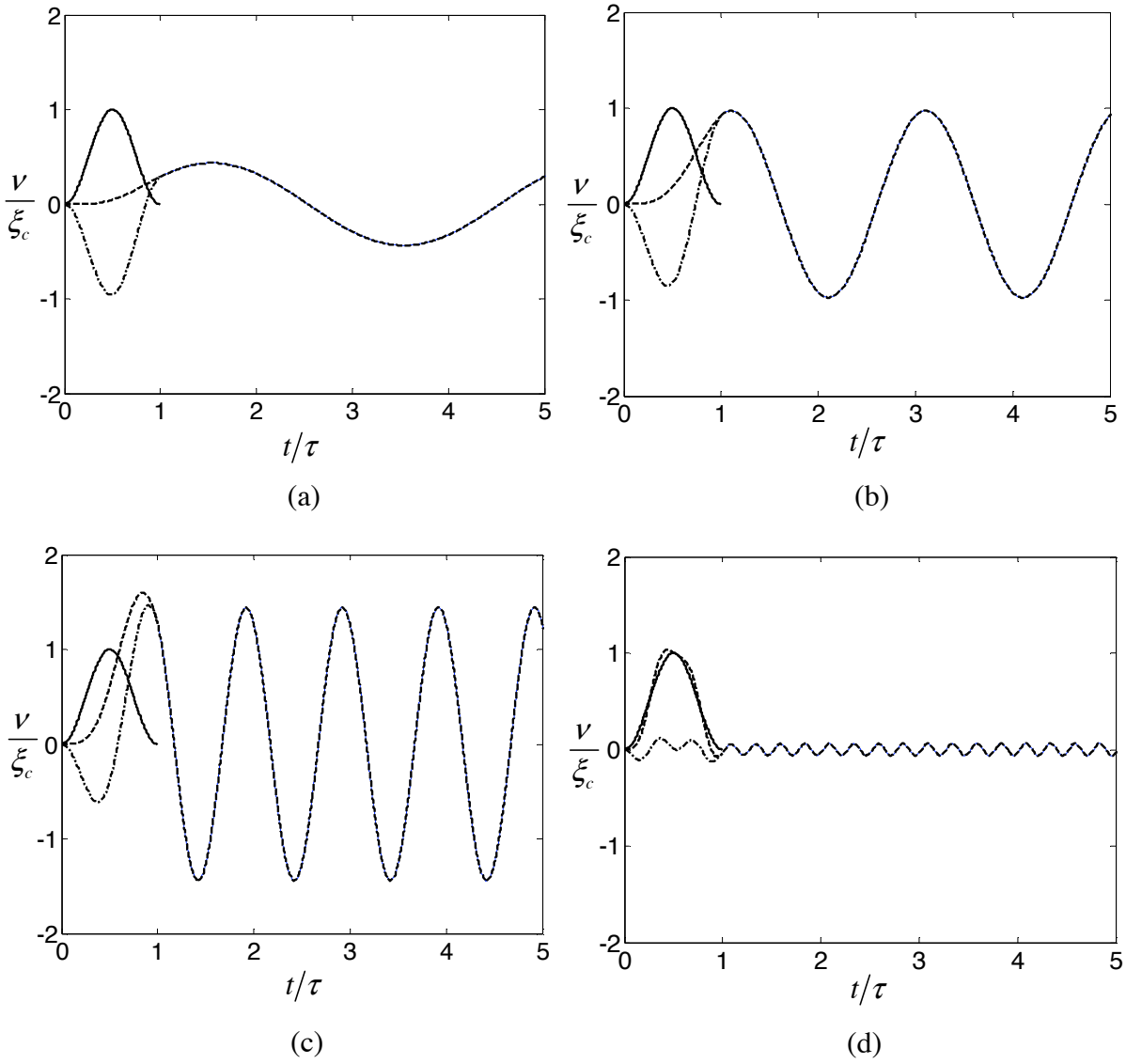


Figure 3.4.Time responses for absolute displacement (dashed) and relative displacement (dash-dot) for stiffness reduction factor $\sigma = 0.5$ and different values of the period ratio $\hat{\tau}_{\text{high}}$. The solid line represents the versed sine excitation. (a) $\hat{\tau}_{\text{high}} = 0.25$, (b) $\hat{\tau}_{\text{high}} = 0.5$, (c) $\hat{\tau}_{\text{high}} = 1$, (d) $\hat{\tau}_{\text{high}} = 2$.

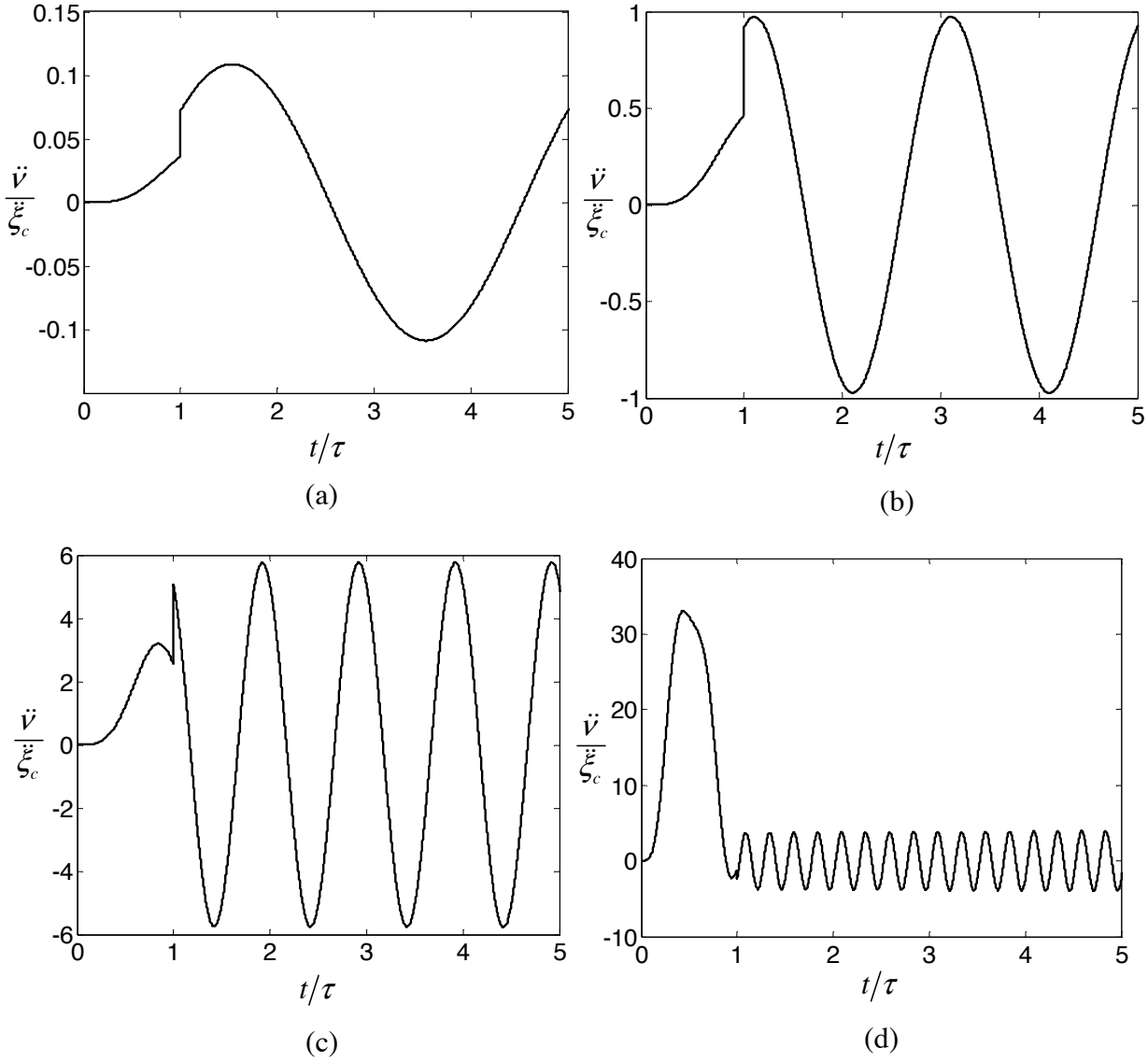


Figure 3.5 Time responses for absolute acceleration considering a stiffness reduction factor $\sigma = 0.5$ and different values of the period ratio period ratio $\hat{\tau}_{\text{high}}$. (a) $\hat{\tau}_{\text{high}} = 0.25$, (b) $\hat{\tau}_{\text{high}} = 0.5$, (c) $\hat{\tau}_{\text{high}} = 1$, (d) $\hat{\tau}_{\text{high}} = 2$.

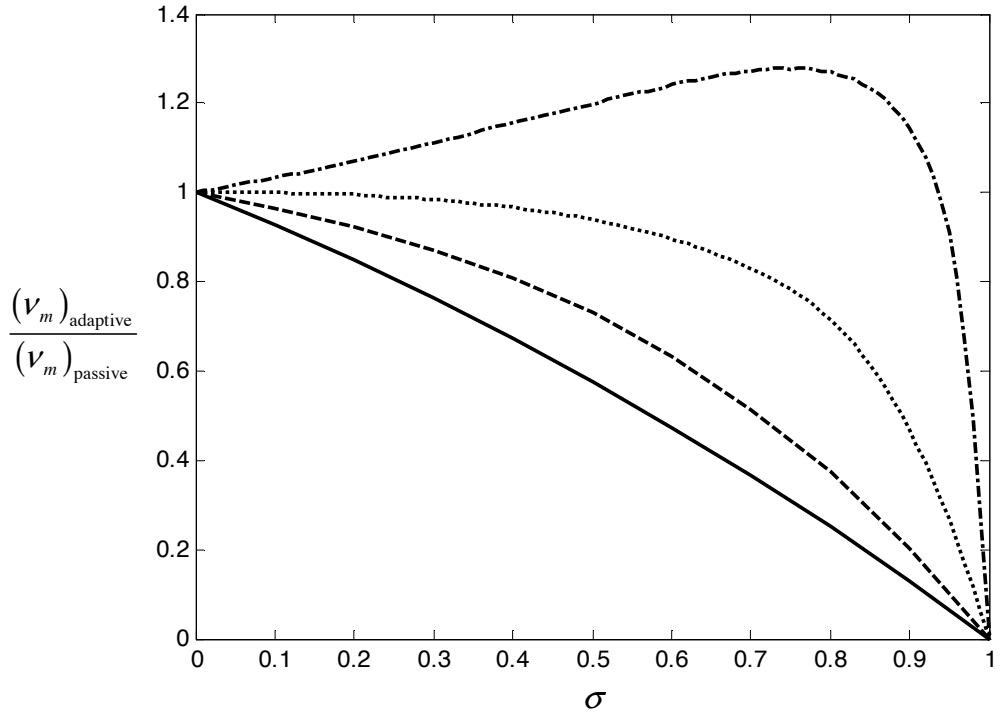


Figure 3.6. Ratio between the absolute displacement responses of the switchable stiffness model $(\nu_m)_{\text{adaptive}}$ and the passive model $(\nu_m)_{\text{passive}}$ as a function of the stiffness reduction factor $(-\hat{\tau}_{\text{high}} = 0.25\,;\, --\hat{\tau}_{\text{high}} = 0.5\,;\, \cdots\ \hat{\tau}_{\text{high}} = 1\,;\, \text{-·-}\ \hat{\tau}_{\text{high}} = 2)$.

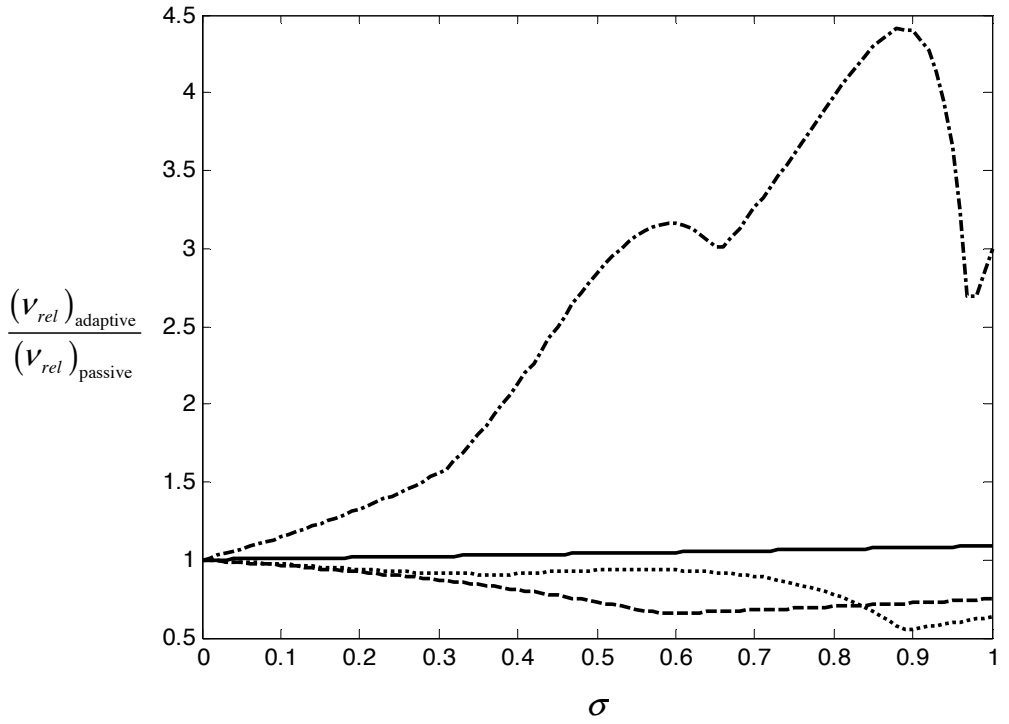


Figure 3.7. Ratio between the relative displacement responses of the switchable stiffness model $(\nu_{rel})_{\text{adaptive}}$ and the passive model $(\nu_{rel})_{\text{passive}}$ as a function of the stiffness reduction factor $\sigma$. $(-\hat{\tau}_{\text{high}} = 0.25\,;\, --\hat{\tau}_{\text{high}} = 0.5\,;\, \cdots\ \hat{\tau}_{\text{high}} = 1\,;\, \text{-·-}\ \hat{\tau}_{\text{high}} = 2)$.

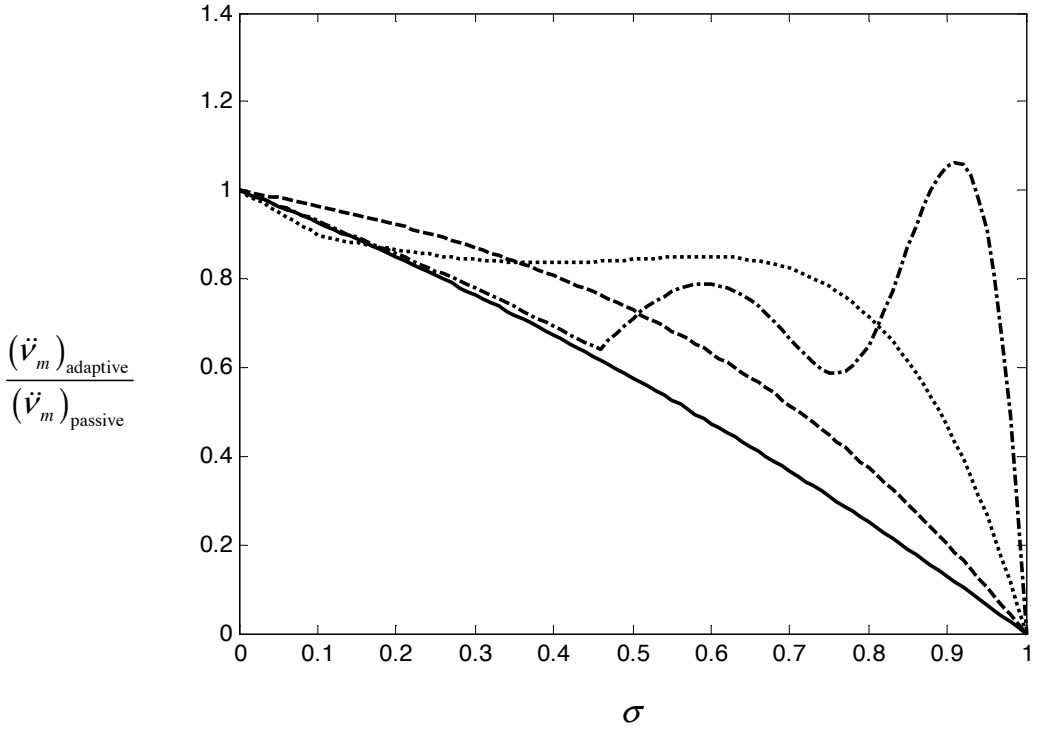


Figure 3.8. Ratio between the absolute acceleration response of the switchable stiffness model $(\ddot{v}_m)_{\text{adaptive}}$ and the passive model $(\ddot{v}_m)_{\text{adaptive}}$ as a function of the stiffness factor ($-\hat{\tau}_{\text{high}} = 0.25$ ; $--\hat{\tau}_{\text{high}} = 0.5$ ; ··· $\hat{\tau}_{\text{high}} = 1$ ; -·- $\hat{\tau}_{\text{high}} = 2$ ).

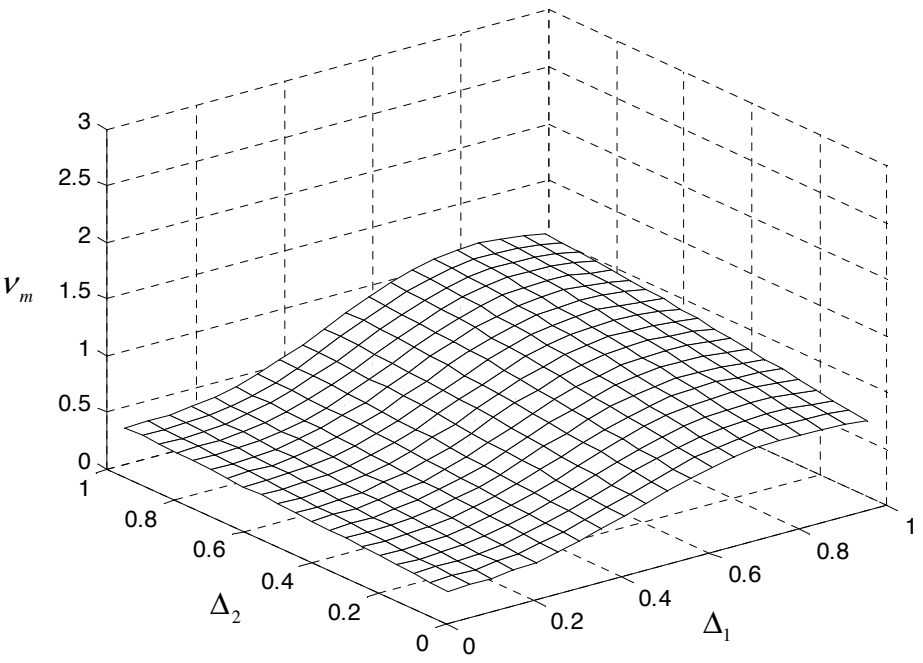


(a)

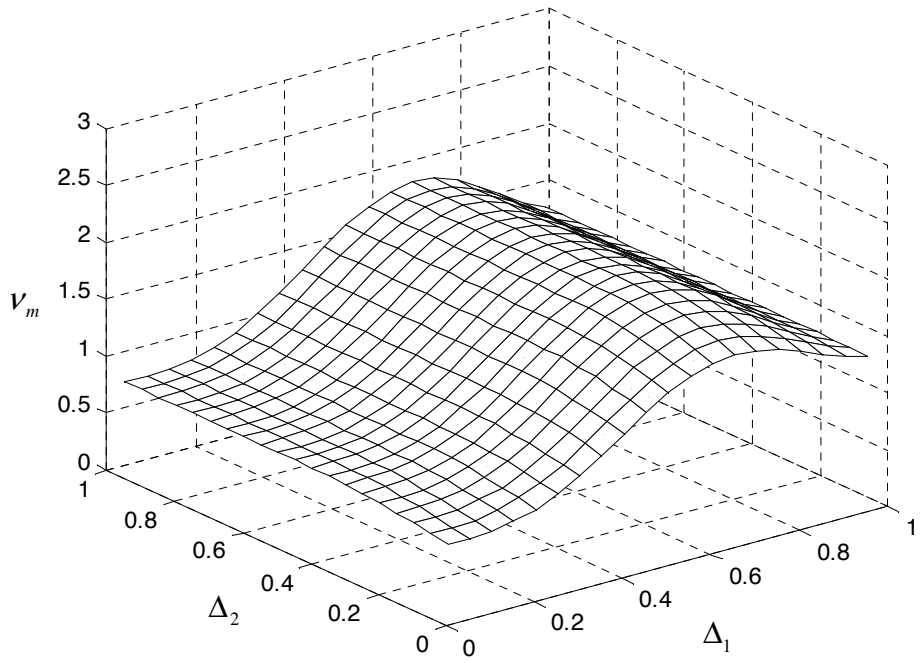


(b)

Figure 3.9. Effect of a time delay in the stiffness reduction $\Delta_1 = \frac{\Delta t_1}{\tau}$ and in the stiffness recovery $\Delta_2 = \frac{\Delta t_2}{\tau}$ on the maximax response of the normalised absolute displacement, for a switchable stiffness system, under a versed sine pulse excitation. (a) $\hat{\tau}_{\text{initial}} = 0.25$, (b) $\hat{\tau}_{\text{initial}} = 0.5$.

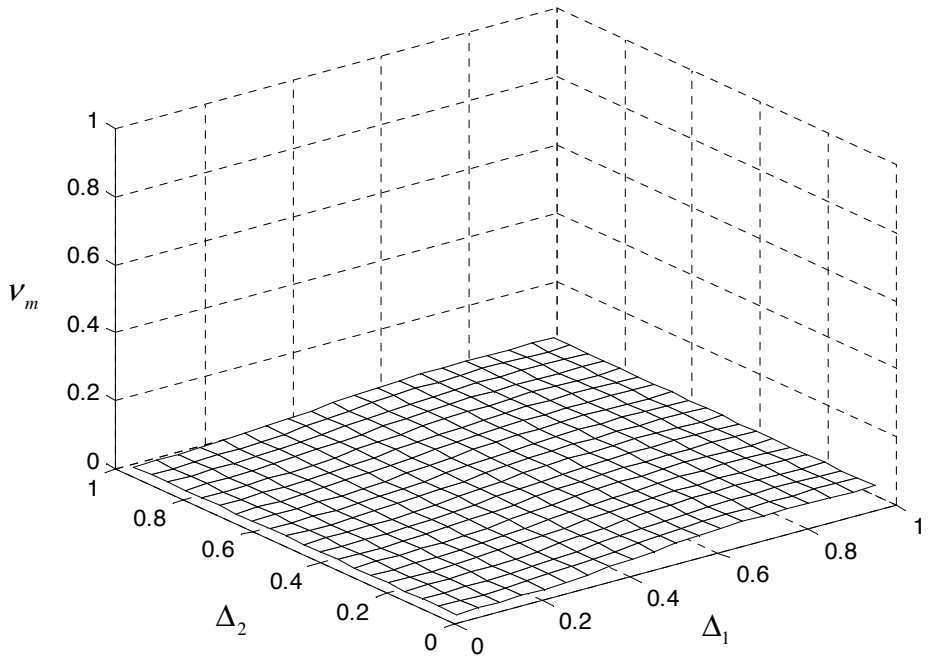


(a)

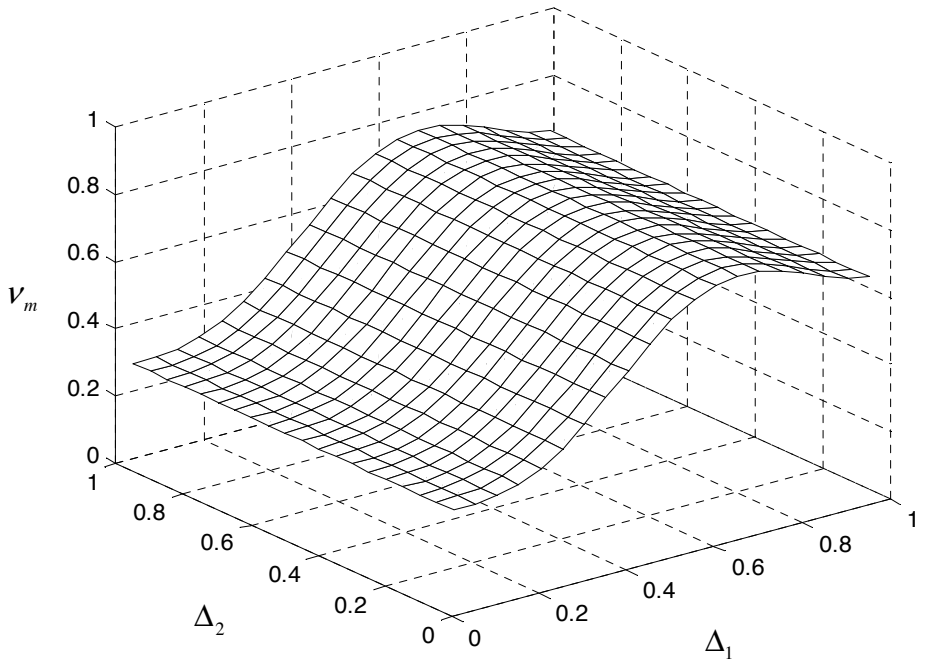


(b)

Figure 3.10. Effect of a time delay in the stiffness reduction $\Delta_1 = \frac{\Delta t_1}{\tau}$ and in the stiffness recovery $\Delta_2 = \frac{\Delta t_2}{\tau}$ on the maximax response of the normalised absolute acceleration, for a variable stiffness system, under a versed sine pulse excitation. (a) $\hat{\tau}_{\text{initial}} = 0.25$, (b) $\hat{\tau}_{\text{initial}} = 0.5$.

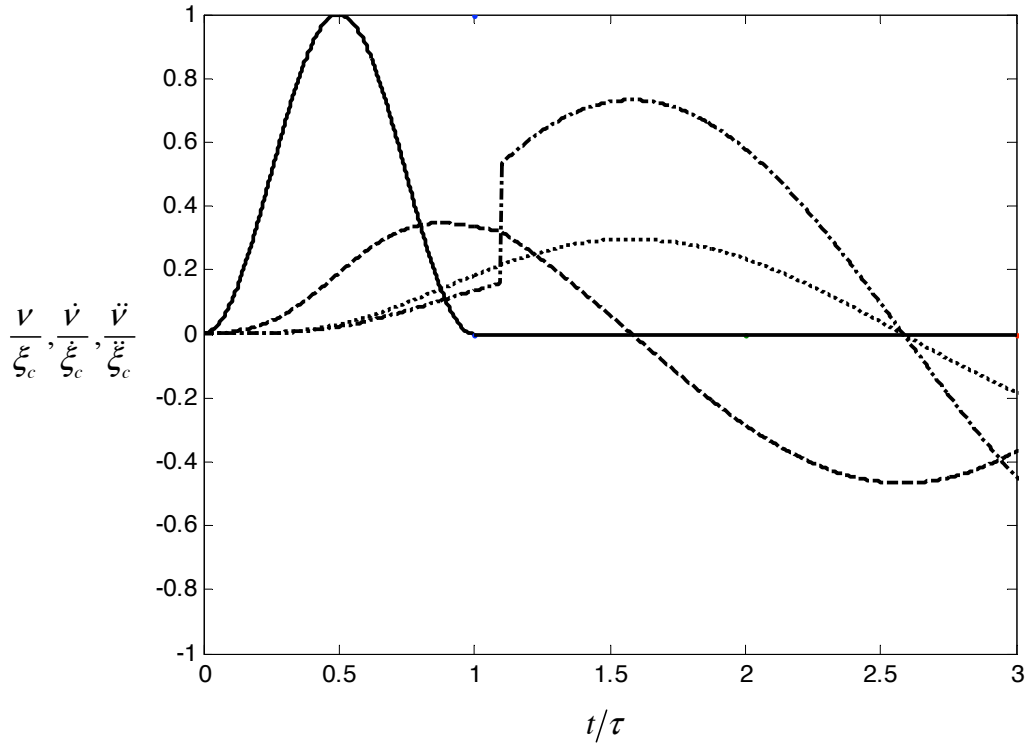


Figure 3.11. Example of time responses for a system with switchable stiffness for versed sine excitation. $\sigma = 0.7$, $\hat{\tau}_{\text{high}} = 0.25$ and delays $\Delta_1 = \Delta_2 = 0.1$. (— Pulse, --- $\frac{\nu}{\xi_c}$, ··· $\frac{\dot{\nu}}{\dot{\xi}_c}$, -·- $\frac{\ddot{\nu}}{\ddot{\xi}_c}$)

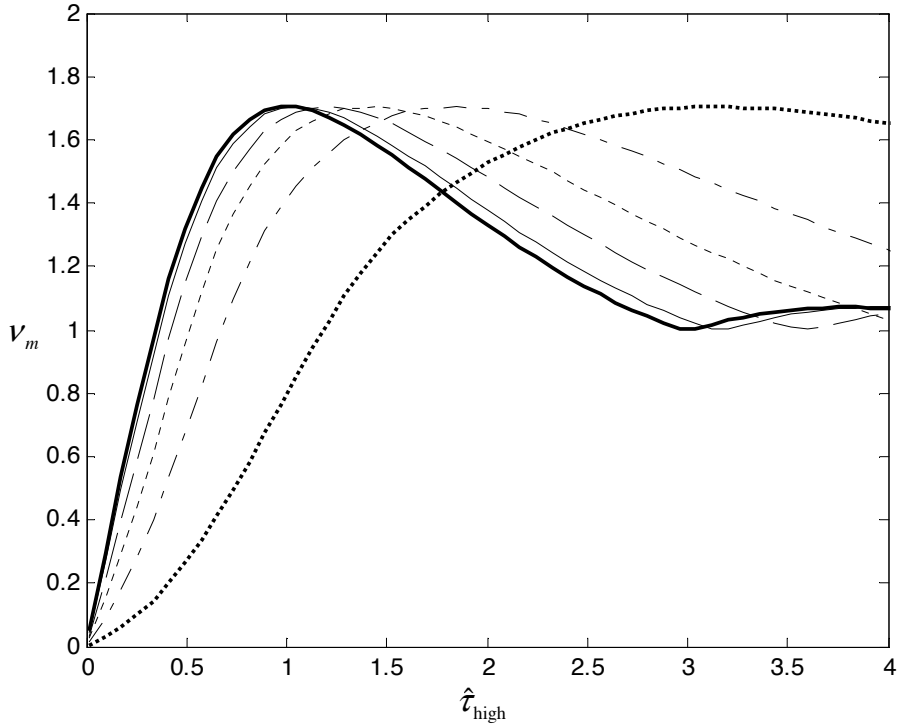


Figure 3.12. Shock Response Spectra of the switching stiffness adaptive systems for versed sine pulse excitation and delays $\Delta_1 = \Delta_2 = 0.01$. The bold line represents the passive system. (— $\sigma = 0$; — $\sigma = 0.1$; – – $\sigma = 0.3$; - - $\sigma = 0.5$; – - – $\sigma = 0.7$; ··· $\sigma = 0.9$).

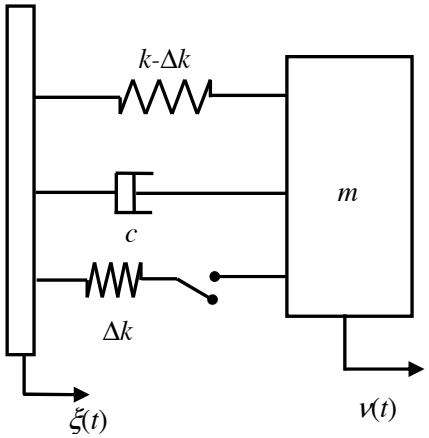


Figure 3.13. Viscously damped single degree-of-freedom model with switchable stiffness under shock excitation $\xi(t)$ applied at the base.

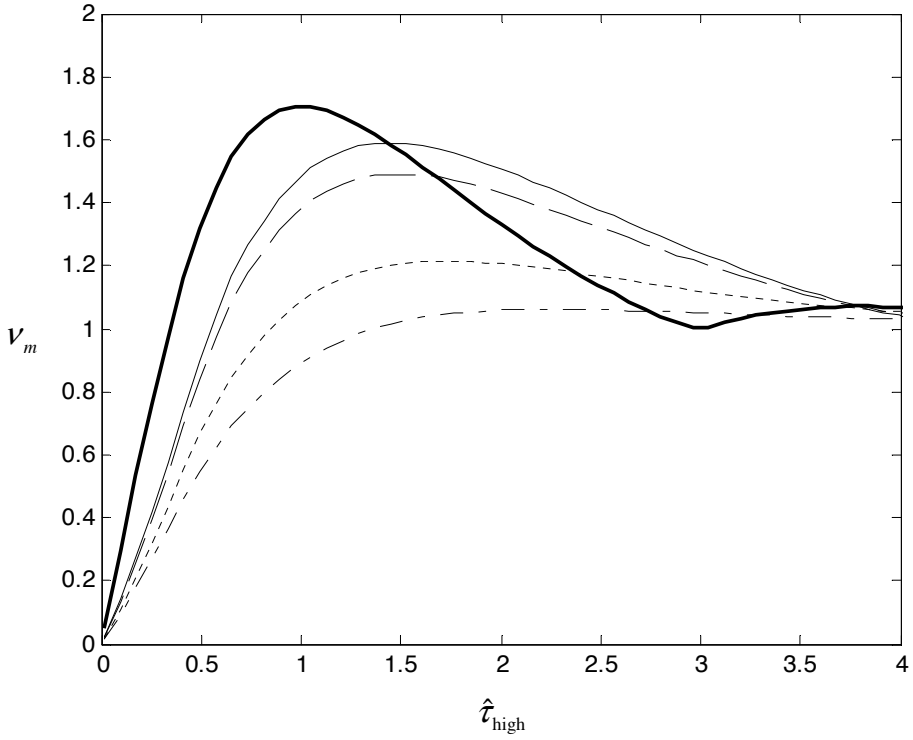


Figure 3.14. Shock Response Spectra for a versed sine pulse considering the effect of viscous damping, for a stiffness reduction factor $\sigma = 0.5$. The bold line is for a passive undamped model. (— $\zeta = 0.05$; – – $\zeta = 0.1$; - - $\zeta = 0.3$; – - – $\zeta = 0.5$).

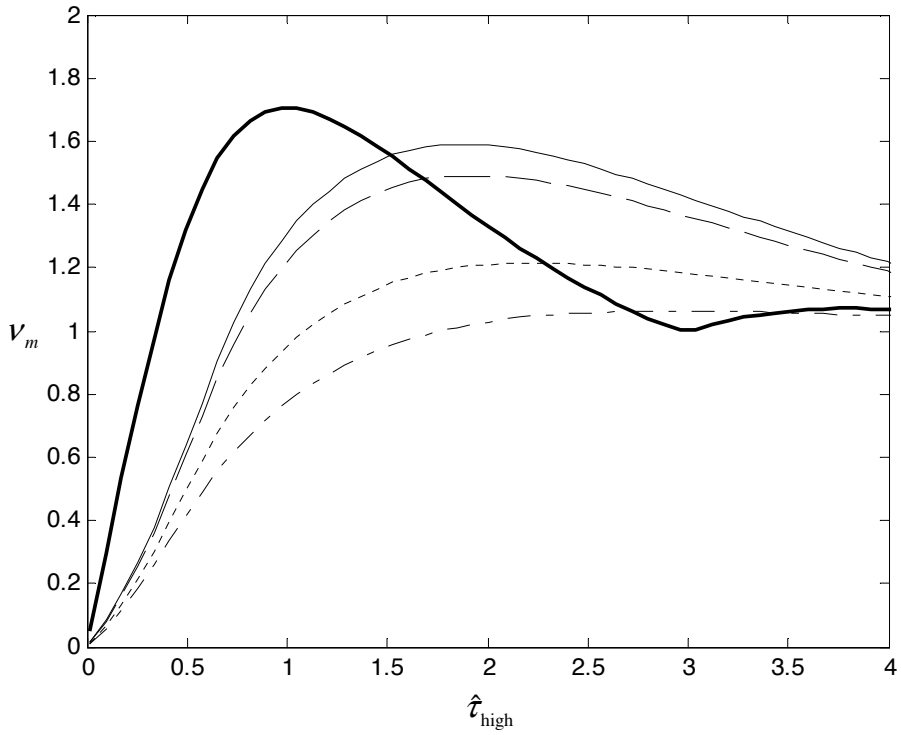


Figure 3.15. Displacement Shock Response Spectra for a versed sine pulse considering the effect of viscous damping, for a stiffness reduction factor $\sigma = 0.7$. The bold line is for a passive undamped model. (— $\zeta = 0.05$; – – $\zeta = 0.1$; - - $\zeta = 0.3$; – - – $\zeta = 0.5$)

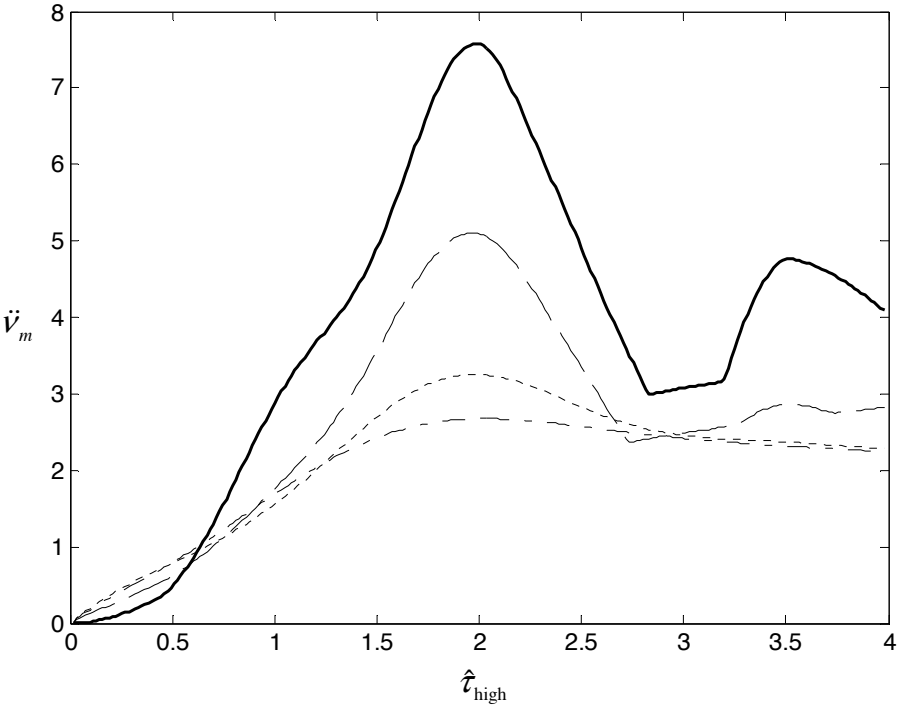


Figure 3.16. Acceleration Shock Response Spectra for a versed sine pulse considering the effect of viscous damping, for a stiffness reduction factor $\sigma = 0.5$. The bold line is for a passive undamped model. — $\zeta = 0$; – – $\zeta = 0.1$; - - $\zeta = 0.3$; – - – $\zeta = 0.5$)

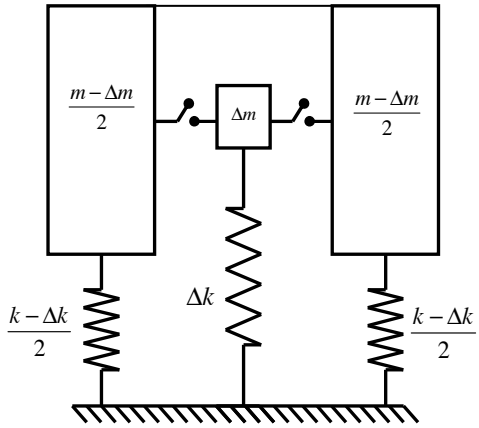


Figure 3.17. Conceptual sketch for a switchable stiffness/mass system. The secondary mass can oscillate independently inside the main mass while it is disconnected.

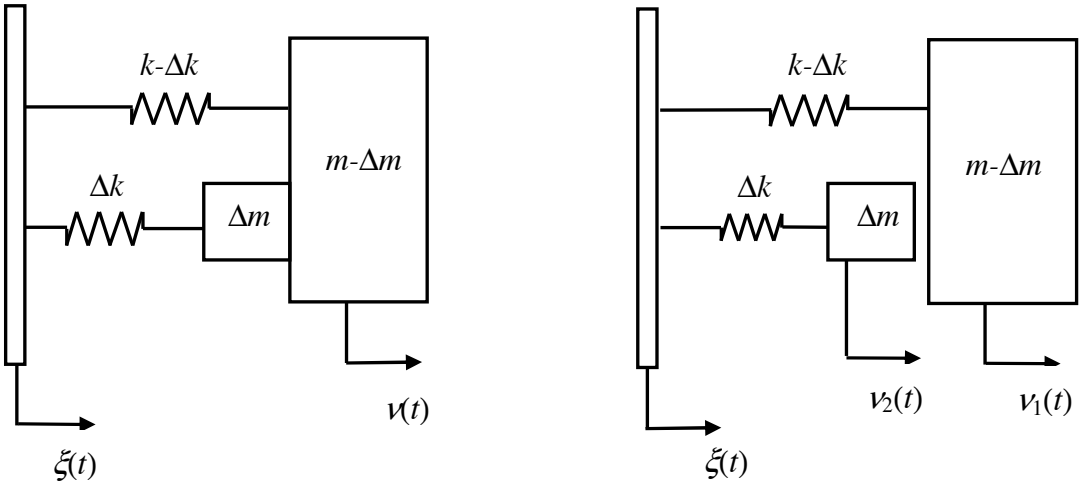


Figure 3.18. Compound model comprising two single degree-of-freedom models that can oscillate together (a) or independently (b).

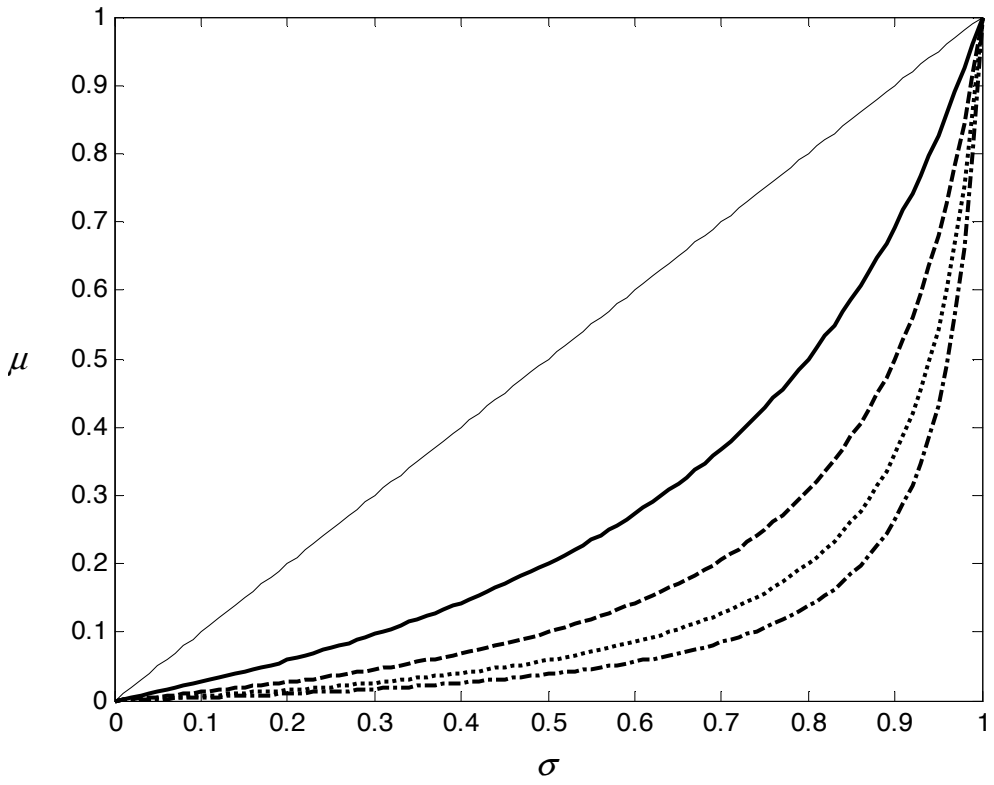


Figure 3.19. Values of the mass ratio $\mu = \frac{\Delta m}{m}$ and the stiffness reduction ratio $\sigma = \frac{\Delta k}{k}$ corresponding to several integer values of the frequency ratio $\Omega = \frac{\omega_s}{\omega_p}$.

(— Ω = 1; ─ Ω = 2; --- Ω = 3; ··· Ω = 4; -·- Ω = 5).

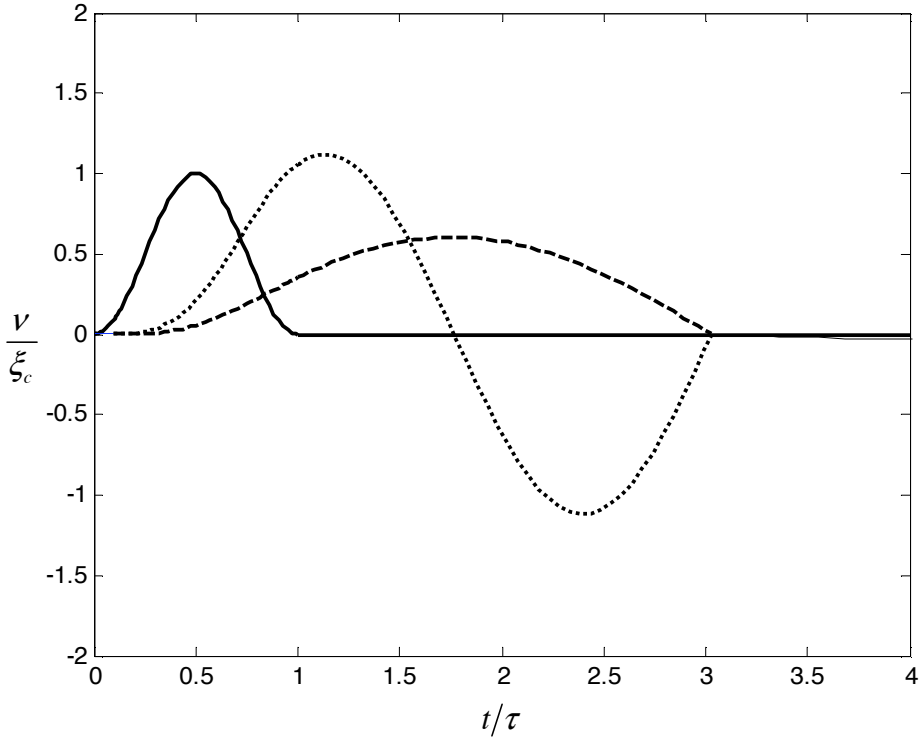


(a)

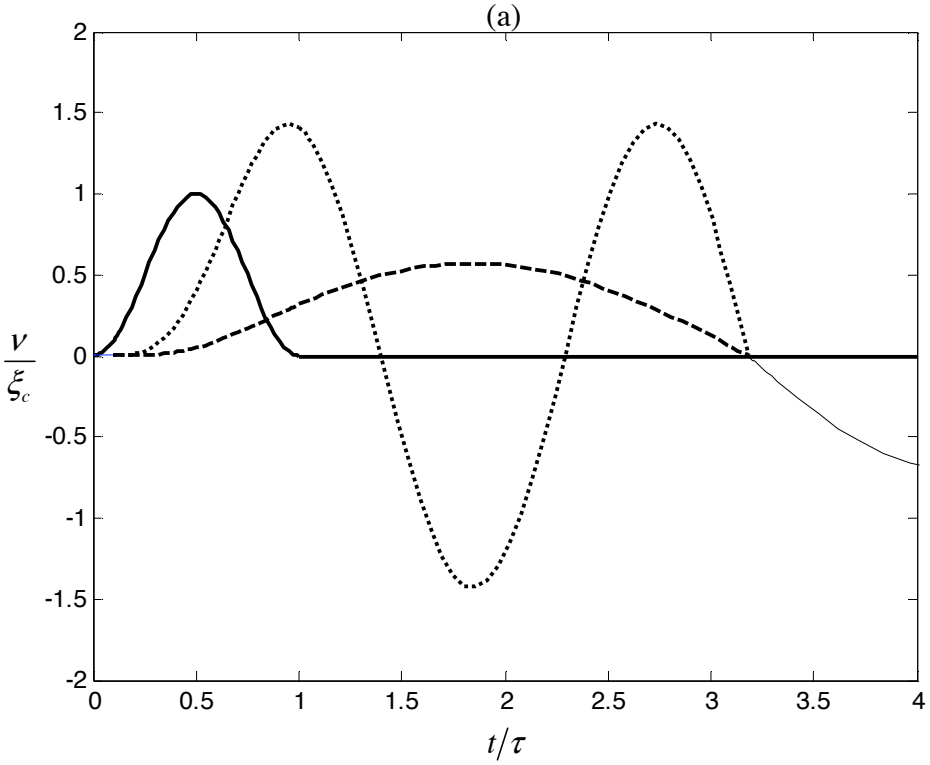


(b)

Figure 3.20. Displacement time response for the primary (---) and secondary (····) masses, showing the moment when the systems recombine with an inelastic impact. The continuous bold line represents the versed sine input. The thin line represents the response after the systems reconnect. The period ratio is $\hat{\tau}_{\text{high}} = 0.25$ , and the values of frequency ratio Ω are: (a) Ω = 2 and (b) Ω = 3.

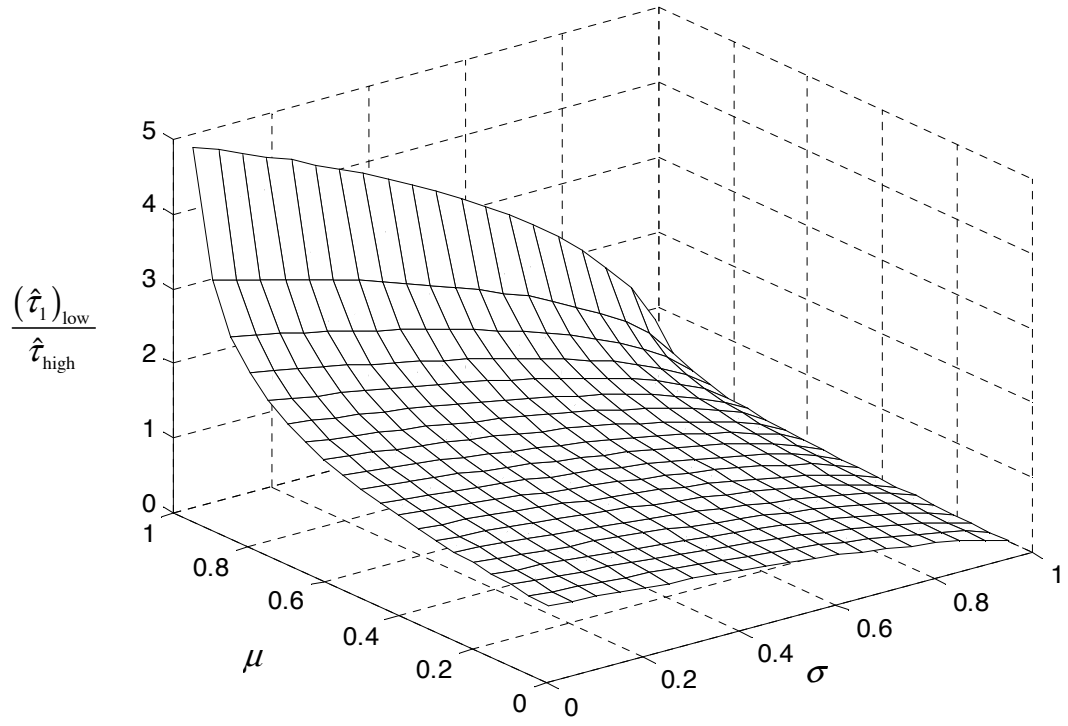


(a)

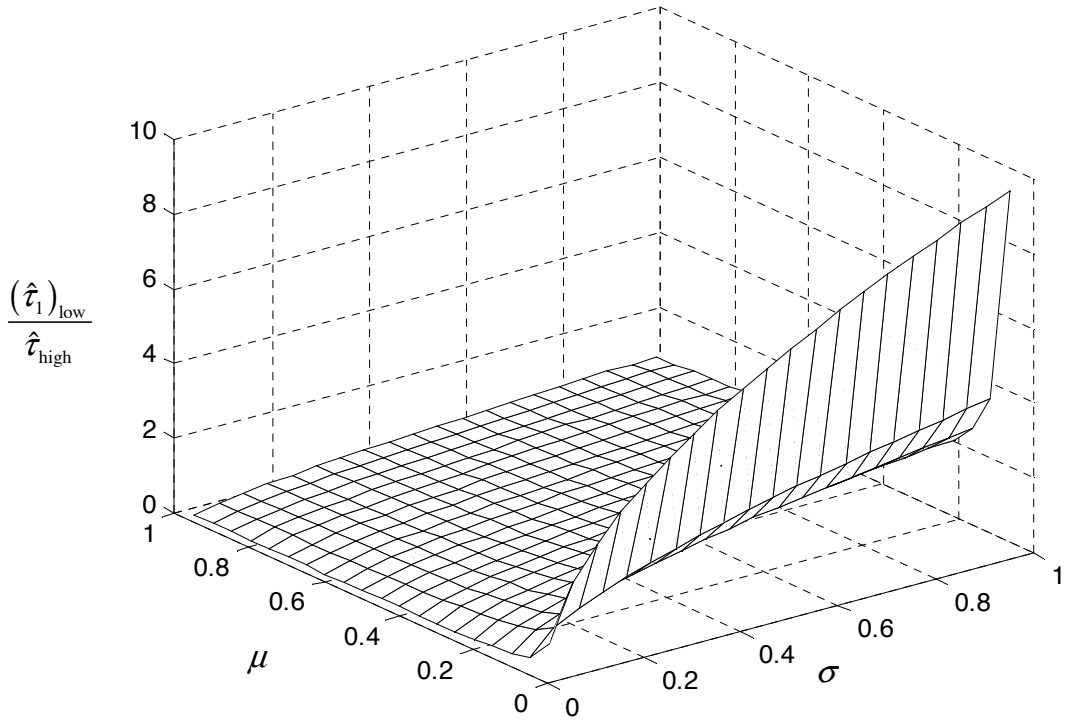


(b)

Figure 3.21. Variation in the period ratio $\hat{\tau}$ as a result of the stiffness and mass change. (a) Primary system and (b) Secondary system.

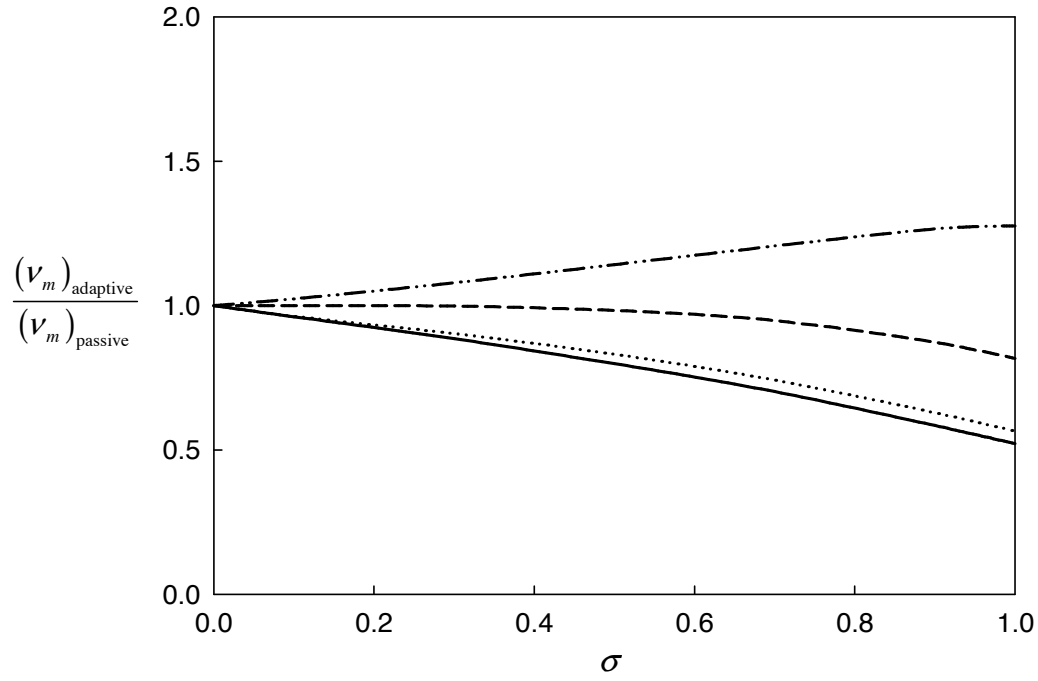


(a)

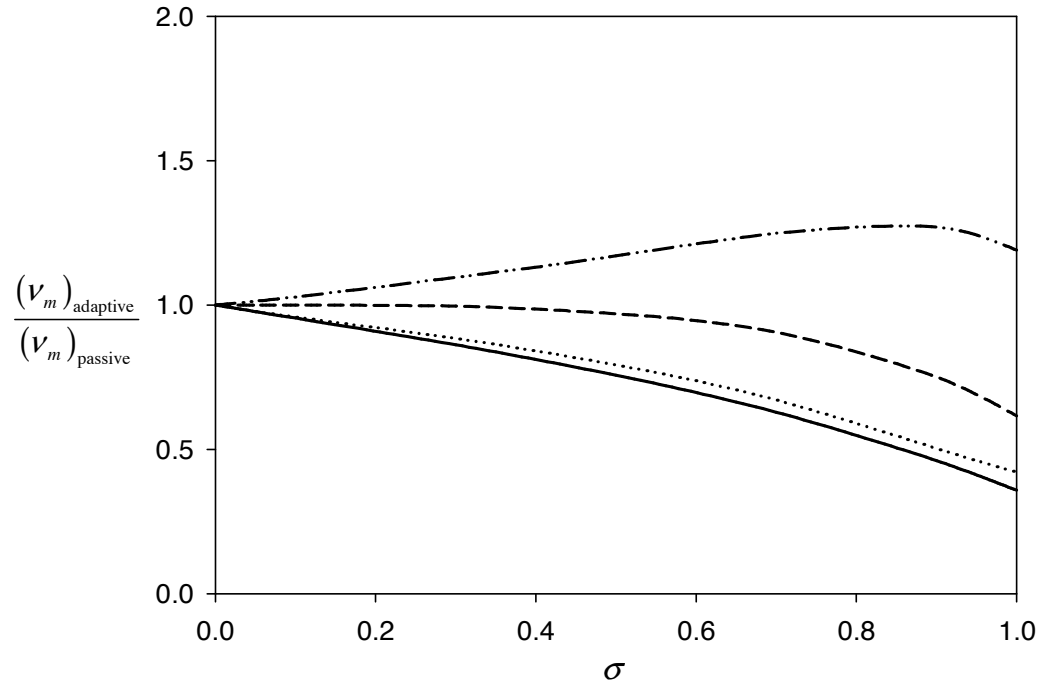


(b)

Figure 3.22. Ratio between the displacement response of the compound model and the passive model under a versed sine pulse, as a function of the stiffness reduction factor $\sigma$ given for two values of the frequency ratio between the primary and secondary systems (a) $\Omega = 2$ and (b) $\Omega = 3$ (— $\hat{\tau}_{\text{high}} = 0.25$ ;··· $\hat{\tau}_{\text{high}} = 0.5$ ;--- $\hat{\tau}_{\text{high}} = 1$ ; -·-· $\hat{\tau}_{\text{high}} = 2$ ).

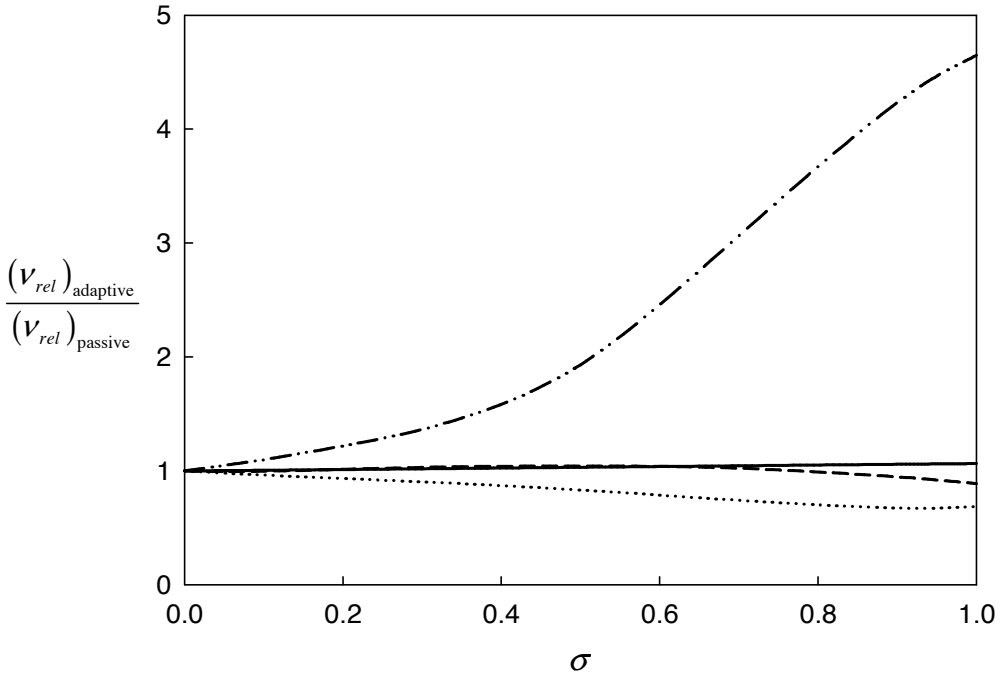


(a)

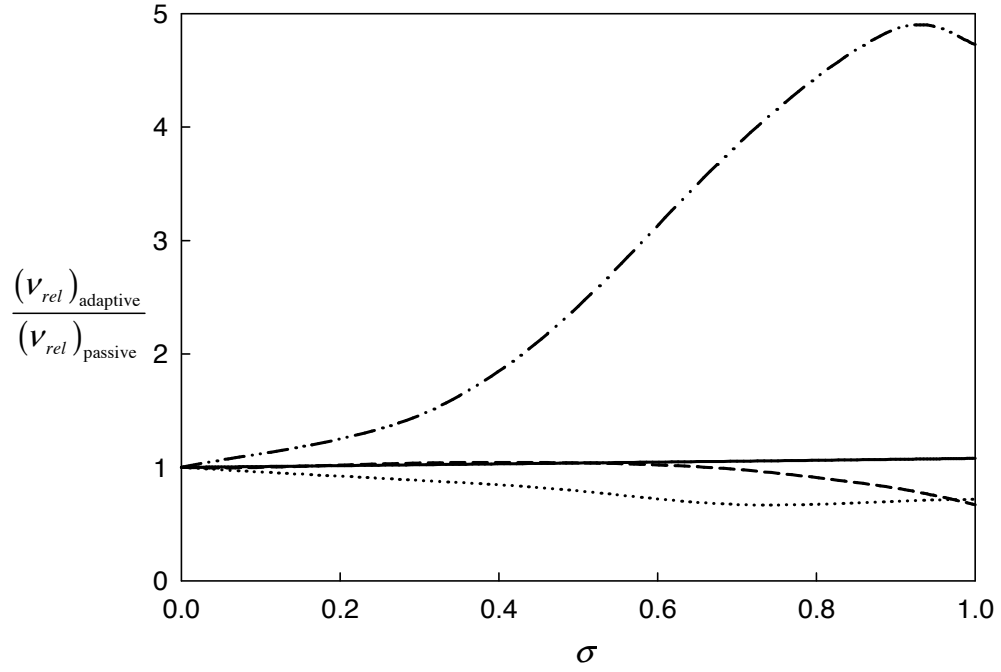


(b)

Figure 3.23. Ratio between the relative displacement response of the compound model and the passive model under a versed sine pulse, as a function of reduction factor $\sigma$ given for two values of the frequency ratio between the primary and secondary systems (a) $\Omega = 2$ and (b) $\Omega = 3$ ($-\hat{\tau}_{\text{high}} = 0.25$ ; $\cdots\ \hat{\tau}_{\text{high}} = 0.5$ ; $---\ \hat{\tau}_{\text{high}} = 1$ ; $-\cdots-\ \hat{\tau}_{\text{high}} = 2$ ).

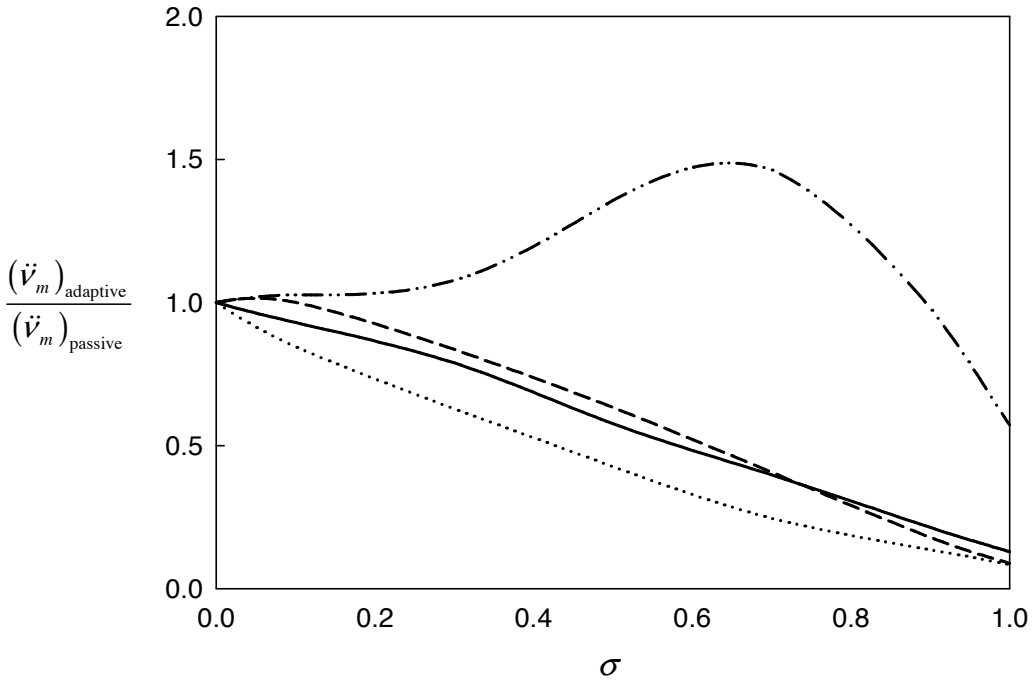


(a)

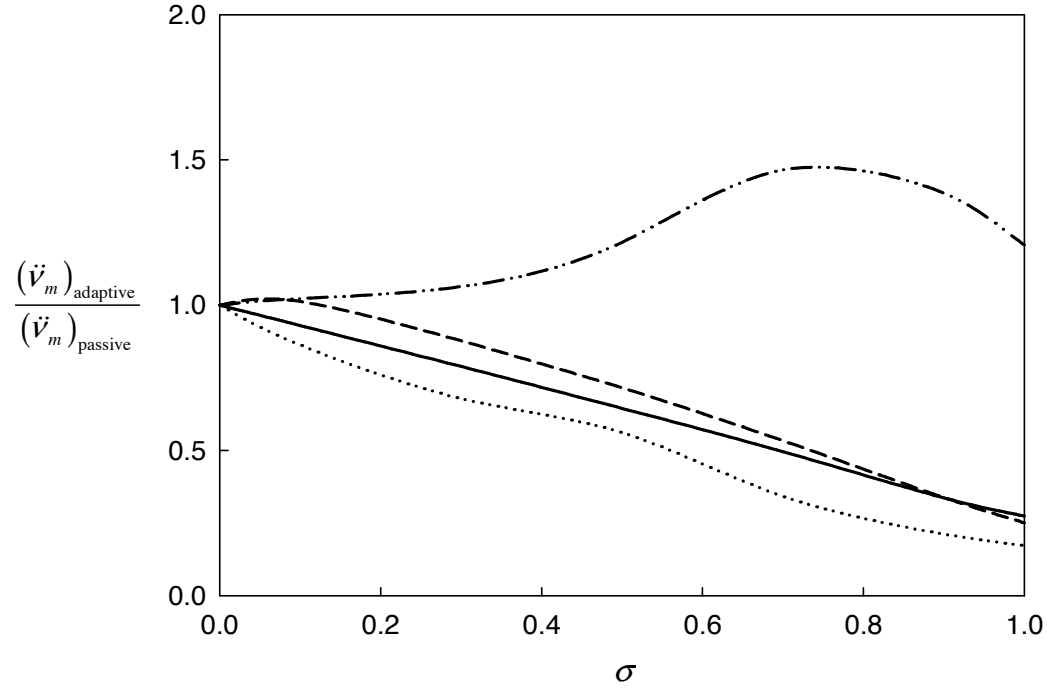


(b)

Figure 3.24. Ratio between the absolute acceleration response of the compound model and the passive model under a versed sine pulse, as a function of the reduction factor $\sigma$ given for two values of the frequency ratio between the primary and secondary systems (a) $\Omega = 2$ and (b) $\Omega = 3$ ($-\hat{\tau}_{\text{high}} = 0.25$ ; $\cdots\, \hat{\tau}_{\text{high}} = 0.5$ ; $\text{---}\, \hat{\tau}_{\text{high}} = 1$ ; $\text{-}\cdot\text{-}\, \hat{\tau}_{\text{high}} = 2$ ).

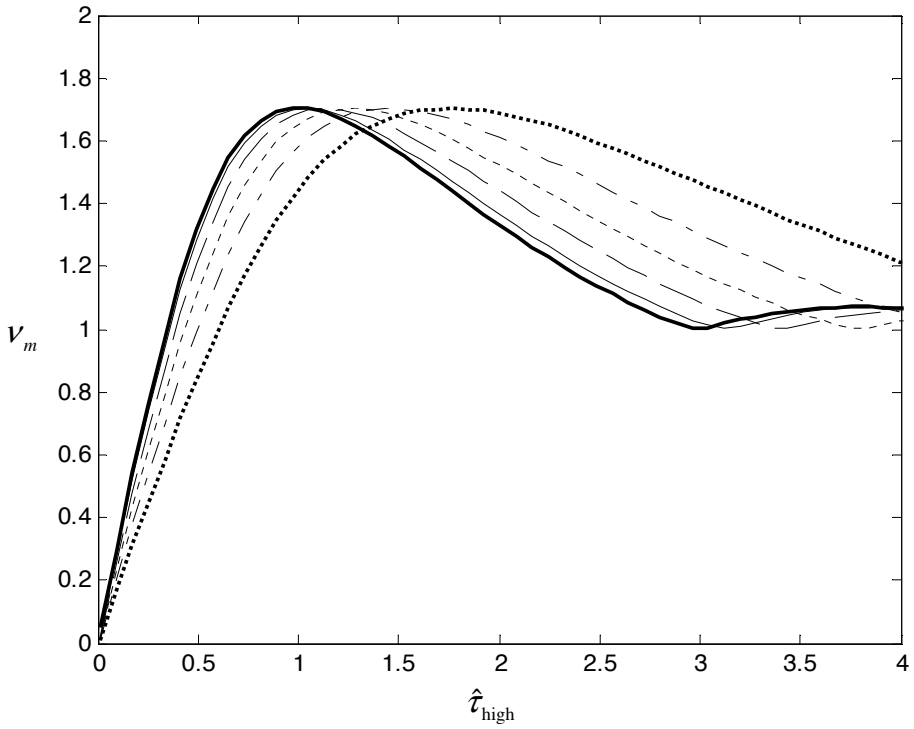


(a)

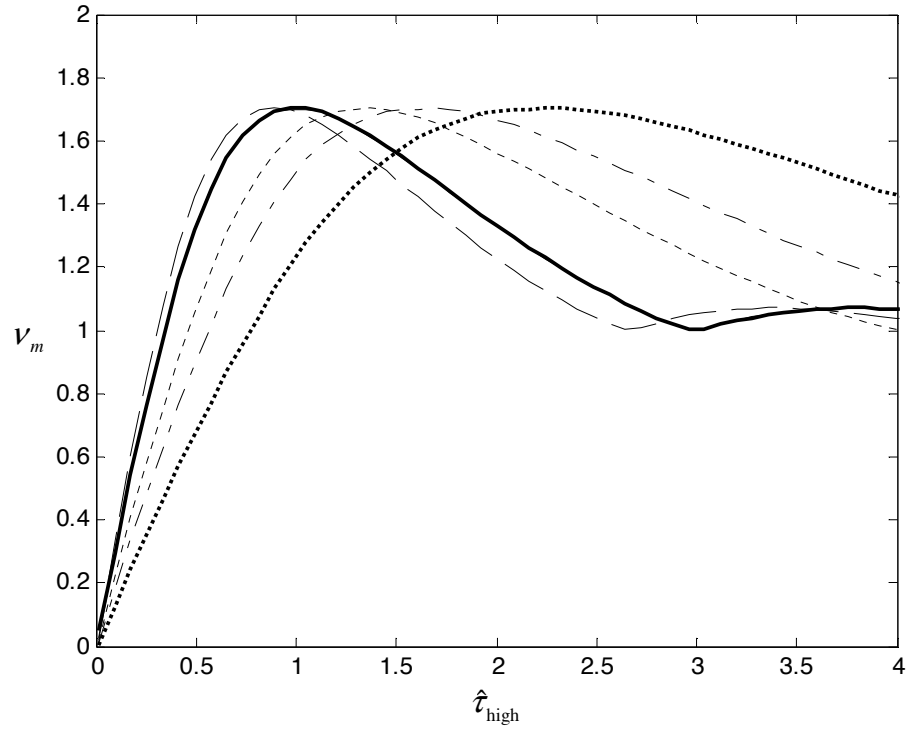


(b)

Figure 3.25. Shock response spectra for the compound model under versed sine excitation. The frequency ratio between primary and secondary systems are (a) $\Omega = 2$ and (b) $\Omega = 3$. The bold line represents the SRS corresponding to the undamped single degree-of-freedom model, while the other curves are given for different values of the stiffness reduction ratio $\sigma$. (—$\sigma = 0$; – $\sigma = 0.1$; – – $\sigma = 0.3$; - - - $\sigma = 0.5$; – - – $\sigma = 0.7$; ··· $\sigma = 0.9$)

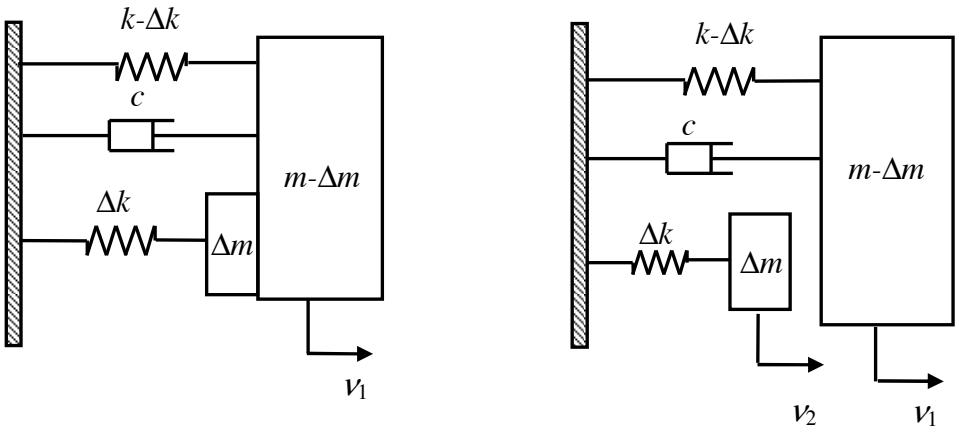


Figure 3.26. Conceptual compound model with viscous damping.

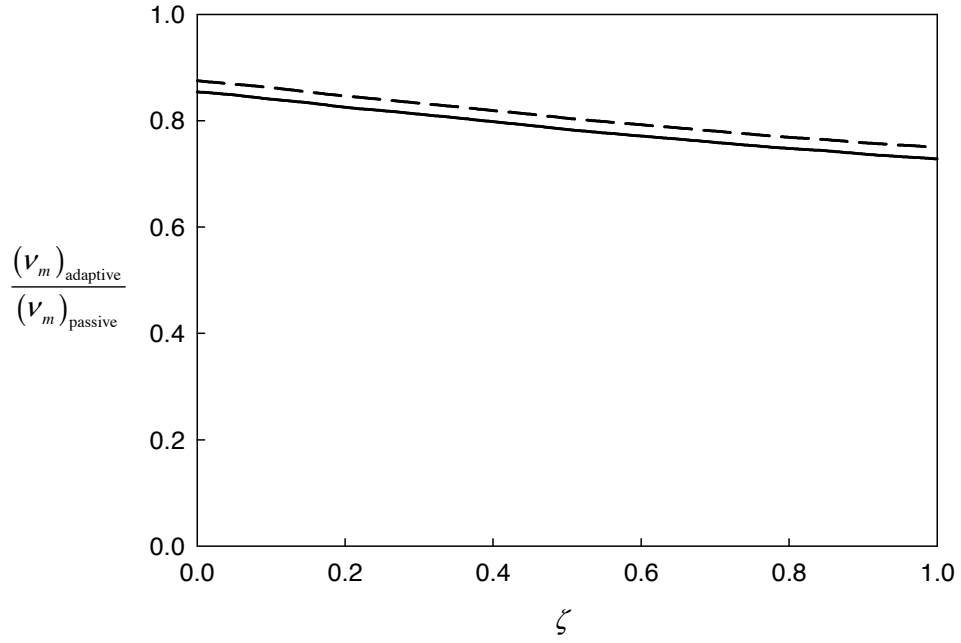


Figure 3.27. Effect of viscous damping in the different switchable stiffness models considered. The input is a versed sine considering a period ratio of $\hat{\tau}_{\text{high}} = 1$. The compound model comprises two single degree-of-freedom systems considering a stiffness reduiction ratio of $\sigma = 0.7$, a mass ratio of $\mu = 0.085$ and an undamped frequency ratio of $\Omega = 5$. The damping ratio is given by the initial state as $\zeta = \frac{c}{2\sqrt{km}}$ .

(– – Simple model; —— Compound model).

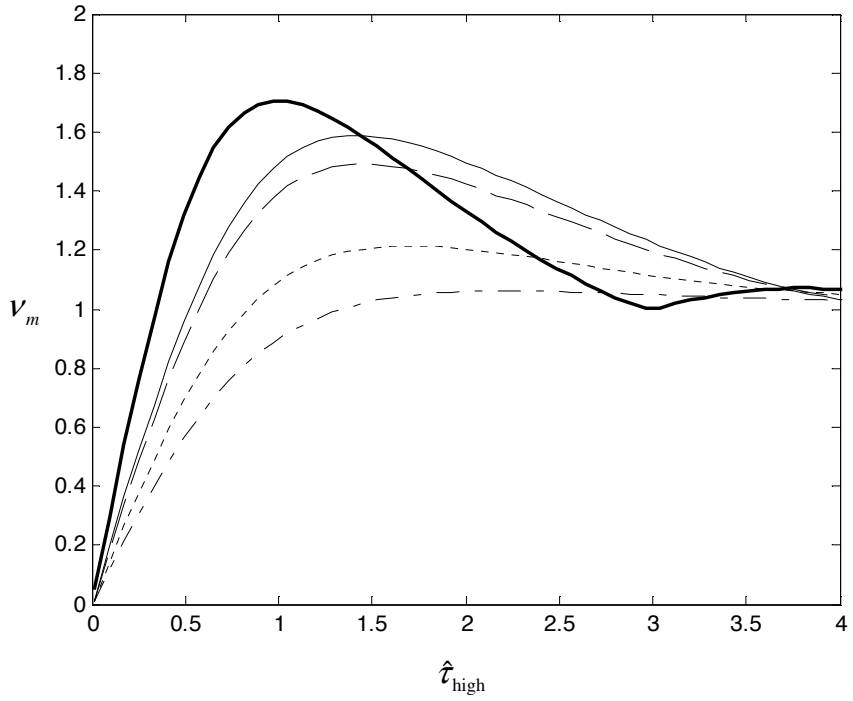


Figure 3.28. Shock Response Spectra for the switchable compound models showing the effect of viscous damping for a stiffness ratio of $\sigma = 0.5$, The bold line included represents the passive undamped model. The mass ratio $\mu$ is chosen so that the frequency ratio is $\Omega = 5$. ($-\ \zeta = 0.05$; $--\ \zeta = 0.1$; $\cdot\cdot\ \zeta = 0.3$; $-\cdot-\ \zeta = 0.5$).

# Chapter 4.

# Residual vibration suppression using switchable stiffness.

## 4.1. Introduction.

The objective of this chapter is to present a strategy to suppress the residual vibration that occurs after a shock pulse input to a simple mechanical system, which is idealized as a mass-spring system. As seen in the previous chapter, the objective was to minimize the shock response during a transient excitation by reducing the stiffness but there are residual effects after a shock that need to be rapidly suppressed. The approach in this case considers a different switchable stiffness strategy. A particular control strategy for transient vibration suppression originally proposed by Onoda and Watanabe [91] is investigated and developed. It involves an on-off logic to connect/disconnect a stiffness element, with the aim of providing high energy dissipation for lightly damped systems. The theoretical investigation presented in this chapter is based on such a strategy. Additionally, the models introduced in chapter 3 are considered again for the analysis, but the control strategies are different.

Although the approach by Onoda and Watanabe considered a simple system, there are several points that remain unclear. In particular, how does stiffness change produce energy dissipation or loss and what assumptions have been made in the existing published studies? In

this chapter the analysis of this model is extended in order to clarify its behaviour. Moreover, new numerical results and conclusions are provided for subsequent studies. Firstly, the basic on-off stiffness model found in the literature is revisited and its advantages and physical limitations discussed. As seen in chapter 3 a compound model involving an energy dissipation mechanism due to the inelastic collision between the two masses is considered, and then viscous damping is introduced and its effects analyzed as an extended development of the simplest configuration. The objective throughout the modelling of the various alternative systems is to consider the physical behaviour in comparison to the results for a viscously damped single degree-of-freedom system that can be considered as the benchmark or reference case. Similarly the decay in the switchable stiffness systems can be associated with an equivalent decay rate or logarithmic decrement for direct comparison.

## 4.2. Simple model (massless secondary spring).

According to Chen [106], it is possible to control the vibration of structural members by varying their stiffness. The author claimed that this approach is particularly useful in reducing the vibration of lightly damped systems. To understand how the vibration can be reduced by varying the stiffness, first consider the simple system shown in figure 4.1. The model is a single-degree-of-freedom (SDOF) undamped system consisting of a mass $m$ supported by a variable in time linear elastic spring $k_v(t)$.

The equation of motion for free vibration is given by:

$$m\ddot{v} + k_{effective}v = 0 \tag{4.1}$$

where $k_{effective} = k_v(t)$ is the instantaneous value of the effective stiffness at a time $t$. The free vibration solution of equation (4.1) is $v = Ve^{i\omega t}$, for a given constant value of the stiffness, which can be expressed using the concept of the phase-plane, which relates the variation of the velocity of the mass to its displacement. The solution can be represented by a family of phase trajectory curves represented in the $v - \dot{v}$ plane or phase plane. It satisfies [107]:

$$v^2 + \left(m/k_{effective}\right)\dot{v}^2 = a^2 \tag{4.2}$$

where $a$ is a constant that depends upon the initial conditions. Equation (4.2) represents a response that includes both $v$ and $\dot{v}$, which follows the path of an ellipse moving clockwise in the phase plane as shown in figure 4.2 considering a constant stiffness. For a system with a given mass and a low stiffness the solution forms a horizontal ellipse as shown in figure 4.2(a). For a system with the same mass but a larger value of stiffness the ellipse is vertical as shown in figure 4.2(b). In order to reduce the free vibration every cycle the state point $\left(v,\dot{v}\right)$ should approach the origin as if the system were damped, as shown in figure 4.3 for the case when viscous damping is included. However, for the undamped system considered one can reduce the vibration by having a large value of stiffness during the first and third quadrants of the phase plane, and a low constant stiffness in the second and third quadrant. This would cause the trajectory to become closer to the origin every cycle. In this case the orbit would be continuous but not smooth. Its derivatives, particularly the acceleration, would not be continuous and it would undergo a step change at each stiffness change.

As presented in chapter 3 a conceptual model comprising a mass $m$ supported by two springs in parallel of stiffness $k$-$\Delta k$ and $\Delta k$ respectively is considered. However, in this case it experiences residual free vibration after a shock pulse has been applied. For simplicity in this chapter free vibration is considered after a single impulse is applied to the system.

The equation of motion for free vibration of a switchable stiffness system is still given by equation (4.1), but now the instantaneous value of the stiffness $k_v$ can take either the value of $k$ or $k$-$\Delta k$ depending on the control or switching law used. Since the objective of this system is to provide vibration suppression, the switching logic for the spring $\Delta k$ has to ensure that the amplitude of vibration decreases every cycle. Based on the phase plane concept, the stiffness should be maximum and equal to $k$ when the product $v\dot{v}$ is positive and minimum equal to $k$-$\Delta k$ when $v\dot{v}$ is negative. This can be expressed mathematically by a control law as [91]:

$$k_v = \begin{cases} k & v\dot{v} \geq 0 \\ k-\Delta k & v\dot{v} < 0 \end{cases} \qquad (4.3)$$

The time when the response satisfies the condition $v\dot{v} \geq 0$ is equivalent to when the displacement $v$ and the velocity $\dot{v}$ have the same sign. The solution of equation (4.1) is given by equation (4.2) considering the stiffness value depending upon the control law. As a result of using this logic the spring $\Delta k$ is disconnected when the absolute value of the displacement of the mass is a maximum. It is connected again when the absolute value of the velocity is maximum, which corresponds to the displacement $v$ being zero and occurs when the system is passing through its equilibrium position. It is important to note that it is assumed the unconnected spring has returned to its unstretched position when it is reconnected. The introduction of a time lag or delay in the switching of the stiffness could potentially cause the system to become unstable. This phenomenon is analyzed briefly in appendix D.

As introduced in chapter 3 the stiffness reduction factor $\sigma$ is given by:

$$\sigma = \frac{\Delta k}{k} \tag{4.4}$$

The phase plane plot shown in figure 4.5(a) represents the solution when the control law described above is implemented and shows schematically what happens at each switching point. Additionally, the corresponding displacement as a function of time is shown in figure 4.5(b). The system is piecewise linear between switching times and an analytical solution can be found when it is assumed that the spring is reconnected at the static equilibrium position. Consider that the system has an initial velocity $\dot{v}_0 = a$ and an initial displacement $v_0 = 0$. These initial conditions are given by the point marked **A** in figures 4.5(a) and 4.5(b), and the stiffness is $k$. When the displacement is maximum at point **B** the stiffness $\Delta k$ is disconnected and the resulting stiffness is $k$-$\Delta k$ until point **C,** when the displacement is zero. The stiffness is then recovered and is equal to $k$. It is assumed that the spring $\Delta k$ has returned to its zero extension position to allow the reconnection to take place. At point **D** the displacement is given by $v_{\max}\sqrt{1-\sigma}$. The stiffness $\Delta k$ is disconnected again and reconnected at **E**. The result is a stiffness change every quarter cycle and so the peak amplitude at the $n^{th}$ cycle will be:

$$v_n = v_{n-1}\left(1-\sigma\right) \tag{4.5}$$

where $v_{n\text{-}1}$ is the maximum peak amplitude of the previous cycle. This means that the amplitude is reduced by a multiplicative factor of $(1-\sigma)$ every cycle. A typical response as a function of time including displacement, velocity and acceleration is shown in figure 4.6 for two values of $\sigma$, i.e. stiffness reductions of 50% for figure 4.6(a) and 80% for figure 4.6(b). These responses were calculated using a fixed step numeric solver implemented in MATLAB using the Runge-Kutta method. The response calculated was evaluated by multiplying the velocity and displacement within the solver to determine the switching points. The displacement $v$, velocity $\dot{v}$ and acceleration $\ddot{v}$ have been normalised with respect to the corresponding maximum absolute response parameters and the time $t$ normalised with respect to the mean period $T_m = \frac{T_{on}}{2} + \frac{T_{off}}{2}$, where $T_{on}$ and $T_{off}$ are the natural periods during the on ($\Delta k$ connected) and the off ($\Delta k$ disconnected) stiffness states respectively. Note that the amplitude of displacement decreases at a greater rate for the larger value of the stiffness reduction factor $\sigma$.

An important detail in the behaviour of this system is the fact that the value of the restoring force on the mass is discontinuous at the points of stiffness reduction (points **B** and **D** in figure 4.5). This condition results in sudden instantaneous acceleration changes of the mass at these points, which might be a potential drawback of this system. However, it is important to note that the analysis performed in this section is purely theoretical and several assumptions have been made, for example instantaneous stiffness switching and massless springs. Previous investigations [89-97] have generally ignored the acceleration discontinuity in their analysis and subsequent discussion.

The strategy described in this chapter disconnects (turns off) the secondary spring $\Delta k$ when its deformation is maximum, i.e. when the potential energy stored in this spring is maximum. It is assumed that this amount of energy in the disconnected spring is all dissipated in the interval whilst it is disconnected. A discussion concerning this assumption follows later in the chapter. For this to be achieved, massless springs and immediate switching between high and low stiffness states are considered. Figure 4.7 shows the kinetic, potential and total system energies for a given initial velocity and zero initial displacement. These are normalised with respect to the initial energy in the system. The total energy decreases in steps corresponding to the times when switching occurs. When the secondary spring $\Delta k$ is disconnected an amount

of energy $\frac{1}{2}\Delta k v_n^2$ is lost, where $v_n$ is the peak displacement of the $n^{th}$ cycle given by equation (4.5). This amount of energy is assumed to be removed or lost from the system. Considering that the maximum energy at the beginning of one cycle is $\frac{1}{2}kv_{n-1}^2$, and at the next cycle is $\frac{1}{2}kv_n^2$, thus the total energy lost during the $n^{th}$ cycle is given by

$$\frac{1}{2}kv_{n-1}^2 - \frac{1}{2}kv_n^2 = \frac{1}{2}kv_{n-1}^2\sigma\left(2-\sigma\right) \tag{4.6}$$

This energy seems to 'disappear' from the system using the present assumptions, which is physically impossible. In practice one can have several mechanisms that effectively contribute to this energy dissipation; real springs might possess friction or hysteretic damping in addition to having mass characteristics. Moreover, in complex systems the energy can be transferred to higher modes of vibration where it is easier to dissipate energy, as some previous investigations have suggested [91]. Also, it can be related to the parametric excitation phenomena, which might occur when the system properties change with time [108]. Nevertheless, the equation of motion for this system does not consider any of these factors and it is interesting to investigate how energy can be dissipated or lost with only conservative terms in the equation.

Although the model considered is undamped, any real system will include a certain amount of damping. Moreover, if the secondary elastic element is massless, its oscillation frequency tends to infinity. However, if viscous damping is present, even if it is infinitesimal, the secondary system could return to the equilibrium position. The model can then be represented as in figure 4.8, where viscous damping has been included. Note that the damping is assumed to be only active when the secondary system is disconnected, as the switch in figure 4.8(a) indicates. As a result, the secondary system becomes a first order system, whose response is given by [102]:

$$v = v(0)e^{-\frac{\Delta k}{c}t} \tag{4.7}$$

where $v(0)$ is the displacement of the secondary system at the time of disconnection $t = 0$. An important point is to ensure that the secondary spring $\Delta k$ returns to its equilibrium position, and this depends upon the amount of damping present. The upper limit for the damping permissible for the secondary spring-damper system can be calculated considering the time whilst it is disconnected, which is a quarter of the natural period for the main system in its low stiffness state and can be written as:

$$t_0 = \frac{\pi}{2\sqrt{\frac{k-\Delta k}{m}}} \tag{4.8}$$

As a result, the required damping constant $c$ is a function of the stiffness reduction factor $\sigma$. Rearranging equation (4.7) for $c$ and substituting the settling time to $t_0$, one can write:

$$c = \frac{-\Delta k t_0}{\ln\left(\frac{v_{final}}{v(0)}\right)} \tag{4.9}$$

where $v_{final}$ is the final displacement of the secondary spring-damper system and it must be as close as zero as possible. The latter expression can be written in non dimensional form as:

$$\frac{c}{2\sqrt{km}} = \frac{-\sigma\pi}{2(1-\sigma)} \frac{1}{\ln\left(\frac{v_{final}}{v(0)}\right)} \tag{4.10}$$

The damping should be equal to or smaller than the value given by equation (4.10) in order to guarantee a proper settling time. Figure 4.9 shows the value of the damping constant as a function of the stiffness reduction factor. This plot gives the maximum permissible damping constant provided $v_{final}$ is 0.1% of the initial displacement at the time of disconnection. A larger amount of damping is permissible as the stiffness reduction factor increases, however the objective is to apply this strategy to lightly damped systems.

The corresponding time histories for both the main and the secondary systems are presented in figure 4.10. It can be observed that the secondary system, comprising the stiffness element $\Delta k$ and the dashpot $c$ returns to the equilibrium position whilst disconnected and then reconnects again when the mass is at its static equilibrium position. Note that the smaller the damping the less time it takes to return to rest. If the damping is negligible, the model further reduces to the simplest model described at the beginning of the chapter, but the secondary stiffness element will be oscillating at an infinite frequency because it is assumed to have zero mass. The addition of an infinitesimal amount of viscous damping solves this physically unrealisable problem, as the stiffness element returns to the rest position, thus dissipating the stored energy in the elastic element.

Having discussed the energy dissipation mechanism using the concept of a first order secondary system with an infinitesimal amount of damping, the undamped system is considered again for the sake of simplicity. It is important to relate and compare the decay of the undamped semi-active system with a damped passive system. To do this, it is possible to obtain an equivalent viscous damping ratio corresponding to a particular value of the stiffness reduction factor. It has been shown graphically that a switchable reduction in the stiffness results in vibration decay. However, it is beneficial to have a mathematical relationship for predicting an equivalent damping ratio. Onoda, *et al* [91] plotted the equivalent damping ratio for the on-off system described above, and later Winthrop *et al* [81] obtained an analytical expression for it. Recalling the definition of logarithmic decrement $\hat{\delta}$ for a viscously damped single degree-of-freedom system undergoing oscillatory free motion[102]:

$$\hat{\delta} = \ln\left(\frac{v_{n-1}}{v_n}\right) \tag{4.11}$$

where $v_n$ and $v_{n\text{-}1}$ are the peak amplitudes of displacement in consecutive cycles. For the on-off system, the corresponding peak amplitudes are given by equation (4.5) since the reduction in amplitude each cycle is given by $(1-\sigma)$. Thus, the equivalent logarithmic decrement for the on-off system is given by combining equations (4.5) and (4.11) to give:

$$\hat{\delta} = \ln\left(\frac{1}{1-\sigma}\right) = -\ln(1-\sigma) \tag{4.12}$$

Using the relationship between the viscous damping ratio and the logarithmic decrement [102] the equivalent viscous damping ratio for the on-off system is given by:

$$\zeta_{eq} = \frac{\hat{\delta}}{\sqrt{4\pi^2 + \hat{\delta}^2}} \tag{4.13}$$

where $\hat{\delta}$ is given by equation (4.12). Equation (4.13) gives the equivalent ratio in the sense of the decay per cycle, although the time history given in figure 4.6 shows that the displacement response is not strictly governed by an exponential decay in time or oscillation at one unique frequency. The equivalent viscous damping ratio $\zeta_{eq}$ is plotted in figure 4.11 as a function of the stiffness reduction factor $\sigma$. The figure shows the asymptote $\zeta_{eq} = \frac{\sigma}{2\pi}$, which is valid for reasonably small values of $\sigma$ which might be realisable in practice. In the limit as $\sigma \to 1$ oscillation no longer occurs and the equivalent viscous damping ratio tends to unity.

4.2.1. Effect of damping.

The objective of the on-off switchable stiffness strategy is to provide residual vibration suppression after a shock has been applied to the system. This strategy is intended for lightly damped systems. The next problem to analyse and consider is to determine if this strategy would have any benefit if applied to a system that has already an appreciable amount of damping. This section is concerned with the damped problem.

Figure 4.12 represents a viscously damped single degree-of-freedom with two parallel springs one of which can be disconnected using the control law given by equation (4.3)

To evaluate the performance of this system a key parameter to examine is the equivalent damping ratio of the system. It is difficult to obtain an analytical expression for the equivalent damping since the equivalent damping will comprise the effect of the viscous damping present in the system and the energy dissipated by the stiffness reduction. Moreover, the damping ratio of the system will change over time because of the stiffness variations. However, it is relatively straightforward to find the effective damping numerically by

evaluating the responses of the system at the peaks and then calculating an equivalent logarithmic decrement. The resulting equivalent damping plot is shown in figure 4.13 for several values of the initial damping ratio in the system for the on-period, which is given by $\zeta = \frac{c}{2\sqrt{km}}$, as a function of the stiffness reduction factor. It is assumed here that the secondary elastic element loses its stored energy when disconnected. A general observation from this figure is that the curves are similar to the undamped case, but that the level is increased depending upon the actual damping initially present. One can see that the asymptote previously shown in figure 4.11 for small values of $\sigma$ now can be expressed by $\zeta_{eq} = \zeta + \frac{\sigma}{2\pi}$, but this is valid only if the passive damping in the system is small.

A particular observation that must be made about figure 4.13 is that the value of initial viscous damping existing in the system is considered to be fixed, i.e. the viscous damping constant remains unaltered for a particular value of damping ratio. The value shown in the figures is the initial damping ratio in the system for that fixed damping constant. The actual value of damping ratio in the system will change as a result of the stiffness switching. Consequently, the actual damping ratio of the system for the high stiffness and low stiffness state is given by the expressions:

$$\zeta_{on} = \frac{c}{2\sqrt{km}} \tag{4.14}$$

$$\zeta_{off} = \frac{c}{2\sqrt{(k - \Delta k)m}} \tag{4.15}$$

It can be said that a mean damping ratio exists for this system, as the stiffness is switched every quarter of cycle. This value of damping ratio can be written as:

$$\zeta_m = \frac{\zeta_{on}}{2} + \frac{\zeta_{off}}{2} \tag{4.16}$$

The damping ratio for the on state remains constant whilst the value for the off state depends upon the stiffness reduction value. As expressed by equation (4.15), a higher stiffness reduction will lead to an increase in the damping ratio for the off period. This will cause the mean damping ratio to be slightly higher than the initial damping ratio. In addition to the effect of the switching strategy alone, this phenomenon helps increase the energy dissipation. A plot of the initial viscous damping ratio versus the mean viscous damping ratio for several values of the stiffness reduction factor $\sigma$ is shown in figure 4.14, where this effect is easily seen. The initial and the mean damping ratios have a linear relationship that can be expressed combining equations (4.14), (4.15) and (4.16) resulting in:

$$\zeta_m = \frac{c}{4\sqrt{km}}\left(1+\frac{1}{\sqrt{1-\sigma}}\right) \tag{4.17}$$

It is also interesting to investigate if the addition of damping can alleviate to some extent the acceleration peaks observed previously. As can be seen in figure 4.15, which shows the time-domain acceleration response of the switchable stiffness model, normalized considering the maximum acceleration of the undamped switchable stiffness model, the effect is not very significant unless the system is highly damped, and in this situation, implementing the on-off strategy is not recommended since there are no advantages. However, small quantities of existing passive damping still contribute to diminishing to some degree the acceleration levels and the discontinuities that occur in it.

## 4.3. Compound model (mass-spring secondary system)

### 4.3.1. Undamped system

In chapter 3 for shock response reduction, a compound model comprising a secondary mass-spring system was introduced. In this chapter, however, this compound model is analyzed in the context of the residual vibration suppression strategy.

The secondary spring-mass system is allowed to connect and disconnect from the main mass following the control law as given by equation (4.3). Recalling the behaviour of the control law discussed previously, it requires stiffness reduction at the point of maximum

displacement, and recovery at zero displacement in order to get maximum energy dissipation. Considering that the secondary mass-spring system will oscillate independently during the off part of the control law (low stiffness stage), it is important to ensure that the secondary mass is exactly at the static equilibrium position at the moment of stiffness recovery, when the secondary stiffness $\Delta k$ reconnects to the primary mass. If this is achieved, both the main and the secondary system will coincide at the correct time as given by the control law. As presented in the conceptual model shown in figure 3.16, the primary and secondary systems are considered to oscillate in different spaces and they do not collide during the time they are disconnected. The model described in chapter 3 is used here and it is reproduced in figure 4.16 for ease of reference.

One of the principal characteristics of the simple model considered previously is the immediate energy loss at the time at which the secondary stiffness is disconnected, which are the stiffness reduction points shown in figure 4.7. However, the new approach shown in figure 4.16 considers no energy lost during the disconnection. The total energy is the sum of the energy in the main and the secondary system, the latter has a certain amount of potential energy when it is disconnected, and no external or internal form of damping is considered.

For this model the energy dissipation mechanism is attributed solely to the subsequent connection and the impact between the main mass $m-\Delta m$ and the secondary mass $\Delta m$. When the impacting masses stick together after the impact then the collision is said to be perfectly inelastic. In this case, the ratio between the velocities of separation and approach of the two masses involved in the impact, also called the coefficient of restitution [107], is zero. The masses will then have the same velocity immediately after the impact, which is according to the conservation of momentum principle given by:

$$\dot{v}_0 = \frac{\left(m-\Delta m\right)\dot{v}_1 + \Delta m\dot{v}_2}{m} \tag{4.18}$$

where $\dot{v}_1$ and $\dot{v}_2$ are the velocities of the two masses immediately before the impact, and $\dot{v}_0$ is the common velocity of the masses once they are moving together immediately after the impact. This condition on the collision might be achieved practically if a rapid clamping mechanism is used to attach the secondary mass to the primary mass.

The process of disconnection and connection of the secondary mass-spring system for this model follows the same control logic described in section 4.2, i.e. disconnection at points of maximum absolute displacement and reconnection when the primary mass has zero displacement.

When the systems are attached, the equation of motion is as given by equation (4.1), which is repeated here for convenience:

$$m\ddot{v} + k_{effective}v = 0 \tag{4.19}$$

where $m$ is the total mass and $k$ is the effective total stiffness in the system. Following the control logic described in section 4.2, when the displacement of the mass is maximum the stiffness is switched to its low value. At this point, the primary and secondary systems will oscillate independently and their equations of motion are:

$$\left(m-\Delta m\right)\ddot{v}_1 + \left(k-\Delta k\right)v_1 = 0 \tag{4.20}$$

$$\Delta m\ddot{v}_2 + \Delta k v_2 = 0 \tag{4.21}$$

The point at which the spring is disconnected is shown in figure 4.17 as point **B** at time $t = t_0$. Figure 4.17 also shows a general time-displacement response for the main mass $m-\Delta m$ until the stiffness recovery point. The system oscillates with a new natural frequency resulting from the effective stiffness and mass change until point **C**. The second mass is allowed to oscillate independently in a way that they do not collide or come together until a specified point in the cycle of vibration, which is marked as **C** in figure 4.17 of the primary mass $m-\Delta m$. This process will repeat again from point **D** where the systems will be disconnected and eventually recombined at point **E**

To obtain an expression for the energy dissipated during the impact, it is necessary to consider the exact values of velocity for each mass at the moment of contact. Considering the control law, the main mass $m-\Delta m$ is assumed to be passing through the static equilibrium position at the moment of contact or recovery, and the solution for the displacement of each mass can

be found provided that the initial conditions are those from the stiffness reduction point **B** in figure 4.17, i.e. maximum displacement and zero velocity.

$$v_1 = v_{\max} \cos \omega_p (t - t_0) \tag{4.22}$$

$$v_2 = v_{\max} \cos \omega_s (t - t_0) \tag{4.23}$$

The corresponding velocities are given by:

$$\dot{v}_1 = -\omega_p v_{\max} \sin \omega_p (t - t_0) \tag{4.24}$$

$$\dot{v}_2 = -\omega_s v_{\max} \sin \omega_s (t - t_0) \tag{4.25}$$

The natural frequencies for the disconnected single-degree-of-freedom systems $\omega_p$ and $\omega_s$ (primary and secondary systems) are given, as in chapter 3 by

$$\omega_p = \sqrt{\frac{k - \Delta k}{m - \Delta m}} \tag{4.26}$$

$$\omega_s = \sqrt{\frac{\Delta k}{\Delta m}} \tag{4.26}$$

The time $t_0$ is the time it takes for both masses to oscillate for the first quarter of the cycle and it can be expressed as:

$$t_0 = \frac{\pi}{2\omega_n} \tag{4.28}$$

where $\omega_n$ is the natural frequency of the compound system when the masses are connected, and is given by $\omega_n = \sqrt{\frac{k}{m}}$. At the moment of contact between the masses (marked as **C** in

figure 4.17), $t - t_0 = \frac{\pi}{2\omega_p}$ and the corresponding displacements and velocities of each mass can now be rewritten as:

$$v_1 = 0 \tag{4.29}$$

$$v_2 = v_{\max} \cos\left(\frac{\pi\omega_s}{2\omega_p}\right) \tag{4.30}$$

$$\dot{v}_1 = -\omega_p v_{\max} \tag{4.31}$$

$$\dot{v}_2 = -\omega_s v_{\max} \sin\left(\frac{\pi\omega_s}{2\omega_p}\right) \tag{4.32}$$

As stated by the control law the secondary mass needs to be at its static equilibrium point since its velocity is maximum and this will increase the energy dissipation. It can be seen from equation (4.30) that this condition is possible only when the frequency ratio $\frac{\omega_s}{\omega_p}$ takes odd integer values. i.e. $\frac{\omega_s}{\omega_p} = 1,3,5,7....$ The subsequent results are calculated using this condition. Thus, it is useful at this point to recall the frequency ratio $\Omega = \frac{\omega_s}{\omega_p}$, the frequency ratio for the disconnected systems as introduced in chapter 3.

It is now possible to calculate the energy lost during each impact. The kinetic energy after the impact is given by:

$$T_0 = \frac{1}{2} m \dot{v}_0^2 \tag{4.33}$$

where $\dot{v}_0$ is the common velocity after the masses collide as given by equation (4.18). The initial total potential energy of the system is $\frac{1}{2}kv_{\max}^2 = \frac{1}{2}m\dot{v}_{\max}^2$ , where $v_{\max}$ is the maximum peak displacement of the main system just before the secondary system is disconnected, and there is no energy lost until the point of zero displacement for the primary mass $m-\Delta m$ when the impact occurs. At this point, the energy dissipated during the impact is:

$$E_d = \frac{1}{2}kv_{\max}^2 - \frac{1}{2}m\dot{v}_0^2 \tag{4.34}$$

Hence the corresponding percentage of energy dissipated can be expressed as a percentage of the energy in the system before the impact:

$$\%E_d = \left(1 - \frac{m\dot{v}_0^2}{kv_{\max}^2}\right) \times 100 \tag{4.35}$$

Combining equations (4.18) (4.34) and (4.35) the common velocity after the impact can be written as:

$$\dot{v}_0 = \frac{v_{\max}}{m}\left[(m-\Delta m)\omega_p + \Delta m\omega_s \sin\left(\frac{\pi\omega_s}{2\omega_p}\right)\right] \tag{4.36}$$

Equations (4.35) and (4.36) can be combined to give the percentage of energy dissipated as:

$$\%E_d = \left[1 - \frac{1}{km}\left[(m-\Delta m)\omega_p + \Delta m\omega_p \sin\left(\frac{\pi\omega_s}{2\omega_p}\right)\right]^2\right] \times 100 \tag{4.37}$$

Equation (4.37) can be written in a non dimensional form by using the parameters $\sigma = \frac{\Delta k}{k}$, the stiffness reduction ratio and the frequency ratio $\Omega = \frac{\omega_s}{\omega_p}$, the frequency ratio, to give:

$$\%E_d = \left[1 - \frac{\sigma}{1+\Omega^2\left(\frac{1}{\sigma}-1\right)}\left[\left(\frac{1}{\sigma}-1\right)\Omega + \sin\left(\frac{\pi}{2}\Omega\right)\right]^2\right] \times 100 \qquad (4.38)$$

The mass ratio $\mu = \frac{\Delta m}{m}$ as defined in chapter 3 is used again. To guarantee that the masses coincide at the static equilibrium displacement position at the time required, $\mu$ and $\sigma$ must have values that satisfy $\Omega = \frac{\omega_s}{\omega_p} = 1,3,5,...$, i.e. odd integers. However, in the case of $\mu = \sigma$, which gives $\Omega = 1$, the amount of energy dissipated is zero. This is because the velocity of the secondary mass is equal in magnitude and phase to the velocity of the main mass when they collide, i.e. the relative approach velocity is zero. There is no change in the velocity of the masses before and after the impact, so there is no energy lost during the contact.

In order to assure maximum energy dissipation during the impact the common velocity of the masses after the contact must be as small as possible, i.e. the kinetic energy is minimized. Since the velocity of the mass $m - \Delta m$ is always maximum just before the impact, the velocity of $\Delta m$ should preferably be a maximum and have opposite sign at the point of impact. This is not necessarily true for all the odd integer values of $\Omega$ as seen in figure 4.18, which shows the percentage of energy dissipated for odd integer values of $\Omega$ between 1 and 15. It can be seen that the energy dissipated is considerably higher when $\Omega = 3,7,11,...$. On the other hand, when $\Omega = 5,9,13,...$ the energy dissipated is smaller. It is possible to maximize the energy dissipation when $\Omega = 3,7,11,...$ because the velocity of the masses are out of phase at the moment of impact. However, when $\Omega = 5,9,13,...$ the velocities, although different in magnitude, have the same phase, therefore the energy dissipation is considerably less compared with the previous case. This fact can be seen clearly in figure 4.19 which shows the energy dissipation as a function of the stiffness ratio, for the values of $\Omega$ mentioned above. Furthermore, a plot of the equivalent viscous damping ratio as a function of the stiffness reduction factor $\sigma$ is presented for several values of $\Omega$ in figure 4.20. The equivalent damping ratio was estimated using the ratio between consecutive peaks calculated by the energy dissipation given by equation (4.38) This plot further confirms the energy dissipation behaviour. The equivalent viscous damping ratio was obtained numerically by obtaining the

peak displacements for the impacting model, using a fourth order Runge-Kutta routine, and then considering the decay rate. The calculations were made for $\Omega = 3,5,7,9,11,\text{and } 13$ as a function of the stiffness reduction factor. When $\Omega = 3,7,11,...$ there is an optimum combination of $\mu$ and $\sigma$ for each value of $\Omega$, which dissipates all the energy during the first impact. As a result both masses return to rest immediately after the impact. This condition can be stated mathematically considering the total momentum after the impact is zero, as follows:

$$\left(m - \Delta m\right) x_{\max} \omega_p - \Delta m x_{\max} \omega_s = 0 \tag{4.39}$$

Noting that $\Omega = \frac{\omega_s}{\omega_p}$, equation (4.39) can be written as

$$\frac{m - \Delta m}{\Delta m} = \Omega \tag{4.40}$$

Thus, for $\Omega = 3,7,11,...$ the relationship between the optimum mass ratio and the frequency ratio is given by:

$$\mu = \frac{1}{\Omega + 1} \tag{4.41}$$

Using equations (4.26) and (4.27) the frequency ratio can also be expressed as $\Omega = \sqrt{\frac{(1-\mu)\sigma}{(1-\sigma)\mu}}$. As a result, the relationship between the stiffness ratio and the frequency ratio can be calculated as:

$$\sigma = \frac{\Omega}{\Omega + 1} \tag{4.42}$$

The values of $\mu$ and $\sigma$ calculated using equations (4.41) and (4.42) represent the peaks observed in figure 4.20 for $\Omega = 3,7,11,...$ These peaks tend to indicate an equivalent damping ratio of 1, which is true considering the definition of critical damping as the system no longer posesses oscillation. Hence, it is possible to maximize the energy dissipation for these

situations. This can be further validated by obtaining the derivative of equation (4.38), which can be used to obtain the maximum value of energy dissipation for particular values of $\Omega$. The full derivation can be found in appendix E. However, as $\Omega$ increases, the stiffness reduction required also increases, which could be difficult to achieve in practice. The corresponding values of $\mu$ and $\sigma$, for discrete values of $\Omega$ which give maximum energy dissipation are shown in figure 4.21, where it is clearly seen that higher stiffness reduction is needed as $\Omega$ increases. In general the stiffness and mass ratios can be related using the following equation:

$$\mu = \frac{1}{1+\Omega^2\left(\frac{1}{\sigma}-1\right)} \tag{4.43}$$

Equation (4.43) is plotted in figure 4.22 as a function of $\sigma$ for several values of $\Omega$.

As an example, consider the plot shown in figure 4.23(a) which depicts a time history showing the displacement, velocity and acceleration responses for the impacting model (bold line) where $\sigma$=0.5 and $\mu$ =0.1. The sudden changes in velocity are due to the impact between the masses after every half cycle. This combination will give $\Omega = 3$ but is not optimized for the case of maximum energy dissipation. The optimum situation when the energy dissipated is maximized, i.e. $\mu$ =0.25 and $\sigma$= 0.75 is presented in figure 4.23(b).

Figure 4.24(a) shows the secondary system response (dashed line) during the times it remains disconnected and oscillates independently, showing that both masses coincide at the same point during the impact. Figure 4.24(b) shows the kinetic, potential and total energy for the system. This plot shows the sum of the energies in the primary and the secondary systems. Both figures 4.24(a) and 4.24(b) are for values of $\sigma$=0.5 and $\mu$=0.1. The results coresponding for the optimum situation $\mu$=0.25 and $\sigma$ = 0.75 are shown in figure 4.25, where it is clearly seen that the masses are at rest immediately after the first impact.

In order to establish a relationship between this impacting model and the basic model considered in section 4.2, one can consider the behaviour of the impacting model when the secondary mass tends to zero. From section 4.2, the maximum energy in the basic switchable

stiffness model can be written in terms of the potential energy as $\frac{1}{2}kv_{\max}^2$, for the basic model. The percentage of energy dissipated after the first stiffness reduction (half a cycle) can be expressed as

$$\%E_d = \frac{\frac{1}{2}kv_{\max}^2 - \frac{1}{2}kv_{\min}^2}{\frac{1}{2}kv_{\max}^2} \times 100 \tag{4.44}$$

where $v_{\min}$ is the subsequent negative peak displacement (marked as **D** in figure 4.17) and it is related to $v_{\max}$ by $v_{\min} = v_{\max}\sqrt{1-\sigma}$. It is important to note that there are two stiffness reductions for the basic model, as there are in general apart from the optimum cases two impacts in the impacting model each cycle. Hence, equation (4.44) reduces to:

$$\%E_d = \sigma \times 100 \tag{4.45}$$

Equation (4.45), which gives the energy dissipation as a result of the first stiffness reduction in the cycle, coincides with the energy dissipation in the impacting model during the first impact, assuming a very small fixed value of the secondary mass, i.e. $\mu \approx 0$. This can be easily shown if equation (4.38) is expressed in terms of the mass ratio $\mu$ and the stiffness ratio reduction $\sigma$ giving:

$$\%E_d = \left[1 - \left[\sqrt{1-\sigma}\sqrt{1-\mu} + \sqrt{\mu\sigma}\sin\left(\frac{\pi}{2}\sqrt{\frac{(1-\mu)\sigma}{(1-\sigma)\mu}}\right)\right]^2\right] \times 100 \tag{4.46}$$

By setting $\mu = 0$ in equation (4.46) and simplifying the resulting expression it is the same as equation (4.45) thus showing how the compound model reduces to the simple model when the secondary mass is negligible.

4.3.2. Effect of damping.

The objective of the switchable stiffness strategy is to reduce or minimise the residual vibration in lightly damped systems after a shock has been applied to a system. So far, the impacting model has been analyzed, without taking into account any damping. In this section, a brief investigation is conducted as to whether the impact strategy would have any benefit if applied to a system that already has some damping present. This is important because all real systems inherently have some form of damping.

Figure 4.26 represents a viscously damped single degree-of-freedom with two parallel springs one of which can be disconnected using the control law given by equation (4.3). When disconnected there are two independent mass-spring-damper systems. When both systems are attached an equivalent damping constant is calculated from the constants $c_p$ and $c_s$ corresponding to the damping constants of the primary and secondary systems respectively.

The displacement response for the primary and secondary masses from the maximum displacement point (i.e. point **B** in figure 4.17, but now considering damping) is given respectively by:

$$v_1 = 0 \tag{4.47}$$

$$v_2 = v_{\max} e^{-\zeta_s \omega_s (t-t_0)} \cos\left(\omega_s \sqrt{1-\zeta_s^2}\,(t-t_0)\right) \tag{4.48}$$

The time $t_0$ is given by equation (4.26) as in the undamped case. The percentage of the energy dissipated can be obtained calculating the common velocity of the masses $\dot{v}_0$ after they impact and oscillate together, as expressed by equation (4.18). Using the derivatives of equations (4.47) and (4.48) and then combining them into equation (4.18) gives the common velocity after the impact. As a result the percentage of energy dissipated during the impact in the damped impacting model can be expressed as:

$$\%E_d = \left[1 - \frac{\sigma}{1+\Omega_d^2\left(\frac{1}{\sigma}-1\right)}\left[e^{-\frac{\pi\zeta_p}{2\sqrt{1-\zeta_s^2}}}\left(\frac{1}{\sigma}-1\right)\Omega_d\sqrt{1-\zeta_p^2} + e^{\frac{\pi\zeta_s\Omega_d}{2\sqrt{1-\zeta_p^2}}}\left[\zeta_s\cos\left(\frac{\pi}{2}\Omega_d\right)+\sqrt{1-\zeta_s^2}\sin\left(\frac{\pi}{2}\Omega_d\right)\right]\right]^2\right]\times 100$$

(4.49)

where the frequency ratio $\Omega$ has been replaced by the damped frequency ratio, since the model is now damped. This ratio is defined as:

$$\Omega_d = \frac{\omega_s\sqrt{1-\zeta_s^2}}{\omega_p\sqrt{1-\zeta_p^2}} \tag{4.50}$$

As described in the previous section, one wants the frequency ratio to have values $\Omega_d = 3,7,11,...$ in order to maximize energy dissipation and ensure the systems can recombine at the required times. Thus, the physical properties of the system must be tuned to keep the required frequency ratio.

In order to evaluate the performance of this system a key parameter to compare is the equivalent damping ratio of the system. The analysis to obtain the percentage of energy dissipation and the subsequent equivalent damping ratio is similar to the analysis presented in section 4.3.1. It is difficult to obtain an analytical expression for the equivalent damping, since the effective damping will comprise the effect of the viscous damping present in the system and the energy dissipated by the stiffness reduction. Additionally, the damping ratio of the system will change over time as a result of the stiffness and mass variations. However, it is relatively straightforward to estimate the effective damping by using equation (4.47) to calculate the energy dissipation and then find the consecutive peaks used to obtain the equivalent logarithmic decrement. For the numerical results in this section, the damping constants $c_p$ and $c_s$ are selected so that the damping ratio for both systems is the same, i.e. $\zeta_1 = \zeta_2$. The effective damping ratio is shown in figure 4.27 for several values of the initial damping ratio in the system for the on period, as a function of the stiffness reduction factor,

considering $\Omega_d = 3$. This condition will shift the optimum values of $\mu$ and $\sigma$, but the frequency ratio $\Omega_d$ will remain the same. The equivalent damping ratio will be enhanced as the viscous damping in the system increases. However, the main conclusion from this figure is that there is no significant change if the system is lightly damped. For instance, when the fraction of critical damping is less than 5%. There is a limit on how much equivalent damping can be obtained depending on the amount of physical damping present in the system. It is important to remember that the strategy is suitable for low damping systems, where the addition of any other form of damping is not straightforward. Otherwise, if the system is already highly damped it can be more convenient from a practical point of view not to use a semi-active strategy, but simply add another form of passive damping.

Finally, figure 4.28 compares two situations, the first one depicted by the continuous line represents the equivalent damping ratio when $\Omega_d = 3$, and a damping ratio of 0.01. On the other hand, the dotted line shows the equivalent damping for the basic model introduced in section 4.2, considering a damping ratio of 0.01. As a result, it can be seen that the impacting model presents a practical limiting value of stiffness reduction where the energy dissipation is optimized, rather than the physically unrealisable value of 100% stiffness reduction of the basic model when energy dissipation is maximized. Moreover, it appears that the impacting model at low values of stiffness reduction always exceeds the performance of the basic on-off stiffness model in terms of energy dissipation. If the parameters of the model are adequately chosen, the energy lost by the inelastic impacts is higher than the energy lost in the simple model by the disconnecting spring.

## 4.4. Conclusions.

The performance of a system for enhancing the decay of residual vibration, which uses an on-off logic to adaptively reduce the stiffness, has been revisited. This particular system can be found in the literature but there are some aspects that were unclear, particularly those related to the energy dissipation and physical implementation. Previous studies have not considered the conservation of energy in the system, as no dissipative terms have been included in the analysis. Moreover, issues with acceleration discontinuities have not been reported although present in this system due to the sudden stiffness changes. As a result in this chapter, the details of the control logic and the existing switchable stiffness model have been extensively examined including a means by which the disconnected spring can in conjunction with a damper, dissipate the energy and account for the system energy reduction.

An alternative modelling approach has been proposed, in order to investigate the energy dissipation in a switchable stiffness system and to provide a valid mathematical and physical model. This approach involved a secondary spring with a small mass and considers the impact between this mass and the main mass at the moment of stiffness recovery. The energy is solely dissipated due to this inelastic impact. There is a trade-off between the mass and stiffness ratios; high energy dissipation can be achieved for certain combinations of these parameters which are physically allowed. It was found that as the secondary mass is reduced to zero, this system effectively reduces to the basic on-off model and their energy dissipation characteristics are the same for this particular configuration.

Furthermore, the inclusion of viscous damping was studied in both the basic and the impacting systems. The main conclusion obtained being that when the system is lightly damped the performance is not affected. However, highly damped systems experience a drawback in vibration suppression, and the effective damping ratio could become lower than that for the viscous damping ratio present for the passive linear original system. This supports the hypothesis that the strategy is only suitable and beneficial for lightly damped systems.

The theoretical results and assumptions presented in this chapter will form the basis for the design of an experimental setup used to validate the switching strategy. Later in the thesis both strategies for shock control and residual vibration suppression will be implemented.

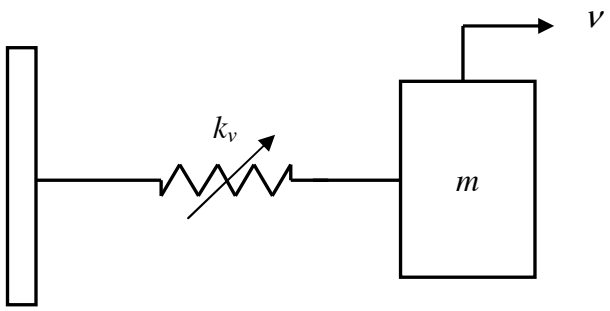


Figure 4.1. Single-degree-of-freedom system with variable stiffness.

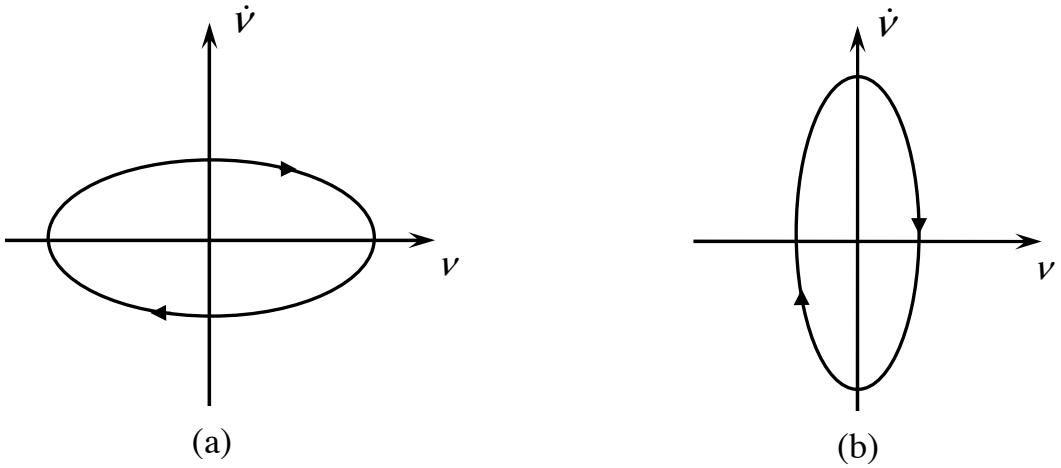


Figure 4.2. Phase plane representation of the free vibration motion of a single degree-of-freedom undamped system. (a) low stiffness and (b) high stiffness for a given fixed mass $m$.

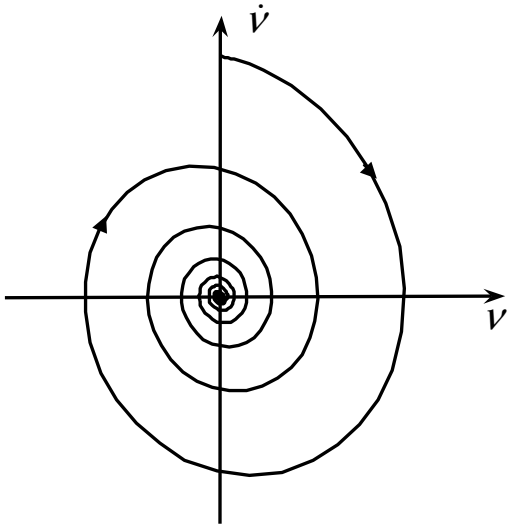


Figure 4.3. Phase plane representation of the motion of a single degree-of-freedom viscously damped system.

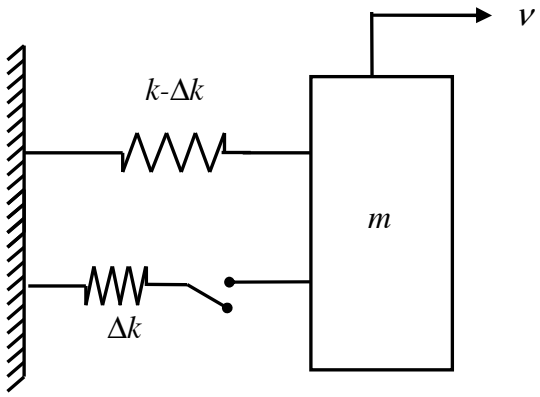


Figure 4.4. Single-degree-of-freedom system with on-off switchable stiffness.

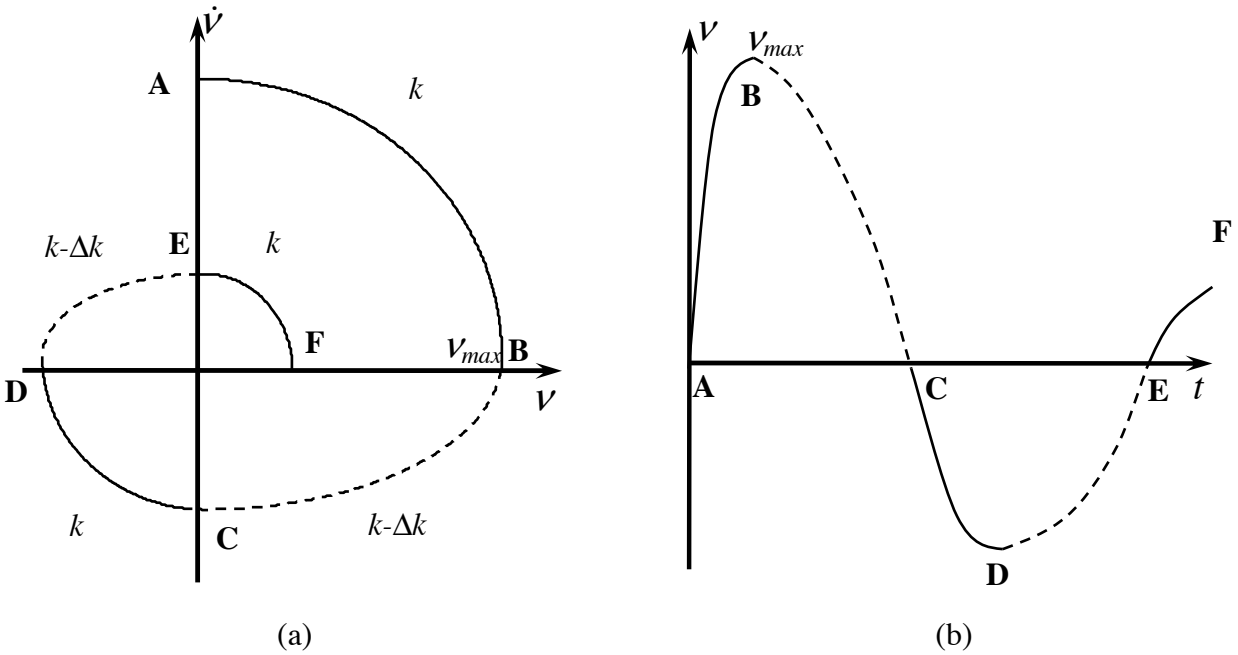


Figure 4.5. Free vibration of the on-off switchable system illustrating the effects of the stiffness change (—— High stiffness; --- low stiffness). (a) Phase plane plot (b) Time history of the displacement response.

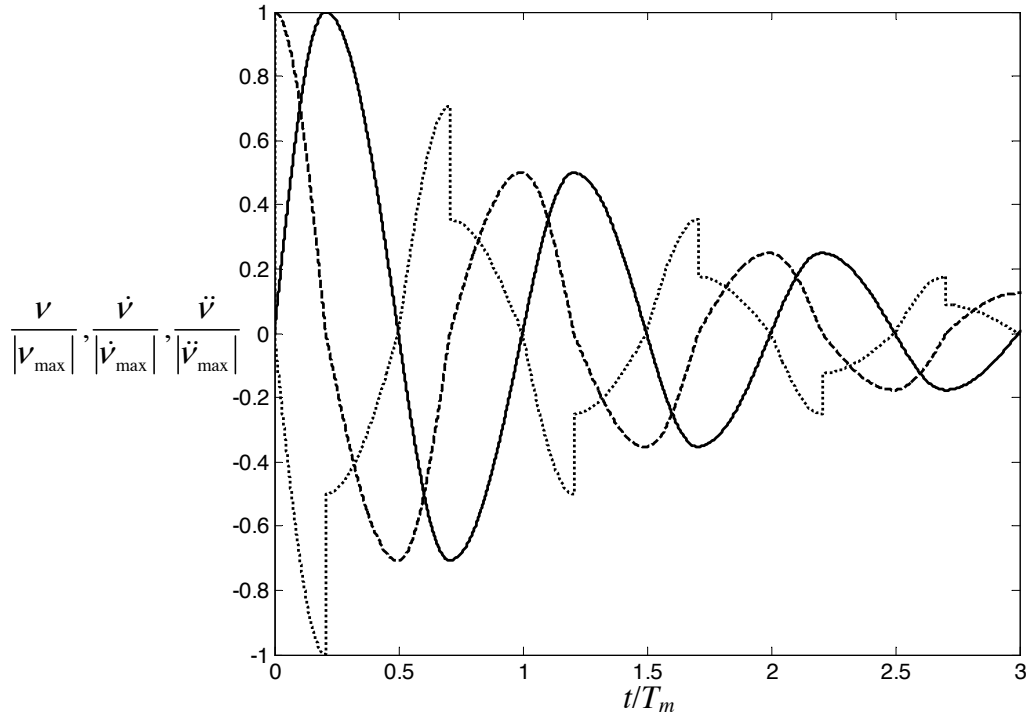


(a)

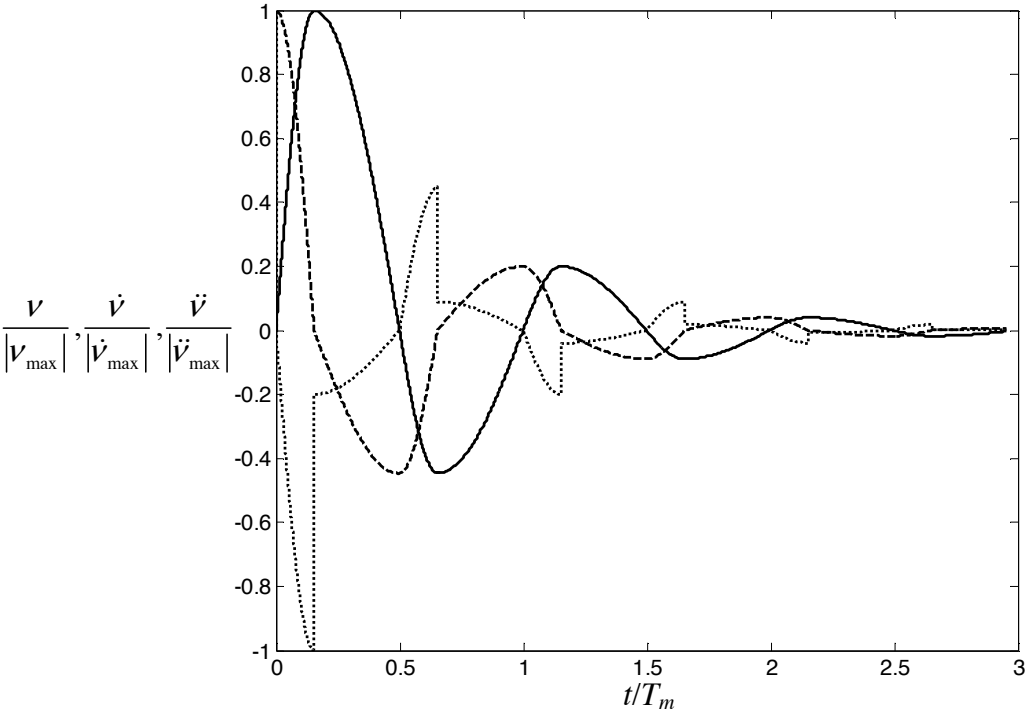


(b)

Figure 4.6. Typical response for the switchable stiffness system of figure 4.4 showing curves for displacement, velocity and acceleration. $T_m = \frac{T_{on}}{2} + \frac{T_{off}}{2}$, where $T_{on}$ and $T_{off}$ are the natural period during the high and the low stiffness states respectively. (a) $\sigma =$ 0.5 (b) $\sigma =$ 0.8. (——Displacement; ----- Velocity; ····· Acceleration)

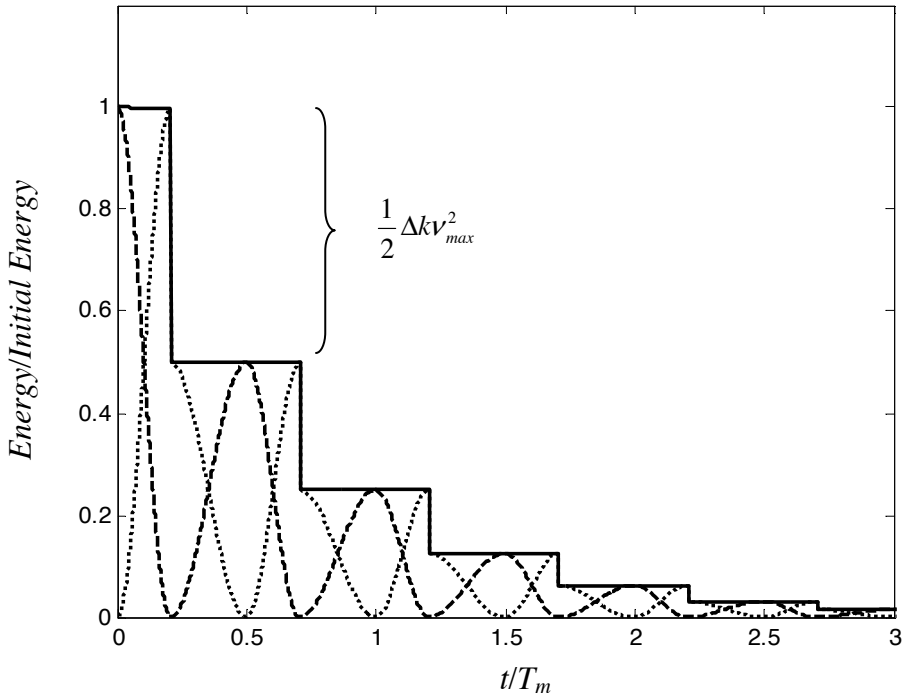


Figure 4.7. Example of energy levels for the switchable stiffness system with a stiffness reduction ratio of $\sigma = 0.5$. The horizontal axis represents time normalised with respect to the mean period and vertical axis is the energy normalised with respect to the initial energy (—— Total energy; --- Kinetic energy; ···· Potential energy).

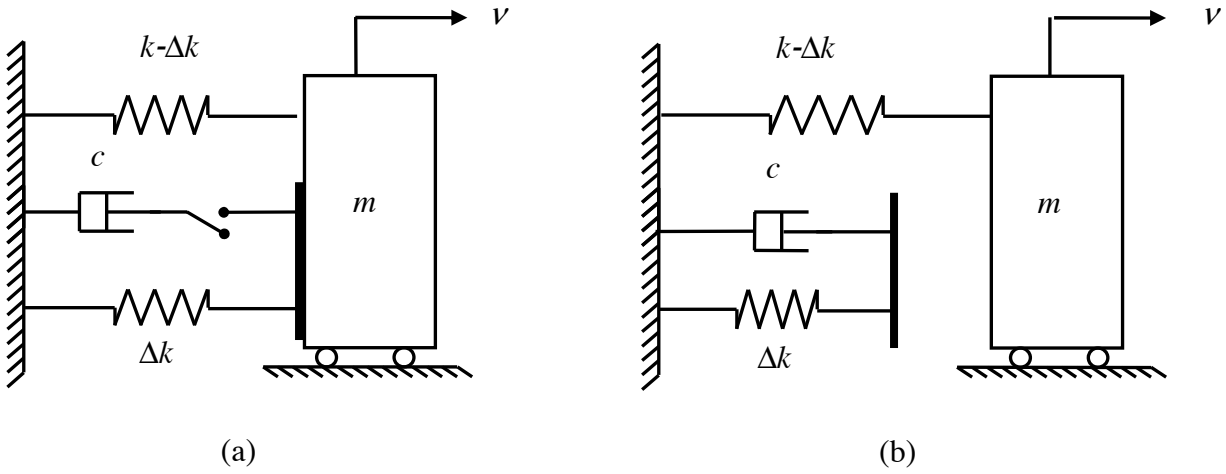


Figure 4.8. Switchable on-off model with viscous damping. (a) High stiffness state with both elastic elements connected and the dashpot disconnected. (b) Low stiffness state, the secondary spring has been disconnected and the dashpot is connected to it.

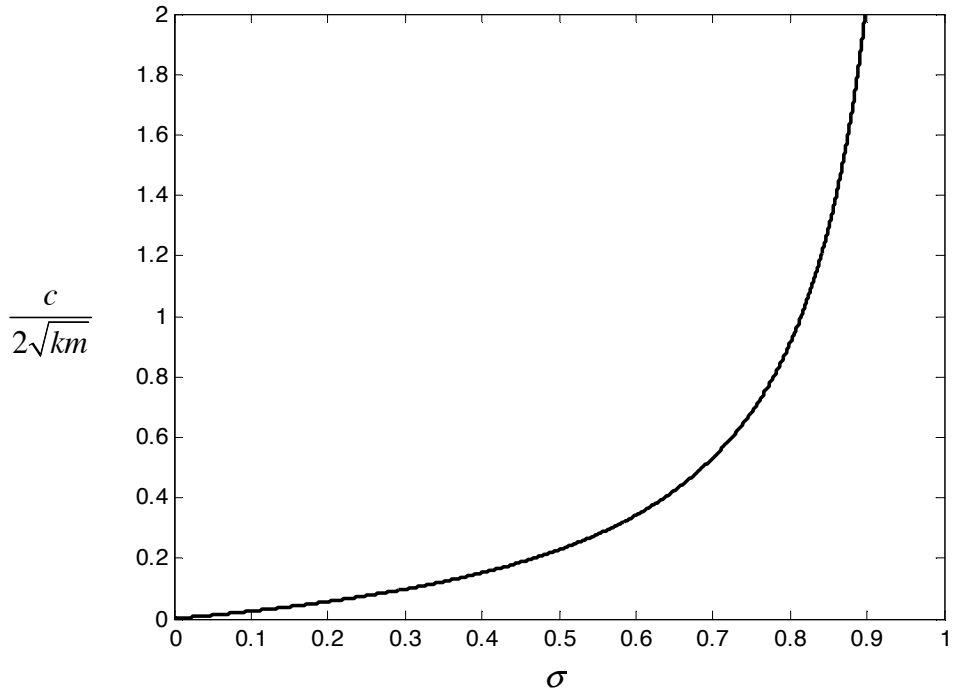


Figure 4.9. Maximum damping permissible in the secondary spring-damper system as a function of the stiffness reduction ratio $\sigma$ to allow the secondary spring to return to the equilibrium position whilst it is disconnected.

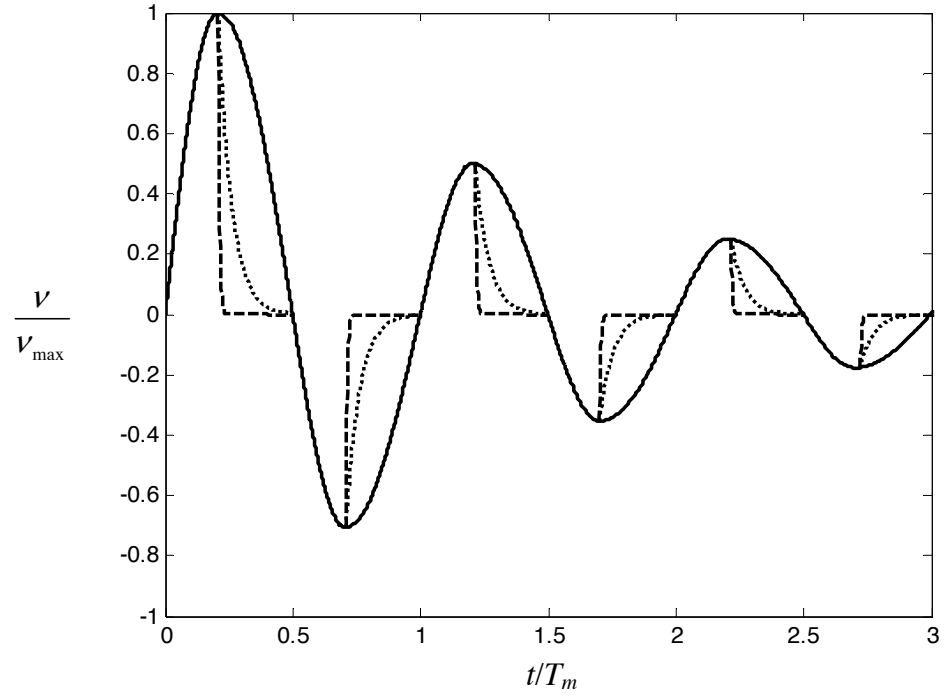


Figure 4.10. Response of the combined main system (▬) and the secondary spring-damper system for different damping values considering a stiffness reduction ratio of $\sigma = 0.5$. (···· $c/2\sqrt{km} = 0.1$; --- $c/2\sqrt{km} = 0.01$).

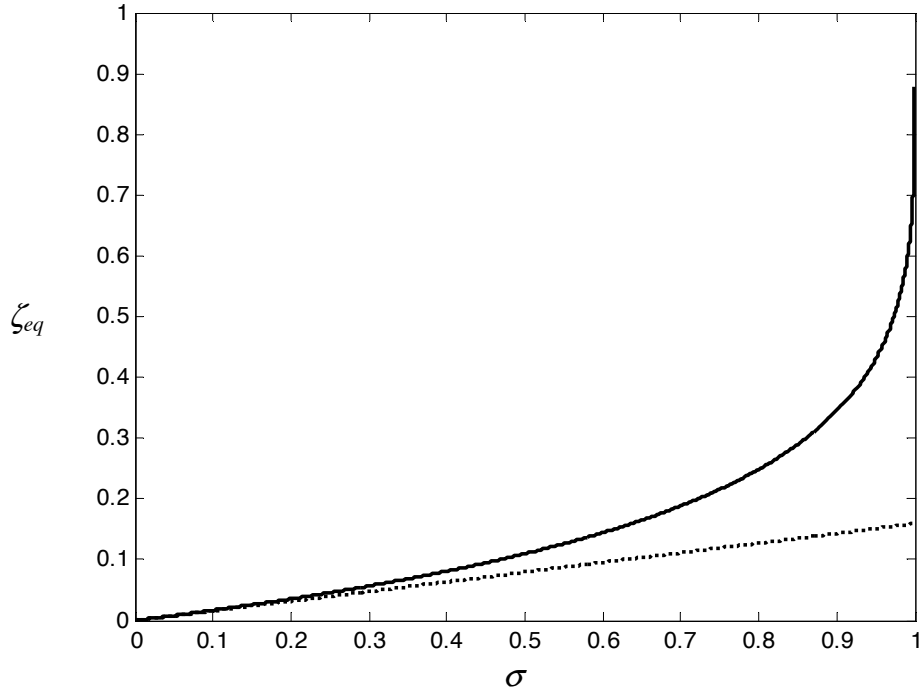


Figure 4.11. Equivalent damping ratio as a function of the stiffness reduction ratio $\sigma$ where the straight line represents the asymptote given by $\zeta_{eq} = \sigma/2\pi$ for small values of $\sigma = \Delta k/k$.

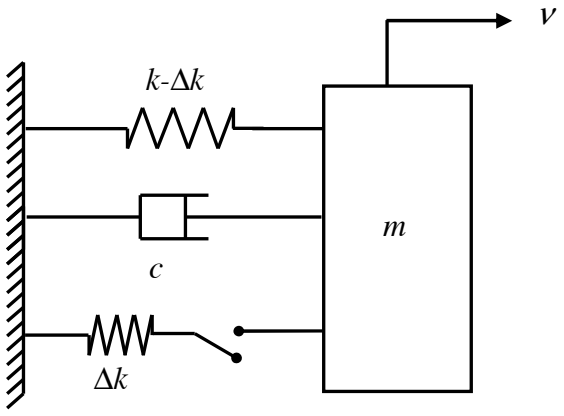


Figure 4.12. Single-degree-of-freedom viscously damped system with on-off switchable stiffness.

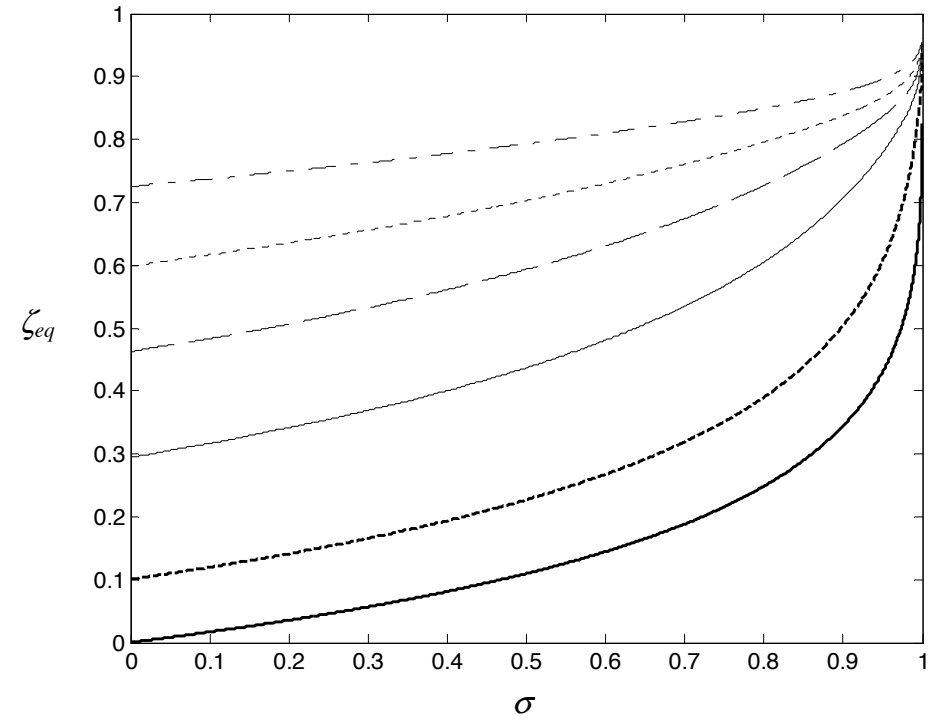


Figure 4.13. Equivalent damping ratio as a function of the stiffness reduction factor for different values of the actual damping ratio in the system.
(——$\zeta = 0$; --$\zeta = 0.1$; — $\zeta = 0.3$; – – $\zeta = 0.5$; - - $\zeta = 0.7$; – - –$\zeta = 0.9$)

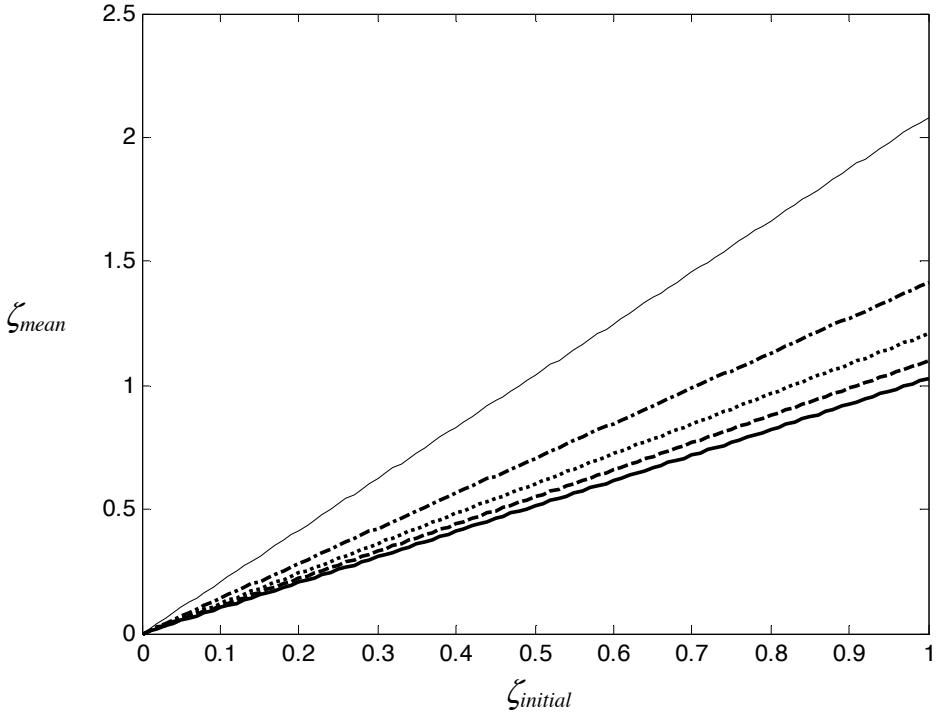


Figure 4.14. Effect of the switching stiffness in the actual damping ratio for various values of the stiffness reduction ratio σ. The horizontal axis represents the initial damping ratio and the vertical axis the mean damping ratio. (—$\sigma = 0.1$; -- $\sigma = 0.3$; ···· $\sigma = 0.5$; -·- $\sigma = 0.7$ – $\sigma = 0.9$)

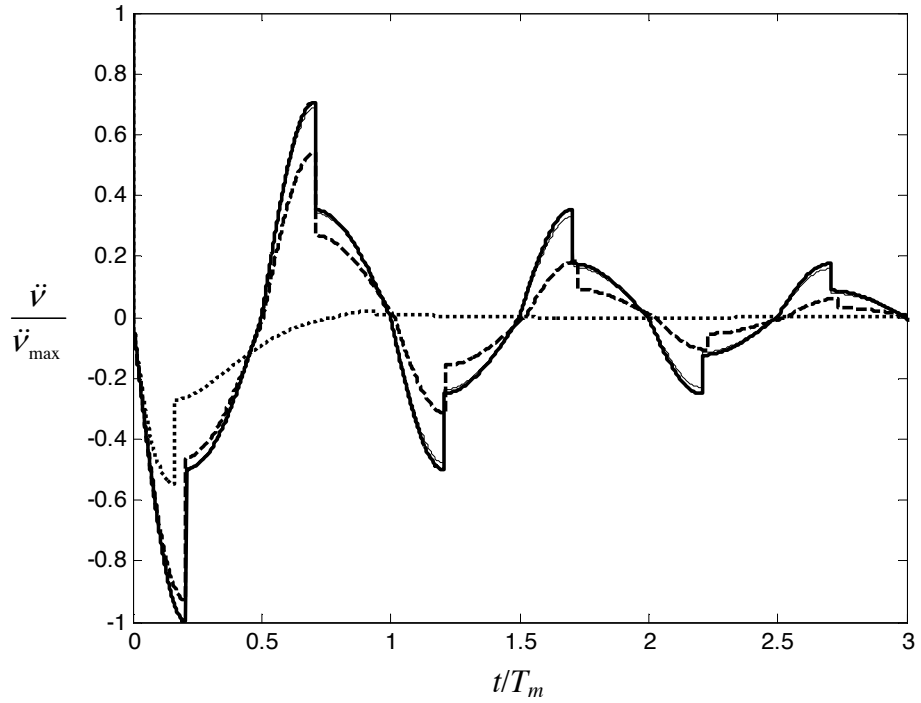


Figure 4.15. Acceleration response for the on-off variable stiffness system with damping. (—$\zeta = 0$; –$\zeta = 0.01$; -- $\zeta = 0.1$; ····$\zeta = 0.3$).

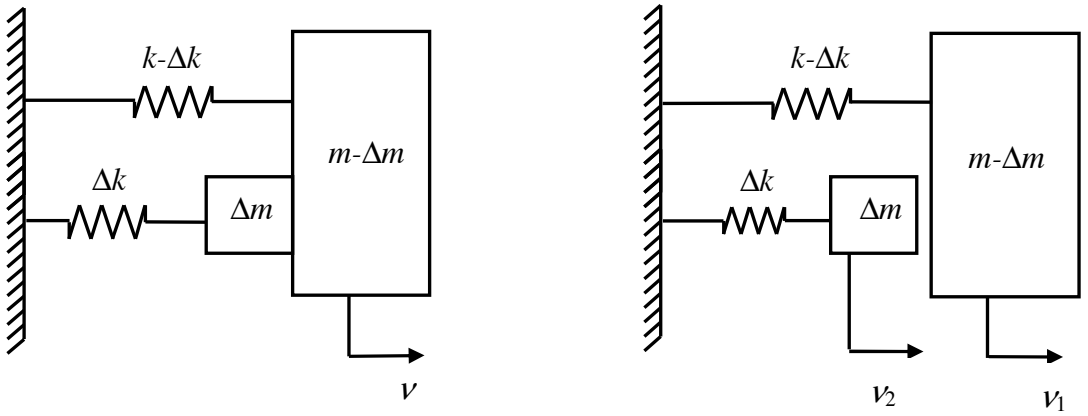


Figure 4.16. On-off stiffness model considering a secondary spring with mass: (a) The systems are rigidly attached, (b) The secondary mass is disconnected and oscillates independently from the main mass.

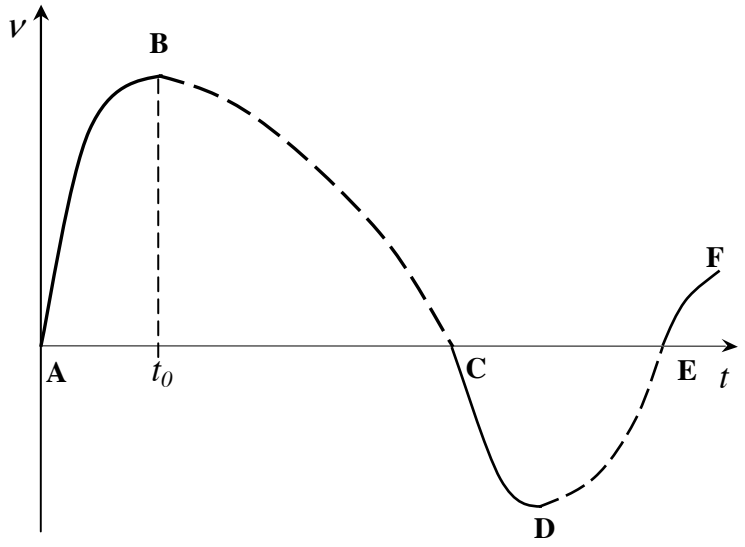


Figure 4.17. Response of the main mass $m - \Delta m$ before the stiffness reduction (—) and after the reduction (— —).

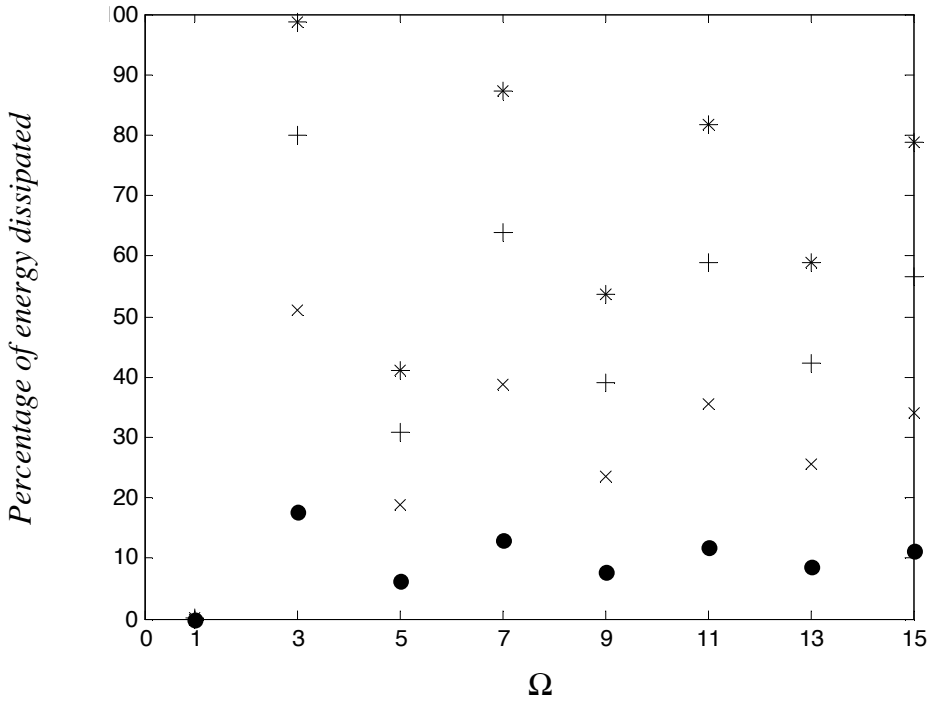


Figure 4.18. Percentage of energy dissipated as a function of the secondary to primary system frequency ratio Ω, for several values of the stiffness reduction ratio $\sigma$. (● $\sigma = 0.1$; × $\sigma = 0.3$; + $\sigma = 0.5$; ✳ $\sigma = 0.7$)

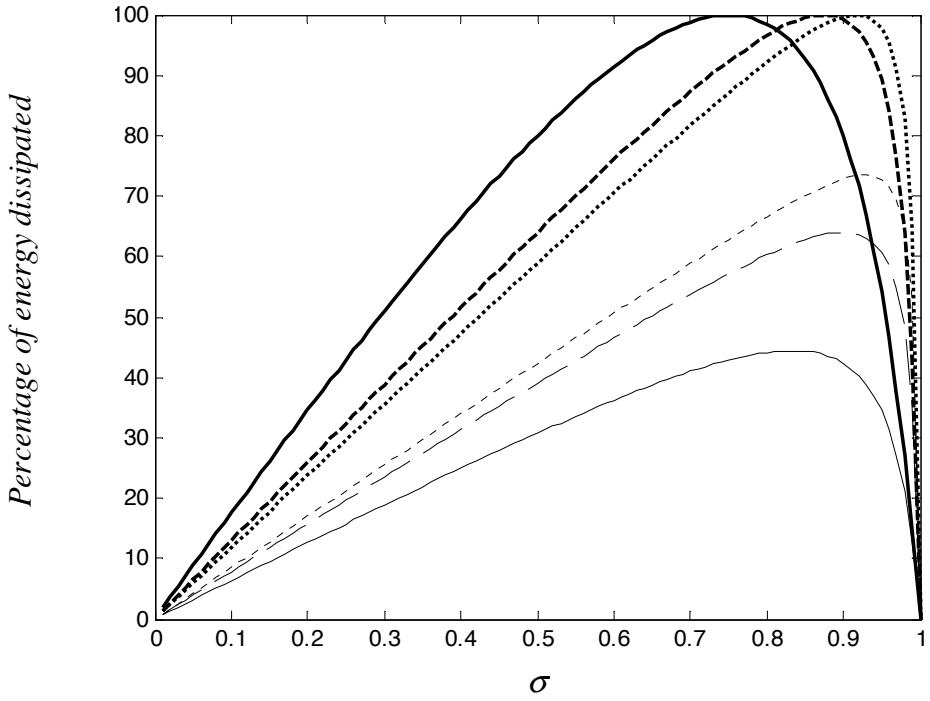


Figure. 4.19. Percentage of energy dissipated at the first reconnection as a function of the stiffness reduction ratio $\sigma$ for different values of the secondary to primary systems frequency ratio Ω. (—— Ω = 3; --- Ω = 7; ···· Ω = 11; — Ω = 5; – – Ω = 9; - - - Ω = 13).

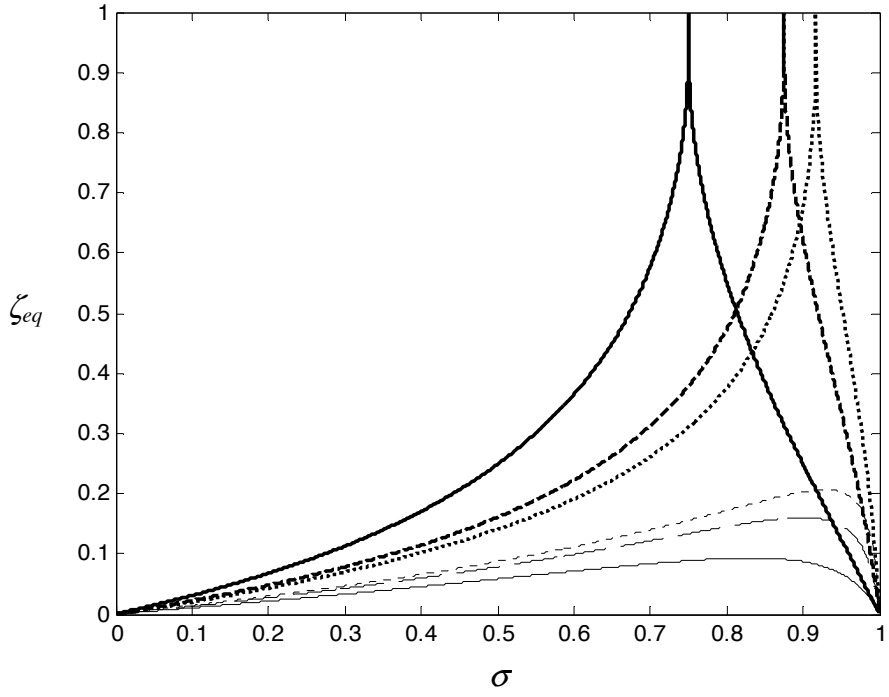


Figure. 4.20. Equivalent damping ratio $\zeta_{eq}$ as a function of the stiffness reduction ratio $\sigma$ for different values of the secondary to primary system frequency ratio Ω.
(—— Ω = 3; --- Ω = 7; ···· Ω = 11; — Ω = 5; – – Ω = 9; - - - Ω = 13).

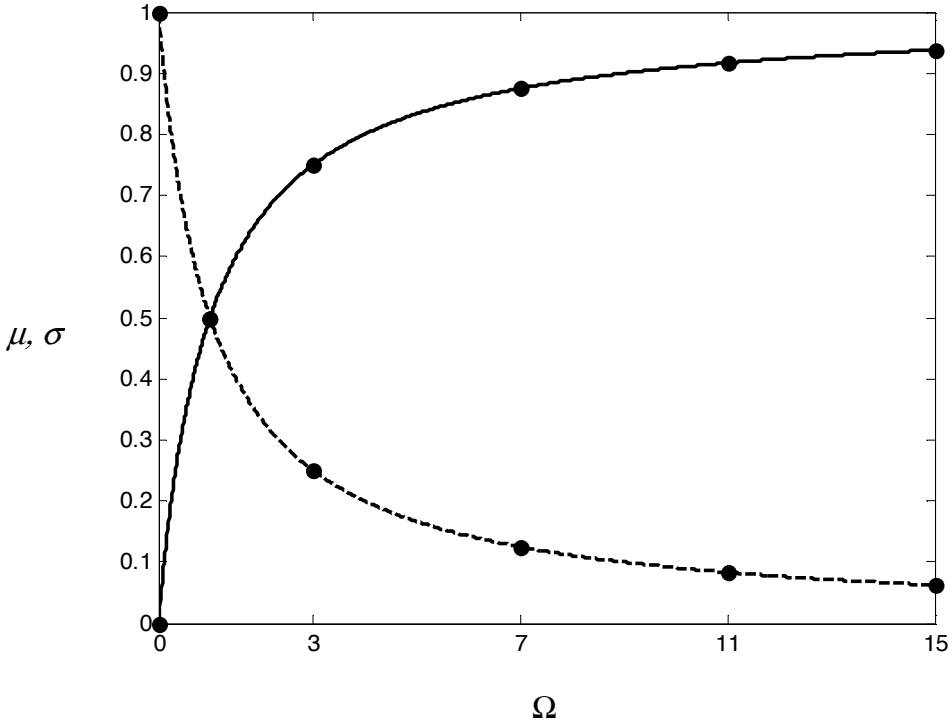


4.21. Values of the stiffness reduction ratio $\sigma$, and mass ratio $\mu$ corresponding to different values of secondary to primary system frequency ratio Ω which give maximum energy dissipation in the impacting model. (—— $\sigma$; --- $\mu$).

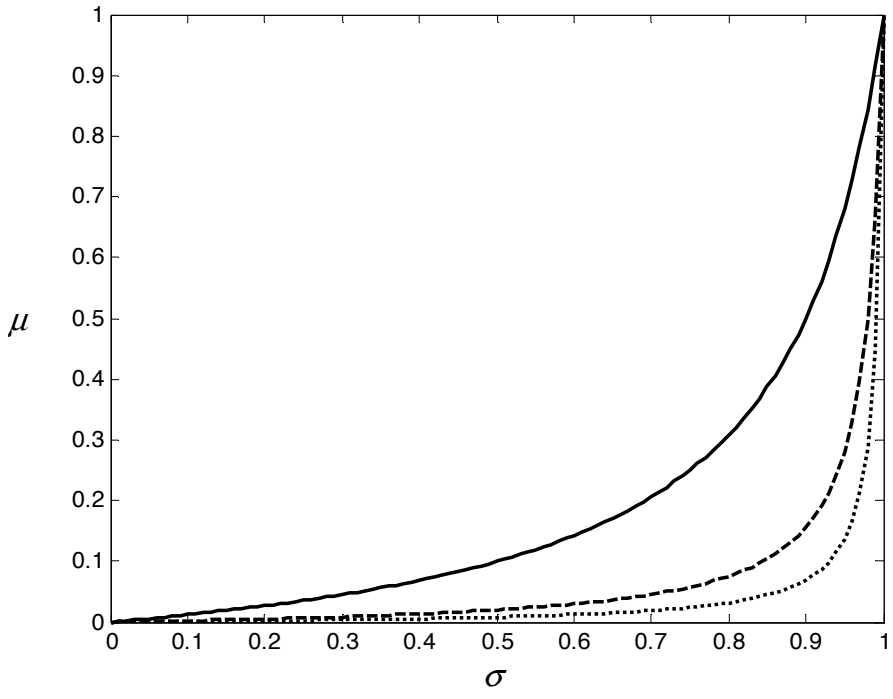


Figure. 4.22. Combinations of the stiffness reduction ratio $\sigma$, and mass ratio $\mu$ causing the secondary mass to be exactly at the static equilibrium position at the moment of impact, for optimum vales of the secondary to primary system frequency ratio Ω.

(—— Ω = 3; --- Ω = 7; ····· Ω = 11).

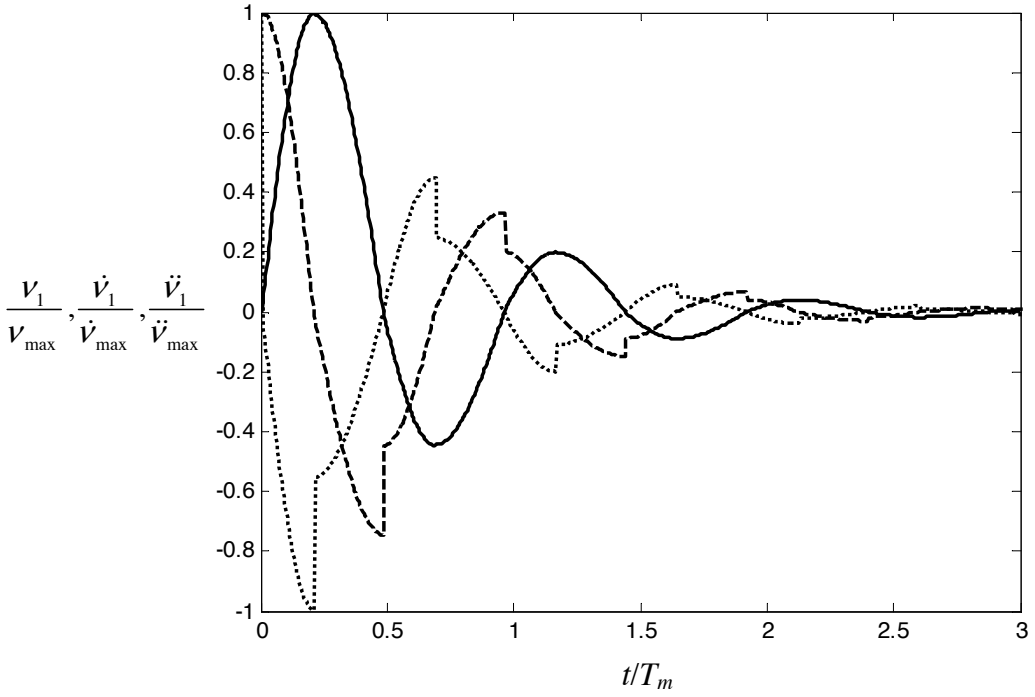


(a)

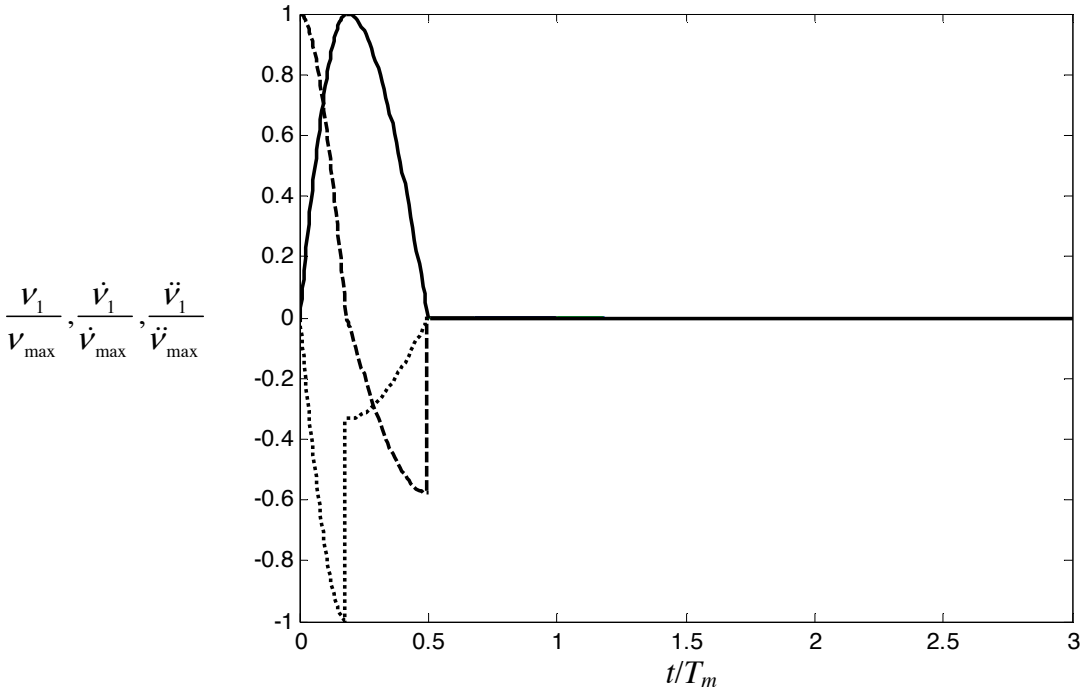


(b)

Figure 4.23. Time response for the impacting model. The time is normalised with respect to the mean period $T_m$. (a) $\sigma = 0.5$ and $\mu = 0.1$, (b) $\sigma = 0.75$ and $\mu = 0.25$. The frequency ratio between secondary and primary system is $\Omega = 3$. (──Displacement; ----- Velocity; ····· Acceleration),

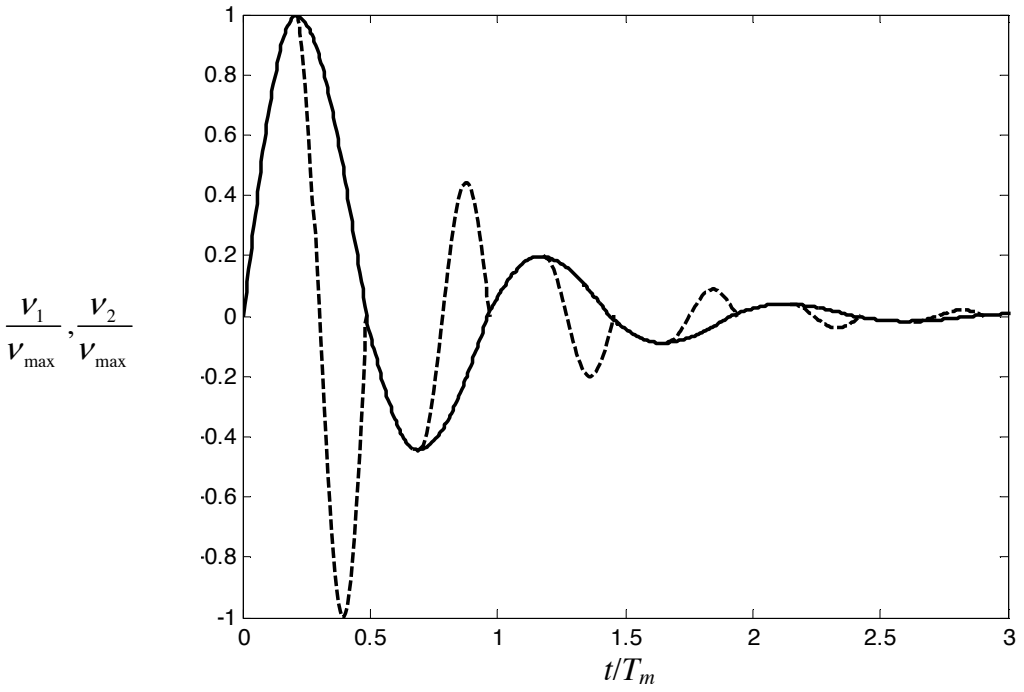


(a)

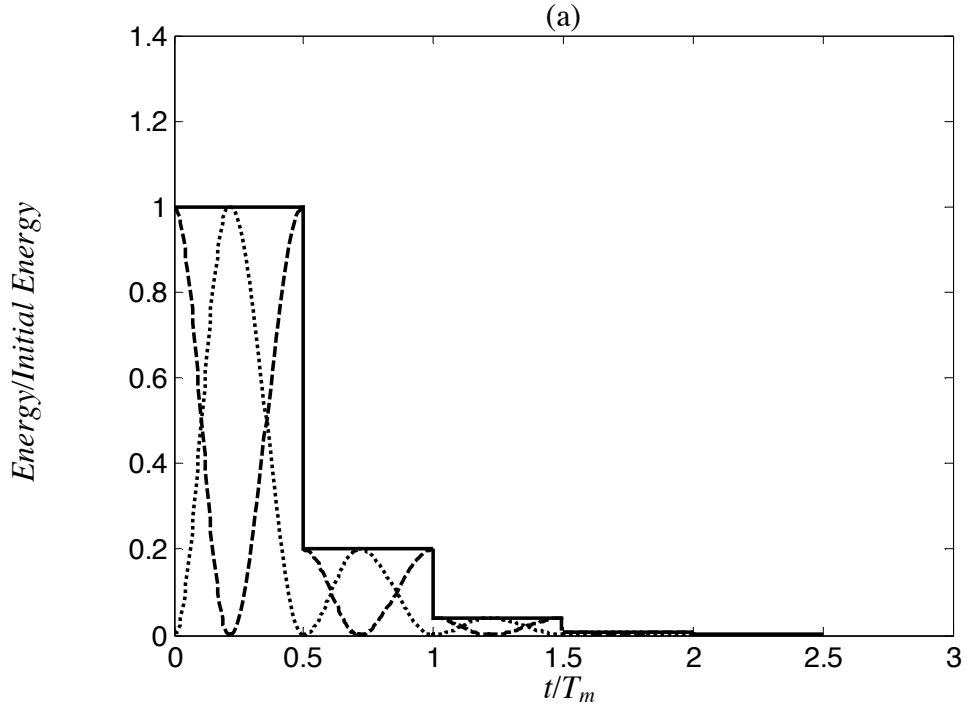


(b)

Figure 4.24. (a) Displacement response for both the main (——) and the secondary system (---). (b) Energy levels in the system. (—— Total energy; --- Kinetic energy; ···· Potential energy). Time is normalised with respect to the mean period $T_m$.. For this example the stiffness reduction ratio is $\sigma = 0.5$ and the mass ratio $\mu = 0.1$, giving a secondary to primary system frequency ratio $\Omega = 3$

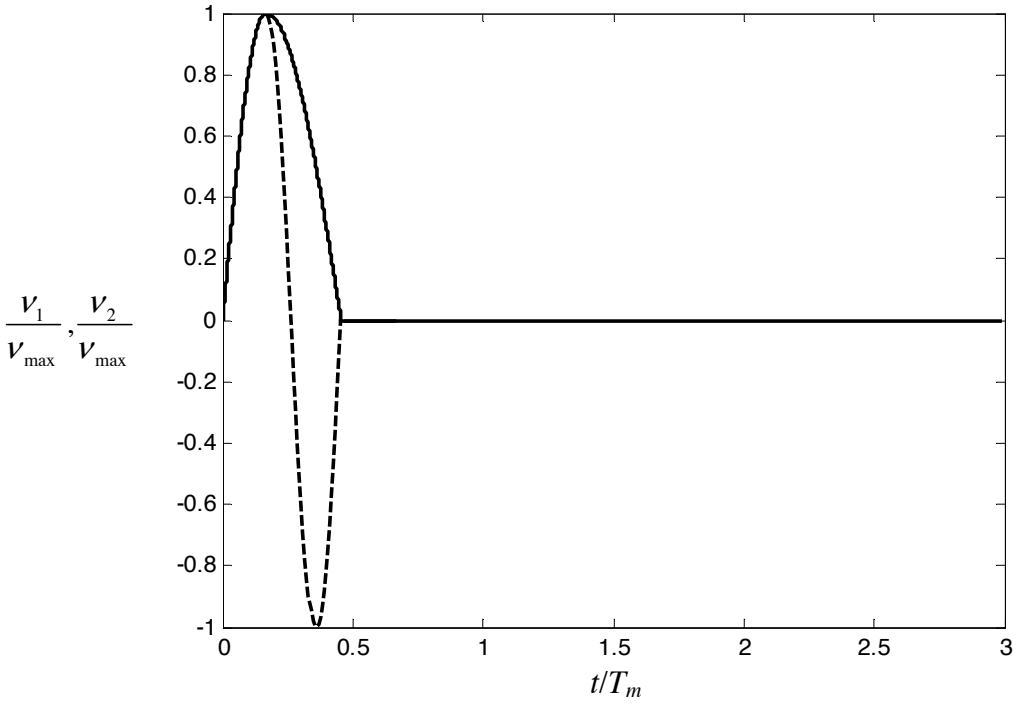


(a)

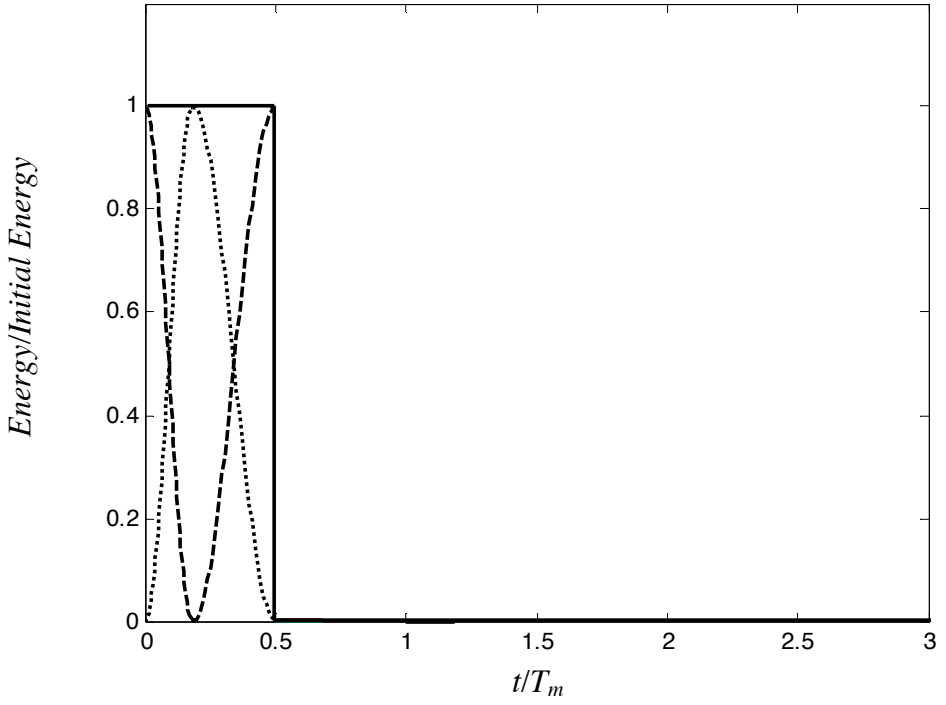


(b)

Figure 4.25. (a) Displacement response for both the main (——) and the secondary system (---). (b) Energy levels in the system. (—— Total energy; --- Kinetic energy; ···· Potential energy). Time is normalised with respect to the mean period $T_m$. For this example the stiffness reduction ratio is $\sigma = 0.75$ and the mass ratio $\mu = 0.25$, giving a secondary to primary system frequency ratio $\Omega = 3$ and maximum energy dissipation.

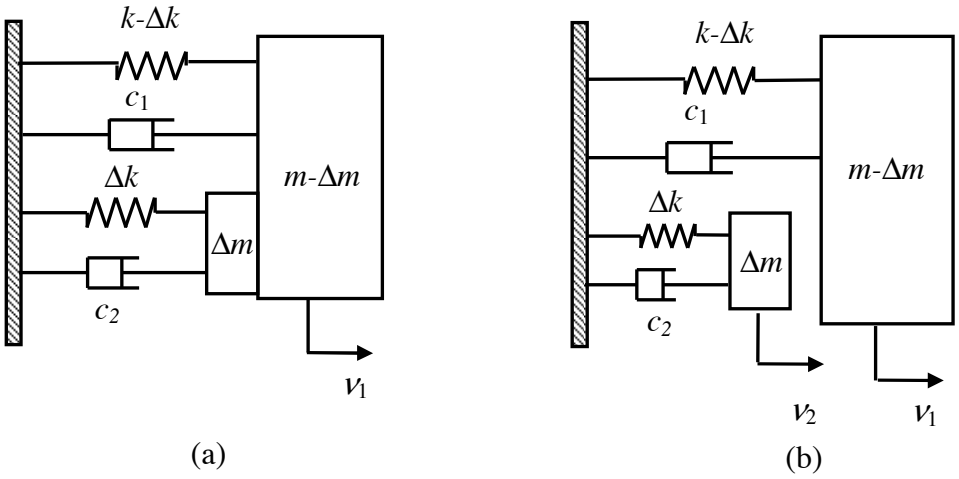


Figure 4.26 On-off stiffness model with viscous damping model considering a secondary spring with mass: (a) The systems are rigidly attached. (b) The secondary mass is disconnected and oscillates independently from the main mass.

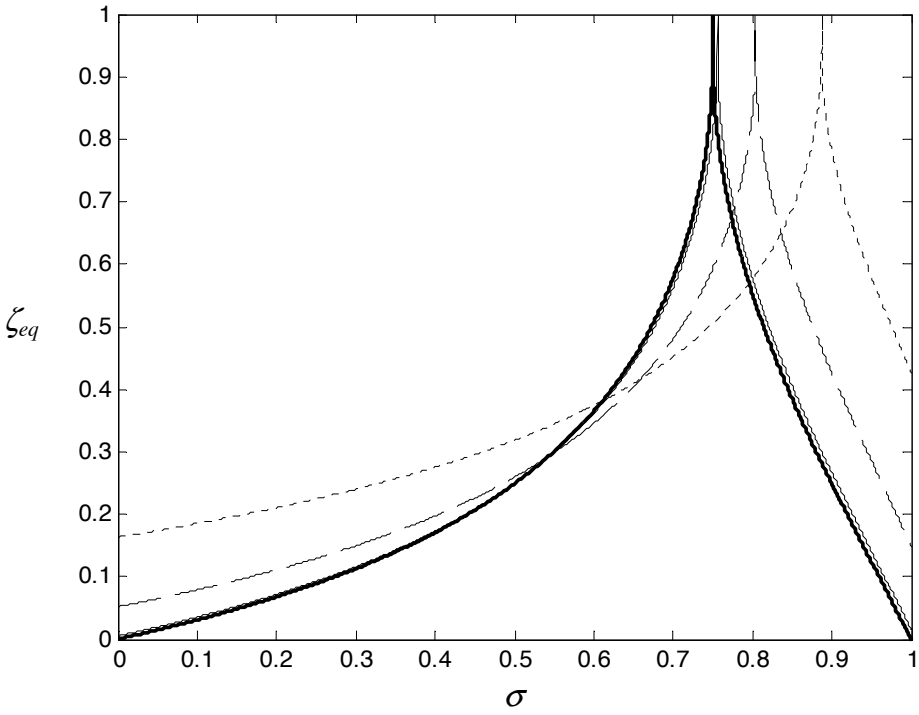


Figure 4.27. Equivalent damping ratio $\zeta_{eq}$ for the impacting system considering viscous damping in both primary and secondary systems, considering the same damping ratio in both systems, so $\zeta = \zeta_1 = \zeta_2$. The frequency ratio is $\Omega_d = 3$. (——$\zeta = 0$; —·—$\zeta = 0.01$; – – $\zeta = 0.1$; - - - $\zeta = 0.3$).

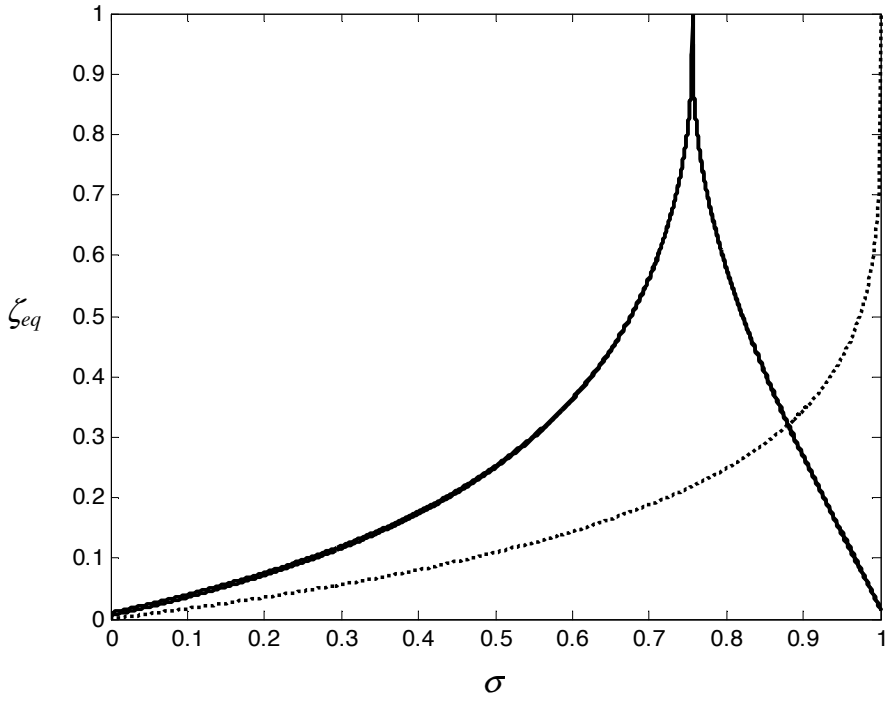


Figure 4.28. Equivalent damping ratio comparison between an impacting model, considering a frequency ratio of $\Omega = 3$ (——), and the same model when the secondary mass approaches to zero (·····).The viscous damping ratio considered for both models is the same and is equal to 1%.

# Chapter 5.

# Design of a switchable stiffness experimental model.

## 5.1. Introduction.

The main objective of this chapter is to describe the design and several tests on a test rig where the stiffness could be changed in real time. For the sake of simplicity in the design a simple switchable spring was chosen for the experimental rig, rather than a compound model involving impacts. It has been shown previously that both the simple and compound (impacting) models have similar performance characteristics. The physical properties of the experimental model are estimated in terms of the percentage stiffness change and effective damping ratio when switched between two constant stiffness states. The linearity of the system is also studied by means of static and dynamic tests. This experimental rig was used to validate experimentally the analysis and theoretical findings presented in chapters 3 and 4. The experiments regarding the implementation of the real time control strategies are described in chapter 6.

## 5.2. Description of the rig.

In order to successfully replicate and validate the theoretical concepts presented in chapters 3 and 4, an experimental variable stiffness design must fulfil certain conditions. Firstly, in order to be able to gain benefits and appreciate the effect of the stiffness reduction, the system must be capable of achieving a high stiffness change, at least a factor of two. Secondly, this change has to be made very rapidly, since the stiffness change needs to be performed in real time every quarter of cycle. The actual absolute time in which the stiffness switchings will be performed will depend upon the natural frequency of the system. Consequently it is preferable to have an original system with a low natural frequency in order to allow for a greater interval between low and high frequency states. Moreover, that the system should be lightly damped in order to observe a significant change in the residual decay rate due to the switching and losses of energy through the switching system. It is also desirable that the system approaches a single degree-of-freedom model.

In order to have a system with these characteristics, a variable rate elastic element was conceived and designed using electromagnetic forces. The fundamental idea behind the model is similar to the concept of magnetic levitation. If one has two magnets aligned with their opposite poles facing, as shown in figure 5.1, the resulting repulsive force when suitably configured acts essentially as a restoring force. If one uses an electromagnet instead of a permanent magnet the magnetic field can be changed, therefore the restoring force, which can be considered to be due to an equivalent effective stiffness, will be changed. As a result, one can obtain a variable rate or switchable stiffness element depending upon the voltage supplied to the electromagnets. However, there are some disadvantages of the simple system described above, as the system is highly nonlinear because of the magnetic forces involved; the repulsive force is not proportional to the separation of the magnets. Also, an unstable system is likely to be present unless some restraints are implemented.

In order to take advantage of the magnetic spring concept and to avoid the inconveniences it introduces, a modified design was proposed. As depicted in figure 5.2(a), the system comprises two permanent, disc shaped neodymium magnets (1, 2) which are suspended

between two electromagnets (3, 4), in a symmetric arrangement. The permanent magnets are held by an aluminium ring (8), which is suspended using four tensioned wires. Only two of them are shown in the figure (6, 7), which are attached to the main frame (5). Figure 5.2.(b) shows a photograph of the actual system. The total mass of the permanent magnets and the aluminum ring is 0.0753 kg, which is the isolated mass. By varying the voltage applied to the electromagnets, the repulsive force changes, and the effective combined stiffness of the system is varied. It is important to note that although the system in the figures is shown in the vertical position, the experiments were made with the system in the horizontal position to avoid the effect of gravity.

When the electromagnets are turned off, the effective stiffness of the system is said to be in the low or softer state. This stiffness setting is basically defined by two mechanisms. The first one is given by the wires, which provide part of the effective residual stiffness of the system. The second mechanism is given by a softening effect produced as a result of the attraction between the iron core of the electromagnets when turned off and the permanent magnets. This effect becomes more evident as the permanent magnets approach the electromagnets, due to the nonlinear nature of the magnetic forces. The system is designed in such a way that the supporting wires can be changed for others of different material and/or thickness in order to have different stiffness properties.

The high stiffness state is then engaged when the electromagnets are activated. Once the electromagnets have been switched on in the repulsive configuration, the effective stiffness increases, thus the system is in a high stiffness state. This state differs considerably from the low stiffness state. In this case, the repulsive force between the electromagnets and the permanent magnets causes a hardening effect. The electromagnets used are capable of working in the 0-24V voltage range. However, to avoid excessive heating only a maximum of 18 V is used, since the electromagnets draw a considerable current (between 1 A and 3 A). For the purposes of this study and subsequent analyses, only the extreme stiffness states are of interest as this corresponds to the maximum stiffness changes. This means the electromagnets are turned on or off depending upon the control law. Consequently, the change in stiffness is approximately immediate.

A possible issue in this setup is the tension in the supporting wires. It was observed during the tests that the wires tended to slacken as the tests were running. It was necessary to keep them tensioned by occasional adjustment. This problem also caused slight variations in the resonance frequency and damping ratio when the tests were repeated, as it is very difficult to ensure that the same tension is applied to the four wires for all the tests.

## 5.3. Procedure.

The main objective of estimating the physical properties of the system was achieved by measuring the transmissibility of the rig using broadband random excitation applied to the base. The resonance peak for different applied voltages was determined and the effective stiffness change was found. These tests were performed for two different supporting wires, namely titanium and nylon. Additionally, a simple static test was developed in order to check the linearity of the system, and the transmissibility tests were also measured for different amplitude values.

The equipment and apparatus used were:

- Data Physics analyzer.
- Hameg triple power source HM7042-5.
- PCB accelerometer 352C22 (2).
- Derritron shaker VP4.
- Power amplifier.
- PCB Signal conditioner.

A block diagram showing the setup of the equipment is shown in figure 5.3. Two accelerometers were used to acquire the signals from the base of the shaker and the suspended magnets respectively. The Data Physics analyzer was used to calculate the frequency response function using the input signals from the accelerometers. Additionally, the same analyzer was used to send an excitation to the shaker through a power amplifier. The peak

signal levels measured on the base were between 0.08 g and 1 g for the minimum and maximum amplifier gains used in the tests. The frequency response functions were acquired using a Hanning window, 1600 lines of resolution, a frequency span of 0-200 Hz, 40 averages and 50% data window overlap.

## 5.4. Results.

A preliminary transmissibility test used to assess the degree of linearity of the system was first performed. The transmissibility was measured over a range of excitation amplitudes. Figure 5.4 presents the magnitude of the frequency response function (FRF) for the minimum and the maximum excitation levels (0.08 g and 1 g respectively). This particular example corresponds to the system supported by nylon wires with the electromagnets turned off.

Transmissibility plots are presented in figures 5.5 to 5.12 comprising magnitude, phase angle and coherence. The plots are presented in a dB scale for the magnitude (V/V) and for a linear frequency scale (Hz). Figure 5.5 corresponds to having no electromagnets, figure 5.6 for the case with the electromagnets attached but turned off, figure 5.7 for electromagnets turned on at 12 V, and figure 5.8 for electromagnets turned on at 18 V, all for nylon supporting wires. Additionally, figures 5.9 to 5.12 depict the same corresponding situations described above but for titanium wires.

## 5.5. Discussion.

The first concern about the experimental setup was the high possibility of nonlinearities due to the magnetic forces involved. As mentioned previously, the system exhibits a softening behaviour when the electromagnets are turned off, because the permanent magnets are attracted to the iron of the electromagnets. In contrast, a hardening effect is present when the electromagnets are turned on, due to the repulsive magnetic force, which is essentially nonlinear. A first test involving the measurement of the FRF for different amplitudes of the excitation force was developed. This test was performed for both nylon and titanium, for their respective high and low stiffness states. The peak amplitude values for the suspended magnet were between 0.06 mm and 1 mm for the lowest and highest amplitude settings.

Similar results were obtained for all the cases. Several FRF magnitude curves overlapped each other showing only small variations. Moreover, a simple static test carried out between those displacements limits also show the linearity of the system. Thus this test demonstrates that at least in the displacement range of interest the system behaves fairly linearly. Further measurements had peak displacements of approximately 0.8 mm and rarely surpassed 1 mm. Between these limits the system approaches very well a linear single degree of freedom model which is necessary to accurately validate the theoretical studies previously presented.

Further observation and insight into the possible nonlinearities of the model can be obtained from the transmissibility and coherence plots presented in figures 5.5 to 5.12. The transmissibility has been calculated for different input amplitude values and the comparable transmissibility plots show a good degree of linearity (see figure 5.4 for an example).

Figures 5.5 and 5.9 shows the FRF for the case of no electromagnets, when the permanent magnet is suspended by nylon wires and titanium wires respectively. In particular, it is interesting to observe figures 5.5(a) and 5.9(b) which show poor coherence above the resonance peak. It is very likely that the cause of this problem could be noise as a result of the measured suspended magnet response being too low compared with the base amplitude. It is unlikely that nonlinear effects can cause this behaviour as it has been shown before the high degree of linearity present in the system. However, the significance of this figure is to estimate the natural frequency, in this case being approximately 17.37 Hz. This configuration with no electromagnets has been included for comparison with the other situations as will be seen later, and this particular configuration was not considered for subsequent tests.

In contrast, when the electromagnets were attached the coherence improved significantly, especially when the permanent magnet was supported by nylon wires (figure 5.6). When the electromagnets were turned on the coherence was also affected (figure 5.7), but improved again when the voltage was increased (figure 5.8). These problems in the coherence are probably due to the nonlinear effects of the magnetic forces although small. In general, the coherence showed acceptable values. A similar behaviour was observed when titanium wires where used. Moreover, there was the possibility of a rotational mode occurring on the suspended magnet assembly, which can be easier to appreciate in the case of nylon wires. In this case a rapid

change in the phase angle can be observed at approximately 46 Hz, coinciding with a sudden drop in the coherence. Effectively the configuration of the supported magnets might lead to a rocking mode being excited, as the tension in the wires may not be equal. This phenomenon was much more prominent in the case of nylon wires, probably due to the lower stiffness, and decreases as the stiffness of the system was increased.

Having discussed the non-linear issues, the estimation of the system properties was the next step. The main objective here was to evaluate the physical properties and performance in terms of the equivalent stiffness reduction and damping ratio. These parameters can be easily obtained from the transmissibility plots presented previously. From the theory presented in chapters 3 and 4, the high and low natural frequencies are related to the stiffness reduction ratio by the following expression:

$$\sigma = 1 - \left( \frac{\omega_{off}}{\omega_{on}} \right)^2 \tag{5.1}$$

The damping ratio was calculated by the half power bandwidth method [2] from the FRF resonance peak as:

$$\zeta = \frac{\omega_2 - \omega_1}{2\omega_n} \tag{5.2}$$

It is important to note, however, that for lightly damped systems the resonance region of the FRF is susceptible to errors in the estimation of the damping ratio due to frequency resolution. For low damping, the resonance peak is very sharp, and the number of points is very small. As a result, in this zone the peak value might be based in a single point on the FRF [109]. This resolution problem was only observed in the situations when no electromagnets attached, where the system has a very low damping. However, this case was included as a reference for comparison and was not used for other tests. This problem was not present for the system with the electromagnets attached. The results for the system properties corresponding to the various situations are summarized in table 5.1.

The effect of the magnetic force in changing the effective stiffness of the system is fairly easily visible from the inspection of the transmissibility plots. The resonance peak was effectively shifted when the electromagnets are switched on. Although the effect is small when the titanium wires are used, there is still a stiffness change of 31.4% and 41.5% for applied voltages of 12 V and 18 V respectively. However, since the nylon wires produce a softer residual stiffness, the effective relative stiffness change using the electromagnets in this case was considerable higher, being 48.4% and 55% for 12 V and 18 V respectively. Another point of interest is the fact that the inclusion of the electromagnets causes the aforementioned softening effect when turned off. The natural frequency is drastically reduced when the electromagnets are attached, compared to the case with no electromagnets are present.

As expected, the system has a very low damping ratio. Thus one of the most important requirements for the system, i.e. to be lightly damped, was achieved. Damping values ranging from 0.007 to 0.04 for nylon wires and from 0.004 to 0.07 for titanium were found depending upon the different configurations. By adding the electromagnets the effective damping ratio increased. The damping ratio also increased when the electromagnets were operating. This increase in the damping might be a result of the formation of Eddy currents due to the conductive element moving through the magnetic field [111]. Another important thing to note is that the effective damping ratio was higher for the titanium wires, most probably due to the friction in the joints between the metallic frame and the wires. However, the damping in general was small, consequently the rig is suitable for investigating the switching strategy. The preferred situation, which can lead to better results for several stiffness strategies, was when nylon wires support the permanent magnet, since the stiffness change was higher and the inherent passive damping ratio was lower. Figure 5.13 presents the situation most suitable for the experiments presented in the next chapter. This configuration is for the system supported with nylon wires and the solid and dashed lines represent the off state and the on state with 12 V supplied respectively. This situation was chosen due to the considerable stiffness change with a reasonable voltage applied to avoid overheating.

## 5.6. Conclusions.

An experimental rig designed to achieve a switchable stiffness element has been introduced in this chapter. This experimental rig is based on electromagnetic forces used to obtain different stiffness settings. The rig comprises a couple of disc shaped permanent magnets suspended between two electromagnets. The stiffness variation is achieved by adjusting the voltage supplied to the electromagnets. The behaviour of the system has been investigated by performing static and dynamic tests and the linearity of the system has been evaluated. The system behaves approximately linearly in the displacement range of interest, i.e. for small displacements. Moreover, the parameters of the system have been estimated. For the configurations studied a stiffness reduction of approximately 50% has been achieved, with inherent low passive damping. The stiffness change can be made very quickly since it only depends on turning on or off the electromagnets. The experimental rig has the requirements for the validation of the theoretical strategies presented in previous chapters. The full implementation of the switching stiffness control is performed and presented in chapter 6.

| Configuration | | Damping ratio | Natural frequency Hz | Stiffness N/m | Stiffness reduction ratio |
|---|---|---|---|---|---|
| **Nylon** | No electromagnets | 0.007 | 17.37 | 898.0 | |
| | Electromagnets off | 0.034 | 12.75 | 483.3 | |
| | 12V | 0.045 | 17.75 | 936.6 | 0.484 |
| | 18V | 0.039 | 19.00 | 1073 | 0.550 |
| **Titanium** | No electromagnets | 0.004 | 16.12 | 772.5 | |
| | Electromagnets off | 0.064 | 17.62 | 922.9 | |
| | 12V | 0.072 | 21.50 | 1374 | 0.314 |
| | 18V | 0.030 | 22.87 | 1556 | 0.415 |

Table 5.1. Properties of the switchable stiffness model for the different configurations considered.

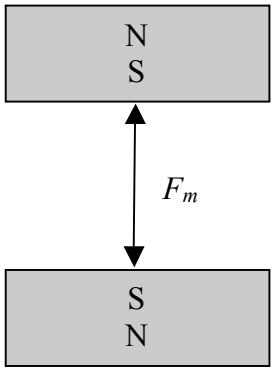


Figure 5.1. Concept of magnetic levitation. Two magnets with the same poles facing will produce a repulsive force $F_m$.

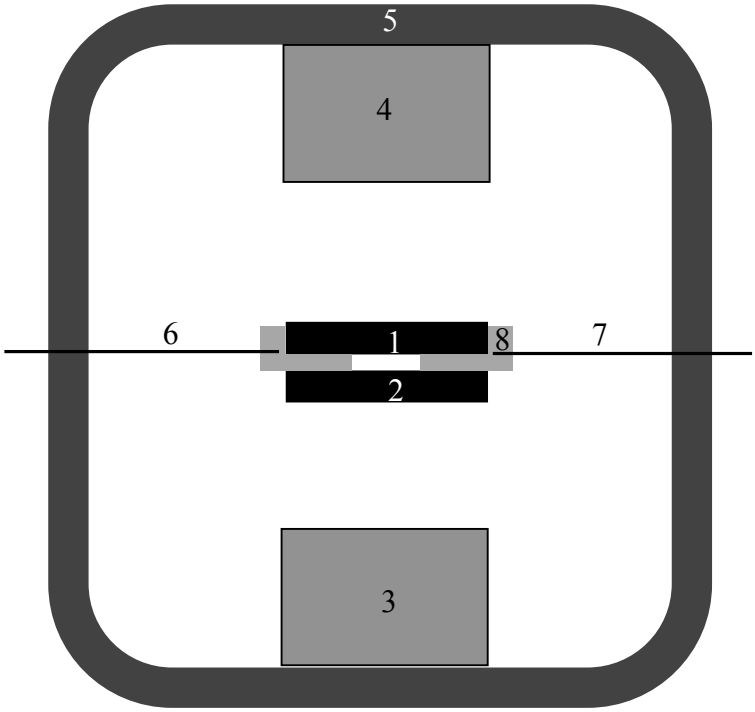


(a)

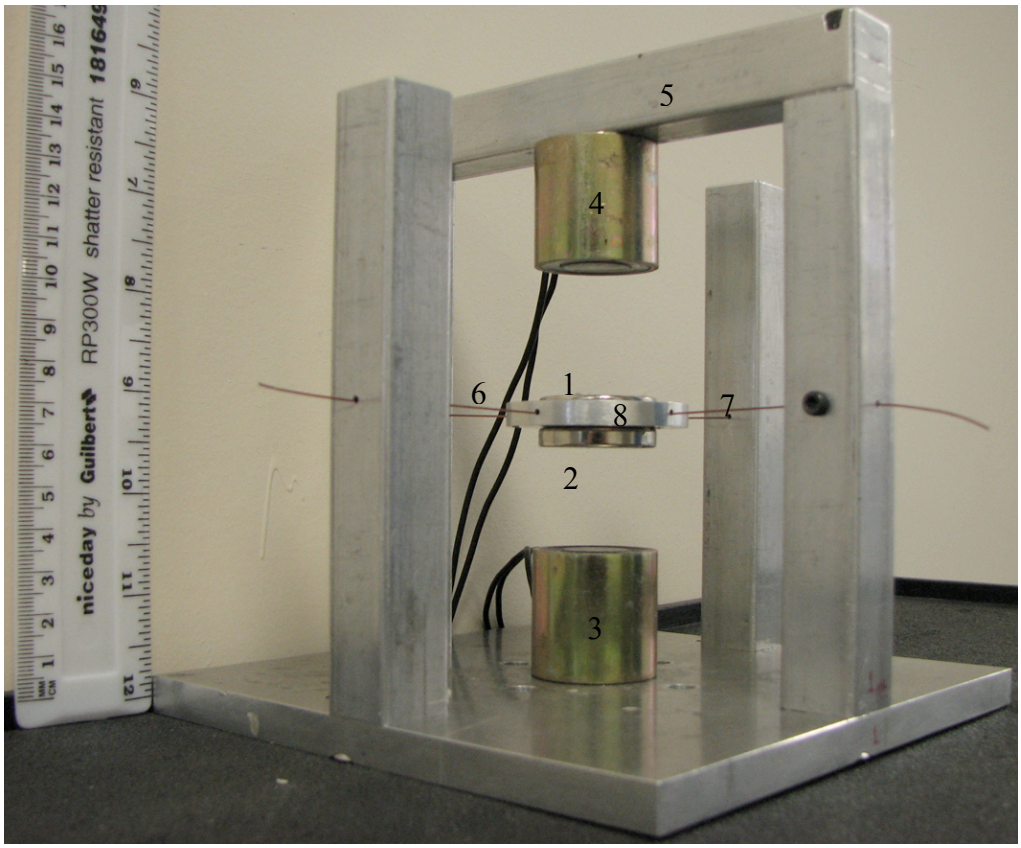


(b)

Figure 5.2. (a) Diagram of the switchable stiffness experimental rig in the vertical position. The permanent magnets (1, 2) are suspended between two electromagnets (3, 4) using four wires (6, 7) that also join the magnet to the main frame (5). (b) Photograph of the actual rig.

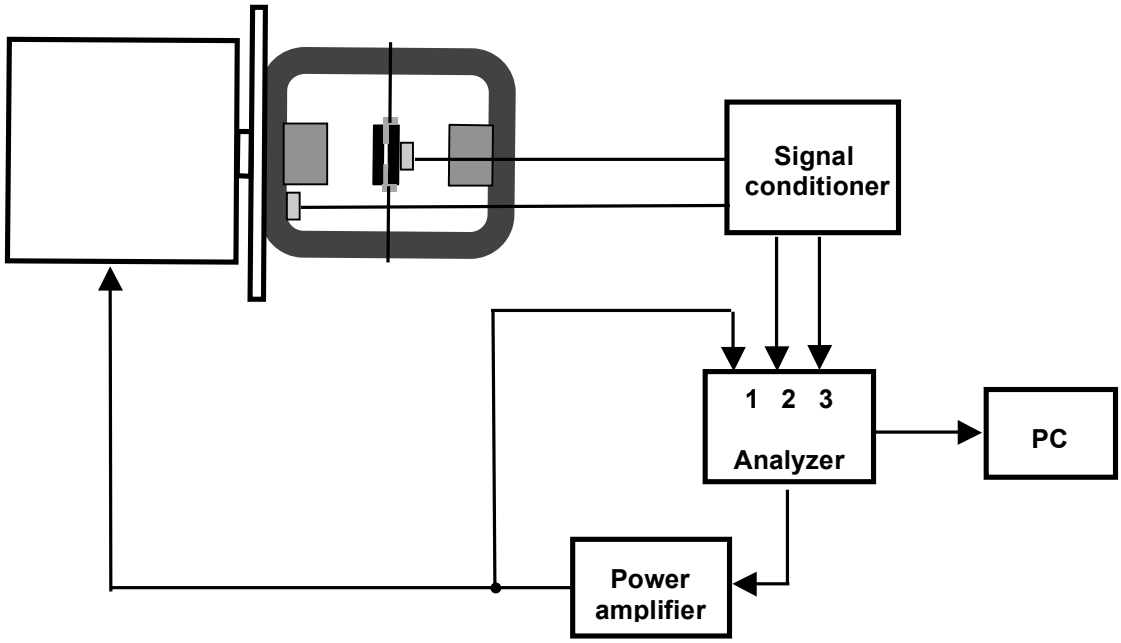


Figure 5.3. Schematic diagram of the setup used for the laboratory tests.

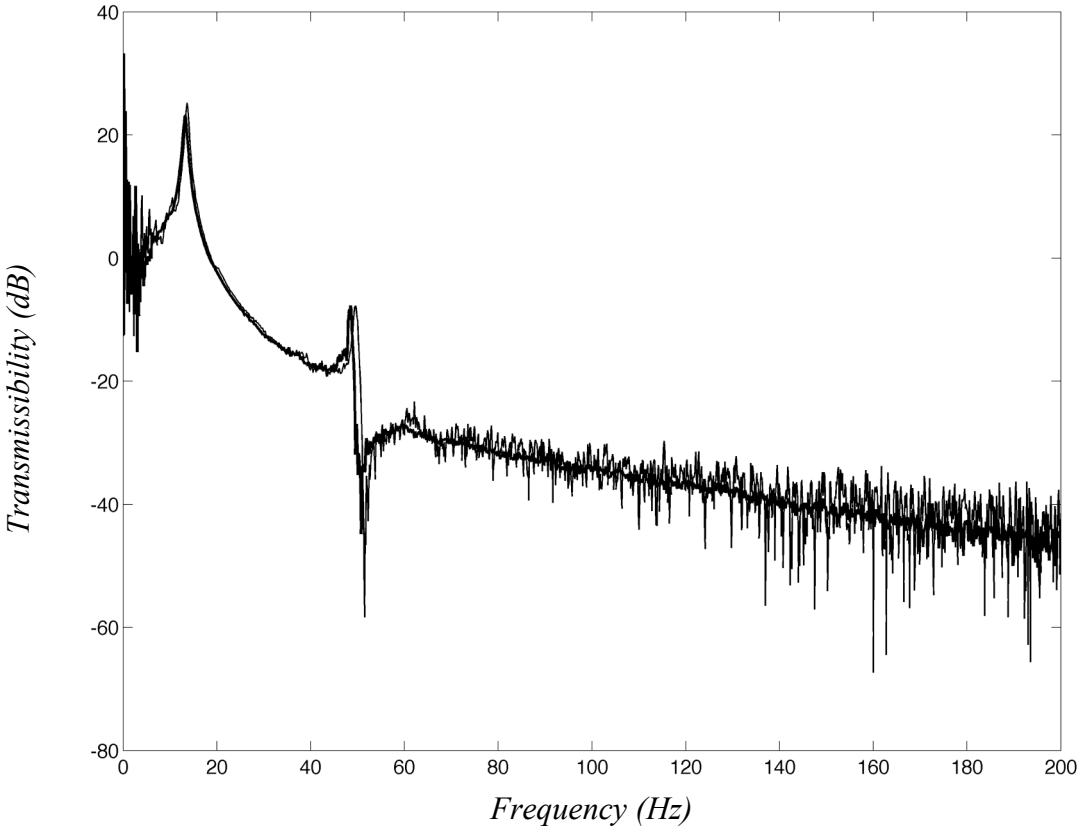


Figure 5.4. Example of frequency response function magnitude measured for two different amplitudes of the excitation signal. The bold line represents the minimum input amplitude range and the thin line represents the maximum input amplitude range. This particular example corresponds to nylon wires in the off setting.

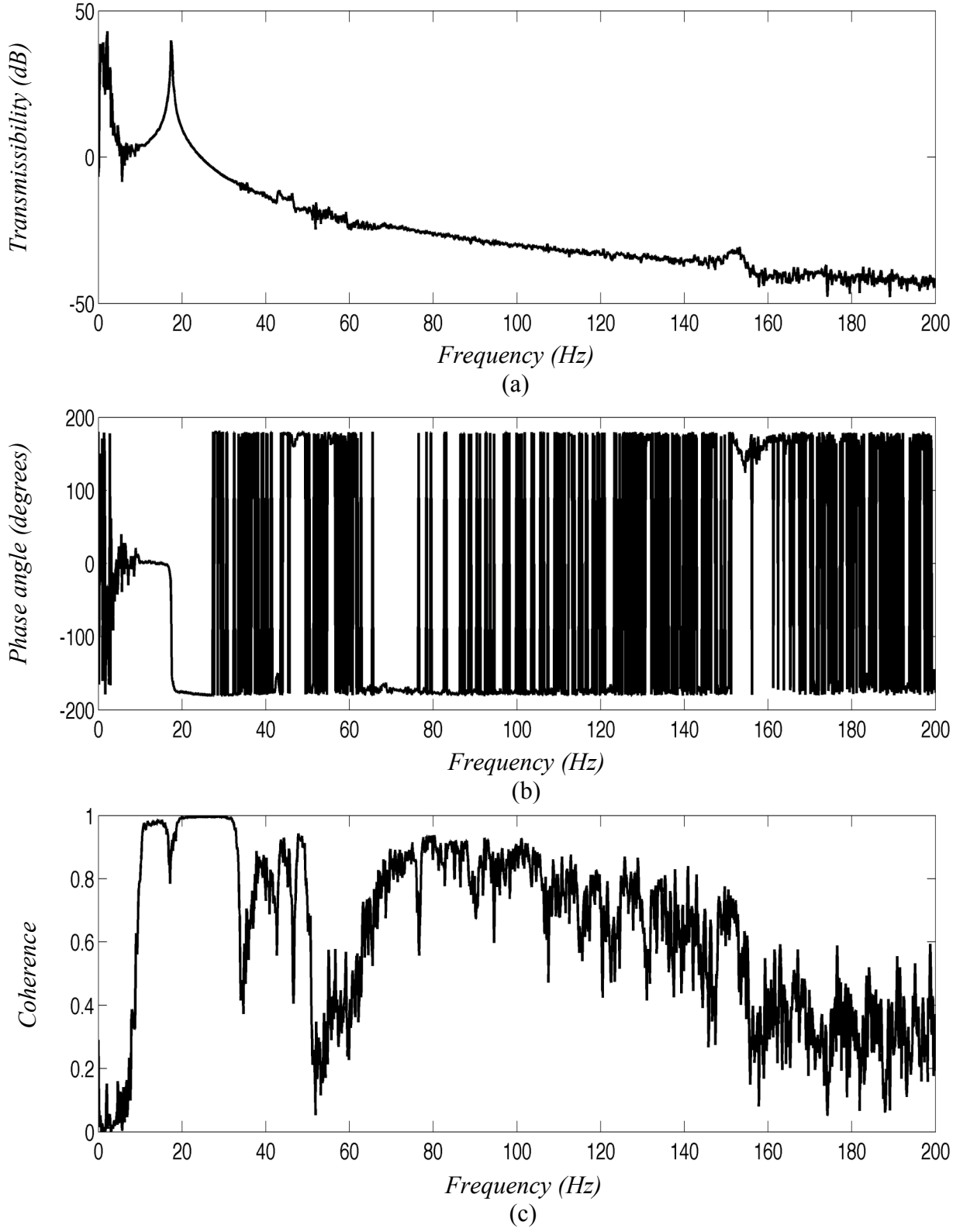


Figure 5.5. Transmissibility of the magnetic spring with no electromagnets attached and supported by nylon wires. (a) Magnitude, (b) phase angle. (c) Coherence function.

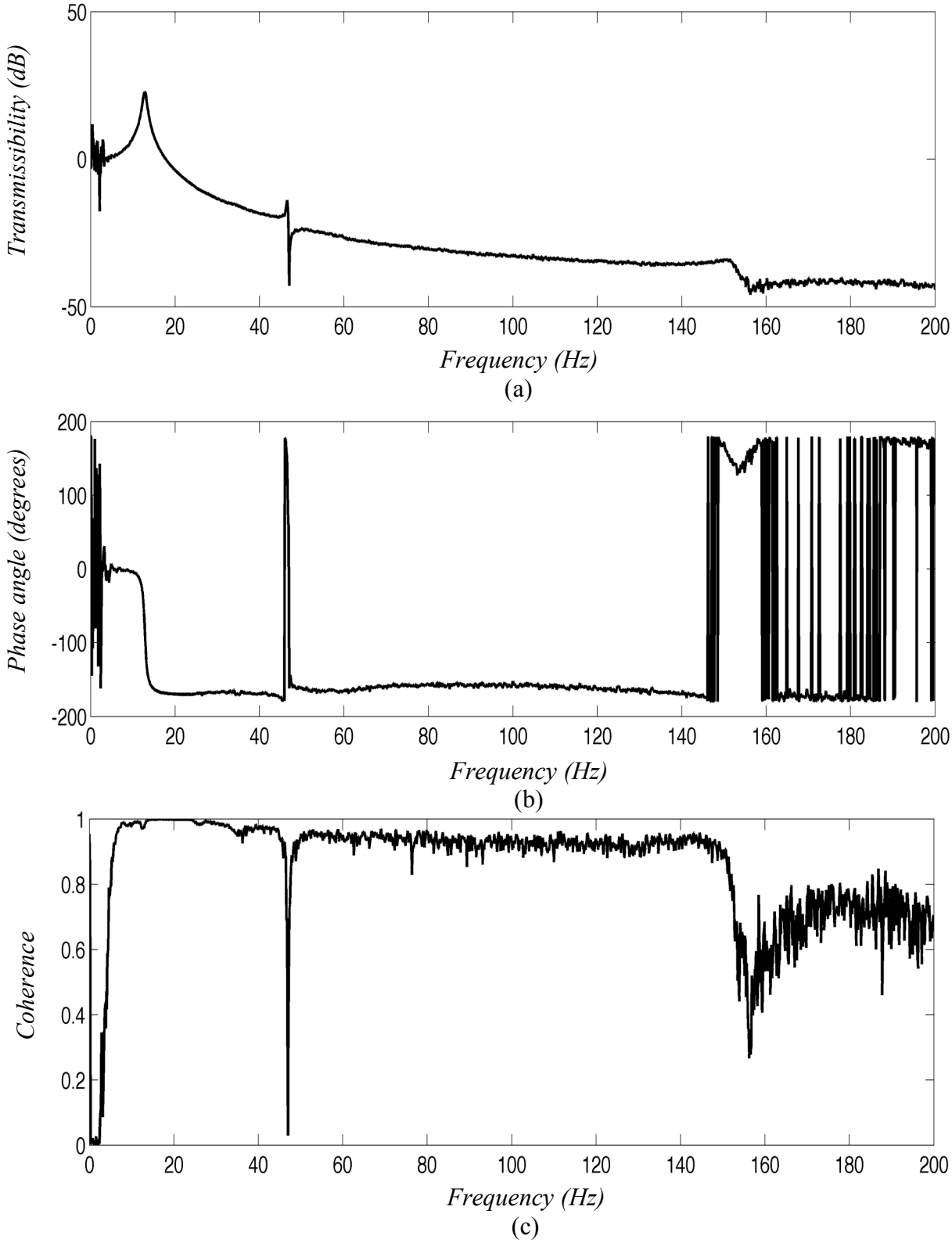


Figure 5.6. Transmissibility of the magnetic spring with the electromagnets attached but turned off. The permanent magnet is supported by nylon wires. (a) Magnitude, (b) phase angle. (c) Coherence function.

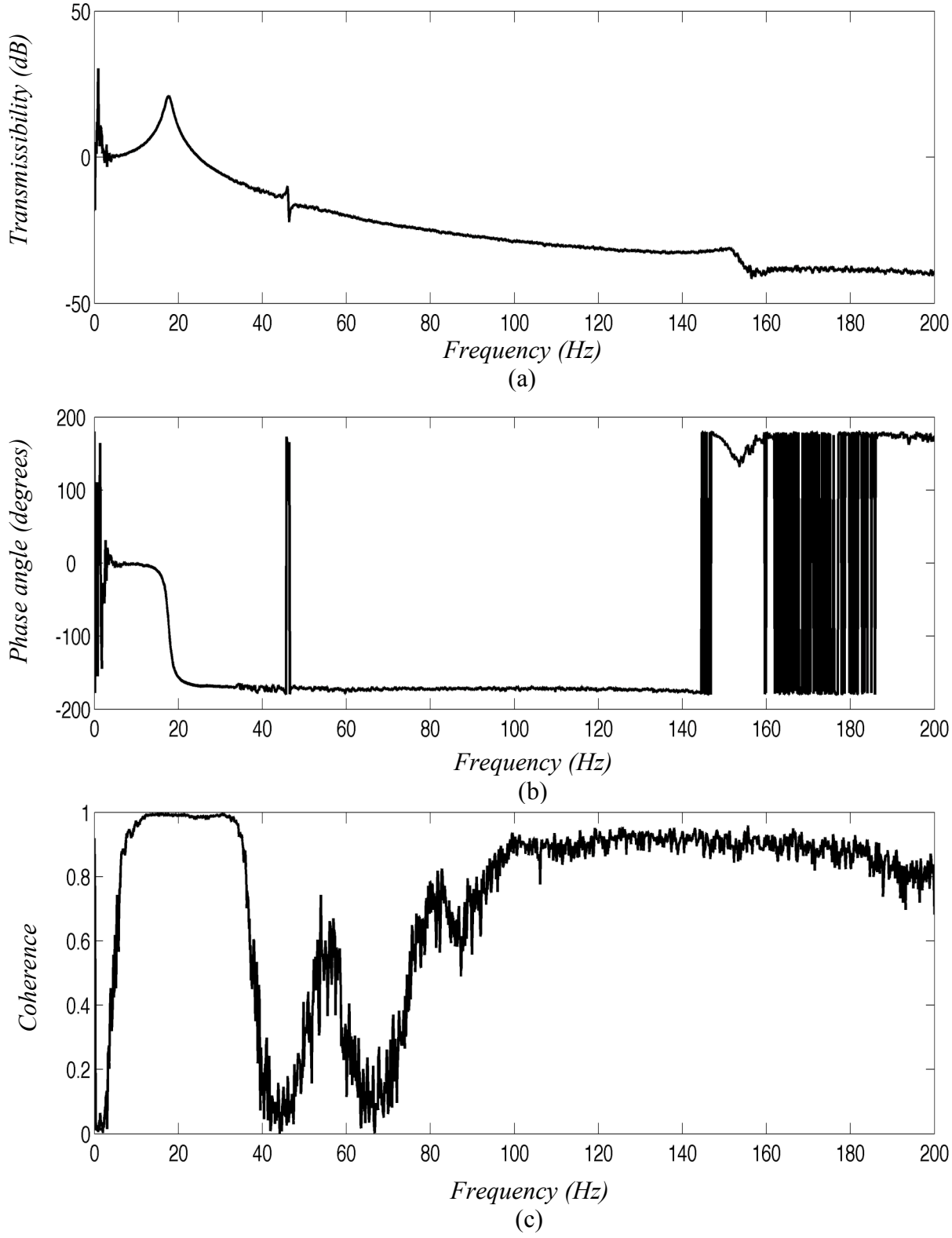


Figure 5.7. Transmissibility of the magnetic spring with the electromagnets powered with 12 V. The permanent magnet is supported by nylon wires. (a) Magnitude, (b) phase angle. (c) Coherence function.

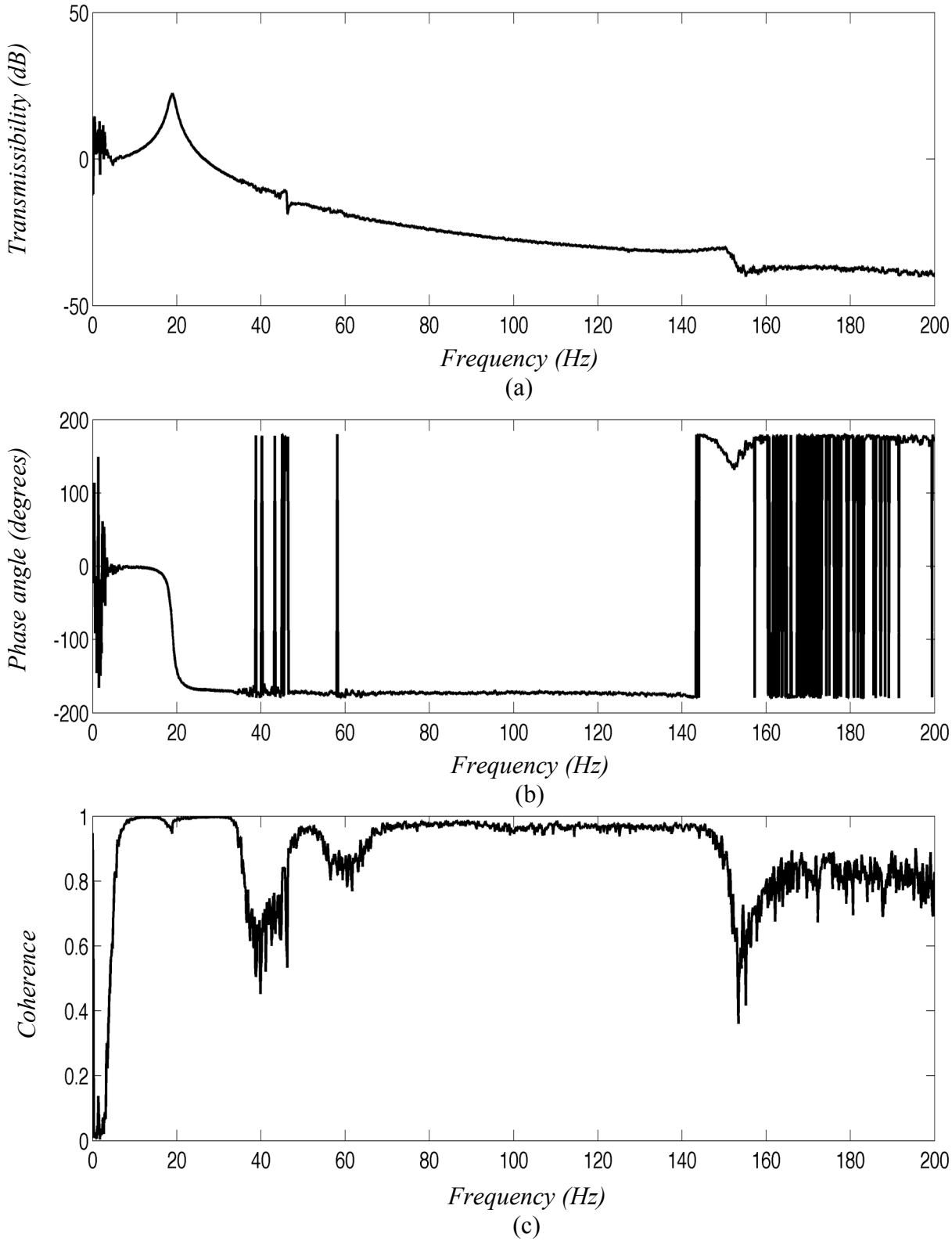


Figure 5.8. Transmissibility of the magnetic spring with the electromagnets powered with 18 V. The permanent magnet is supported by nylon wires. (a) Magnitude, (b) phase angle. (c) Coherence function.

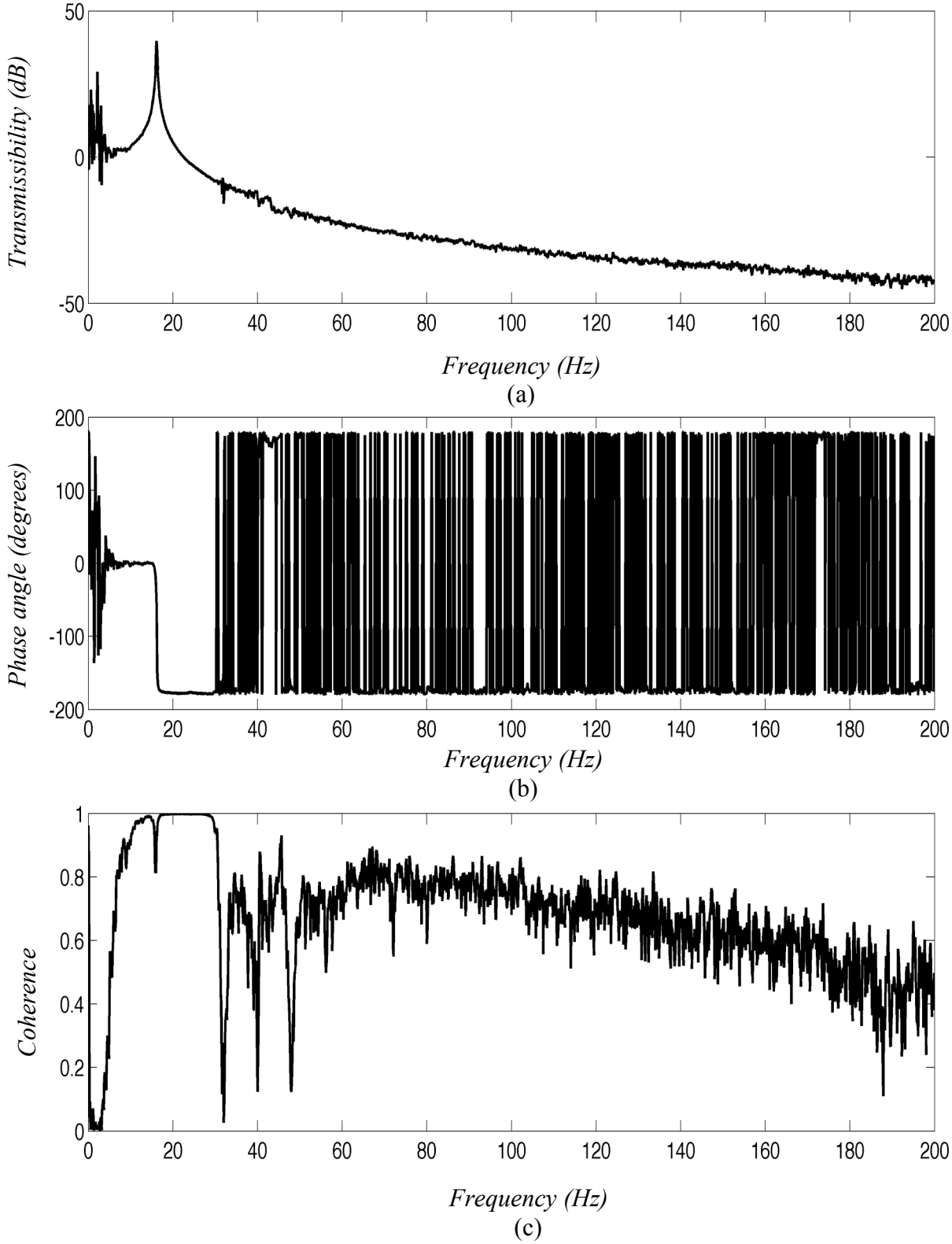


Figure 5.9. Transmissibility of the magnetic spring with no electromagnets attached and supported by titanium wires. (a) Magnitude, (b) phase angle. (c) Coherence function.

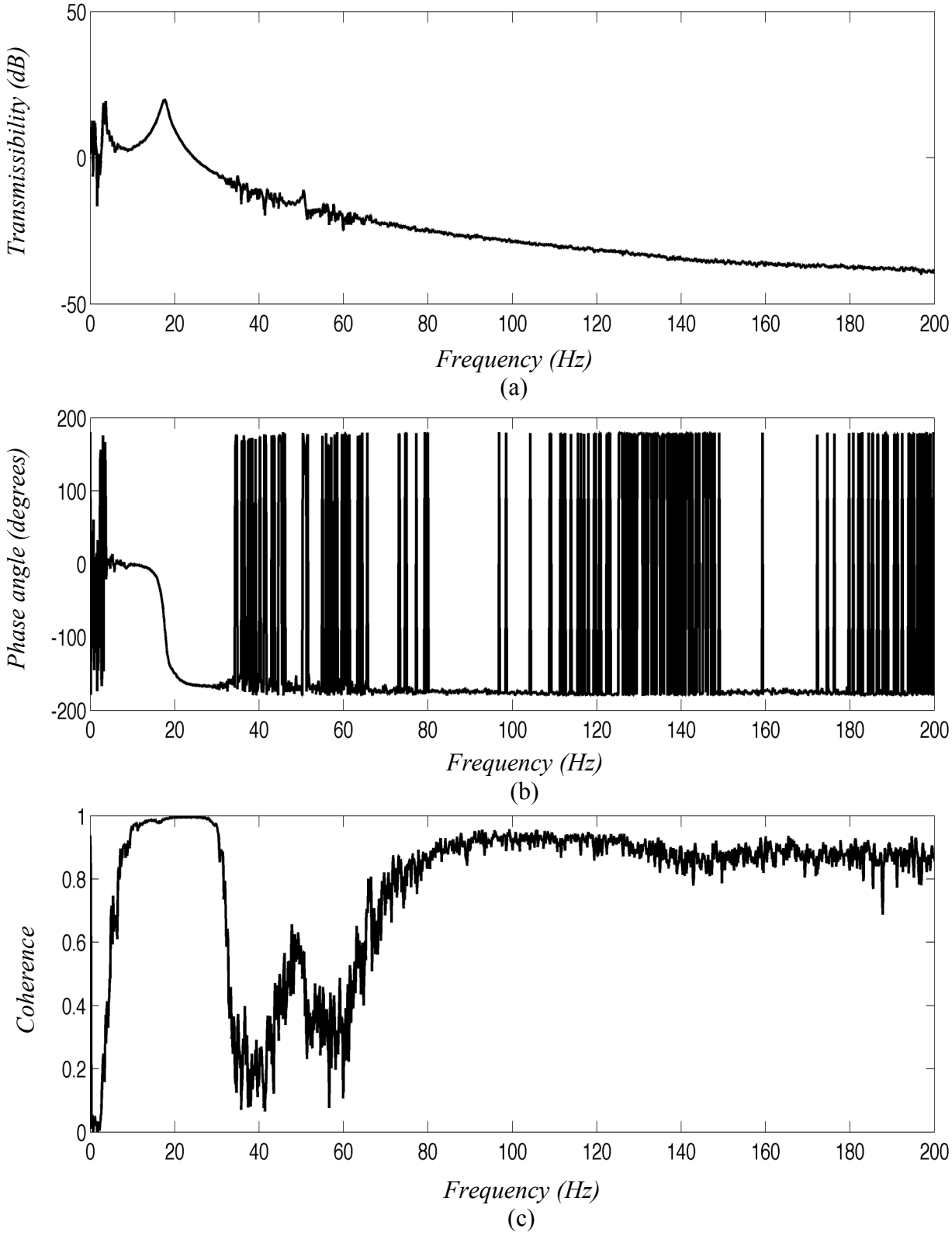


Figure 5.10. Transmissibility of the magnetic spring with the electromagnets attached but turned off. The permanent magnet is supported by titanium wires. (a) Magnitude, (b) phase angle. (c) Coherence function.

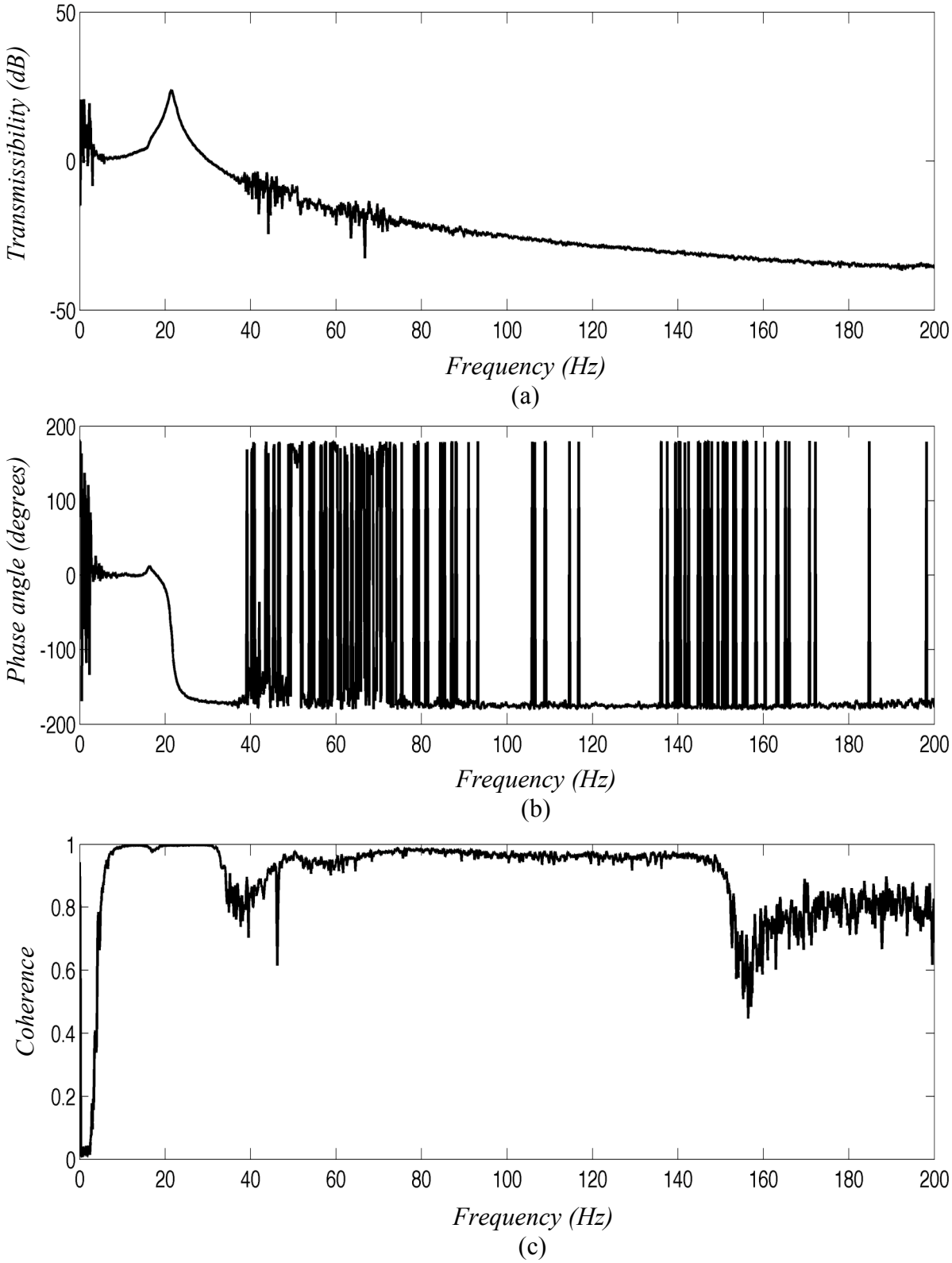


Figure 5.11. Transmissibility of the magnetic spring with the electromagnets powered with 12 V. The permanent magnet is supported by titanium wires. (a) Magnitude, (b) phase angle. (c) Coherence function.

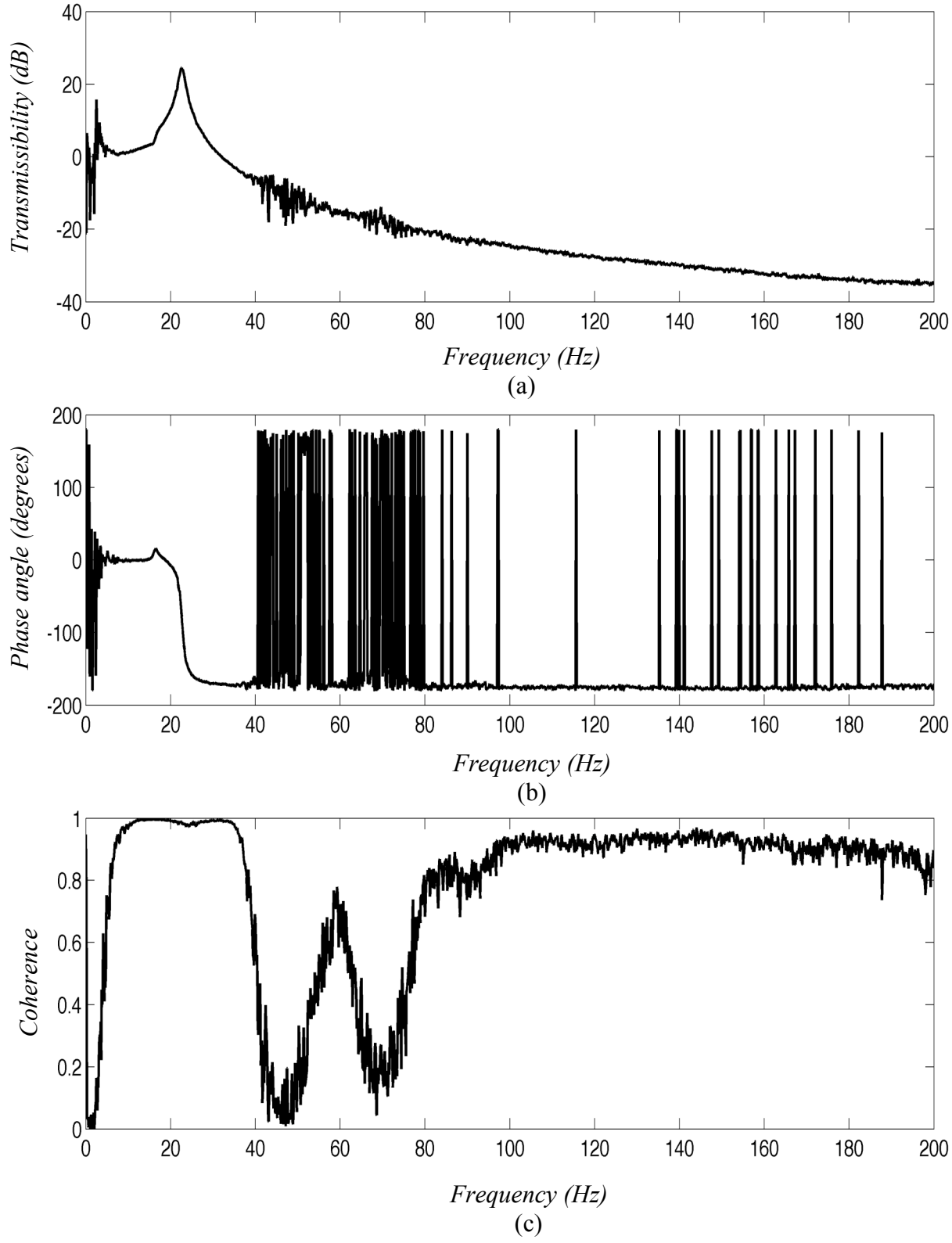


Figure 5.12. Transmissibility of the magnetic spring with the electromagnets powered with 18 V. The permanent magnet is supported by titanium wires. (a) Magnitude, (b) phase angle. (c) Coherence function.

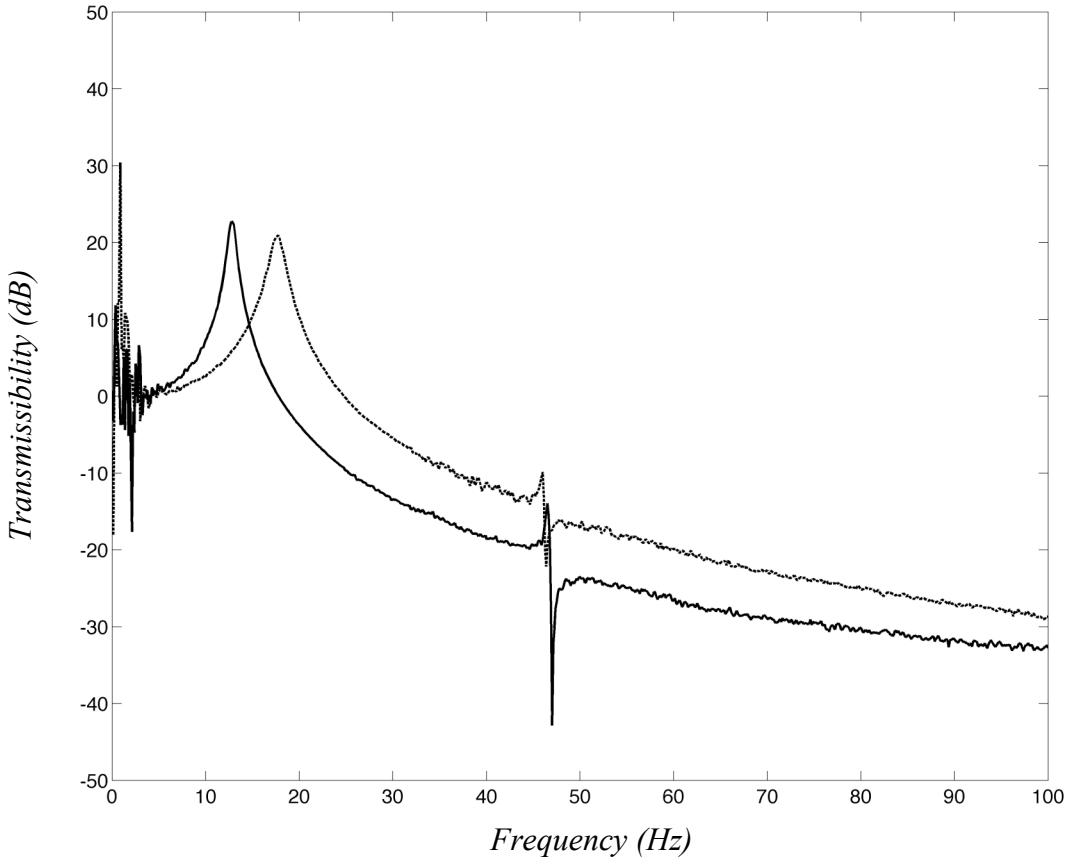


Figure 5.13. Transmissibility magnitude of the system supported by nylon wires. The solid line gives the off state (low stiffness) and the dotted line represents the on state for 12 V (high stiffness).

# Chapter 6.

# Experimental validation of the switching stiffness strategies.

## 6.1. Introduction.

The purpose of building a switchable stiffness device was to replicate and validate the switching strategies presented theoretically in chapters 3 and 4. As presented previously the stiffness control strategy comprises two parts, namely control during the shock, for which reduction in the maximax response is intended, and residual control, which can suppress free vibration after the shock pulse. In this chapter the experimental setup introduced in chapter 5 was applied. In the first section a brief description of the shock generation procedure and the passive response of the experimental rig to shock pulses is given. This is followed by the implementation of the stiffness control in real time and the subsequent comparison with the passive system and the theoretical predictions.

## 6.2. Generation of a shock pulse.

For the shock response simulations presented in chapters 2 and 3, several simple shaped symmetrical pulses were used. These pulses are mathematically simple and convenient for theoretical simulations, and they replicate with a high degree of accuracy the behaviour of real shock pulses. In particular, a versed sine pulse was used in the later simulations involving stiffness control during shock pulses. However, there are some issues related with the generation of simple pulses using an electrodynamic shaker, like the one used in the experimental tests.

The initial idea for the experimental tests was to generate a versed sine pulse using MATLAB and export it as a waveform audio format (WAV) file. As a result, this file can be played through a PC D/A converter and a power amplifier to finally drive the shaker. An example of a pulse generated in this way is shown in figure 6.1. However, the shaker is not able to reproduce an exact symmetric pulse, due to its physical characteristics. This is because the shaker is effectively a mass-spring-damper system, which is being excited with the shock pulse, and it exhibits residual vibration. This is the behaviour seen in the laboratory tests, as shown in figure 6.2 which presents the shaker response as the dotted line to the ideal pulse given in figure 6.1. The amplitude response in this case is the absolute acceleration $\ddot{\xi}$ and is presented in g. The horizontal axis represents absolute time in seconds. This is the recorded time history using an accelerometer on the top of the shaker, i.e. at the base of the rig and is the effective pulse that excites the model. The effective pulse duration is the interval between the two first peaks of the recorded time history. It is important to remember that this time history corresponds to the acceleration profile resulting from a versed sine displacement pulse. The second derivative of a theoretical versed sine pulse of similar characteristics is represented by the solid bold line in figure 6.2, in order to have a better understanding of the behaviour of the shock pulse. The residual vibration always has the same natural frequency (approximately 20 Hz), i.e. the frequency of the shaker plus the mass of the rig. One can regard this kind of pulse as a decaying sinusoidal base input for theoretical comparison.

Bearing the previous considerations in mind, it is important to analyze the effect of having an excitation of this kind in the experimental tests. As the system is still excited after the theoretical input pulse signal to the shaker has finished, in this section this situation is investigated by performing several experimental tests and mathematical simulations.

### 6.2.1. Experimental measurement of SRS.

In order to understand the behaviour of the experimental rig under this particular kind of shock, the corresponding shock response spectra (SRS) were obtained experimentally. The method for calculating the SRS is to excite the system using pulses of different durations, acquire the time responses and obtain the maximum response. The response is then normalised considering the maximum amplitude of the pulse and it is plotted against the ratio between the duration of the pulse and the natural period of the system. Several pulse durations were used to give various values of $\tau/T$ between 0.25 and 4 to cover the main areas of the SRS. This experiment was performed for the high and low stiffness states corresponding to the system supported by nylon wires. As the pulse can be regarded as a decaying sinusoid, these experimental results are compared with the theoretical SRS calculated for decaying sinusoidals, corresponding to the high and low stiffness states. This comparison is shown in figure 6.3. The theoretical high and low stiffness SRS curves calculated in the simulations are depicted by the solid and dotted lines respectively, whilst the experimental SRS are marked in the figure as + and × for high and low stiffness respectively. The comparison shows that the behaviour of the system can be reproduced better using a decaying sinusoidal for the simulations, since the experimental SRS approaches fairly well the theoretical predictions. Another important point in this comparison is the fact that the SRS demonstrates similar behaviour compared to that of simple symmetric pulses, i.e. it comprises three regions, namely the isolation, the amplification and the quasi-static regions as shown in figure 6.3. Additionally, it is important to note that the conclusions based on the versed sine case still hold for this particular input. This means that a reduction in the stiffness of the system will cause a decrease in the maximum response, which is the basis for the stiffness control strategy during the shock input.

6.2.2. Modified shock pulse.

Although the decaying sinusoidal could be used for the experimental tests, it is preferable to have a pulse with as small a residual response as possible, so that it approaches a theoretical versed sine. It has been shown in the previous section that the effect of reducing the stiffness is similar to that when a simple symmetrical pulse is applied. However, in the case of decaying sinusoidal it is not easy to determine when to recover the stiffness to its original value, i.e. when the shock pulse has finished. One can consider the pulse duration as the time the theoretical versed sine is applied, but in practice the actual shock input is still active after this time. It might be possible as well to recover the stiffness at the second peak of the decaying sinusoidal, or even when the shock vibrations have largely diminished. But this method will need a considerable number of trial and error tests, which can be avoided if a more suitable shock pulse is used.

Shin and Brennan [112] developed a method for suppressing residual vibrations using two pulses of the same shape with different amplitudes and applied at different times. If the amplitudes and times are properly chosen, the response of the second pulse will have exactly the opposite phase of the response for the second pulse. Effectively, the vibrations of the system could be cancelled.

This method can be applied to the generation of a single pulse using an electrodynamic shaker. Considering a pulse of very short duration applied to the shaker it will oscillate freely at its natural frequency. If another pulse of the same characteristics but different amplitude is applied exactly at the half of the first cycle, then the response of the second pulse will cancel the response of the first pulse. This idea is represented schematically in figure 6.4 considering two impulses (delta functions) and the response of the system due to these impulses. From [112] the amplitude of the second pulse needs to be scaled such that:

$$\frac{A}{B} = e^{\zeta \omega_n t_0} \tag{6.1}$$

where $A$ is the amplitude of the first pulse, $B$ the amplitude of the second pulse and $t_0$ the time when pulse $B$ is applied, in this case half the natural period of the shaker free response.

Taking into account that the shaker includes the mass of the experimental model and it has a natural frequency of approximately 20Hz giving a natural period of 0.05s, the duration of the pulses was chosen to be 0.005s. It is possible to use shorter duration pulses, but as will be seen later, this might cause higher modes of the frame structure of the model to be excited since the frequency content of the short pulses is high. Considering equation (6.1) and assuming that the system is linear, the amplitude of the second pulse was estimated to be 77% of the amplitude of the first pulse (these actual values were used in the production of figure 6.4, but the figure is presented with normalised values as it is a numerical simulation). The second pulse was applied at time 0.025s i.e. half the period of the system. The actual shaker acceleration response is shown in figure 6.5 by the bold line along with the response resulting from the single pulse only represented by the thin line. In this plot the two short impulses are easily recognized. It can be seen that although there is some residual vibration, the residual response is greatly minimized when the second pulse is applied, and the main base input resulting from this procedure is closer to a single theoretical input. The effective duration of this pulse is 0.025 seconds, which gives a period ratio of $\tau/T = 0.443$ considering the natural frequency of the system supported by nylon wires in its high stiffness state (17.75Hz). An issue with this method of pulse generation is the fact that the number of effective pulses is limited, since its duration depends upon the properties of the shaker, namely its stiffness and mass, which are fixed. However, an additional mass can be added in order to obtain different pulse durations, but these pulses will have longer durations due to the lower natural frequency. Two more pulses were generated for the later experimental validations adding mass to the system. A pulse of duration 0.03 seconds ($\tau/T = 0.532$) was produced adding 1 kilogram and another pulse of 0.035 seconds ($\tau/T = 0.621$) was generated by adding 2 kilograms. Another issue concerning these pulses is that there is high frequency content in the pulses generated in this way, probably due to some modes of the supporting frame being excited by the short impulses.

In order to estimate the benefits obtained from reducing the stiffness the response of the actual rig for the high and low stiffness states were measured. The same shock excitation described previously was used considering the shortest pulse i.e. $\tau/T = 0.443$. Since the best performance in terms of stiffness reduction was obtained for nylon wires, the following tests were performed using this material. For this case the stiffness reduction is around 50%. The absolute acceleration responses shown in figure 6.6 are given in *g* and the time is presented in seconds. The fact that a low stiffness suspension causes the amplitude to decrease is easily visible, presenting in this case an amplitude difference of about 53%, which is to be expected in the implementation of the switching strategy for shock response.

## 6.3. Maximax response control strategy tests.

### 6.3.1. Set-up information.

As introduced in chapter 3, the objective of this strategy is to reduce the stiffness whilst a shock is applied to the system. For the theoretical analysis a versed sine pulse was considered and it was shown that it is feasible to obtain better isolation performance with this control strategy. However, for the purposes of experimental simulation it was not possible to reproduce an exact versed sine pulse. The pulse described in section 6.2.2 was used for the experimental validations. This pulse approaches a versed sine pulse. It is important to recall that the results shown here are acceleration responses and the shock pulses recorded need to be directly compared with the acceleration profile of a versed sine pulse, as shown in figure 6.2.

An analogue circuit was made specifically in order to implement the stiffness switching for shock control. This circuit uses the signal of the shock pulse acquired using an accelerometer and finds the first two minima points of the signal. As shown in figure 6.5, the effective shock pulse when the residual response is ignored can be located between the first two minima points. What the circuit exactly does is to detect a rise in the signal after the first minima and turn off the voltage supply, thus reducing the effective stiffness. After this event, the circuit detects when the signal rises again at the second minima and recovers the power supply, increasing the stiffness to its original value. More information about this circuit is given in appendix F. The same setup and equipment used in chapter 5 was used for this part of the

experiments (see figure 5.3). The acceleration responses were recorded using the Data Physics analyzer. Additionally, the output voltage applied to the electromagnets was recorded. The free vibration was measured with teardrop miniature PCB accelerometers with a sensitivity of 9.36 mV/g for the accelerometer placed on the suspended magnet, and 9.90 mV/g for the one on the base. The gain used in the signal conditioner amplified the signal 100 times. This was necessary because the control circuit needs input signals of amplitude no less than approximately 2 V to perform the switching logic. It is important to note that the results presented were acquired using a trigger in the analyzer considering a time delay of 0.05 s.

### 6.3.2. Results.

An example of the acceleration response of the switching stiffness model (using nylon wires) is presented in figure 6.7. The shortest pulse (0.025s) was used for this test. For comparison, the acceleration response of the passive system (high stiffness state) is given by figure 6.7(a). Figure 6.7(b) gives the actual response of the switching strategy. The shock pulse is presented in figure 6.7(c) and figure 6.7(d) shows the voltage applied to the electromagnets. The acceleration amplitudes are presented in *g* and the voltage is given in volts. The time axis is represented in seconds.

Figures 6.8 and 6.9 present a comparison considering two pulses of longer duration. Figure 6.8 presents results of the system when a mass of 1 kg was added resulting in a pulse of 0.032s, and figure 6.9 was produced with an extra 2 kg, which caused the pulse duration to increase to 0.035s. The subplots are presented in the same order than in the previous case of figure 6.7, i.e. passive response, switching response, shock pulse and voltage respectively.

### 6.3.3. Discussion

The behaviour of the switching strategy is clearly depicted by figures 6.7 6.8 and 6.9. The voltage history presented in those figures is a direct indicator of the stiffness switching. The system is initially in its on state, which means the stiffness is in its high value. The voltage reduction to zero when the shock begins is easily visible. At this point the electromagnets are completely turned off resulting in a lower stiffness value. At the end of the shock the voltage returns to its initial value thus recovering the stiffness.

There are some interesting points to discuss from the experimental results. Firstly, it can be observed that the response amplitude of the suspended magnet rises in the first cycles, and then after reaching the maximum the decay begins. This behaviour has been observed before when the passive response of the system was studied. The reason can be attributed to beating phenomena, as the natural frequency of the shaker considering the mass of the rig (20 Hz) is very close to the natural frequency of the suspended magnet (17.75 Hz). It is known that when a system is excited by a harmonic motion whose frequency is close to the natural frequency of the system, this beating phenomenon occurs [2]. However, in this case a decaying sinusoidal is affecting the system, rather than a sustained vibration, and the phenomenon disappears quickly.

Another point worth noting is the small jump present in the response of the suspended magnet when the stiffness is recovered. This small jump occurs after the point when the maximum response is reached. It is attributed to the sudden voltage applied that transmits a small pulse and causes the suspended magnet to experience this small but sudden motion. The same behaviour has been observed when manually turning on the electromagnets as the magnet is slightly but very quickly lifted from its original position. However, this jump is very small causing only an amplitude increase of approximately 6% from the previous maximum.

Finally, the voltage records shows two overshoots when the voltage is removed and when it is applied again. This corresponds to the inductive nature of the circuit, which tends to oppose the changes in current, thus it causes transients when the voltage is applied or removed.

However, the most important part of the analysis is to study the shock isolation performance of the system and compare it with the passive case. This comparison is made by taking the passive model in its high stiffness state as a reference case, since this state is the original configuration of the system.

The two following comparisons consider the shock response resulting from the shortest pulse as discussed above (0.025s). The effect of the switching strategy for the longer pulses is considered later.

When compared to the passive response of the high stiffness setting, one can easily see a considerable reduction in the response. Effectively, the response of a system with high stiffness subjected to a short duration shock pulse is higher when compared to a system with lower stiffness. In this case the effectiveness of reducing the stiffness only during the shock response is readily visible. The reduction of the response is around 53% taking the maximum response of the passive system during the shock for comparison. After the stiffness recovery, the switching response is slightly greater than the passive response, but only for the second cycle. However, this part of the response corresponds to the residual phase, and this strategy alone is intended only to reduce the response during the shock. Nonetheless, it is important to note at this point that, as expected, the vibration decay is very similar for both situations.

It is also of interest to investigate the effect of the switching strategy when longer pulses are applied. As introduced in section 6.2.2 it was possible to generate two longer pulses by adding up to 2 kg of extra mass to the rig. The response due to the first shock obtained with an effective duration of 0.03 seconds resulting in a period ratio of $\tau/T = 0.532$ is shown in figure 6.8. For this case there is still a benefit in using the switching strategy, as a reduction in the response of about 46% is present. However, for the response to the second pulse of 0.035 seconds and $\tau/T = 0.621$ presented in figure 6.9 the situation is different. In this case the reduction in the response is very small, being about 12% and the residual response after the pulse is even amplified. This shows that the switching strategy is only advantageous for short pulses, and as the pulse duration increases the response can be worst compared to the passive system, as predicted by the theory in chapter 3.

Another point investigated was the relative and absolute displacement response behaviour. As stated before, the main objective of this study is to evaluate the performance of this strategy in terms of the acceleration response of the system. The acceleration response is significant in the assessment of the transmitted forces and the estimation of the possible damage resulting from a shock. However, the relative displacement is another important parameter related to the space constraints of the isolation system. In the theoretical analysis in chapter 3 it was observed that the use of the stiffness switching for shock control normally leads to negligible benefit or no difference in relative response unless the shock duration is short compared to the pulse. Otherwise it can cause a large increase in the relative response. Moreover, it is

important to remember that the relative response is particularly important during the application of the shock because after the pulse the relative response is equal to the absolute residual response. For the experimental setup considered here, the pulse is short enough not to increase the relative response and some benefits could still be obtained. The absolute and relative displacements were obtained by numerical integration of the acceleration time series in MATLAB. The discussion on displacement response is given only for the shortest pulse when the results can be readily observed and the benefits are more evident. Figure 6.10 presents the relative displacement calculated from the experimental acceleration results. The absolute displacement response $v$ for the switching system is presented in figure 6.10(a). For comparison the absolute response of displacement $v$ for the passive system is given in figure 6.10(b). In this case, taking into account the maximum response during the shock, a decrease of 40% in the absolute displacement response was observed by using the stiffness switching.

The absolute displacement responses presented in figures 6.10(a) and 6.10(b) are used to calculate the relative displacement as $v_{rel} = v - \xi$ and the results are presented in figure 6.10(c) for the switching system and in figure 6.10(d) for the passive system. Comparing the switching response with the passive response one can observe a very similar behaviour. As expected, there is not great advantage for relative response, but there is also no detriment in the isolation performance. For this case, a decrease of 14% in the relative response was found during the impulse input.

A summary of the performance benefits and a comparison with the theoretical predictions given by chapter 3 is presented in table 6.1 for acceleration results, and table 6.2. for displacement response. The theoretical results were obtained according the methods presented in chapter 3 related to the simple model with no secondary mass. Table 6.1 shows the comparison between the theoretical absolute acceleration reduction expected for the three pulses considered and the actual values of reduction in the response obtained in the experimental tests. This is presented accordingly to the maximum absolute response during the shock. Table 6.2. gives the theoretical and experimental response reductions in absolute and relative displacement only for the first pulse considered. The results obtained experimentally show a reasonable degree of agreement with the theoretical results. A possible

reason of discrepancy between theoretical and experimental results is the difference between the simple pulses considered in the simulations, and the more complex pulse used for the experimental validations.

## 6.4. Decay and switching logic tests

### 6.4.1. Set-up information

It was intended to use the switchable stiffness element for experimental validation of both the shock response reduction *and* the residual response suppression. Now that the behaviour of the system had been described and its properties identified, the next stage was to correlate the theoretical predictions with experimental results.

A circuit was built for the validation of the switching strategy used for the residual vibration suppression. As described in chapter 4, the control law for this strategy can be written as:

$$k_v = \begin{Bmatrix} k & x\dot{x} \geq 0 \\ k - \Delta k & x\dot{x} < 0 \end{Bmatrix} \tag{6.2}$$

The control logic involves two parameters, namely the absolute displacement and absolute velocity. As the system is small and lightweight it is necessary to use small transducers that will not add extra significant mass to the system. Consequently, using small accelerometers one can obtain the system response and then integrate the signal once to get velocity and twice to get displacement. This can add noise to the signal.

In order to avoid the use of a double integrator, it was possible to use a single acceleration signal to perform the control law. Considering that the control logic searches the phase of two signals to find the points of maximum and zero displacement, it also can be expressed as:

$$k_v = \begin{Bmatrix} k & \ddot{x}\dot{x} \leq 0 \\ k - \Delta k & \ddot{x}\dot{x} > 0 \end{Bmatrix} \tag{6.3}$$

By using the acceleration and velocity of the isolated mass, it was possible to perform just a single integration, thus reducing the possibility of additional noise in the signals. The circuit was built following this consideration. In fact, only one acceleration signal was used, since it is split into two and one signal was integrated whilst the other not. The circuit also has a multiplier and then the multiplied signal passes through a comparator that performed the control law, sending a voltage to the electromagnets if the product was less than zero, or switching them off otherwise. However, the maximum permissible voltage in the circuit was 12 V. As a result, it was not possible to use the maximum stiffness change obtained in the previous experiments, but it was expected that the effect of the control law could be demonstrated using 12 V, which gives a 48.4% and 31.4% stiffness change for nylon and titanium wires respectively. It is also important to mention that it was necessary to amplify the signal acquired from the accelerometer using a signal conditioner. Otherwise the signal level would be too small for the circuit to perform the control logic. Details of the circuit and the set-up used can be found in appendix F. Moreover, in this chapter only the results for the system with nylon wires are presented since the performance was greater than with titanium. Although similar behaviour was observed, the system supported by nylon wires was considered to be adequate to demonstrate the effect of the stiffness change.

### 6.4.2. Results.

The system was subjected to a very short pulse compared to the natural period of the system ($\tau/T$ =0.01) in order to approach an impulse excitation. The same set-up for data acquisition used in the shock testing was considered again here, i.e. the same accelerometers and signal conditioning unit. The following results are given for absolute acceleration response of the suspended magnets in *g* and the time is presented in seconds.

The responses for the switching strategy are shown in figure 6.11. These plots include the acceleration response, as well as the voltage applied to the electromagnets. Figure 6.11(a) depicts the free vibration acceleration response of the passive system in the high stiffness state, which is taken as a basis for comparison. The switching response is presented in figure 6.11(b) and the voltage applied to the electromagnets is given in figure 6.11(c).

### 6.4.3. Discussion.

The absolute acceleration and voltage plots shown in figures 6.11 reveal the behaviour of the switching strategy. It can be seen that the switching events occur at the points required by the theoretical control law. The plot of voltage confirms this, which is an indicator of the stiffness state in the system. The voltage supply is turned off at the point of absolute maximum response, i.e. the stiffness is reduced. Afterwards, the voltage is supplied again when the response is passing through the equilibrium position i.e. the stiffness is recovered to its high value. The characteristic waveform of the applied voltage closely resembles a rectangular train of pulses, as the on-off switching logic requires. However, there were some sharp peaks present probably due to the inductive nature of the electromagnets. Another interesting point is the number of switching events present during the system decay. For instance, there were only four cycles of stiffness change. This phenomenon corresponds to the fact that the circuit requires the input signals to have a certain minimum voltage level to perform the control, which was approximately 0.7 V. When the input voltage was lower, the switching stopped. Even using the signal conditioner with the maximum gain, it was not possible to sustain the control for a longer time.

A comparison between the decay responses of the system for the fixed high stiffness state is possible with the aid of figure 6.11. The switching response should be compared with the high stiffness value since it is the original state of the system. When compared to the passive case, the system performance in terms of faster vibration decay is far superior when the switching logic was applied. Although the control acts only for the first two vibration cycles, this was enough to suppress the vibrations more rapidly.

In order to evaluate the performance of the system it is necessary to compare the previous experimental results with theoretical predictions. The main performance indicator for the on-off switching logic is the equivalent damping ratio, which can be derived from the stiffness reduction factor. For an undamped system under the switching strategy the logarithmic decrement can be expressed as:

$$\delta = \ln\left(\frac{1}{1-\sigma}\right) \tag{6.4}$$

This can be used to calculate the theoretical equivalent damping ratio $\zeta_{eq}$ from equation (4.13). However, in this case the passive system has initially some amount of damping $\zeta_{initial}$. Assuming that this amount of damping is viscous, the total equivalent damping ratio $\zeta_t$ can be expressed as $\zeta_t = \zeta_{initial} + \zeta_{eq}$ when the initial amount of damping $\zeta_{eq}$ is approximately less than $0.3$, as described in chapter 4 (refer to figure 4.13). Bearing this in mind, the theoretical equivalent damping can be obtained for the experimental rig, considering the actual physical properties of the rig given in table 5.2. Moreover, an equivalent damping can be calculated from the experimental decay measurements and compared with the expected theoretical value. This experimentally obtained viscous damping ratio was obtained calculating the logarithmic decrement of the switching system from the amplitude of the peaks and then calculating the damping ratio using equation (4.13). However, this calculation was made considering the absolute displacement response of the system, obtained by numerical integration of the acceleration results in MATLAB. For reference, the displacement response is depicted in figure 6.12(a) for the switching system and figure 6.12(b) for the passive system. This plot further shows the advantage and more rapid vibration decay of the switching strategy, and it is used to estimate the viscous damping ratio. The results of damping ratio are shown in table 6.2 compared with the theoretical predictions.

There is reasonable correlation between the predicted damping ratio and the experimental damping for the nylon suspension. This comparison can be easier to understand by examining figure 6.13, which presents the responses for the theoretical model and the experimental setup. For the simulation, shown in thin line, the physical parameters of the rig have been considered, and also the same initial conditions. It is important to mention that the actual excitation is not exactly a short pulse, but a decaying sinusoidal due to the dynamics of the electrodynamic actuator (shaker). When compared to the experimental response (bold line) there is a good agreement between theory and practice. It is important to observe and recognize the presence of the acceleration peaks discussed previously in chapter 4, which are a result of the sudden stiffness changes.

## 6.5. Energy dissipation in the experimental design.

In chapter 4 several theoretical assumptions were made in order to explain the energy dissipation of the switchable stiffness models. However, in the experimental design the lost energy seen in the results has to be dissipated in some way. The reason attributed to be the cause of the energy dissipation mechanism is the inductive nature of the design used since the setup is basically a resistor-inductor (RL) circuit. The main components of the model are the electromagnets, which are essentially inductors. An inductor is an electrical element that opposes the changes in current, as a capacitor opposes the changes in voltage. It can be shown that an inductor has the capacity of storing energy. This stored energy is necessary to build up a current in the inductance. This energy is given by [111]:

$$E = \frac{1}{2} L I^2 \tag{6.5}$$

where $L$ is the inductance, $E$ the energy and $I$ the current. If the voltage source is removed suddenly the inductance tries to maintain a constant current thus releasing its stored energy, which is then dissipated by the resistive element. The sudden application or removal of the voltage will cause a momentary changing response. This phenomenon is called a transient. When the voltage is suddenly removed the energy stored is released in the form of a current that decays exponentially. This can be represented schematically by the RL circuit shown in figure 6.14 that represents the fundaments of the switching system. When the circuit is open the current decreases exponentially thus generating a transient. The exponential decays present in figure 6.11 (c) indicate the current decay since the current is related to the voltage as:

$$i(t) = I_0 e^{-t/\tau} = \frac{V}{R} e^{-t/\tau} \tag{6.6}$$

where $\tau$ is known as the time constant, in this case representing the time it takes to the current to fall to the value $1/e$ of the initial value $I_0$. This is shown schematically in figure 6.15, which shows a schematically drawn zoom of the voltage time history.

A way of examining the energy in the system is to study at the peak voltages. If the system is conservative the energy at the moment when voltage is applied (stiffness recovery) should be the same compared with the energy at the moment of voltage removal (stiffness reduction). This means no energy is dissipated. However, it has been shown that this system effectively dissipates energy. From figure 6.16 the voltage at the point of stiffness recovery (A) is higher than the voltage at the point of stiffness reduction (B). In a DC circuit the current is directly proportional to the voltage, thus the energy levels are also different. This means that a certain amount of energy is added to the electromagnetic system each time the voltage is connected to the electromagnets. This energy must come from the mechanical system, and it has to be equal to the amount of energy lost due to the stiffness reduction. Considering the previous assumptions, the electromagnetic energy added can be expressed as:

$$E_{added} = \frac{1}{2} L I_A^2 - \frac{1}{2} L I_B^2 \tag{6.7}$$

This energy addition occurs twice each cycle of the mechanical system. Assuming this is equal to the mechanical energy lost per cycle one can write:

$$L\left(I_A^2 - I_B^2\right) = \frac{1}{2} k \left(v_{n-1}^2 - v_n^2\right) \tag{6.8}$$

This can be numerically validated using the experimental results obtained. All the parameters involved can be calculated or measured. The voltage in the circuit is known and equal to 12 V in each electromagnet since they are arranged in parallel. The measured resistance from the electromagnets is 37.3 Ω and 38 Ω for the bottom and top electromagnets respectively. These resistances give an effective resistance of 18.82 Ω as the electromagnets are in parallel. Additionally, the inductance from the electromagnets was also measured, giving values of 5.18 mH and 5.05 mH, which result in an equivalent inductance of 2.55 mH. The instantaneous peak current at the point of stiffness recovery (A) calculated considering the effective resistance and the voltage at that point as $I = \frac{V}{R_{effective}}$ is 0.62 A and the current at the stiffness reduction point (B) is 0.47 A. Taking the left hand side of equation (6.8) the electromagnetic energy is 0.417 mJ. The mechanical energy dissipated can be calculated using the peak displacement values and the stiffness of the system. From the experimental

data, two averaged sample displacement values from consecutive peaks are $v_{n-1} = 1.36\text{mm}$ and $v_{n-1} = 0.82\text{mm}$ and the stiffness of the system being 936 N/m the energy in this cycle is 0.415 mJ which is in very good agreement with the energy added to the electromagnetic system.

## 6.6. Full implementation of the switching strategies.

The final experimental objective for this project is to combine both switching stiffness strategies. This means that the stiffness control during the shock is performed, and after the shock has finished the switching stiffness for residual vibration is activated. The combination of these strategies should further demonstrate the feasibility of the control, and the performance advantages found in the separate implementation of the strategy. Moreover, it will show the behaviour of the system in a complete shock scenario which comprises both maximum response during the application and the residual response left after the shock finishes. Thus the final objective is to minimize the response and at the same time mitigate residual vibrations quickly.

In order to achieve this objective, the circuits explained previously for the different stiffness strategies needed to be modified. This modification is basically a link between the two separate logics. As a result, the shock control part of the logic, which uses an acceleration signal from the base, is responsible for triggering the second switching logic for the residual part once the pulse has finished. At this point, the control signal is the response of the magnet used to implement the switching as before. Detailed information can be found in appendix F.

Figure 6.16 shows the result of the complete implementation, in this case only the shortest pulse (0.25s) was considered for the experiment. The subplots presented are as follow (a) passive response, (b) switching response, (c) shock pulse and (d) voltage applied to the electromagnets. The voltage history shows that after the shock has finished the stiffness remains in its low value, because the shock ends around the point of maximum acceleration, thus the residual switching logic indicates at this point a stiffness reduction. After this stage, the residual switching continues reducing and recovering the stiffness at the required points, until the amplitude of the control signal is too low and the switching ends. It is important to mention that after the signal becomes so low for the switching circuit, it stops performing the

switching at the required times and the switching becomes erratic. However, at this point the amplitude of the suspended magnet has become very small, and the switching might be stopped to avoid further problems. Moreover, it is also of interest to note that the spikes at the points of stiffness reduction are still present, as observed when the stiffness switching for residual response was implemented alone. During the shock pulse, the response is almost the same as the case studied in section 6.3 for the control of stiffness during the shock only. After the shock has finished, it is when the advantages are observed, in this case the residual vibration is clearly more rapidly reduced. As the stiffness reduction factor is the same (approximately 50% of stiffness reduction) the estimated equivalent viscous damping ratio is 0.133, very similar to the damping ratio of 0.134 obtained when the residual vibration strategy was implemented alone. This figure clearly depicts the enhanced shock isolation performance of the switching system over the system with no control, for both maximax and residual response.

## 6.7. Conclusions.

The switchable stiffness experimental rig has been used to validate the theoretical methods for shock isolation and residual vibration isolation. The first stage involved the validation of the stiffness control during the shock. For this part the generation of a suitable shock input was analyzed and as a result a shock pulse with very low residual amplitude was generated using two separated short impulses out of phase. The shock response of the passive system was obtained, and later compared with the switching model. It was shown that reducing the stiffness during the shock is effective in reducing the response of the system and good correlation with the theoretical findings was obtained.

The second part involved the stiffness switching for residual vibration suppression. In this case the free vibration response of the system was considered and the switching control was implemented using an analogue circuit. Good improvement in the energy dissipation properties of the system were found, thus suppressing residual vibrations more quickly than in the passive system. There was good agreement between theory and practice for this situation. Additionally, the energy dissipation mechanism in the experimental model was attributed to the inductive elements that show an energy increase during the stiffness recovery.

Finally, both stiffness control during the shock and residual vibration control were implemented together in the same circuit. This combination led to a better performance in both the shock response reduction and a rapid suppression of residual vibration compared to the original passive system.

| Period ratio $\tau/T$ | Predicted reduction in the response | Experimental reduction in the response |
|---|---|---|
| **0.44** | 61% | 53% |
| **0.53** | 25% | 46% |
| **0.62** | 17% | 12% |

Table 6.1. Comparison between the theoretically predicted acceleration response reduction using the shock stiffness control and the experimental results, for the particular shock pulses used in the tests.

| Reduction in the response | Predicted reduction in the response | Experimental reduction in the response |
|---|---|---|
| **Relative** | 23% | 14% |
| **Absolute** | 30% | 40% |

Table 6.2. Reduction of the absolute and relative displacement response for the system with stiffness switching during the shock in terms of percentage. The results are for the shortest pulse. i.e. $\tau/T = 0.44$.

| Suspension configuration | Theoretically calculated damping ratio | Experimentally measured damping ratio |
|---|---|---|
| **Nylon** | 0.150 | 0.134 |

Table 6.3. Comparative results of the theoretical total damping ratio under the switching strategy, and the experimental results for the system supported by nylon wires.

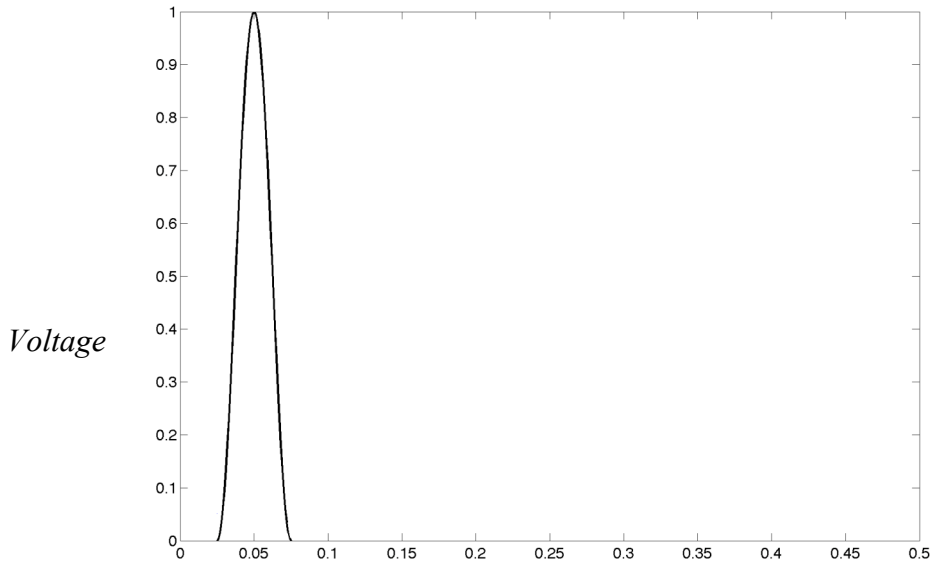


Figure 6.1. Ideal versed sine pulse generated as a WAV file using MATLAB. This particular pulse was generated to give $\tau/T = 0.25$.

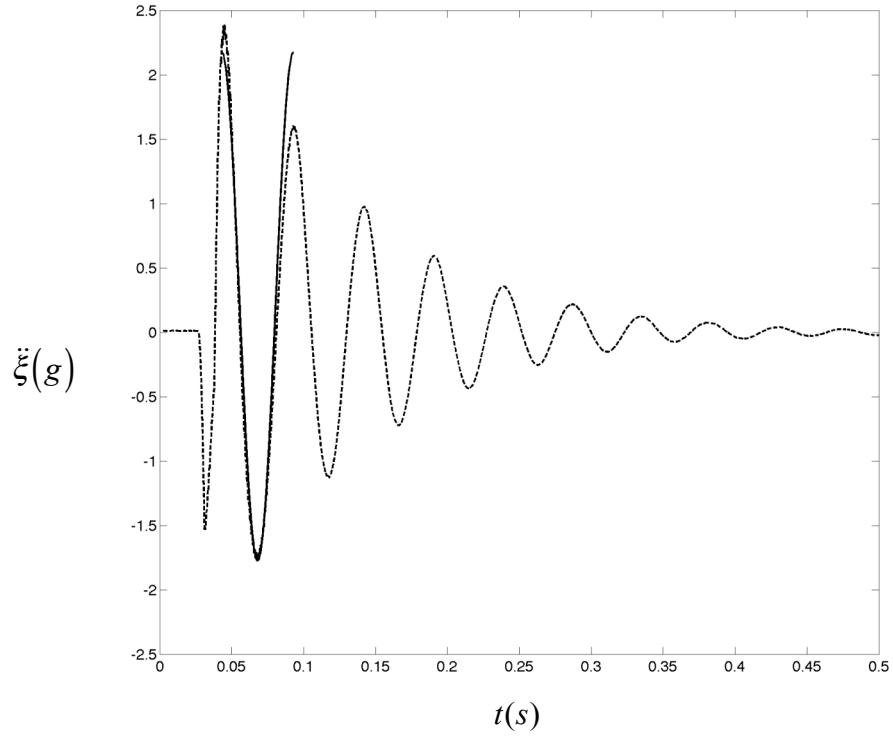


Figure 6.2. Acceleration response ($g$) measured on top of the shaker showing the decaying sinusoidal nature of the shock response of the shaker (dotted). The solid curve represents the expected theoretical acceleration pulse. The vertical acceleration axis is given in $g$ and the time in seconds.

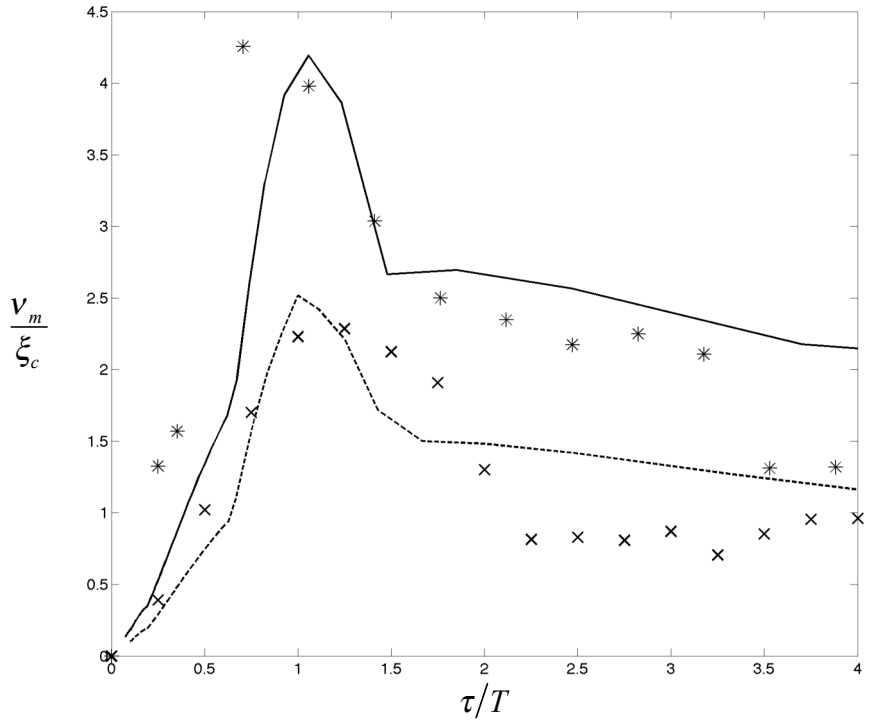


Figure 6.3. Shock response spectra obtained experimentally and theoretically for a decaying sinusoidal for both low and high stiffness states. Nylon wires used. The solid and the dotted line depict the theoretical high and low stiffness results respectively. The experimental results are represented by the markers ✳ for high stiffness and × for low stiffness.

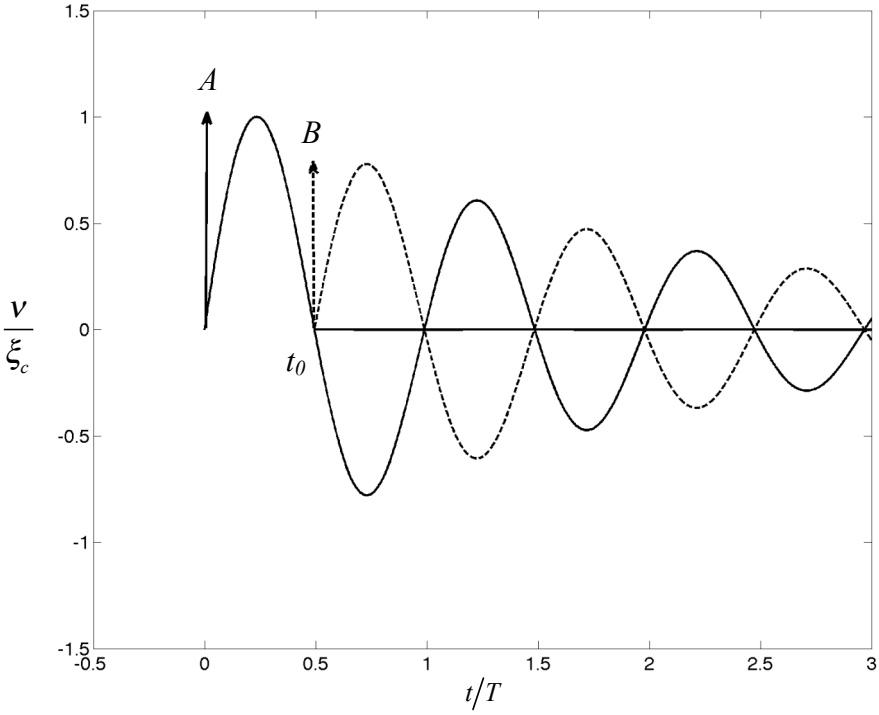


Figure 6.4. Suppression of residual vibration using two impulses $A$ and $B$. The second impulse is applied at $t = 0.5T$ in order to cancel the response of the first impulse.

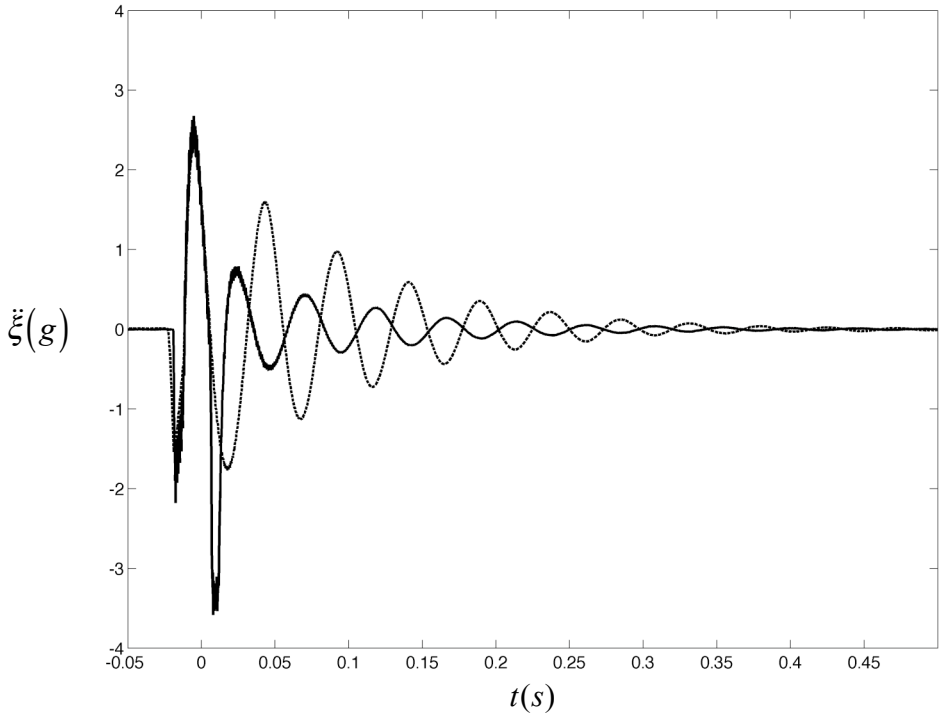


Figure 6.5. Effective shaker acceleration resulting from two impulses sent to the shaker (bold line). The second impulse is applied at $t = 0.5T = .025s$ to gain residual vibration suppression. The dotted line represents the response when only the first impulse is applied. The vertical axis is given in $g$ and the time in seconds.

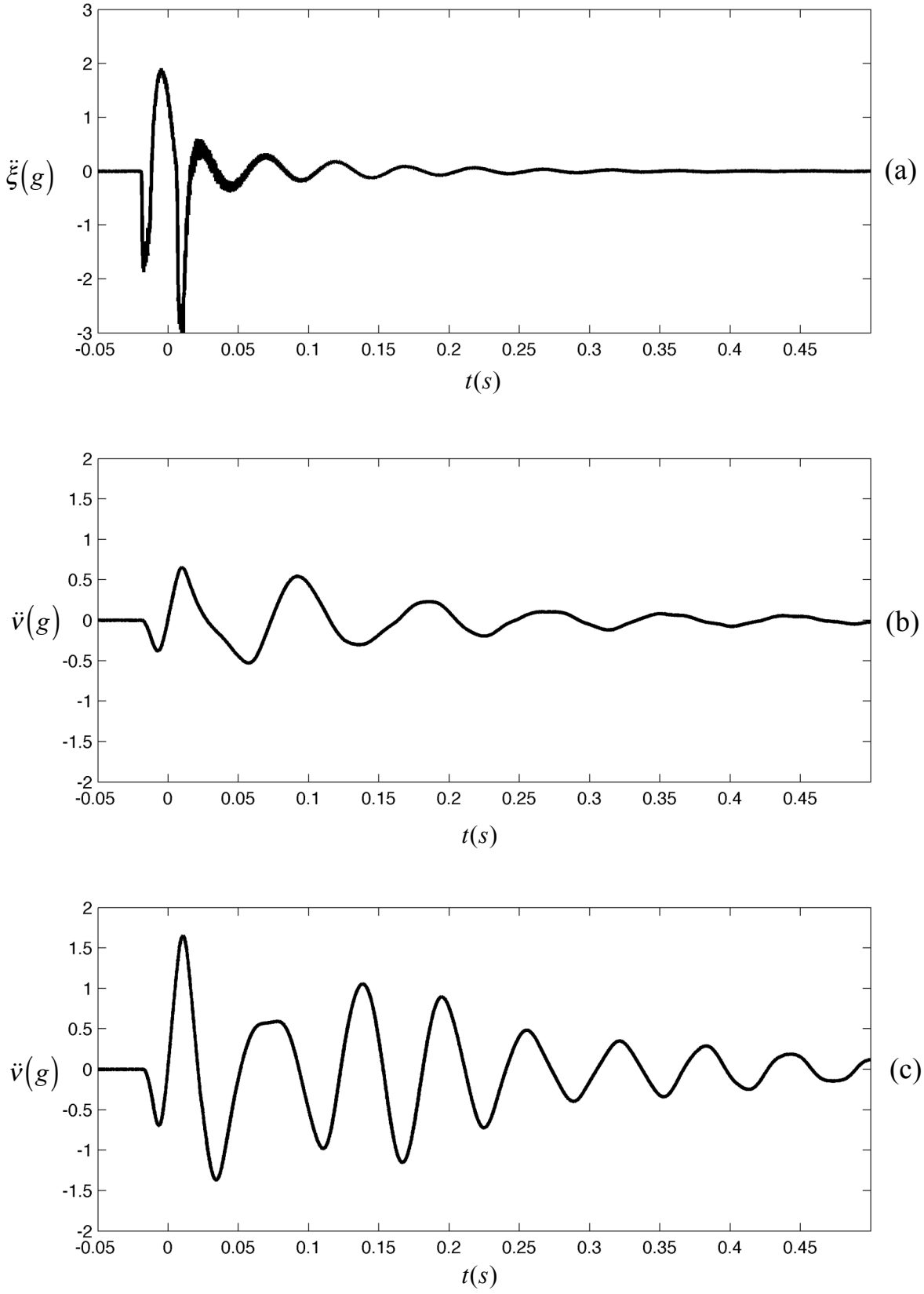


Figure 6.6. Passive shock response of the experimental rig. (a) Shock pulse, (b) low stiffness response and (c) high stiffness response. The vertical axis is given in *g* and the time in seconds.

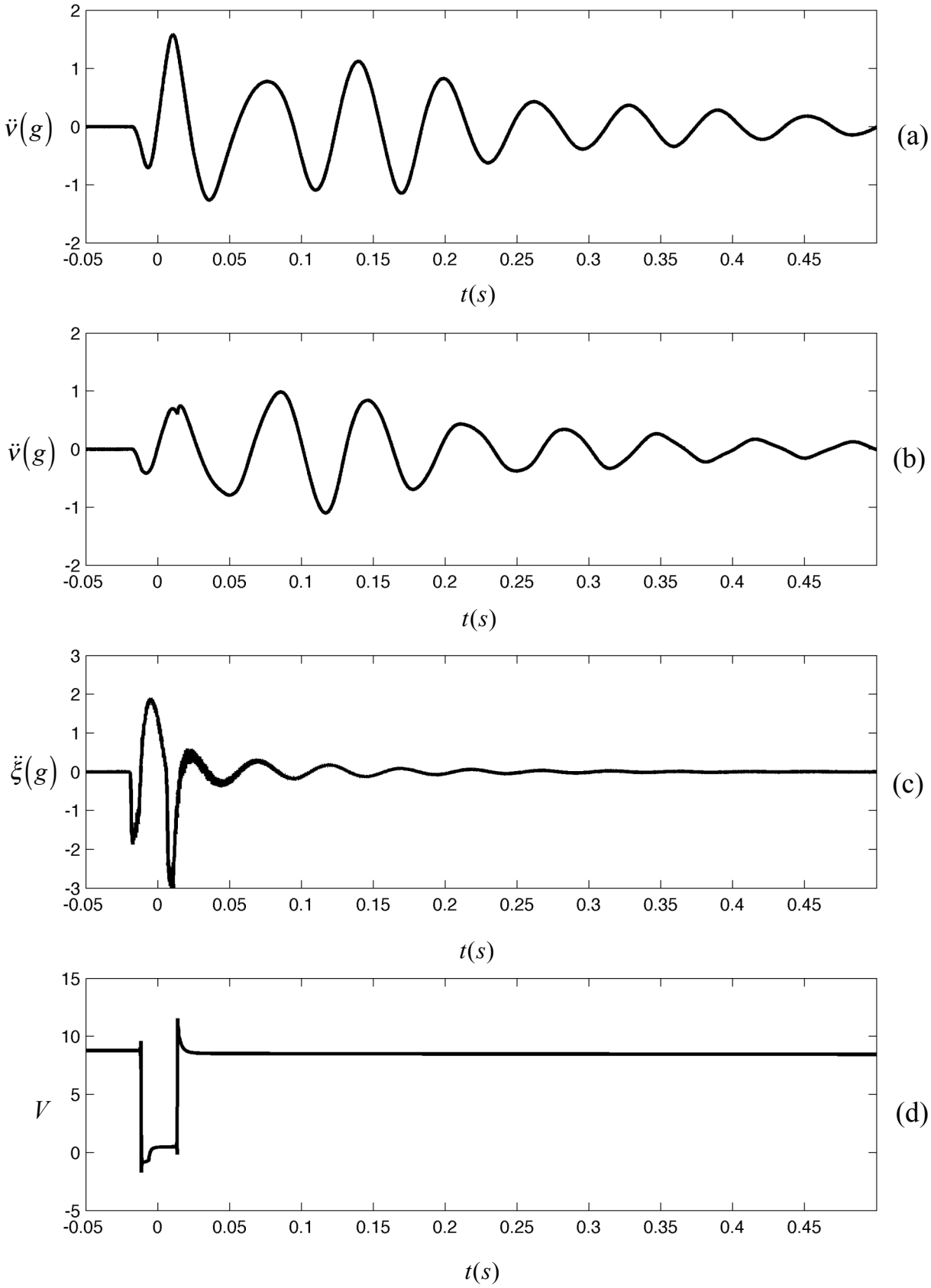


Figure 6.7. Stiffness switching strategy for shock response. (a) Passive response, (b) switching response, (c) shock pulse and (d) voltage applied to the electromagnets. Acceleration is given in *g*, voltage in volts and time in seconds.

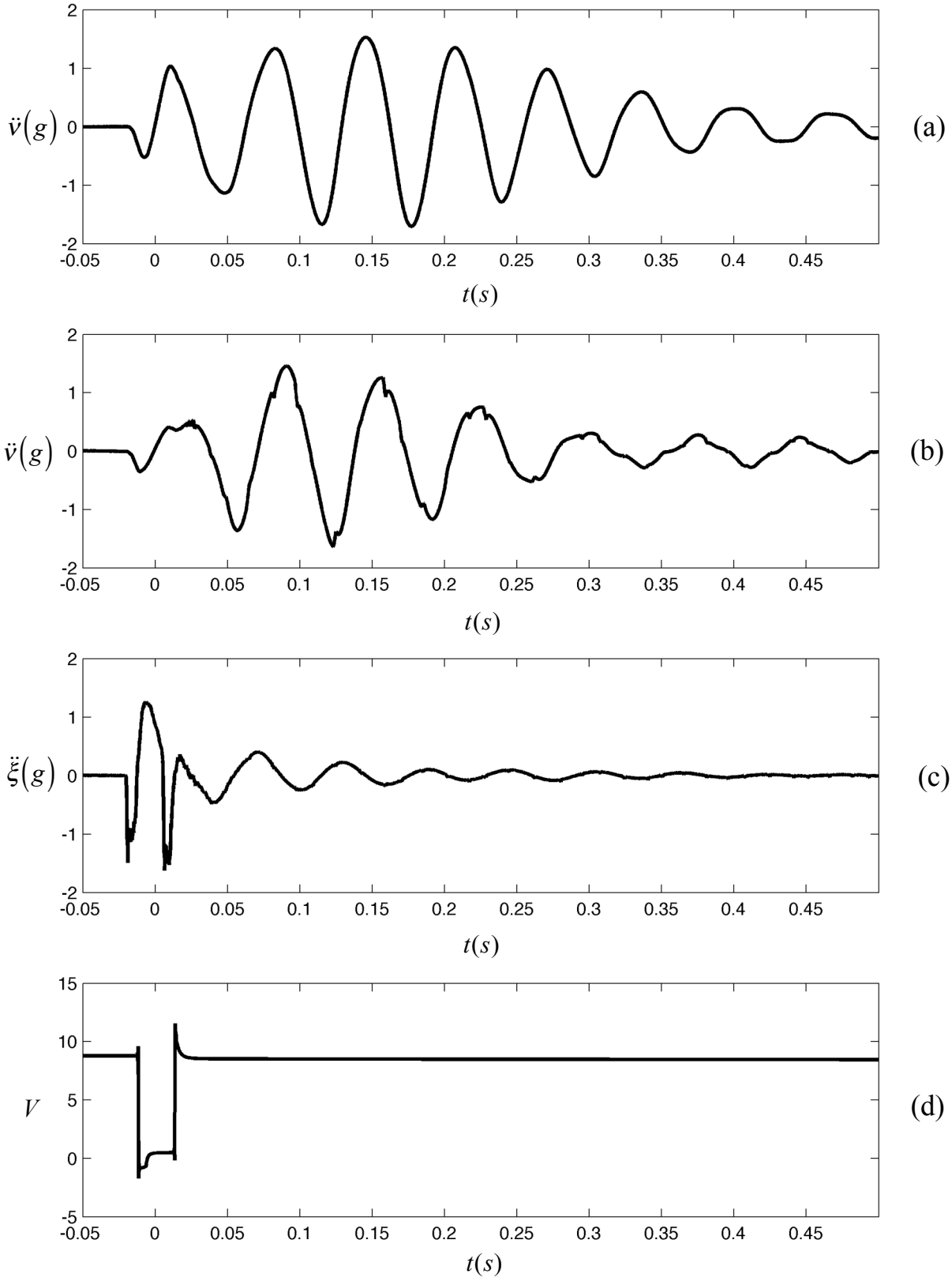


Figure 6.8. Stiffness switching strategy for shock response considering a longer pulse obtained adding a mass of 1 kg to the rig, resulting in a pulse of duration 0.03s. (a) Passive response, (b) switching response, (c) shock pulse and (d) voltage applied to the electromagnets. Acceleration is given in *g*, voltage in volts and time in seconds.

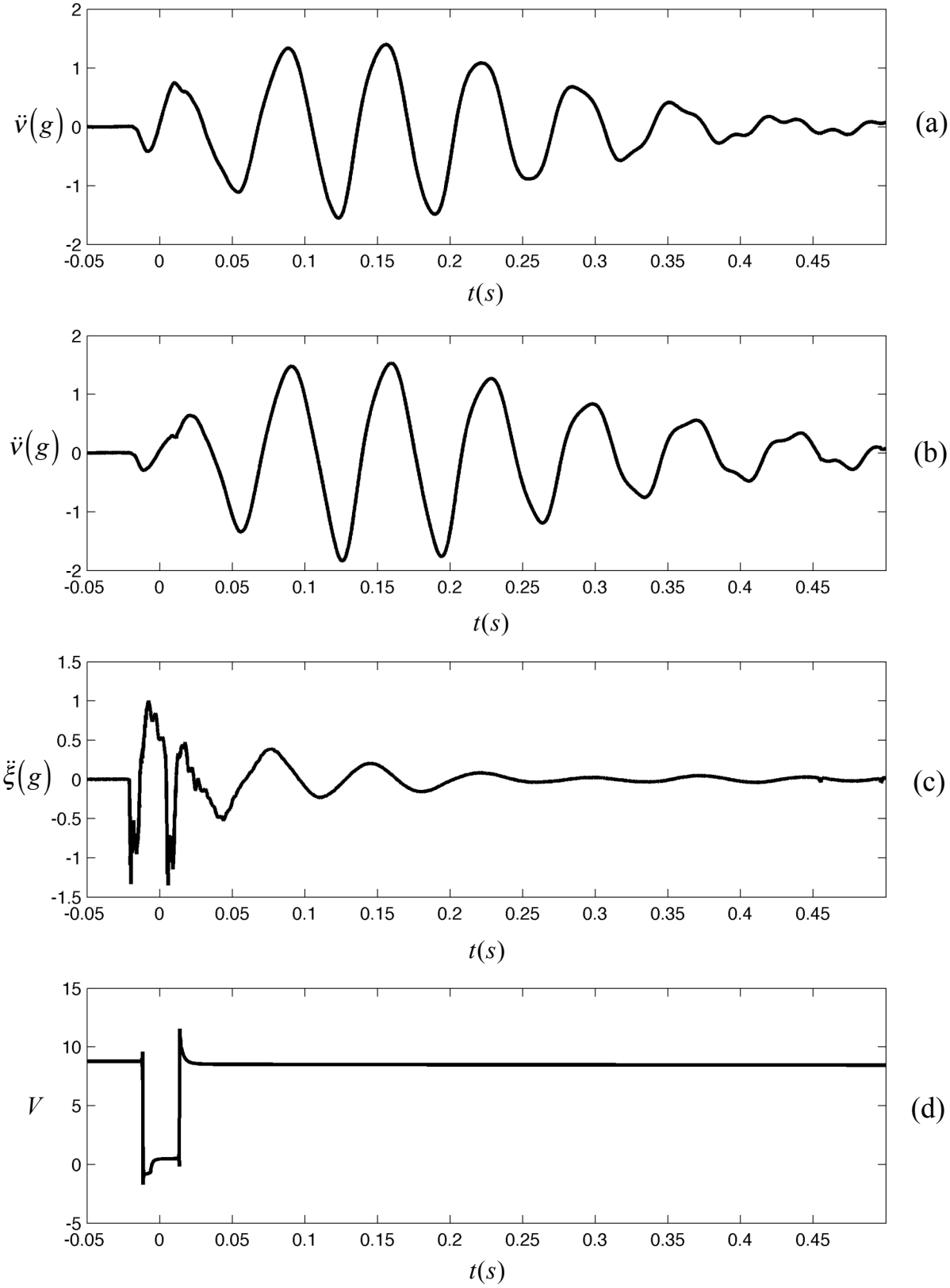


Figure 6.9. Stiffness switching strategy for shock response considering a longer pulse obtained adding a mass of 2 kg to the rig, resulting in a pulse of duration 0.035s. (a) Passive response, (b) switching response, (c) shock pulse and (d) voltage applied to the electromagnets. Acceleration is given in *g*, voltage in volts and time in seconds.

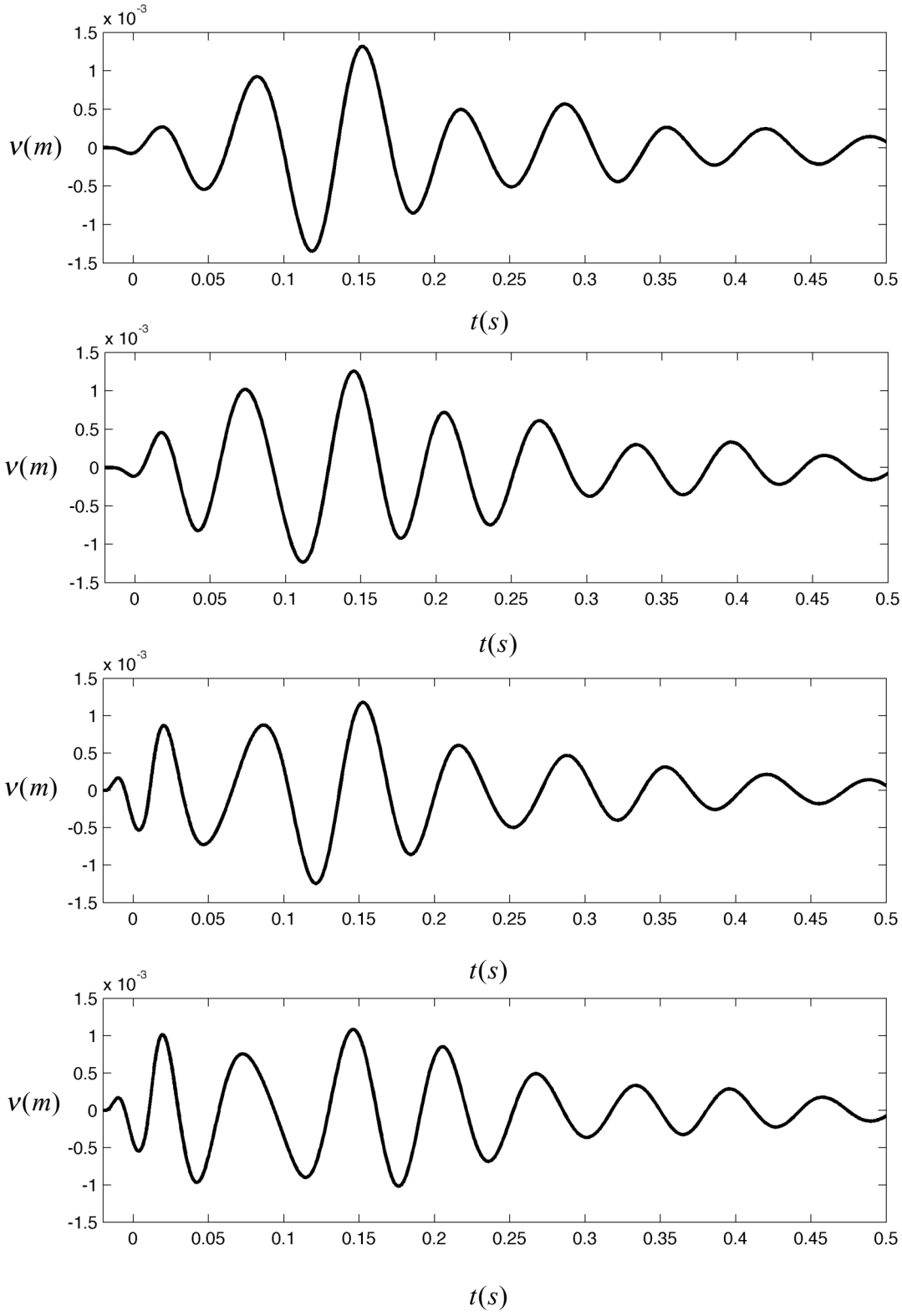


Figure 6.10. Displacement response for the model with stiffness control during shock (a) absolute displacement for switching system, (b) absolute displacement for passive system. (c) relative displacement for switching system and (d) relative displacement for passive system. The vertical axis is given in metres and the horizontal axis in seconds.

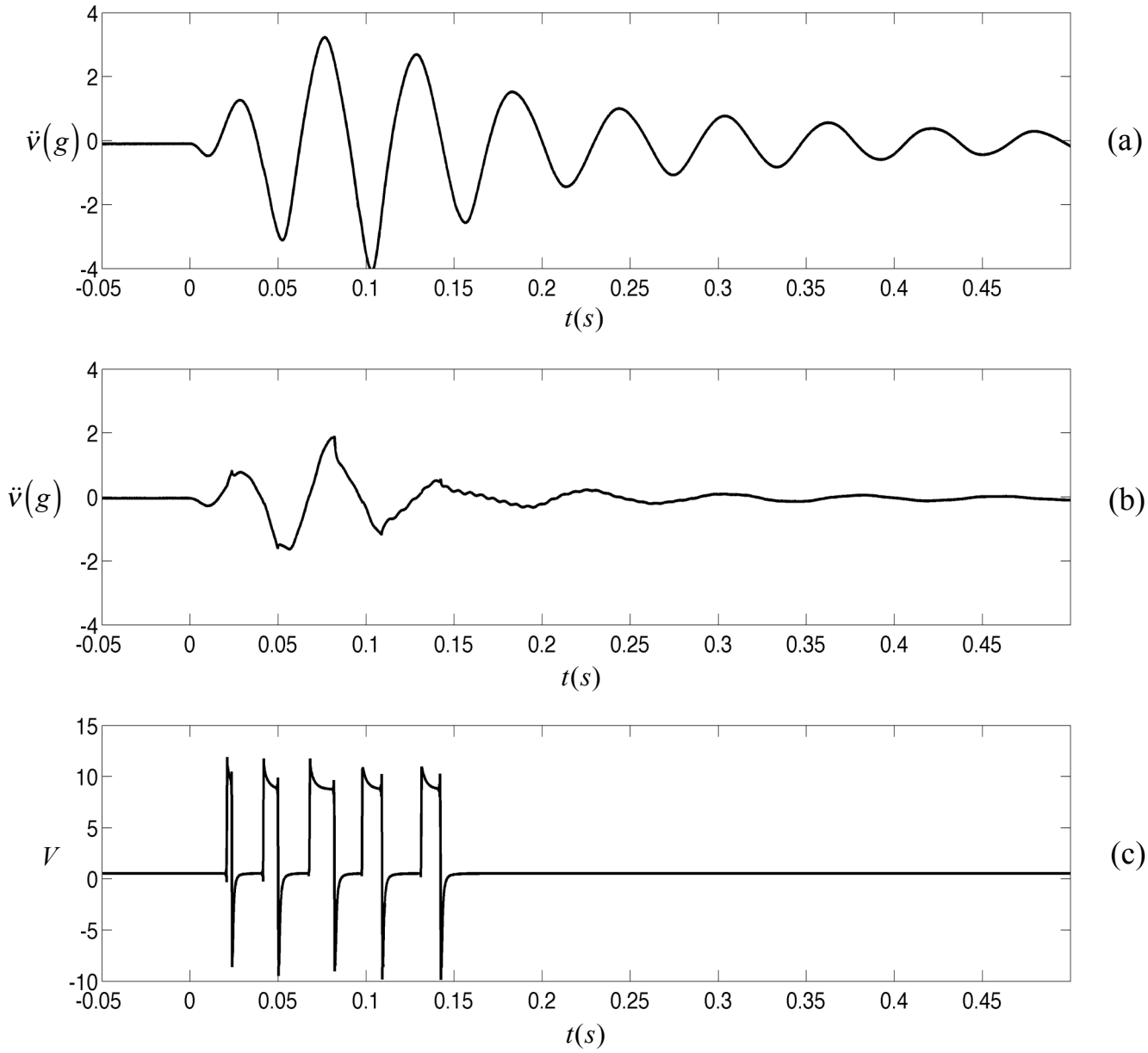


Figure 6.11. Switching stiffness response for residual vibration suppression applied to nylon wires suspension. (a) Passive response, (b) switching response and (c) voltage. Acceleration is given in *g*´s, voltage in volts and time in seconds.

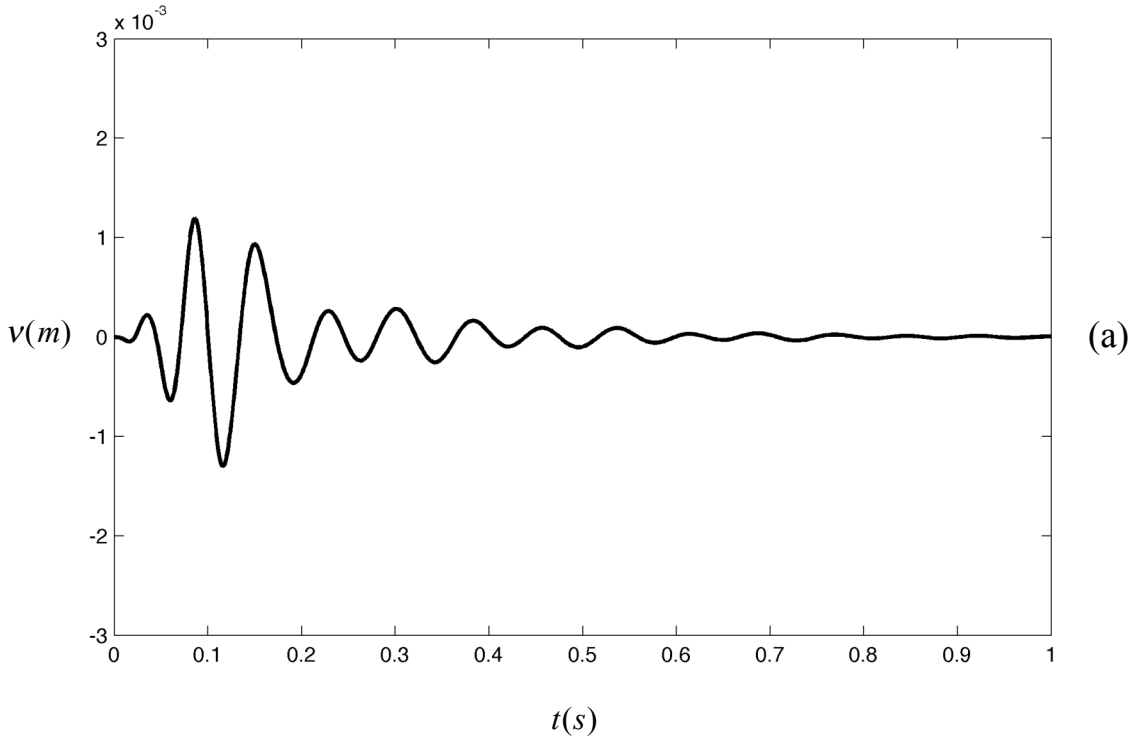


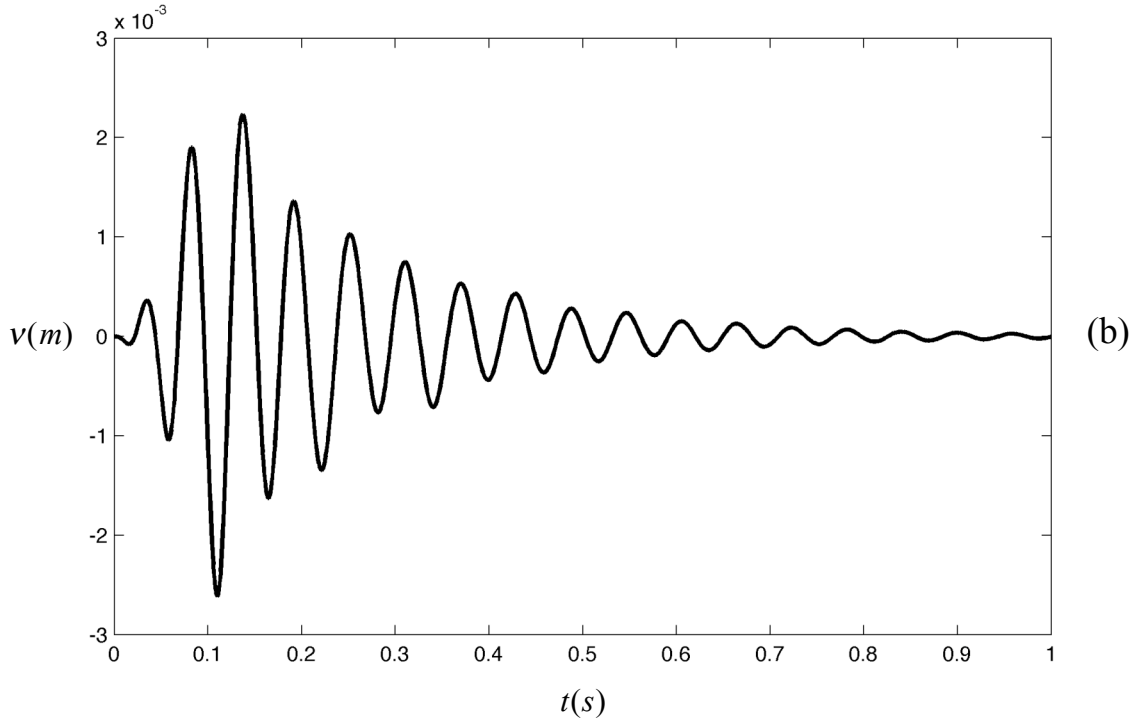


Figure 6.12. Absolute displacement free response for the experimental rig. (a) switching strategy applied. (b) passive response. The vertical axis is given in metres and the horizontal axis in seconds.

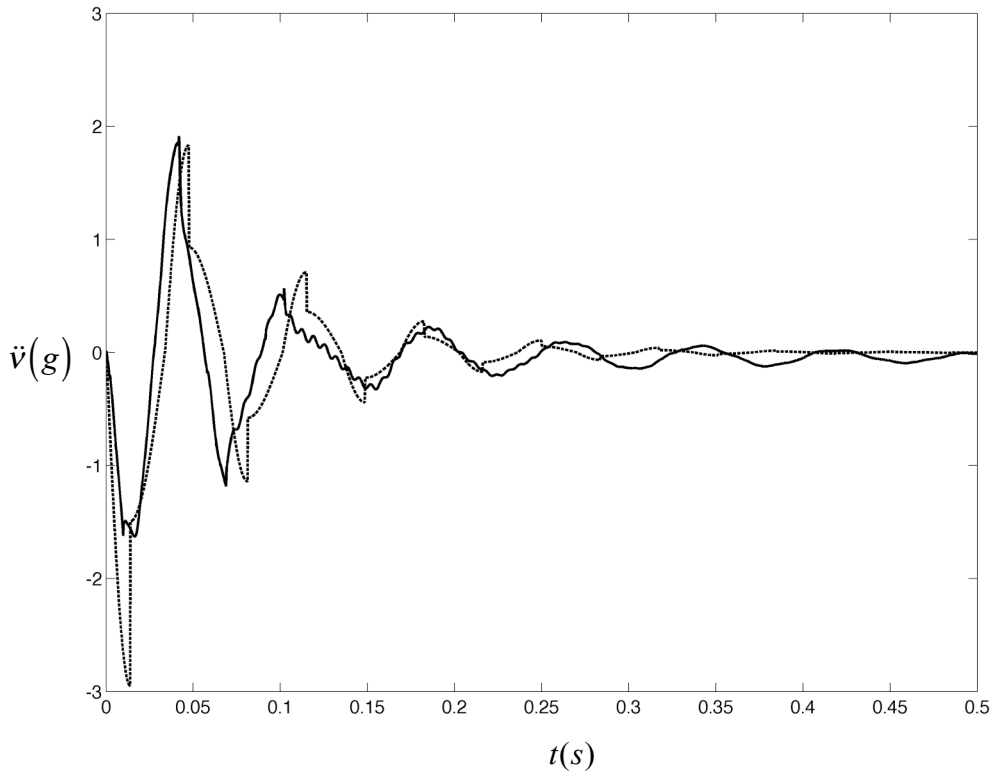


Figure 6.13. Comparison between the experimental response of the switching strategy for residual vibrations (bold line) and a simulation considering the parameters of the actual model (thin line). Acceleration is given in *g*, and time in seconds.

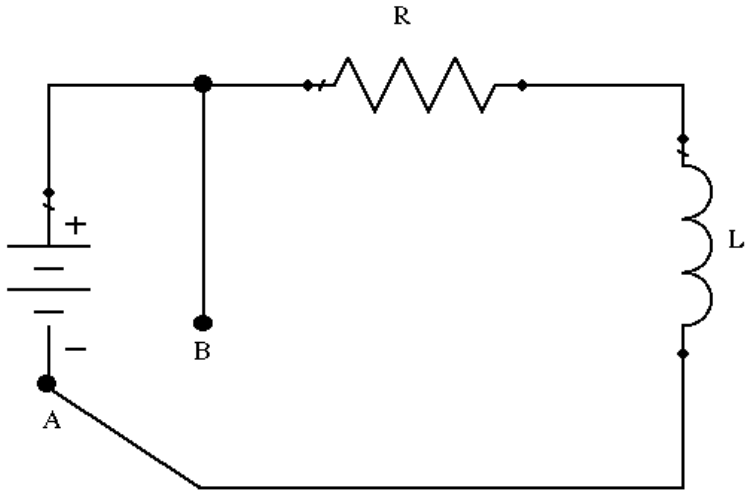


Figure 6.14. RL circuit representing the switchable stiffness system based in electromagnets. The switch moves from A to B to disconnect the electromagnets thus generating a transient as the current decays exponentially.

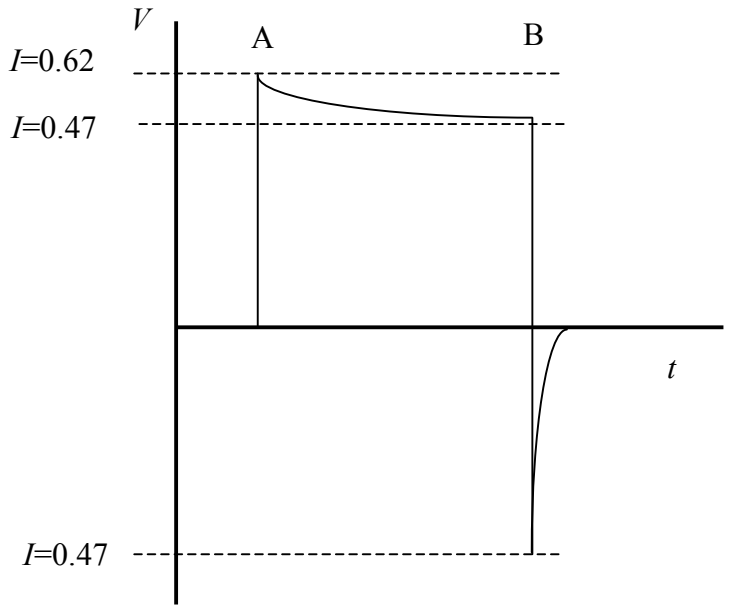


Figure 6.15. Schematical representation of the voltage variation of the electromagnetic system. The points shown are A for the stiffness recovery and B for the stiffness reduction.

The *instantaneous* current for points A and B is calculated as $I = \frac{V}{R}$.

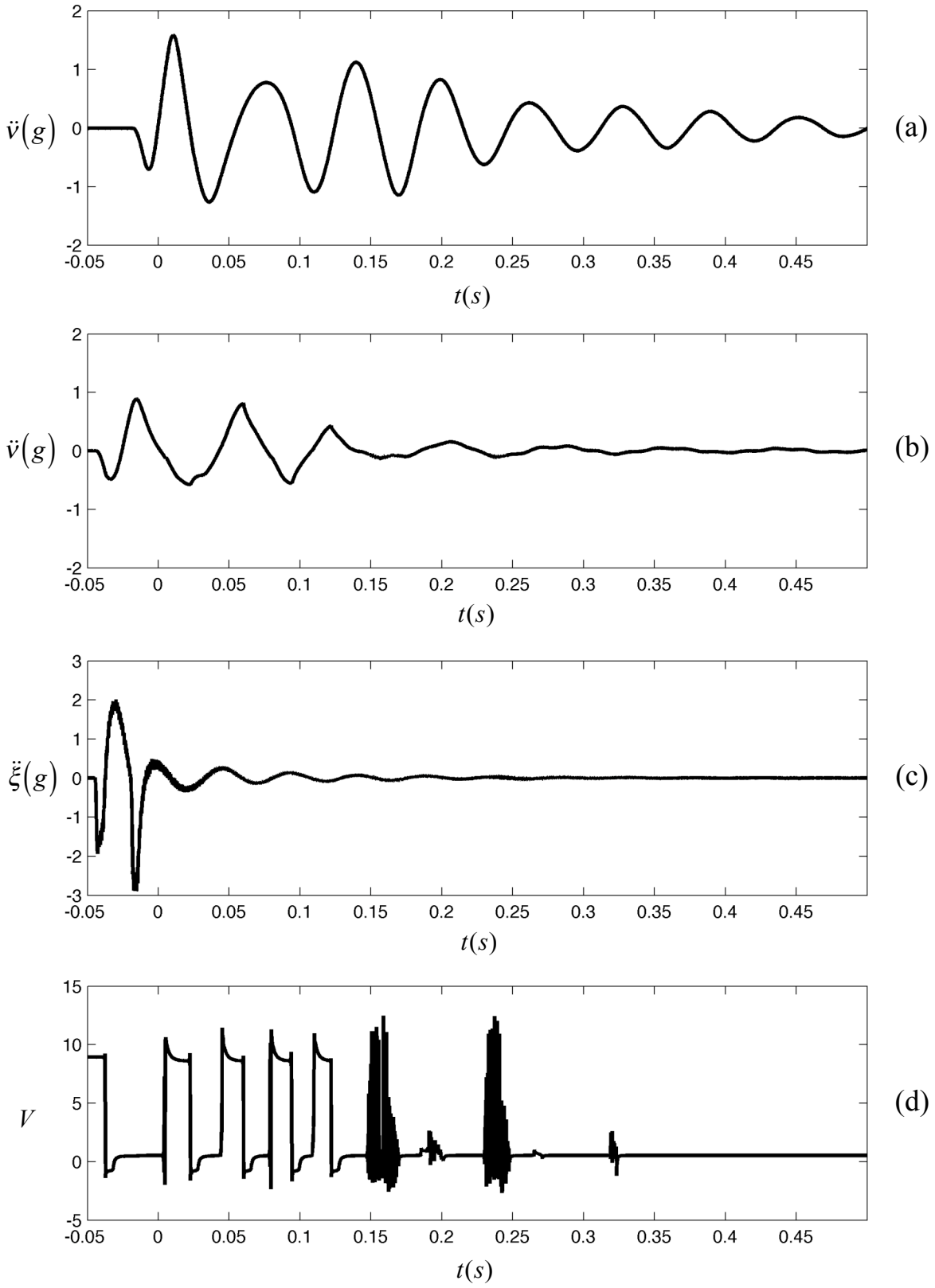


Figure 6.16. Response of the switchable stiffness model to both stiffness control during the shock, and control for residual vibration. (a) Passive response, (b) switching response, (c) shock pulse, and (d) voltage. Acceleration is given in *g*, voltage in volts and time in seconds.

# Chapter 7.

# Conclusions and recommendations for further work

The investigation of novel semi-active and adaptive methods for shock isolation and residual vibration control using switchable stiffness have been presented in this thesis. This chapter gives overall conclusions of the study and presents recommendations for future work.

## 7.1. General conclusions.

Shock is a source of vibration, which is very important to study because of its highly detrimental effects. Normally high accelerations and deformations are involved, thus the need to design and select proper isolators for those systems subjected to shock. Typically passive isolators based on elastic elements have been used as shock isolators, along with a dissipative elements, and/or viscoelastic elements. The modelling of those isolators is normally based on single degree-of-freedom models subjected to transient excitation in the form of symmetric pulses. This analysis is normally made in the time domain, where the Shock Response Spectra (SRS) plays an important role. These isolation systems have proven their reliability and relative good performance over the years. However, there are some disadvantages involved. For instance, passive isolators have fixed properties and are normally designed for a particular

kind of shock whereas a different excitation could reduce the isolator performance. Normally, if a high isolation performance is needed for a given shock excitation, the supports need to be soft, i.e. to have a low stiffness. However, this increases the relative displacement, thus it can be an issue when space is limited.

This thesis presented a theoretical analysis on alternative methods of shock isolation considering the use of semi-active and adaptive control strategies. In particularly, the use of switchable stiffness was analyzed. The problem was divided in two stages, namely the control of the maximum response during a shock, and the later suppression of residual vibration.

For control of the response during the shock, a particular stiffness switching strategy was proposed. This control scheme is based on the shock input, and it reduces the stiffness during the application of the shock. The analysis of the strategy was performed firstly on a single degree-of-freedom model with an elastic element called the secondary spring capable of disconnection or connection from the main supported mass in order to reduce the effective stiffness. Secondly, a compound system was considered in which the secondary element comprises another mass-spring model. This secondary element is also switchable as in the simple model. The analysis of these models was made using a versed sine base displacement excitation, and the different response parameters such as absolute displacement, relative displacement and absolute acceleration were studied. The performance of the passive single degree-of-freedom model was considered as a performance benchmark. It was found that reducing the stiffness during the application of the shock increases the isolation performance. The percentage of stiffness reduction is a direct indicator of the reduction in the response, where higher stiffness reduction will lead to better isolation performances. This performance gain was reflected more in the absolute displacement and acceleration responses, while the relative displacement experienced smaller benefits. However, it was also found that this strategy works better for pulses of short duration in comparison with the natural period of the system. For longer pulses, especially those approaching the quasistatic area of the Shock Response Spectra the response can be amplified. Similar behaviour was observed for both the simple and the compound model. Additionally, the effect of damping was introduced, showing that it increases further the isolation, but the effect is small. It is also important to note the effect of the delay in the stiffness switching, which can affect the isolation performance if it is very high. However, small delays will cause no visible effect.

The second part of the strategy was related to the rapid suppression of the residual vibrations that occur after the shock has passed. For this objective a different switching stiffness strategy was used. The strategy used in this case was semi-active, because the stiffness is switched every quarter of cycle. This control method is intended primarily to provide high energy dissipation in lightly damped systems. The investigation mainly focused on the energy dissipation mechanism and its quantification. As in the previous stage, two models were considered, i.e. a simple undamped single degree-of-freedom with a switchable stiffness element, and a compound model with a secondary mass-spring system. The former model represents the basic behaviour of the switching strategy using massless elastic elements, where the secondary elastic element carries and dissipates some energy while it is disconnected due to the addition of an infinitesimal amount of damping. The latter impacting model was conceived as a further explanation of the energy dissipation mechanism. In this case, the secondary mass and the primary mass experience an inelastic impact that is responsible for the energy lost in the system. The effect of damping was also incorporated later into the analysis of both models, showing that the strategy is not suitable for highly damped systems, where no benefits are found. Otherwise, the use of this strategy gives enhanced energy dissipation thus suppressing residual vibrations rapidly without the implementation of another passive means of damping, which can be helpful in systems where the addition of damping is difficult for design reasons, for instance.

The theoretical studies have been experimentally validated with a specifically designed rig. The experimental model uses electromagnetic forces in order to obtain a switchable stiffness force. This model has been designed having in mind the principal assumptions considered in theory, i.e. a system which is capable of obtaining high stiffness changes, at least in a factor of two, but is also capable of doing this change very quickly. Additionally, the system should be lightly damped. The laboratory tests on the rig confirmed these properties.

Validation of both theoretical strategies using the experimental rig gave good results. For the first stage, a shock motion was generated using an electrodynamic shaker used to excite the system. The switching response obtained using a control circuit was recorded and compared with the passive response of the system. Significant improvements in the isolation performances were found, giving a good agreement with the theoretical predictions. Another circuit was used to implement the residual vibration control, in this case with the system in free vibration an certain impulse. The effective damping ratio of the experimental system was

very similar to the predicted value considering the mechanical properties of the system. Moreover, it was also easy to appreciate how the vibrations were suppressed more rapidly in the switching system compared to the passive case. Finally, both strategies were implemented together, thus demonstrating the feasibility and advantages of the complete control scheme.

Overall, this thesis has presented a novel theoretical method for shock isolation using semi-active control strategies, showing its potential use and advantages over classical passive approaches especially for lightly damped systems. Moreover, the feasibility and validity of the theoretical methods have been tested experimentally with a very good correlation between theory and practice.

## 7.2. Recommendations for further work.

This thesis has given a further insight into the use and application of switchable stiffness for shock excitation. However, there are some aspects found during the investigation that might be worthy of further study as mentioned below.

- The analysis in this thesis has been restricted to single degree-of-freedom systems. A possibility for further study is the use of multi degree-of-freedom models where the energy dissipation could be transferred to higher modes of vibration.

- In the simulation of shock response for the switchable stiffness model only a symmetric versed sine pulse was considered. Although this kind of pulse is widely used in shock analysis, it will be an interesting area to investigate the behaviour of this strategy for more complex shock situations, such as non-symmetric pulses, or other pulses approaching situations like explosions, waves, or earthquakes.

- The effect of delay in the residual response switching strategy was briefly analysed in the thesis, stating that it can cause potential instabilities in the system. However, this a topic which can be further extended in order to have a better understanding of the model.

- The study in this thesis has been limited to transient non periodic excitation. It would be interesting to investigate the effect and behaviour of this or a similar switchable stiffness strategy for other different type of excitations such as harmonic or random sources of vibration. This proposed analysis could be carried out both theoretically and experimentally.

# REFERENCES


1. Mead, D.J., *Passive Vibration Control*. 1999, Chichester, John Wiley and Sons.
2. Harris, C.M., Crede, C.E., *Shock and Vibration Handbook*. 1996, New York: McGraw-Hill.
3. Mindlin, R.D., Dynamics of package cushioning. *Bell Systems Journal*, 1945. **24**.
4. Ayre, R.S., *Engineering Vibrations*. 1958, New York: McGraw-Hill.
5. Snowdon, J.C., Response of nonlinear shock mountings to transient foundation displacements. *Journal of the Acoustical Society of America*, 1961, **33**(10). p. 1295-1304.
6. Snowdon, J.C., Transient response of nonlinear isolation mountings to pulselike displacements. *Journal of the Acoustical Society of America*, 1963, **35(**3). p. 389-396.
7. Snowdon, J.C., Steady-state and transient behavior of two and three element isolation mountings, *Journal of the Acoustical Society of America,* 1963, **35**(3). p. 397-403.
8. Derby, T.F. and Calcaterra, P.C. Response and optimization of an isolation system with relaxation type damping (Optimal damping of impulse- and random-vibration responses of mechanical isolation system using relaxation type damping) *The Shock and Vibration Bulletin*, Shock and Vibration Information Center, 1969. **40**(5).
9. Eshleman, R.L. and P. Rao, Response of mechanical shock isolation elements to high rate input loading. *Shock and Vibration Bulletin*, Shock and Vibration Information Center, 1969, **40**(5): p. 217-34.
10. Parfitt, G.G. and J.C. Snowdon, Incidence and prevention of damage due to mechanical shock, *Journal of the Acoustical Society of America*, 1962, **34**(4). p. 462-468.
11. Chandra, S.N., Hatwal, H. and Mallik, A.K. Performance of non-linear isolators and absorbers to shock excitations. *Journal of Sound and Vibration*, 1999. **227**(2): p. 293-307.
12. Smallwood, D.O., Improved recursive formula for calculating shock response spectra. *Shock and Vibration Bulletin*, Shock and Vibration Information Center,1980 **51**(2): p. 211-217.
13. Lalanne, C., *Mechanical Vibration and Shock: Mechanical shock.* Vol. 2. London Hermes Penton Science, 2002.

14. Kemper, J.D. and Ayre, R.S. Optimum damping and stiffness in a nonlinear four-degree-of-freedom system subject to shock load. T*ransactions of the ASME. Series E, Journal of Applied Mechanics*, 1971. **38**(1): p. 135-42.
15. He Qiwei, Z.S., and Xuetao W. Study on the shock response character of nonlinear shock isolation systems under a type of exponential impulse. *Progress in Safety Science and Technology*. 2002. Taiwan, China: Science Press.
16. Hundal, M.S., Impact absorber with linear spring and quadratic law damper. *Journal of Sound and Vibration*, 1976. **48**(2): p. 189-193.
17. Guntur, R.R. and Sankar, S. Performance of different kinds of dual phase damping shock mounts, *Journal of Sound and Vibration*, 1982. **84**(2): p. 253-267.
18. Shekhar, N.C., Hatwal, H. and Mallik, A.K. Response of non-linear dissipative shock isolators. *Journal of Sound and Vibration*, 1998. **214**(4): p. 589-603.
19. Hundal, M.S., Passive pneumatic shock isolator: analysis and design. *Journal of Sound and Vibration*, 1982. **84**(1): p. 1-9.
20. Hundal, M.S. Response of Pneumatic isolator to standard pulse shape. *Shock and Vibration Bulletin,* Shock and Vibration Information Center, 1982, p. 161-16
21. Hundal, M.S., Linear shock isolator: response to velocity pulse. *Journal of Sound and Vibration*, 1983. **86**(2): p. 293-296.
22. Hundal, M.S. and Fitzmorris D.J. Response of a symmetric self-damped pneumatic shock isolator to an acceleration pulse. *Shock and Vibration Bulletin*, Shock and Vibration Information Center, 1985, p 139-154.
23. Mercer, C.A. and Rees, P.L. An optimum shock isolator. *Journal of Sound and Vibration,* 1971. **18**(4): p. 511-520.
24. Vakakis, A.F., *Passive vibration control through nonlinear energy pumping. Proceedings of the ASME Design Engineering Technical Conference*, Chicago IL, United States, 2003 p 1883-1888.
25. Vanderborck, G. Theoretical and experimental behaviour of equipment under mechanical shocks. *Proceedings of the Annual Technical Meeting*, Institute of environmental Sciences Nashville, TN, USA 1992. p 283-288.
26. Dufour, R. Shock and sine response of rigid structures on nonlinear mounts. *ASME Design Engineering Division Publication*, Miami, FL, USA, 1991, **34** p 171-176.
27. Makris, N. and Chang, S.P. Response of damped oscillators to cycloidal pulses *Journal of Engineering Mechanics,* 2000, **126** (2)p. 122-131.

28. Jennings, P.C., Ground motions pulses and structural response, *Earthquake Engineering Frontiers in the New Millennium*. 2001: Beijing, China.
29. Matsuzaki, Y. and Kibe S, Shock and seismic response spectra in design problems. *Shock and Vibration Digest*, 1983. **15**(10): p. 3-10.
30. Chehab, A.G. and El Naggar M.H. , Response of block foundations to impact loads. *Journal of Sound and Vibration,* 2004. **276**(1-2): p. 293-310.
31. Guoqiang, W. and Zuomin D, Design optimization of low impact transmission foundation for forging hammers. *Engineering Computations*, 2006. **23**(2): p. 166-86.
32. Naggar, M.H.E. and Chehab A.G., Vibration barriers for shock-producing equipment, *Canadian Geotechnical Journal*, 2005. **42**(1): p. 297-306.
33. Goyal, S., Buratynski, E.K. and Elko G.W.. Shock-protection suspension design for printed circuit board. *International Conference on High-Density Interconnect and Systems Packaging*, 2000, Denver, CO, USA. p 274-82.
34. Jin-Seung, S., Strategies for improvement of shock performance in hard disk drives. *Journal of Information Storage and Processing Systems*, 2001. **3**(3-4): p. 229-36.
35. Jayson, E.M. and Talke F.E., Optimization of air bearing contours for shock performance of a hard disk drive. *Journal of Tribology*, 2005. **127**(4): p. 878-883.
36. Goyal, S.E. and Buratynski, E.K. , Role of shock response spectrum in electronic product suspension design. *International Journal of Microcircuits and Electronic Packaging*, 2000. **23**(2): p. 183-190.
37. Johnson, C.D.W. Whole-spacecraft shock isolation system, *Smart Structures and Materials: Damping and Isolation*. 2002. San Diego, CA, USA
38. Wilke, P. Whole-spacecraft vibration isolation for broadband attenuation. *IEEE Aerospace Conference*, 2000, Big Sky, MT USA, **4** p. 315-321.
39. Brown, S.A. and Pickering, M.D. COTS electronics and the naval shock environment, 2002 *International Radar Conference*, Edinburgh, UK., p. 114-117.
40. Tsur, O. Rugged, reliable, and secured data storage solutions for airborne ISR systems. 2004. *Proceedings of the SPIE*, **5409**(1), 9 66-73.
41. Jiang, X.J., Wang, Z.H., Sun, H.X., Zhao, T.L., Zhou, C.Y., Yu, G.H., Zhang, G.L. Suitability analysis of commercial off-the-shelf components for space application. *Proceedings of the Institution of Mechanical Engineers, Part G (Journal of Aerospace Engineering)*, 2006. **220**(5): p. 357-64.

42. Jalili, N., A comparative study and analysis of semi-active vibration-control systems. *Journal of Vibration and Acoustics, Transactions of the ASME*, 2002. **124**(4): p. 593-605.
43. Schwartz, M., *Encyclopaedia of smart materials*. John Wiley and Sons, New York, 2002.
44. Franchek, M.A., Ryan M.W., and Bernhard R.J., Adaptive passive vibration control. *Journal of Sound and Vibration,* 1996. **189**(5): p. 565-585.
45. Liu, Y., Waters, T.P. and Brennan M.J., A comparison of semi-active damping control strategies for vibration isolation of harmonic disturbances. J*ournal of Sound and Vibration*, 2005. **280**, p. 21-39.
46. Alkhatib, R. and Golnaraghi, M.F. Active structural vibration control: a review. *Shock and Vibration Digest*, 2003. **35**(5): p. 367-83.
47. Karnopp, D., Active and semi-active vibration isolation. *Transactions of the ASME. Journal of Vibration and Acoustics*, 1995. **117**(3B): p. 177-85.
48. Eriksson, L.J., Active sound and vibration control: a technology in transition. *Noise Control Engineering Journal*, 1996. **44**(1): p. 1-9.
49. Sevin, E. and Pilkey, W.D. *Optimum Shock and Vibration Isolation*, The Shock and Vibration Information Center, Washington D.C.1971.
50. Balandin, D.V., Bolotnik, N.N. and Pilkey, W. D., Review: Optimal shock and vibration isolation. *Shock and Vibration*, 1998. **5**(2): p. 73-87.
51. Pilkey, W.D. and Lim, T.W., Optimal shock isolation with minimum settling time. *58th Shock and Vibration Symposium*, Huntsville, AL, USA, 1987. NASA Conference Publication, p 379-388.
52. Bolotnik, N.N., Optimization of characteristics and parameters of antishock isolators and vibrotechnological machines. *Izvestiya Akademii Nauk: Tekhnicheskaia Kibernetika,* 1993(1): p. 62-67.
53. Balandin, D.V., Bolotnik, N.N and Pilkey W.D., Pre-acting control for shock and impact isolation systems. *Shock and Vibration,* 2005. **12**(1): p. 49-65.
54. Iwata Y., Optimum preview control of vehicle air suspensions. *Bulletin of the Japan Society of Mechanical Engineers*, 1976. **19**(138): p. 1485-1489.
55. Rakheja, S. and Sankar S. Vibration and shock isolation performance of a semi-active 'on-off' damper. *ASME Design Engineering Technical Conference, 1985* Cincinatti OH, USA.

56. Meller T., Electronically controlled damping systems for cars. *Sixth International Conference on Automotive Electronics*. 1987 London, UK.
57. Rajamani R., Semi-active suspensions - a comparison between theory and experiments, *Proceedings of the 12th IAVSD Symposium on Dynamics of Vehicles on Roads from Tracks*, 1991, Lyon, Fr.
58. Kim, S., Vibration control of a semi-active suspension featuring electrorheological fluid dampers. *Journal of Sound and Vibration*, 2000. **234**(3): p. 537-546.
59. Ghosh, M.K. and Dinavahi, R. Vibration analysis of a vehicle system supported on a damper-controlled variable-spring-stiffness suspension. *Proceedings of the Institution of Mechanical Engineers, Part D: Journal of Automobile Engineering*, 2005. **219**(5): p. 607-619.
60. Alanoly, J. and Sankar, S. Semi-active force generators for shock isolation. *Journal of Sound and Vibration*, 1988. **126**(1): p. 145-156.
61. Muijderman J.H.E.A, Huisman, K.J.J., Veldpaus, R. G. M., and Van Heck F. M., Preview-based control of suspension systems for commercial vehicles. *Vehicle System Dynamics*, 1999. **32**(2): p. 237-247.
62. Moran Antonio, N.M., Analysis and design of active suspensions by HINF robust control theory. J*SME International Journal, Series 3: Vibration, Control Engineering, Engineering for Industry,* 1992. **35**(3): p. 427-437.
63. Yedavalli R.K. and Yong L. Active suspension control design for optimal road roughness isolation and ride comfort. *American Control Conference.* 1994. Baltimore, MD, USA:
64. Al-Assaf, Y. Adaptive control for vehicle active suspension systems. *American Control Conference.* 1995. Seattle, WA, USA.
65. Yoshimura, K., Kurimoto, and Hino, Construction of an active suspension system of a quarter car model using the concept of sliding mode control. *Journal of Sound and Vibration*, 2001. **239**(2): p. 187-99.
66. Griffin, M.J. and Wu, X.A Semi-Active control policy to reduce the occurrence and severity of end stop impacts in a suspension seat with an electrorheological fluid damper. *Journal of Sound and Vibration*, 1996. **203**(5): p. 781-793.
67. McManus, S.J., St. Clair, K.A., Boileau P.E., Boutin, J., and Rakheja, S. Evaluation of vibration and shock attenuation performance of a suspension seat with a semi-active magnetorheological fluid damper. *Journal of Sound and Vibration,* 2002. **253**(1): p. 313-327.

68. Shan, S. and He, L. Semi-active shock isolation technology based on controllable damping. *Journal of Vibration and Shock*, 2006. **25**(5): p. 144-147.
69. Kim, D.H., Lee, P.W., and Lee G. S., Active impact control system design with a hydraulic damper. *Journal of Sound and Vibration,* 2002. **250**(3): p. 485-501.
70. Guangqiang, Y., Spencer B.F., and Leban, F. Shock vibration control using "smart" damping devices, *Sixth International Conference on Motion and Vibration Control*, 2002. Saitama, Japan, **2**, p. 722-727.
71. Choi, Y.T., Wereley, and Norman M. Shock isolation systems using magnetorheological dampers. *Smart Structures and Materials: Damping and Isolation*. 2004. San Diego, CA, United States:
72. Tanaka, N., Kikushima, Y. and Kitada, M. Study on the vibrationless forge hammer. (6th Report: development of Mel Forge). *Nippon Kikai Gakkai Ronbunshu, C Hen/Transactions of the Japan Society of Mechanical Engineers,* Part C, 1989. **55**(515): p. 1590-1596.
73. Tanaka, N. and Kikushima.Y. Active control of impact vibration using feedforward control method, *Journal of Vibration, Acoustics, Stress, and Reliability in Design,* 1989. **111**(1): p. 53-60.
74. Tanaka, N. and Y. Kikushima, Study on the vibrationless forging hammer (5th Report, Experiment Of The Pole-Zero Active Vibration Control Method. *Nippon Kikai Gakkai Ronbunshu, C Hen,* 1987. **53**(496): p. 2515-2520.
75. Tanaka, N. and Kikushima, Y. Study of the preview dynamic damper. *ASME Design Engineering Division Publication,* 1989 **18**(2)
76. Tanaka, N. and Kikushima, Y. Impact vibration control using a semi-active damper. *Journal of Sound and Vibration*, 1992. **158**(2): p. 277-292.
77. Lane, J.S., Ferri, A.A. and Heck, B.S. Vibration control using semi-active friction damping. *ASME Design Engineering Division* 1992, **49**: p 165-171.
78. Ferri, A.A. and Eshleman, E. D. Performance limits of shock isolation mounts for specific deterministic inputs. *ASME Design Engineering Division Publication*, 1996, **93**: p 189-195.
79. Krishna Y, Shrinivasa, S. B. S. Shock isolation using magnetostrictive actuator. *Proceddings of the SPIE* 2003. **5062**(1) p 270-277.
80. Bobrow, J. E. and Jabbari, F. High-performance semiactive controller for structural vibration suppression. *Proceedings of the SPIE, The International Society for Optical Engineering,* 1997, **3041**: p 67-74.

81. Winthrop, M.F., Baker, W.P. and Cobb, R.G. A variable stiffness device selection and design tool for lightly damped structures. *Journal of Sound and Vibration,* 2005. **287**(4-5): p. 667-682.
82. Krishna, Y. and Sarma, B.S. Semiactive vibration isolation of a rigid platform using smart actuator. *Proceddings of the SPIE* 2004. **5388**(1) p 327-337.
83. Liu, Y. Vibration control by a variable damping and stiffness system with magnetorheological dampers. *JSME International Journal, Series C: Mechanical Systems, Machine Elements and Manufacturing*, 2006. **49**(2): p. 411-417.
84. Crosby, M.J. and D.C. Karnopp. The active damper: a new concept for shock and vibration control. *Shock and Vibration Bulletin*, 1973. **43**: p. 119-33.
85. Walsh, P.L. and Lamancusa, J.S. Variable stiffness vibration absorber for minimization of transient vibrations. *Journal of Sound and Vibration,* 1992. **158**(2): p. 195-211.
86. Kidner, M.R.F. and Brennan, M.J. Real-time control of both stiffness and damping in an active vibration neutralize. *Smart Materials and Structures*, 2001. **10**(4): p. 758-769.
87. Bonello, P., Brennan, M.J. and Elliott, S.J. Vibration control using an adaptive tuned vibration absorber with a variable curvature stiffness element. *Smart Materials and Structures*, 2005. **14**(5): p. 1055-1065.
88. Bonello, P., Brenan, M.J., Elliott, S.J., Vincent, J.F.V., Jeronimidis, G. Design for an adaptive tuned vibration absorber with variable stiffness element. *Proceedings of the Royal Society of London, Series A (Mathematical, Physical and Engineering Sciences)*: 2005. **461**(2064): p. 3955-76.
89. Cunefare, K.A. State-switched absorber for semi-active control of plates. *Structures, Structural Dynamics and Materials Conference,* 2001. Seattle, WA, USA, **4**, p. 5850-2856.
90. Onoda, J. and Minesugi, K. Alternative control logic for type-II variable-stiffness system. *AIAA Journal*, 1996. **34**(1): p. 207-209.
91. Onoda, J., Endo, T., Tamaoki, H., Watanabe, N. Vibration suppression by variable-stiffness members. *AIAA Journal,* 1991. **29**(6): p. 977-983.
92. Onoda, J., Sano, T. and Kamiyama, K. Active, passive, and semiactive vibration suppression by stiffness variation. *AIAA Journal,* 1992. **30**(12): p. 2922-2929.
93. Utkin, V.I., Variable structure systems with sliding modes. *IEEE Transactions on Automatic Control,* 1977. **AC-22**(2): p. 212-22.

94. Yamaguchi, H., Yashima, M. and Hirayama, Y. Vibration reduction and isolation performance for on-off control of a friction force at a spring support. *Journal of Sound and Vibration,* 1997. **208**(5): p. 729-743.
95. Warkentin, A. and Semercigil, S.E. Variable stiffness control of a single-link flexible robotic arm. *Journal of Sound and Vibration,* 1995. **187**(1): p. 1-21.
96. Pun, J. and Semercigil, S.E. Semi-active vibration control of a flexible arm using joint stiffness control. *Proceedings of the International Modal Analysis Conference*, Orlando, FL, USA, 1997, **1**: p 195-201.
97. Jalili, N. and Ramaratnam, A. A switched stiffness approach for structural vibration control: theory and real-time implementation. *Journal of Sound and Vibration*. **291**(1-2): p. 258-74.
98. Corr, L.R. and Clark, W.W. Similarities between variable stiffness springs and piezoceramic switching shunts. *AIAA Journal,* 2006. **44**(11): p. 2797-2800.
99. Ramaratnam, A., Jalili, N. and Dawson, D.M. Semi-active vibration control using piezoelectric-based switched stiffness. *Proceedings of the American Control Conference,* Boston, MA, USA, 2004, **6**: p 5461-6.
100. Corr, L.R. and Clark, W.W. Energy dissipation analysis of piezoceramic semi-active vibration control, *Journal of Intelligent Material Systems and Structures*, 2001. **12**(11): p. 729-736.
101. Clark, W.W., Semi-active vibration control with piezoelectric materials as variable stiffness actuators. *Proceedings of SPIE - The International Society for Optical Engineering,* 1999. **3672**: p. 123-130.
102. Palm, W.J., *Mechanical Vibrations*, New York: John Wiley and Sons, 2007
103. Timoshenko S, Young D.H. and Weaver W., *Vibration problems in engineering*, New York: Wiley and sons, 1974
104. Morrow, C.T., *Shock and Vibration Engineering*, New York: John Wiley and Sons, 1963.
105. Snowdon, J.C., *Vibration and Shock in Damped Mechanical Systems.*, New York: Wiley and Sons, 1968.
106. Chen, J.C., Response of Large Spacecraft Structures With Stiffness Control, *Journal of Spacecrafts And Rockets*, September-October 1984, **21**(5), 163-67.
107. Anand, D.K., Cunniff P.F., *Engineering Mechanics: Dynamics,,* Houghton Mifflin Company, Boston, 1973.108.
108. Cartmell, M., *Introduction to Linear, Parametric and non Linear Vibrations,* Chapman

and Hall, London, 1990.

109. Ewins, D.L., *Modal Testing: Theory and Practice,* Letchworth: Research Studies, 1984
110. Ogata, K., *Modern Control Engineering,* Prentice-Hall, New Jersey, 1990.
111. Kip, F.A. *Fundamentals of electricity and magnetism,* McGraw-Hill, Kogakusha, Tokyo, 1969
112. Shin, K. and Brennan, M.J. Two simple methods to supress the residual vibrations of a translating or rotating flexible cantilever beam. *Journal of Sound and Vibration,* 2008 **312**(1-2): p. 140-50.

# Appendix A

## Solution of the equations of motion using Laplace transformations.

### a) Constant slope step.

The equation of motion is given by:

$$\frac{\ddot{v}}{\omega_n^2} + v = \xi(t) \qquad \text{(A1)}$$

where:

$$\xi(t) = \begin{cases} \xi_c \dfrac{t}{\tau} & [0 \le t \le \tau] \\ \xi_c & [\tau \le t] \end{cases} \qquad \text{(A2)}$$

Taking the Laplace transformation of equation (A1):

$$\frac{1}{\omega_n^2}\left(s^2V(s)-sV_0-s\dot{V}_0\right)+V(s)=\xi(s) \tag{A3}$$

Considering that the system is initially at rest and rearranging equation (A3):

$$V(s)=\frac{\omega_n^2\xi(s)}{s^2+\omega_n^2} \tag{A4}$$

The solution of the equation of motion is given by the inverse transformation of equation (A4). From [2], the transformation $\xi(s)$ for this particular case is given by:

$$\xi(s)=\frac{\xi_c}{\tau}\frac{1-e^{s\tau}}{s^2} \tag{A5}$$

As a result, and after an algebraic manipulation of equations (a4) and (a5), the solution is given by:

$$v(t)=\frac{\xi_c}{\tau}\omega_n^2\,\mathrm{L}^{-1}\left[\frac{1}{s^2\left(s^2+\omega_n^2\right)}-\frac{e^{-s\tau}}{s^2\left(s^2+\omega_n^2\right)}\right] \tag{A6}$$

Using Laplace transform pairs from [2], the response is given by:

$$v(t)=\frac{\xi_c}{\omega_n\tau}\left[\omega_n t-\sin(\omega_n t)-\left(\omega_n(t-\tau)-\sin\omega_n(t-\tau)\right)\right] \tag{A7}$$

Using $\sin(A+B)-\sin(A-B)=2\cos A\sin B$ to simplify equation (A7) one can write:

$$v(t)=\begin{Bmatrix}\dfrac{\xi_c}{\omega_n\tau}\left[\omega_n t-\sin(\omega_n t)\right] & 0\le t\le\tau\\ \xi_c\left[1+\dfrac{1}{\omega_n\tau}\left(2\sin\left(\dfrac{\omega_n\tau}{2}\right)\cos\omega_n\left(t-\dfrac{\tau}{2}\right)\right)\right] & \tau\le t\end{Bmatrix} \tag{A8}$$

From the part when $t\ge\tau$, the maximax response $v_m$ is given by the following expression, since it is a constant amplitude value:

$$v_m = \xi_c \left[ 1 + \frac{2}{\omega_n \tau} \left( \sin\left( \frac{\omega_n \tau}{2} \right) \right) \right] \tag{A9}$$

Finally, considering that $\omega_n = \frac{2\pi}{T}$ and rearranging equation (A9):

$$\frac{v_m}{\xi_c} = 1 + \frac{T}{\pi\tau} \left( \sin\left( \frac{\pi\tau}{T} \right) \right) \tag{A10}$$

Equation (A10) gives the normalized maximax response as a function of the period ratio $\frac{\tau}{T}$.

## b) Rectangular pulse.

This is the case of a symmetrical pulse. The forcing function is given by:

$$\xi(t) = \begin{cases} \xi_c & 0 \le t \le \tau \\ 0 & \tau \le t \end{cases} \tag{A11}$$

The Laplace transform of the forcing function is given by [2]:

$$\xi(s) = \xi_c \frac{1 - e^{s\tau}}{s} \tag{A12}$$

From the previous analysis one can take directly equation (A4) and combine with equation (A12) in order to obtain the solution. The solution is given by:

$$v(t) = \xi_c \omega_n^2 \mathrm{L}^{-1} \left[ \frac{1}{s^2 \left( s^2 + \omega_n^2 \right)} - \frac{e^{-s\tau}}{s^2 \left( s^2 + \omega_n^2 \right)} \right] \tag{A13}$$

The inverse transform of equation (A13) is:

$$v(t) = \xi_c \left[1 - \cos(\omega_n t) - (1 - \cos\omega_n (t - \tau))\right] \tag{A14}$$

Using $\cos(A - B) - \cos(A + B) = 2\sin A \sin B$ , one can rewrite equation (a14) as follows:

$$v(t) = \begin{cases} \xi_c \left[1 - \cos(\omega_n t)\right] & 0 \le t \le \tau \\ \xi_c \left[2\sin\left(\dfrac{\omega_n \tau}{2}\right)\sin\omega_n\left(t - \dfrac{\tau}{2}\right)\right] & \tau \le t \end{cases} \tag{A15}$$

The amplitude term during the residual response $v_r$ can be written in terms of the natural period and one can write an expression for the residual response as:

$$\frac{v_r}{\xi_c} = \left[2\sin\left(\frac{\pi\tau}{T}\right)\right] \tag{A16}$$

By differentiating this term with respect to $\tau / T$ and equating it to zero, the value obtained of $\dfrac{\tau}{T} = 0.5$ is substituted into equation (A16) in order to obtain the maximax response, given by:

$$\frac{v_m}{\xi_c} = 2 \tag{A17}$$

This is valid for $\tau / T \ge 1/2$ . For lower values, the maximum residual response is equal to the maximax response.

## c) Half sine pulse.

The forcing function is given by:

$$\xi(t) = \begin{cases} \xi_c \sin\left(\dfrac{\pi t}{\tau}\right) & [0 \le t \le \tau] \\ 0 & [\tau \le t] \end{cases} \tag{A18}$$

The Laplace transform of the forcing function is [2]:

$$\xi_c \frac{\pi/\tau}{s^2 + \left(\pi/\tau\right)^2}\left(1 + e^{-s\tau}\right) \tag{A19}$$

From equation (A4) and (A19), after an algebraic manipulation one can write:

$$v(t) = \xi_c \frac{\pi}{\tau}\omega_n^2 \mathrm{L}^{-1}\left[\frac{1}{\left(s^2 + \omega_n^2\right)\left(s^2 + \left(\pi/\tau\right)^2\right)}\right] + \mathrm{L}^{-1}\left[\frac{e^{-s\tau}}{\left(s^2 + \omega_n^2\right)\left(s^2 + \left(\pi/\tau\right)^2\right)}\right] \tag{A20}$$

Using Laplace transforms pairs given by [2], the solution of the equation can be expressed as follows:

$$v(t) = \xi_c \frac{\pi}{\tau}\omega_n^2 \left[\frac{\omega_n \sin\left(\frac{\pi}{\tau}t\right) - \frac{\pi}{\tau}\sin\left(\omega_n t\right)}{\frac{\omega_n \pi}{\tau}\left(\omega_n^2 + \frac{\pi^2}{\tau^2}\right)} + \frac{\omega_n \sin\frac{\pi}{\tau}\left(t-\tau\right) - \frac{\pi}{\tau}\sin\omega_n\left(t-\tau\right)}{\frac{\omega_n \pi}{\tau}\left(\omega_n^2 + \frac{\pi^2}{\tau^2}\right)}\right] \tag{A21}$$

Simplification of equation (A21) leads to:

$$v(t) = \begin{cases} v(t) = \dfrac{\xi_c}{1 - T^2/4\tau^2}\left(\sin\left(\dfrac{\pi t}{\tau}\right) - \dfrac{T}{2\tau}\sin\omega_n t\right) & 0 \le \mathrm{t} \le \tau \\ v(t) = \xi_c\left[\dfrac{\left(T/\tau\right)\cos\left(\pi\tau/T\right)}{\left(T^2/4\tau^2\right) - 1}\right]\sin\omega_n\left(t - \dfrac{\tau}{2}\right) & \tau \le \mathrm{t} \end{cases} \tag{A22}$$

# Appendix B

## Proof of zero residual response for symmetrical pulses applied to undamped systems.

In the case of symmetrical pulses acting on the mass spring system, for certain values of the ratio $\tau/T$ there is no residual response (see figure 2.4). It means that the system returns to rest immediately when the pulse has finished. The reason for this is the fact that the total work done by the forcing function on the system is equal to zero for the corresponding value of $\tau/T$. The work done during the shock period can be defined as:

$$\int_0^{x_{final}} \xi(t)dx = \int_0^{\tau} \xi(t)\frac{dx}{dt}dt \qquad \text{(B1)}$$

### a) Rectangular pulse.

The forcing function is given by:

$$\xi(t) = \begin{cases} \xi_c & 0 \le t \le \tau \\ 0 & \tau \le t \end{cases} \qquad \text{(B2)}$$

The response during the impulse is:

$$x(t) = \xi_c \left[1 - \cos\left(\omega_n t\right)\right] \qquad \text{(B3)}$$

The velocity is obtained by differentiating equation (B3) as follows:

$$\frac{dx}{dt} = \omega_n \xi_c \sin\left(\omega_n t\right) \qquad \text{(B4)}$$

Equations (B2) and (B4) are substituted in equation (B1) to obtain the following expression:

$$\omega_n \xi_c^2 \int_0^{\tau} \sin\left(\omega_n t\right) dt \qquad \text{(B5)}$$

After evaluating the integral one can write the expression for the total work done by the force.

$$\xi_c^2 \left[\cos\left(\frac{2\pi\tau}{T}\right) - 1\right] \qquad \text{(B6)}$$

From figure 2.5 one can see that residual response is zero when $\tau/T = 1,2,3...$ and also by evaluating these values in equation (b6) it is readily seen that the total work done is zero.

## b) Half sine pulse.

In this case the forcing function can be written as follows:

$$\xi(t)=\begin{cases}\xi_c \sin\left(\dfrac{\pi t}{\tau}\right) & [0 \le t \le \tau] \\ 0 & [\tau \le t]\end{cases} \tag{B7}$$

The displacement of the mass and its corresponding velocity during the disturbance period are given by:

$$x=\frac{\xi_c}{1-T^2/4\tau^2}\left(\sin\left(\frac{\pi t}{\tau}\right)-\frac{T}{2\tau}\sin\left(\frac{2\pi t}{T}\right)\right) \tag{B8}$$

$$\frac{dx}{dt}=\frac{4\xi_c\pi\tau}{4\tau^2-T^2}\left(\cos\left(\frac{\pi t}{\tau}\right)-\cos\left(\frac{2\pi t}{T}\right)\right) \tag{B9}$$

Substituting equation (B9) and (B7) in the integral given by equation (B1):

$$\frac{4\xi_c\pi\tau}{4\tau^2-T^2}\int_0^{\tau}\sin\left(\frac{\pi t}{\tau}\right)\left(\cos\left(\frac{\pi t}{\tau}\right)-\cos\left(\frac{2\pi t}{T}\right)\right)dt \tag{B10}$$

The expression for the total work is obtained after performing the previous integral and one can obtain the next expression:

$$\frac{4\xi_c\pi\tau}{4\tau^2-T^2}\left[\frac{\tau^2\left(\cos\left(\frac{2\pi\tau}{T}\right)+1\right)}{\pi(T+2\tau)}-\frac{\tau^2\left(\cos\left(\frac{2\pi\tau}{T}\right)+1\right)}{\pi(T-2\tau)}-\frac{\tau\left(\cos\left(\frac{2\pi\tau}{T}\right)+1\right)}{\pi}\right] \tag{B11}$$

From figure 2.4 corresponding to the half sine pulse the residual response is zero for $\tau/T=1.5, 2.5, 3.5....$ Evaluating equation (B11) at any of these values the total work done by the force is equal to zero.

# Appendix C

## Shock Response Spectra for rectangular and versed sine pulses.

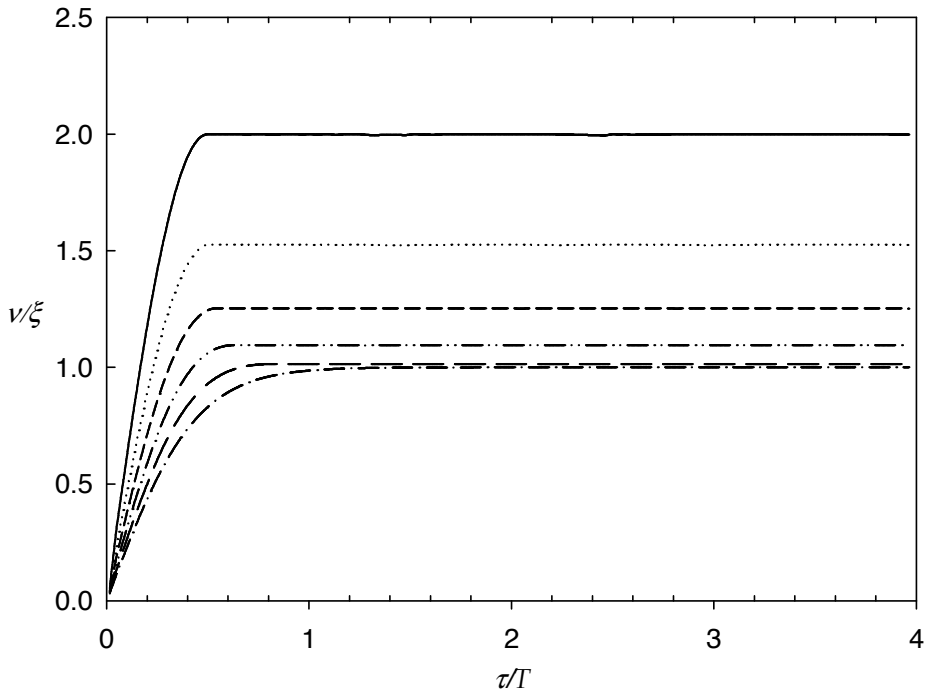


Figure C1. Shock response spectra for a viscously damped SDOF model, for a rectangular pulse excitation. (— $\zeta = 0$; ···$\zeta = 0.2$ ; – – $\zeta = 0.4$; –··– $\zeta = 0.6$; — — $\zeta = 0.8$; – · – $\zeta = 1$)

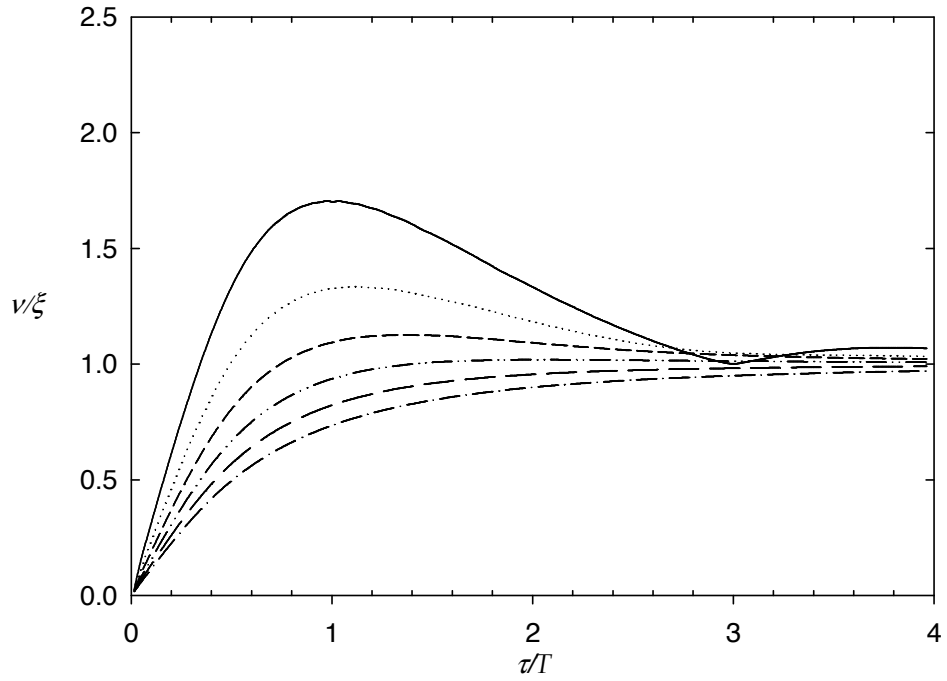


Figure C1. Shock response spectra for a viscously damped SDOF model, for a half sine pulse excitation. (— $\zeta = 0$; ···$\zeta = 0.2$ ; – – $\zeta = 0.4$; –··– $\zeta = 0.6$; — — $\zeta = 0.8$; – · – $\zeta = 1$)

# Appendix D.

## Effect of delay in the switching stiffness strategy for residual vibration.

It can be shown that the switching strategy used for suppressing residual vibrations is stable [97]. This proof is further discussed in this appendix.

Using Lyapunov's direct method [110], one can construct an energy-like function of the system and examining its derivatives the condition of stability can be evaluated. An energy function for the switching stiffness model can be written in terms of the total energy of the system, where the energy is considered after the disconnection of the secondary spring, as follows:

$$V = \frac{1}{2} m\dot{v}^2 + \frac{1}{2}\left(k - \Delta k\right)v^2 \tag{E1}$$

The first time derivative of equation (E1) can be written as:

$$\dot{V} = m\ddot{v}\dot{v} + kv\dot{v} - \Delta kv\dot{v} \tag{E2}$$

This can be further simplified using equation of motion (4.1) and rewritten as

$$\dot{V} = -\Delta kv\dot{v} \tag{E3}$$

Following reference [109], as $V$ is a positive definite function, and $\dot{V}$ is negative semidefinite, it can be said that the system is asymptotically stable. However, it is interesting to note the behaviour of the system when the control law is inverted as:

$$k_v = \begin{Bmatrix} k & v\dot{v} \le 0 \\ k - \Delta k & v\dot{v} > 0 \end{Bmatrix} \tag{E4}$$

In this case, the energy function of the system is expressed as:

$$V = \frac{1}{2} m\dot{v}^2 + \frac{1}{2}(k + \Delta k) v^2 \tag{E5}$$

and the derivative is given by:

$$\dot{V} = \Delta k \dot{v} v \tag{E6}$$

The derivative is a positive function, as a result the system is unstable. This also can be observed in equation (E5) as its second term means that energy is added to the system instead of being dissipated. In fact, at the stiffness reduction points the system is going from a low energy state, to a higher energy state. In a real system this energy, which causes instabilities, must come from a certain source. Figure (E1) shows the response of the actual system using the inverted control law given by equation (E4). In this case the amplitude of the system is bounded. However, the vibration of the system is sustained and while the voltage is supplied it never decays away. The energy responsible of this behaviour comes from the electromagnets used in the system.

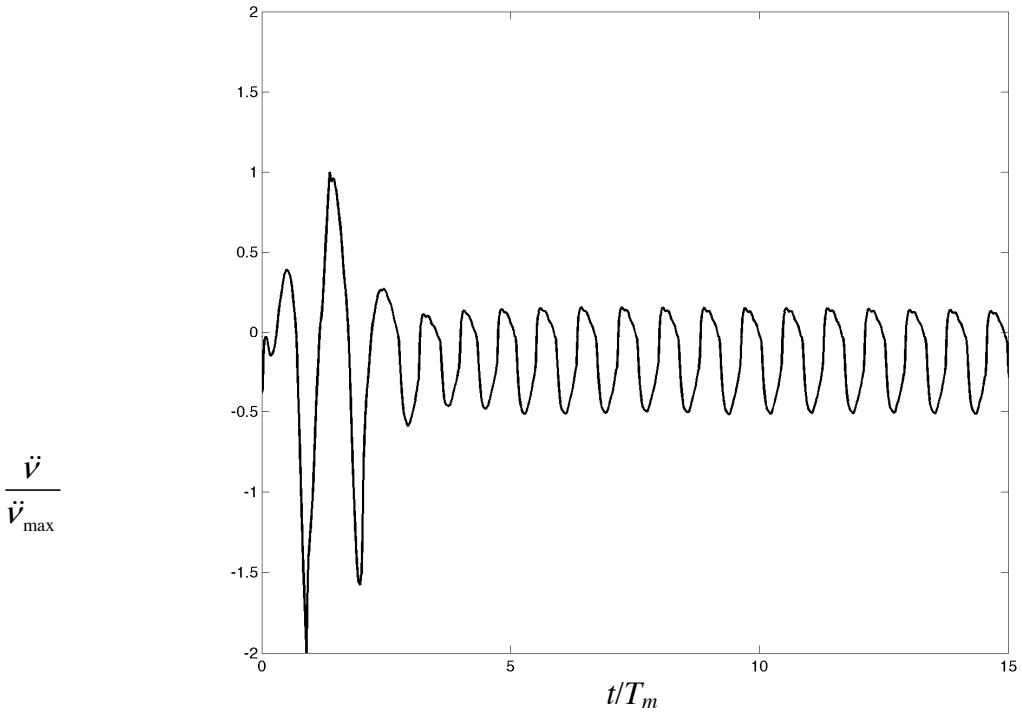


Figure E1. Actual response of the switching system considering the opposite control law as specified by equation (E4)

An interesting point in the study for the stability of this particular strategy is to determine if a delay in the reduction or recovery of the stiffness will cause any possible instability condition. In order to investigate this, a numerical simulation was performed. It is an iterative test that evaluates the amplitude of the system and compares it with the previous cycle. If the amplitude of the next cycle increases with respect to the previous one, the system will be unstable. The comparison is made for values of the stiffness ratio from 0 to 1, and a delay in the application of the strategy is introduced. This delay is given as a fraction of the mean natural period $T_m$. The resulting plot is presented in figure E2.

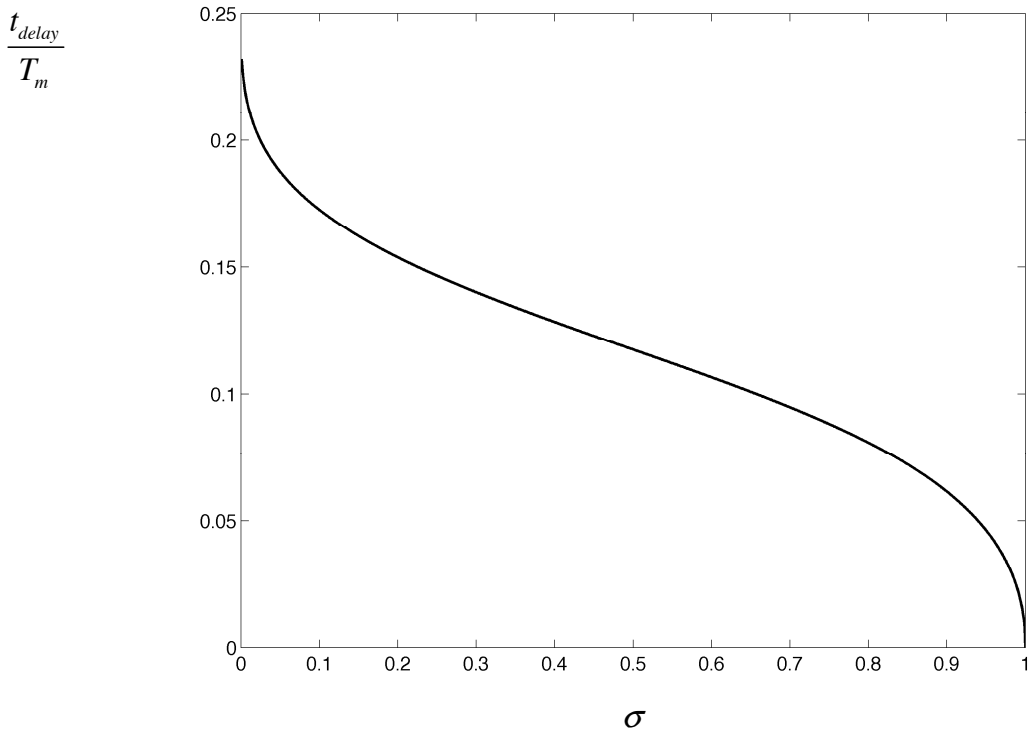


Figure E2. Maximum delay permissible in order to guarantee stability in the switching strategy presented as a function of the stiffness ratio $\sigma$. Values of delay above the curve will cause the system to become unstable.

Figure E2 represents the limiting value of delay permissible in order to achieve stability. The area below the curve represents a "safe" zone where the system is stable. However, it is important to note that although small delays will not cause instabilities, the performance of the system might decrease. The maximum value of delay depends upon the value of stiffness reduction ratio $\sigma$. As the stiffness ratio increases, smaller delays are permitted. A time response example for $\sigma = 0.5$ is shown in figure E2, for three situations. The response of the system with no delay is given by the continuous bold line, whilst the continuous thin line represents the limiting value of delay $d = 0.1176T_m$ for this value of stiffness ratio, and the dotted line, a value exceeding the limit $d = 0.15T_m$.

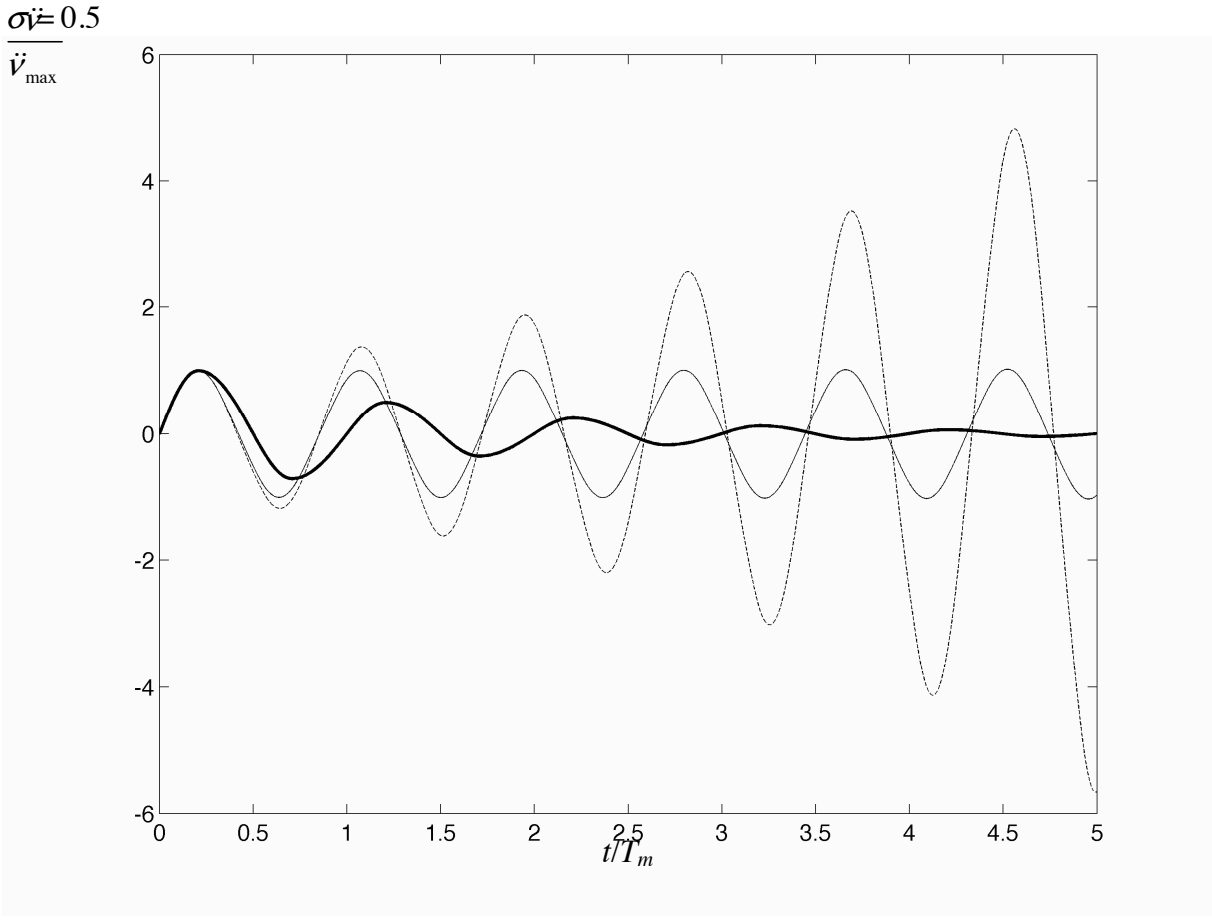


Figure E3. Effect of delay in the switching stiffness strategy. For this example . No delay (continuous bold line), limiting value of delay $d = 0.1176T_m$ (continuous thin line) and $d = 0.15T_m$ (dotted line).

This phenomenon is attributed to two reasons. Firstly, as the stiffness reduction is not made at the point of maximum displacement, the energy dissipated is not maximized. Secondly, the stiffness recovery is performed after the point of equilibrium position. As a result, the secondary spring $\Delta k$ has a certain deformation at the moment of reconnection. This means the secondary spring $\Delta k$ has some energy stored that is returning to the system. If the delay causes the energy returned to be greater than the energy dissipated during the stiffness reduction, the amplitude will grow. Figure E4 shows the energy levels in the unstable system, showing that at some point the energy returned is higher than the energy removed. This will in fact violate energy conservation, which means that in a real system the energy needed to cause the instability must come from an external source. In practice this phenomenon has not been observed because the delay in the real time implementation of the strategy is very small. However, it is important to note that the control law has been changed to the opposite as

expressed by equation E4. As a result, constant amplitude of vibration is sustained (see figure E1). The energy required to sustain this vibration is assumed to come from the electromagnets used in the experimental rig. If the delay is large enough to cause instabilities, in a real system the energy must come from an external source. For the experimental setup used in this project, the electromagnets as inductive devices are capable of storing and releasing energy resulting from sudden voltage or current changes, as was explained in chapter 6.

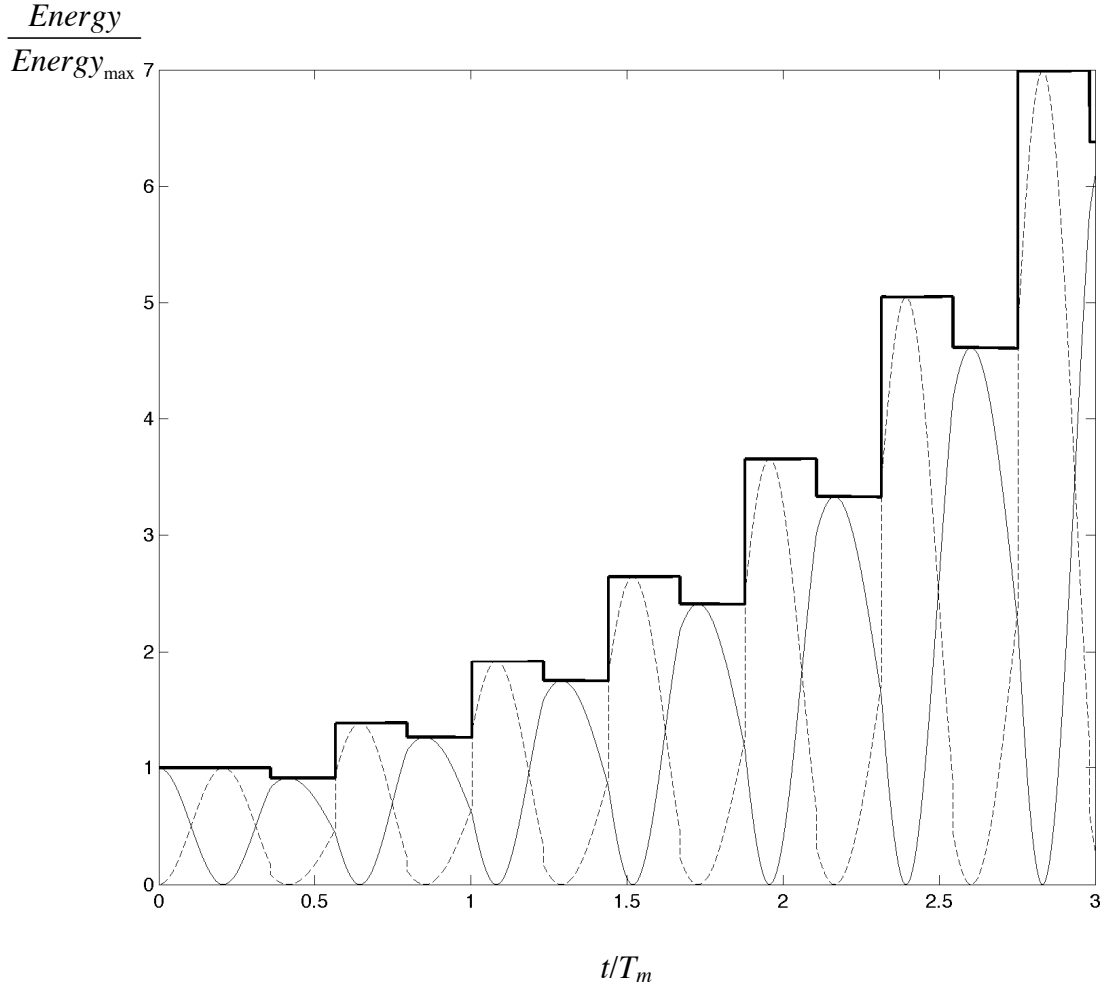


Figure E3. Energy levels in a switchable stiffness system with delay of $d = 0.15T_m$ enough to cause instabilities. The bold line represents the total energy in the system, the thin line represents the kinetic energy, and the dotted line is for the potential energy.

# Appendix E.

## Maximum energy dissipation for the impacting model: an analytical derivation for the optimum parameters.

The energy dissipated per impact of the compound impacting model experiencing free vibrations is given by:

$$E_d = \left[ 1 - \frac{\sigma}{1+\Omega^2\left(\frac{1}{\sigma}-1\right)}\left[\left(\frac{1}{\sigma}-1\right)\Omega + \sin\left(\frac{\pi}{2}\Omega\right)\right]^2 \right] \times 100 \qquad \text{(D1)}$$

For simplicity, the specific case of $\Omega = 3$ is considered. Simplifying equation (D1) yields to:

$$E_d = \frac{\sigma^2}{9-8\sigma}\left(3-4\sigma^2\right) \qquad \text{(D2)}$$

In order to obtain the value of stiffness ratio $\sigma$ which gives the maximum value of energy dissipated, equation (D2) is differentiated with respect to $\sigma$.

$$\frac{dE_d}{d\sigma} = 0 \tag{D3}$$

The derivative is thus given by:

$$\frac{2\sigma(3-4\sigma)}{9-8\sigma}\left[\frac{3-4\sigma}{9-8\sigma}(9-12\sigma)-4\sigma\right] = 0 \tag{D4}$$

Solving equation (D4) for $\sigma$ gives $\sigma = 0.75$. The corresponding value of mass $\mu$ ratio is calculated using the relation $\mu = \dfrac{1}{1+\Omega^2\left(\dfrac{1}{\sigma}-1\right)}$, giving $\mu = 0.25$ for this particular case. This procedure can be used for other values of the frequency ratio $\Omega$.

# Appendix F.

## Details of the switching circuit

The circuits used in the laboratory tests were specifically made for these applications. The circuit is divided in two parts, one dedicated to the voltage switching during the shock pulse, and the other responsible of performing the switching logic for the residual stage.

In the residual stage circuit the input signal used is the acceleration response of the suspended magnet. Inside the circuit, this signal is amplified and then split into two in order to have acceleration and velocity signals. It is important to note that the amplification gain as well as the integrator parameters can be adjusted in the circuit by choosing different values of capacitance and resistance. Then both signals are multiplied and compared with respect to zero. If the product is higher than zero, the voltage is set to the off position. Otherwise, a voltage is sent to the electromagnets. A MOSFET transistor is used to manage the high currents drawn by the electromagnets. Normally no more than 12 volts were used in order to prevent overheating. The schematics for this circuit are shown in figure F1 whilst a block diagram is presented in figure F2.

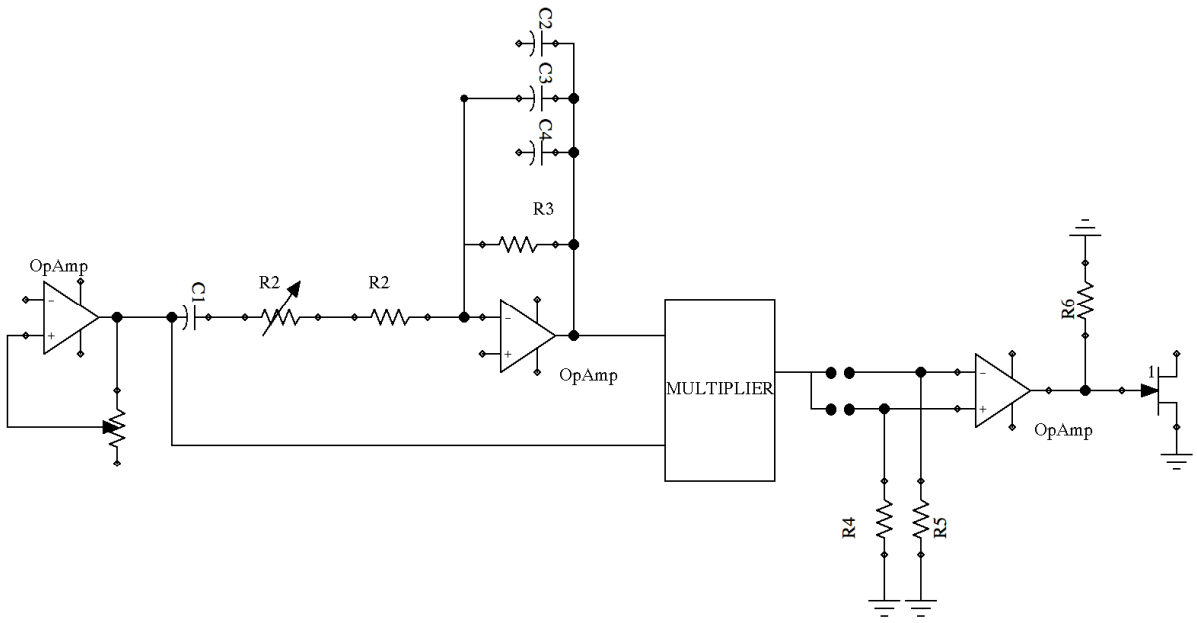


Figure F1. Schematics of the residual stage switching circuit.

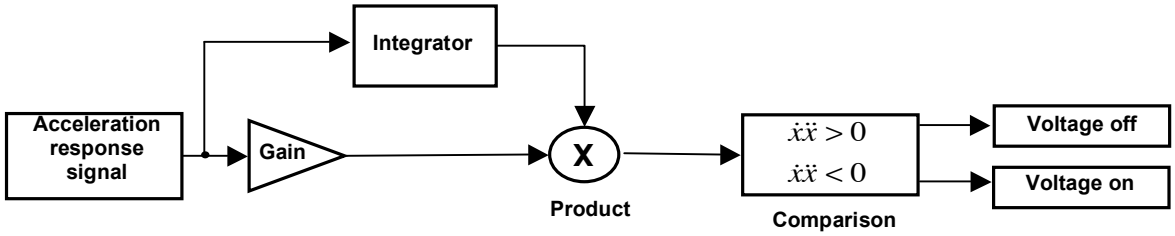


Figure F2. Block diagram for the residual stage switching circuit.

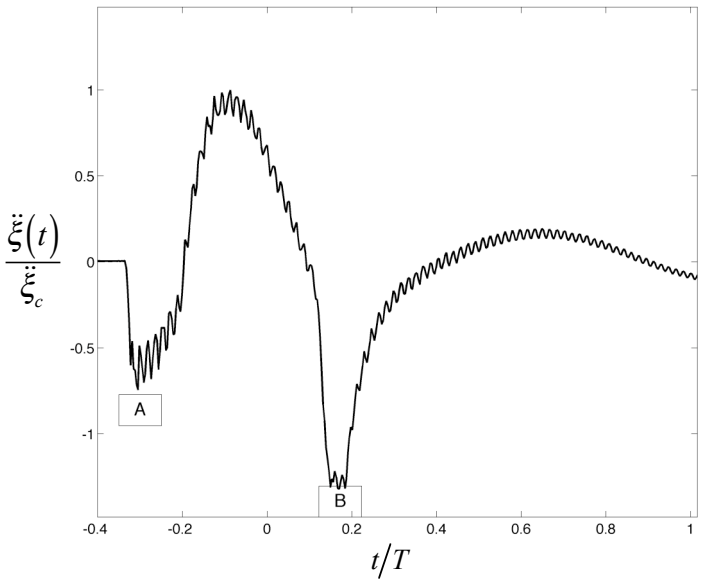


Figure F3. Close up of the typical shock pulse used in the tests showing the two minima. The stiffness is reduced between these points by using a negative peak detector circuit.

The shock strategy part of the circuit involves a negative peak detector after the signal conditioning stage. When a peak is detected, a control signal is sent to a D-type flip-flop. This element has a manual switch that clamps the circuit, setting the voltage to a high value, which is sent to the electromagnets via another MOSFET transistor. After the first minimum which corresponds to the greatest negative peak is detected (according to point A in figure F3) the circuit becomes unclamped and the voltage is set to zero. A second flip-flop is responsible of activating the switching strategy. This second flip-flop remains unclamped until the second minimum negative peak (point B). At this point, the second flip-flop becomes clamped and it activates the switching strategy. Schematics of the circuit and a block diagram are presented in figures F5 and F6 respectively.

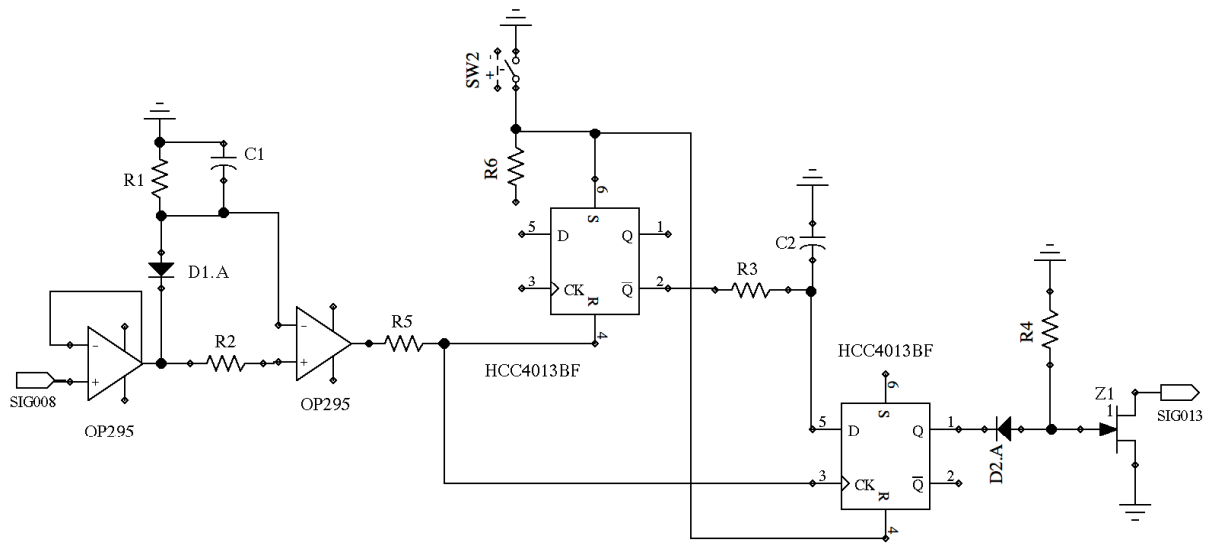


Figure F4. Schematics of the shock pulse stage switching circuit.

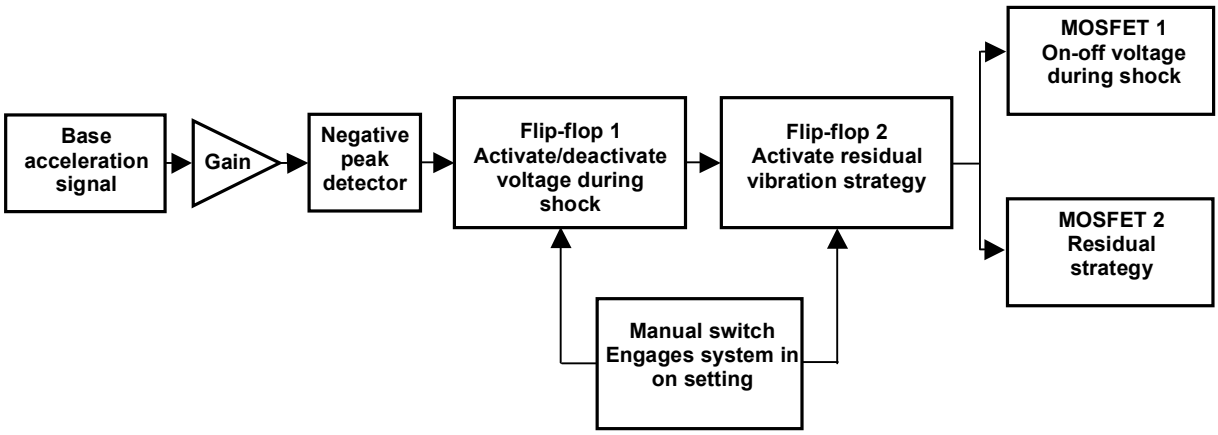


Figure F5. Block diagram of the shock pulse stage switching circuit.